

# **OPERATION AND PERFORMANCE OF A SOLAR HARDWOOD DRYING KILN UTILIZING NATURAL DEHUMIDIFICATION**

by  
Richard Barry Müller

*Thesis presented in partial fulfilment of the requirements for the degree  
Master of Science in Forestry (Wood Products Science) at the University  
of Stellenbosch*



Supervisor: Dr Dieter Steinmann  
Faculty of AgriSciences  
Department of Forest and Wood Science

March 2011

## **DECLARATION**

By submitting this thesis/dissertation electronically, I declare that the entirety of the work contained herein is my own, original work, that I am the sole author thereof (save to the extent explicitly otherwise stated), that reproduction and publication thereof by Stellenbosch University will not infringe any third party rights and that I have not previously in its entirety or in part submitted it for obtaining any qualification.

March 2011

Copyright © 2011 University of Stellenbosch

All rights reserved

## ABSTRACT

The Saasveld solar kiln, valued at US\$ 10,000 (R 70,000), is a greenhouse-type solar kiln requiring no additional heating. A unique auto-regulated process of natural dehumidification at night controls the humidity, and uses no venting system, nor any human/controller intervention. The natural dehumidification is achieved by circulating the humid kiln air through an air jacket on the periphery of the solar kiln. Diurnal temperature fluctuations allow condensation in the air jacket when air is cooled to below its dew-point temperature. The process is simple as colder night temperatures are a certainty. Almost no research has been done on similar kilns.

The purpose of this thesis was to study the operation and performance of a solar drying kiln to dry high density hardwoods utilising natural dehumidification. The kiln load consisted of 20.1m<sup>3</sup> of a high density hardwood, *Eucalyptus diversicolor*, with air-dry density of 893kg/m<sup>3</sup>.

The ZA Dry Q drying quality assessment indicated outstanding moisture distribution with little drying stress, a few surface checks and no internal checks, collapse, short bow or surface discolouration. The results conformed to the ZA Dry Q softwood appearance grade specification, except for end checks – remarkable for the drying of any hardwood. The final moisture content (MC) distribution was extremely tight with MC average of 11.5 per cent (%), standard deviation of 0.97% and the moisture gradient averaged 1.49%, standard deviation of 0.5%. The MC and MG were equally distributed in all three geometric directions throughout the load. The timber dried in 130 days.

The kiln operation was analysed by temperature and humidity parameters at five positions inside and outside the kiln while monitoring the MC. The extent of moisture evaporation from the timber and the dehumidification of air were derived from this data.

The results showed that the average of the daily kiln temperature, independent from the external temperature, increased from 18.0°C initially to 25.7°C. A maximum temperature of 38.1°C was recorded at the end of drying. Cell collapse did not occur under these low temperatures.

Evaporation occurred generally from 07h30 to 16h45. The rate reduced at lower moisture contents. There was no effect of stack width. Natural dehumidification by condensation happened generally from 17h00 to 07h30.

The equilibrium moisture content (EMC) decreased automatically from an initial daily average of 18.1% (variation 5%) to 8% (variation 2%) finally. It was similar to a smoothed T3C2–schedule.

The mild drying conditions, with EMCs above 7.3%, ensured minimal moisture gradients and drying stresses. This reduced surface and internal checks. Nocturnal equalising and conditioning, comparable to intermittent schedules, resulted from: no evaporation, improved diffusion of heated timber and adsorption of moisture on the wood surface. The kiln protected the timber in extreme climatic conditions.

It was found that the main circulating fan could be switched off from 17h00 to 07h30. A 30-minute manual venting at noon was permitted once fibre saturation point had been reached.

Beneficiaries to this study can include hardwood processors who need to dry high density hardwoods within a reasonable time to an excellent drying quality. Processors in developing countries or who have little drying expertise could also benefit.

## OPSOMMING

Die Saasveld sondroër, met 'n beraamde waarde van US\$ 10,000 (R70,000), is 'n groentetunnel-tipe sondroër met geen addisionele verhitting nie. 'n Unieke auto-reguleerder beheer die humiditeit snags deur natuurlike dehumidifikasie. Dit gebruik geen ventileerder of enige menslike/kontroleerder inmenging nie. Die natuurlike dehumidifikasie word verkry deur die vogtige lug te sirkuleer deur 'n lugkussing op die omtrek van die tunnel. Dag-en-nag temperatuur skommelings laat kondensasie toe binne-in die lugkussing sodra die lug benede die doupunt-temperatuur afkoel. Dit is 'n eenvoudige proses aangesien kouer nagte 'n gegewe is. Byna geen navorsing is nog op soortgelyke sondroërs gedoen nie.

Die doel van die tesis was om die werking en werkverrigting van 'n sondroër wat hoë digtheid loofhout met behulp van natuurlike dehumidifikasie droog, te bestudeer. Die houtvrag het bestaan uit  $20.1\text{m}^3$  van hoë digtheid loofhout, *Eucalyptus diversicolor*, met 'n gemiddelde lug-droë digtheid van  $893\text{ kg/m}^3$ .

Die ZA Dry Q drogingskwaliteit toets het uitstaande resultate getoon. Daar was min drogingspannings, 'n paar oppervlak krake en geen interne krake, sel-ineenstorting, kort-boog of oppervlak-verkleuring nie. Die resultate bevredig die ZA Dry Q naaldhout voorkomsgraad spesifikasie, behalwe vir end-krake – merkwaardig vir die droging van enige hoë digtheid loofhout. Die finale vogverspreiding was nou-verspreid met 'n gemiddelde voggehalte van 11.5%, standaard afwyking van 0.97% en 'n gemiddelde vog-gradiënt van 'n 1.49%, standaard afwyking van 0.5%. Die voggehalte en vog-gradiënt was eweredig verspreid in al drie geometriese rigtings van die houtvrag. Die hout het in 130 dae gedroog.

Die werking van die sondroër is geanaliseer deur temperatuur- en humiditeits-parameters by vyf posisies binne- en buite die droogkamer tegelykertyd met die voggehalte te monitor. Die omvang van vogverdamping uit die hout en dehumidifikasie van die lug is afgelei van hierdie data.

Die gemiddelde daaglikse sondroër-temperatuur, wat onafhanklik van die buite temperatuur was, het verhoog van  $18.0^{\circ}\text{C}$  aanvanklik tot  $25.7^{\circ}\text{C}$ . Die maksimum temperatuur van  $38.1^{\circ}\text{C}$  is gemeet aan die end van droging. Sel-ineenstorting het nie voorgekom by hierdie lae temperature nie.

Verdamping het algemeen voorgekom vanaf 07h30 tot 16h45, teen 'n vertragende verdampingstempo by laer voggehaltes. Die stapelwydte-effek was van geen belang nie. Natuurlike dehumidifikasie deur kondensasie het gereeld voorgekom vanaf 17h00 tot 07h30.

Die ewewigsvoggehalte (EVG) het outomaties verminder vanaf 'n aanvanklike daaglikse gemiddelde van 18.1% (variasie van 5%) na 8% (variasie van 2%). Dit was soortgelyk aan 'n gelykmatige T3C2 –drogingskediule. Die matige drogingskondisies, met EVG bokant 7.3%, het minimale vog-gradiënte en drogingsspannings verseker wat oppervlak-krake en interne-krake verhoed het. Nagtelike houtvog egalisasie en kondisionering, vergelykbaar met puls-humiditeit skedules, was die gevolg van: geen verdamping, verbeterde diffusie in verhitte hout en adsorpsie van vog op die hout oppervlak. Die droogkamer het die hout beskerm teen buitengewone klimaatstoestande.

Daar is gevind dat die hoof-waaier afgeskakel kan word vanaf 17h00 tot 07h30 en dat 'n 30-minute nie-outomatiese ventilering smiddae kan plaasvind sodra veselversadigingspunt bereik is.

Hierdie studie sal van nut wees vir die loofhout verwerkers wat hoë-digtheid loofhout moet droog binne 'n redelike tydperk met 'n uitstekende drogings-kwaliteit, asook houtverwerkers in opkomende lande of met gebrekkige drogingsvaardighede.

## **ACKNOWLEDGEMENTS**

I would like to express my sincere gratitude to the following people and organisations:

- My supervisor, Dr. Dieter Steinmann, for his continuous support and enthusiasm;
- Mr. Simon Allpass who donated the timber, stacked the solar kiln and offered general assistance during the drying run;
- Mr. Carel van der Merwe of SANPARKS who donated the solar kiln and shared his experience on this solar kiln;
- Furntech who donated the concrete base for the Saasveld solar kiln;
- Ms. Shann Kieswetter for formatting and editing the thesis;
- My father and role model, Bethel, for his support during all my studies; and
- My wife, Elsie for her love and encouragement – many nights she was woken up as her husband had to see whether the Bergwind blew down his “tent”.

## TABLE OF CONTENTS

ABSTRACT .....	i
OPSOMMING .....	iii
ACKNOWLEDGEMENTS .....	v
LIST OF FIGURES .....	ix
LIST OF TABLES.....	xiii
NOMENCLATURE .....	xvi
1 GENERAL INTRODUCTION .....	1
1.1 Overview of the study .....	1
1.2 Objectives of the research .....	2
1.3 Definition of concepts.....	3
2 LITERATURE REVIEW.....	5
2.1 Solar drying by natural dehumidification .....	5
2.2 Direct radiation solar kilns .....	7
2.3 Solar dehumidifier kilns .....	7
2.4 The drying of hardwoods .....	7
2.4.1 Problems when drying high density hardwoods .....	9
2.4.2 Eucalyptus drying .....	10
2.5 Specific heat capacity of timber .....	11
2.6 Drying quality assessment .....	12
3 MATERIAL AND METHODS .....	12
3.1 Study site.....	12
3.2 Layout and geometry of the Saasveld solar kiln .....	13
3.3 Humidity control .....	15
3.4 Expected climatic conditions inside the Saasveld solar kiln .....	17
3.5 Timber species .....	18
3.6 Stacking.....	18
3.7 Sampling procedure.....	20
3.7.1 Sampling of moisture content during drying .....	20
3.7.2 Sampling for drying quality.....	21
3.7.3 Temperature and humidity sensors.....	22
3.8 Data collection methods.....	22
3.8.1 Moisture content during drying.....	22
3.8.2 Drying quality .....	25
3.8.3 Positioning and management of sensors .....	31
3.8.4 Data-logging .....	32



3.8.5	Thermocouple calibration.....	33
3.9	Data analysis methods.....	34
3.10	Drying run.....	35
4	RESULTS, ANALYSES AND DISCUSSION .....	36
4.1	Drying quality evaluation according to ZA Dry Q.....	36
4.1.1	MC and MG variation through the load .....	36
4.1.2	Assessing mean MC and MG against ZA Dry Q requirements.....	38
4.1.3	Other defects .....	39
4.2	Moisture content during drying.....	44
4.3	Internal and external atmospheric conditions .....	47
4.3.1	Load Inlet temperatures .....	49
4.3.2	Load Inlet EMC's .....	52
4.3.3	Load inlet and outlet air temperatures.....	53
4.3.4	Evaporation of wood moisture from the load inlet to the load outlet.....	57
4.3.5	Dehumidification in the jacket .....	75
4.3.6	Comparison between temperatures inside the kiln and external temperatures.....	88
4.3.7	Comparison between EMC inside and outside the kiln.....	98
4.3.8	Comparison between AH in the kiln and external AH's .....	102
4.4	Comparison with other drying schedules.....	105
4.4.1	Combined air-and-kiln seasoning.....	106
4.4.2	Pre-drying in a solar kiln .....	106
4.4.3	Smoothed schedules .....	107
4.4.4	Intermittent schedules.....	107
4.4.5	Solar drying .....	108
4.4.6	Comparison with an approved schedule .....	110
4.5	Configuration of the Saasveld solar kiln for future research on natural dehumidification.....	112
5	CONCLUSIONS AND RECOMMENDATIONS.....	113
5.1	Conclusions .....	113
5.2	Recommendations.....	116
5.2.1	Recommended modifications to the design and operation of a natural dehumidification based green-house solar kiln .....	116
5.2.2	Suggested research in solar kilns that utilise natural dehumidification .....	118
	REFERENCE LIST .....	120
	APPENDICES.....	124
	APPENDIX A: KILN HARDWARE.....	125
A.1	Plastic cover: .....	125
A.2	Fastening of plastic cover: .....	125

A.3.	Main fan for air circulation .....	127
A.4	Heating of the kiln .....	127
A.5	Small fan for humidity control.....	127
A.6	Stacking.....	127
A.7	Circuit board .....	127
APPENDIX B: DEFINITIONS OF DRYING DEFECTS AS DESCRIBED BY ZA DRY Q .....		129
APPENDIX C: THERMOCOUPLE CALIBRATION.....		130
C.1	Auto calibration and pairing.....	130
C.2	Improved calibration.....	131
APPENDIX D: DATA ANALYSIS METHODS.....		138
D.1	Ambient air pressure.....	138
D.2	Relative humidity .....	138
D.3	Equilibrium moisture content (EMC).....	139
D.4	Absolute humidity (AH) on a mass basis.....	140
D.5	Dew-point temperature .....	140
APPENDIX E: ZA DRY Q RESULTS .....		141
APPENDIX F: MOISTURE CONTENT ANALYSIS.....		147
F.1	MC and MG variation over the width and height of the stacks, as seen from the end of the stack (A).....	148
F.2	MC and MG variation over the length and width of the stacks, as seen from the top of the stack (B):.....	151
F.3	MC and MG variation over the length and height of the stacks, as seen through the stickers of the stack (C), either from the back of the kiln or the plenum chamber .....	155

## LIST OF FIGURES

Figure 3.1: The Saasveld solar kiln.....	13
Figure 3.2: Schematic isometric view of the Saasveld solar kiln (Steinmann, 2001) .....	14
Figure 3.3: Tarpaulin covers the sides and top of the stacks.....	15
Figure 3.4: Air inlet manifold delivering air into the double skin (jacket) .....	16
Figure 3.5: Feedback valve for air to exit the jacket .....	16
Figure 3.6: Position of weeping holes above the fixing rails .....	17
Figure 3.7: Position of the stacks, in brown, in the kiln. Baffles are shown by black lines. Numbers were assigned to each stack.....	19
Figure 3.8: Stacking was done to fill the steel frame opening of the plenum wall. Note the baffle between stacks 1 and 2 .....	19
Figure 3.9: Sectional side-view of the MC sample boards in each of the eight stacks; sample boards rested on short stickers wedged in the sticker opening spaces .....	20
Figure 3.10: ZA Dry Q sample pattern of the stack as seen from the side of the load towards the middle of the kiln (SALMA, 2003b).....	21
Figure 3.11: Preparation of a MC sample board .....	23
Figure 3.12: Preparation of case-hardening test pieces (SALMA, 2003b).....	27
Figure 3.13: Separation and marking of the slices for case-hardening test (SALMA, 2003b) .....	27
Figure 3.14: Test jig for assessment of case-hardening (SALMA, 2003b).....	28
Figure 3.15: Evaluation with the test jig, of case-hardening from a board wider than 100mm (SALMA, 2003b) .....	28
Figure 3.16: Case-hardening is measured with a vernier calliper as a distance between the two slices. ....	28
Figure 3.17: Measurement at the 100mm or 75mm spaced pins (SALMA, 2003b) .....	29
Figure 3.18: Deflection caused by case-hardening of a test piece in a 100mm and 75mm pin position (note that $d_{75} - d_2 = \frac{1}{2} \times (\text{read}_{100} - 10) = d_{100}$ ) .....	29
Figure 3.19: Positioning of the thermocouples .....	32
Figure 4.1: The only surface check encountered .....	44
Figure 4.2: Scatter plot of final MC against green MC of the 24 sample boards.....	46
Figure 4.3: Comparison of the drying of sample boards at different heights in the stacks .....	47
Figure 4.4: Daily average of $T_d$ Load In against the drying days.....	50
Figure 4.5: Daily maximum $T_d$ Load In against the drying days .....	51
Figure 4.6: Average load inlet EMC at various stages of drying seen over the course of a typical day .....	52
Figure 4.7: The specific heat capacity in BTU/lb. °F against MC for two temperatures.....	54
Figure 4.8: TDAL ( $T_d$ Load In- $T_d$ Load Out) against time covering days 1 - 4; MC = 50% .....	55

Figure 4.9: TDAL ( $T_d$ Load In- $T_d$ Load Out) against time covering days 18 - 21; MC = 43% .....	55
Figure 4.10: TDAL ( $T_d$ Load In- $T_d$ Load Out) against time covering days 120 - 123; MC = 10.5% .....	56
Figure 4.11: Difference in AH between load outlet and load inlet (or $\Delta AH_{Load}$ ) during the five stages of drying .....	58
Figure 4.12: $\Delta AH_{load}$ against time for the measuring period of days 1 - 4; MC = 50%.....	60
Figure 4.13: $\Delta AH_{load}$ against time for the measuring period of days 18 - 21; MC = 42%.....	60
Figure 4.14: $\Delta AH_{load}$ against time for the measuring period of days 39 - 42; MC = 29%.....	61
Figure 4.15: $\Delta AH_{load}$ against time for the measuring period of days 63 - 66; MC = 20.5%.....	61
Figure 4.16: $\Delta AH_{load}$ against time for the measuring period of days 90 - 93; MC = 15.3%.....	62
Figure 4.17: Load inlet and outlet EMC against time for days 1 - 4; MC = 50%.....	63
Figure 4.18: Load inlet and outlet EMC against time for days 18 - 21; MC = 43%.....	64
Figure 4.19: Load inlet and outlet and external EMC against time for days 39 - 42; MC = 30% ...	65
Figure 4.20: Load inlet and outlet EMC against time for days 63 - 66; MC = 20.5%.....	66
Figure 4.21: Load inlet and outlet EMC against time for days 90 - 93; MC = 15.3%.....	66
Figure 4.22: Load inlet and outlet and external EMC against time for days 120 - 123; MC=10.3% .. .....	67
Figure 4.23: Load inlet and outlet and external $T_d$ against time for days 120 - 123; MC = 10.3% ..	67
Figure 4.24: $\Delta DP_{load} = \{T_d \text{ Load Out} - DP \text{ Load Out}\}$ temperature at various stages of drying ..	71
Figure 4.25: $\Delta DP_{load}$ against time for the measuring period of days 1 - 4; MC= 50%.....	72
Figure 4.26: $\Delta DP_{load}$ against time for the measuring period of days 18 - 21; MC = 42%.....	72
Figure 4.27: $\Delta DP_{load}$ against time for the measuring period of days 39 - 42; MC = 29%.....	73
Figure 4.28: $\Delta DP_{load}$ against time for the measuring period of days 63 - 66; MC = 20.5%.....	73
Figure 4.29: $\Delta DP_{load}$ against time for the measuring period of days 90 - 93; MC = 15.3%.....	74
Figure 4.30: DP Jacket Out, $T_d$ Jacket out and $T_d$ Exterior during the measuring period of days 1 - 4; MC = 50% .....	76
Figure 4.31: AH Jacket In and AH Jacket Out during the measuring period of days 1 - 4; MC = 50% .....	77
Figure 4.32: Sectional drawing of the possible catchments of condensate.....	78
Figure 4.33: DP Jacket Out, $T_d$ Jacket Out and $T_d$ Exterior during the measuring period of days 18 - 21; MC = 43% .....	79
Figure 4.34: AH Jacket In and AH Jacket Out during the measuring period of days 18 - 21; MC = 43%. .....	80
Figure 4.35: DP Jacket Out, $T_d$ Jacket Out and $T_d$ Exterior during the measuring period of days 39 - 42; MC = 30% .....	81
Figure 4.36: AH Jacket In and AH Jacket Out during the measuring period of days 39 - 42; MC = 30%. .....	82

Figure 4.37: $T_d$ Jacket In, $T_d$ Jacket Out and DP Jacket Out during the measuring period of days 63 - 66; MC = 20.5% .....	83
Figure 4.38: AH Jacket In and AH Jacket Out during the measuring period of days 63 - 66; MC = 20.5% .....	83
Figure 4.39: DP Jacket Out, $T_d$ Jacket Out and $T_d$ Exterior during the measuring period of days 90 - 93; MC = 15.3% .....	84
Figure 4.40: AH Jacket In and AH Jacket Out during the measuring period of days 90 - 93; MC = 15.3%. .....	85
Figure 4.41: Difference between dry bulb and dew-point temperatures at the jacket outlet, .....	87
Figure 4.42: Daily average of the difference between internal and external temperature ( $\Delta T_{day}$ ) ..	89
Figure 4.43: Fluctuation of diurnal exterior temperature, Exterior ( $T_{d\ max} - T_{d\ min}$ ) .....	92
Figure 4.44: Trend lines of the fluctuation of diurnal interior and exterior temperatures, .....	93
Figure 4.45: $T_d$ Load In and $T_d$ Exterior against time covering days 1 - 4; MC = 50% .....	95
Figure 4.46: $T_d$ Load In and $T_d$ Exterior against time covering days 18 - 21; MC = 43% .....	95
Figure 4.47: $T_d$ Load In and $T_d$ Exterior against time covering days 42 - 45; MC = 29% .....	96
Figure 4.48: $T_d$ Load In and $T_d$ Exterior against time covering days 120 - 123; MC = 10.15%.....	96
Figure 4.49: Typical average daily difference between internal and external temperature, average $\Delta T_{time}$ , at various stages of drying .....	97
Figure 4.50: Average $\Delta EMC$ from days 1 - 24; MC = 64% - 42%.....	100
Figure 4.51: Average $\Delta EMC$ from days 25 - 45; MC = 42% - 29.5%.....	100
Figure 4.52: Average $\Delta EMC$ from days 46 - 63; MC = 29.5% - 20.4%.....	100
Figure 4.53: Average $\Delta EMC$ from days 64 - 89; MC = 20.4% - 15.3%.....	101
Figure 4.54: Average $\Delta EMC$ from days 90 - 130; MC = 15.3% - 10.15%.....	101
Figure 4.55: Comparison between AH Load In the kiln and AH Exterior during the measuring period of days 1 - 4; MC = 50%.....	102
Figure 4.56: Comparison between AH Load In the kiln and AH Exterior during the measuring period of days 18 - 21; MC = 43%.....	103
Figure 4.57: Comparison between AH Load In the kiln and AH Exterior during the measuring period of days 39 - 42; MC = 30%.....	103
Figure 4.58: Comparison between AH Load In the kiln and AH Exterior during the measuring period of days 63 - 66; MC = 20.5%.....	104
Figure 4.59: Comparison between AH Load In the kiln and AH Exterior during the measuring period of days 90 - 93; MC = 15.3%.....	104
Figure 4.60: Presentation of a drying schedule by Bauer (2003) for sensitive eucalypt timber in the furnace assisted solar dryer .....	108
Figure 4.61: Comparison between the T3C2- schedule and the temperature experienced inside and outside the Saasveld solar kiln .....	110

Figure 4.62: Comparison between the T3C2- schedule and the EMC experienced inside and outside the Saasveld solar kiln.....	111
Figure 5.1: Alternative to the Saasveld solar kiln (Steinmann, 2001) .....	117
Figure A.1: Damage from the Bergwind. ....	126
Figure A.2: Original rail system. The plastic sheet fits in-between the HDPE profile and the rubber strip. ....	126
Figure A.3: The double rail system used at the leading edges of the Saasveld Solar kiln. The plastic sheet fits in-between the HDPE profile and the HDPE wedge strip. ....	126
Figure A.4: Saasveld solar kiln electrical circuit board.....	128
Figure C.1: The temperature variation during the water calibration procedure.....	132
Figure C.2: Establishment of an algebraic equation of the correction in temperature .....	133
Figure C.3: Improved thermocouple values .....	135
Figure F.1: Observation points to assess the moisture variation in stack 7; the average all MC <sub>½</sub> measurements were 11.7% .....	147
Figure F.2: Observation points to assess the moisture variation in stack 2; the average of all MC <sub>½</sub> measurements were 11.4% .....	147

## LIST OF TABLES

Table 3.1:	Initial mass, initial MC and calculated oven-dry mass of the MC sample boards .....	25
Table 3.2:	The position of thermocouple pairs .....	31
Table 3.3:	Pairing of the thermocouples .....	33
Table 4.1:	A summary of the results for stack 7 and stack 2 .....	37
Table 4.2:	Assessing the mean MC and MG against ZA Dry Q standards .....	38
Table 4.3:	Summary of drying defects in stack 7 with board dimensions of 30mm x 80mm .....	40
Table 4.4:	Summary of drying defects in stack 2 with board dimensions of 30mm x 120mm ....	41
Table 4.5:	Recorded % MC of all sample boards in the load.....	45
Table 4.6:	The five drying stages of the drying run .....	48
Table 4.7:	The six measuring periods during the drying run.....	49
Table 4.8:	Maximum negative values for $\Delta AH_{Load}$ for the five drying stages.....	59
Table 4.9:	Calculated diffusion coefficients for the nocturnal hours inside and outside the kiln as obtained from the average temperatures in each drying stage .....	69
Table 4.10:	Percentage frequency of ( $T_d$ Jacket Out - DP Jacket Out) for the ranges 0-0.2; 0.2-0.4 and >0.4 for the different drying stages at 02h00 .....	88
Table 4.11:	Average $T_d$ Load in, $T_d$ External and $\Delta T_{day}$ for the five drying stages.....	90
Table 4.12:	Correlation coefficients for the day of drying, Exterior ( $T_{d\ max} - T_{d\ min}$ ) and $\Delta T_{day}$ for the five drying stages.....	91
Table 4.13:	MC, Average $\Delta T_{day}$ , Average $\Delta EMC$ and standard deviation for $\Delta EMC$ for the five drying stages. ....	99
Table 4.14:	Typical moisture-content based schedule for drying 43 mm thick blackbutt boards (Haque and Langrish, 2006) .....	109
Table 4.15:	Geometric parameters of the Saasveld solar kiln .....	112
Table C.1:	Pairing of thermocouples. ....	131
Table C.2:	A portion of the table for the initial calculations of polynomial functions to improve temperature values .....	134
Table C.3:	A portion of the table for the new correction values (note that the sum and average at the bottom is for the entire table, and not for the values displayed).....	136
Table C.4:	Regression functions of the correction for the different thermocouples .....	137
Table E.1:	ZA Dry Q MC (%) record for stack 2, 30mm x 124mm green dimensions .....	141
Table E.2:	ZA Dry Q MC (%) record for stack 7; 30mm x 87mm green dimensions .....	144
Table F.1:	Average of six MC values on each board of stack 7 at $\frac{1}{3}$ -depth, as seen from the end of the stack (Face A).....	148
Table F.2:	Standard deviation of six MC values on each board of stack 7 at $\frac{1}{3}$ -depth, as seen from the end of the stack (Face A) .....	149

Table F.3: Average of six MC values on each board of stack 2 at $\frac{1}{3}$ -depth, as seen from the end of the stack (Face A).....	149
Table F.4: Standard deviation of six MC values on each board of stack 2 at $\frac{1}{3}$ -depth, as seen from the end of the stack (Face A) .....	149
Table F.5: Average of six MG values on each board of stack 7, as seen from the end of the stack (Face A).....	150
Table F.6: Standard deviation of six MG values on each board of stack 7, as seen from the end of the stack (Face A).....	150
Table F.7: Average of six MG values on each board of stack 2, as seen from the end of the stack (Face A) .....	151
Table F.8: Standard deviation of six MG values on each board of stack 2, as seen from the end of the stack (Face A).....	151
Table F.9: Average of five MC values on all combinations of position and location of stack 7 at $\frac{1}{3}$ depth, as seen from the top of the stack (Face B) .....	152
Table F.10: Standard deviation of five MC values on all combinations of position and location of stack 7 at $\frac{1}{3}$ depth, as seen from the top of the stack (Face B) .....	152
Table F.11: Average of five MC values on all combinations of position and location of stack 2 at $\frac{1}{3}$ depth, as seen from the top of the stack (Face B) .....	152
Table F.12: Standard deviation of five MC values on all combinations of position and location of stack 2 at $\frac{1}{3}$ depth, as seen from the top of the stack (Face B) .....	153
Table F.13: Average of five MG values on all combinations of position and location of stack 7, as seen from the top of the stack (Face B) .....	153
Table F.14: Standard deviation of five MG values on all combinations of position and location of stack 7, as seen from the top of the stack (Face B).....	153
Table F.15: Average of five MG values on all combinations of position and location of stack 2, as seen from the top of the stack (Face B) .....	154
Table F.16: Standard deviation of five MG values on all combinations of position and location of stack 2, as seen from the top of the stack (Face B).....	154
Table F.17: Average of four MC values on all locations of the five identified layers of stack 7 at $\frac{1}{3}$ depth, as seen through the stickers from the back of the load (Face C) .....	155
Table F.18: Standard deviation of four MC values on all locations of the five identified layers of stack 7 at $\frac{1}{3}$ depth, as seen through the stickers from the back of the load (Face C) .....	156
Table F.19: Average of four MC values on all locations of the five identified layers of stack 2 at $\frac{1}{3}$ depth, as seen through the stickers from the plenum (Face C) .....	156
Table F.20: Standard deviation of four MC values on all locations of the five identified layers of stack 2 at $\frac{1}{3}$ depth, as seen through the stickers from the plenum (Face C) .....	156



Table F.21: Average of four MG values on all locations of the five identified layers of stack 7, as seen through the stickers from the back of the load (Face C)..... 157

Table F.22: Standard deviation of four MG values on all locations of the five identified layers of stack 7, as seen through the stickers from the back of the load (Face C)..... 157

Table F.23: Average of four MG values on all locations of the five identified layers of stack 2, as seen through the stickers from the plenum (Face C)..... 158

Table F.24: Standard deviation of four MG values on all locations of the five identified layers of stack 7, as seen through the stickers from the plenum (Face C) ..... 158

## NOMENCLATURE

### Variables

AH	Absolute humidity	[g water per kg dry air]
$\Delta$ AH	Difference in absolute humidity	[g water per kg dry air]
CH	Case-hardening measurement minus the 10mm pin	[mm]
d	Case-hardening contribution of each test slice = $\frac{1}{2} \times \text{CH}$	[mm]
D	diffusion coefficient	[m/s <sup>2</sup> ]
DP	Dew-point	[°C]
$\Delta$ DP	Difference between the temperature and the dew-point	[°C]
EMC	Equilibrium moisture content	[%]
FSP	Fibre saturation point	[%]
m	Mass	[kg or g]
MC	Moisture content of the timber	[%]
MG	Moisture gradient	[%]
OD	Oven-dry mass	[g]
r	The correlation coefficient between outcomes and their predictors.	
read	Case-hardening measurement including the 10mm pin	[mm]
RH	Relative humidity	[%]
R <sup>2</sup>	Coefficient of determination between a trend-line and actual data.	
T	Temperature	[°C]
$\Delta$ T	Difference in temperature	[°C]
TDAL	Temperature drop across the load	[°C]
TRAL	Temperature rise across the load	[°C]

### Subscripts

$\frac{1}{6}$	Measurement at one-sixth thickness
$\frac{1}{3}$	Measurement at one-third thickness
$\frac{1}{2}$	Measurement at half thickness
d	Dry bulb
day	Daily average over the 130 day drying run
External	Outside the kiln
Jact	Jacket
Load	Measurement across the load
Load In	Measurement at the air inlet to the load

max	Maximum
min	Minimum
Sect1	Section 1 of the sample board
Sect2	Section 2 of the sample board
SB	Sample board
SB Green	Sample board still green before drying
t	Target
time	Average at a specific time of the day
w	Wet bulb
75	as measured over the pins 75mm apart
100	as measured over the pins 100mm apart

## Abbreviations and symbols

A	Parallel to the face of the stack as indicated by A
B	Parallel to the face of the stack as indicated by B
C	Parallel to the face of the stack as indicated by C
Ch	Channel
DB	Dry bulb thermocouple
DQ	Drying quality
SB	Sample board
WB	Wet bulb thermocouple

# **1 GENERAL INTRODUCTION**

Energy, mostly thermal energy, is required to dry timber. The use of solar energy as a thermal energy source for the drying of wood has been studied since the beginning of the last century and utilised around the globe in various designs of kilns (Bauer, 2003). The main objective of solar drying is to utilise the advantages of both air-drying and kiln drying. Air-drying exploits the free heat available from sun radiation. The disadvantages of this system include that it is slow and that little or no drying occurs during the night-time hours. Drying control is also hampered by varying climatic conditions. It is further difficult to control drying defects (Cech & Pfaff, 1980).

## **1.1 Overview of the study**

Solar drying has been found to be more effective than air-drying for small operations where the magnitude of the operation does not justify the capital layout for a conventional kiln. It is also used where conventional sources of energy for conventional kilns are not available (Banks, 1969).

After numerous efforts through the years, it has generally been found that, irrespective of design or locality, solar drying is faster, can achieve lower moisture content (MC) values, and produce less degradation than air-drying (Banks, 1969). The high cost of installing and running a conventional kiln thus makes solar drying a viable alternative, especially for smaller operations.

Various solar kiln designs have been developed. This thesis was based on the research conducted on a solar kiln with a unique way of humidity control. It is a “greenhouse-type” solar kiln which operates on the principle that the air passing through the load is heated inside the kiln. The temperature is not controlled, but relies purely on solar heat collection of materials inside the kiln. Humidity control, or rather auto-regulation, is achieved by a process of natural dehumidification at night. This type of humidity control is extremely simple as cooler night temperatures are a certainty, with no control system or human intervention necessary. This study investigated the results in terms of drying defects and the within and between board MC variations. The study will proceed to investigate the kiln design and auto-operation, since it relies entirely on climatic input.

The natural dehumidification principle of this solar kiln was first described by Lumley & Choong (1979). The first practical documentation of a solar kiln that operated on this principle was an anonymous brochure by the Solar Kiln Company, Inc, located in Mazomanie, Wisconsin, USA. Apparently, the initial design used a greenhouse-type kiln using traditional vents to control humidity (Steinmann, personal communication, 28 February 2001). A double plastic skin was used for better insulation. The skin was kept inflated using a small centrifugal fan, with feedback valves allowing

air back into the kiln. It was found that water collected at the bottom, in-between the two plastic skins. The water was then drained through small weeping holes to the outside. The vapour from the wood condensed during the night, with the condensate forming on the inside of the outer plastic skin. In the initial research, it was found that refractory timbers dried at best when the kiln was air tight and this natural dehumidification proved that the vents became obsolete since there was no control system necessary to remove humid air (Steinmann, personal communication, 28 February 2001). Without vents, there was no transfer of air between the inside and outside of the kiln. Conditions inside the kiln were merely dependent on the natural heat collection by day and natural dehumidification by night (Steinmann, personal communication, 28 February 2001).

A solar kiln operating in a similar manner to that discussed by Steinmann, (personal communication, 28 February 2001) has been developed by Steinmann and the researcher of this study. This kiln is situated at Saasveld, 5 km from George in the Southern Cape Region of the Western Cape, South Africa. For the purpose of this study, the kiln shall be called the “Saasveld solar kiln”. This solar kiln has a capacity of 20.1m<sup>3</sup>. During the period of June 2000 to February 2009, the researcher conducted a number of high density hardwood drying runs which produced timber dried to an excellent quality. Simpson (1991) identified the characteristics of timber having dried to an excellent quality as:

- i. having a narrow moisture content range to limit shrinkage and swelling,
- ii. stress-free timber to machine more efficiently,
- iii. free of any form of warp and
- iv. without cracks or checks.

The purpose here was to investigate the reason for this good drying quality and whether the operation at the Saasveld solar kiln can be improved upon.

## **1.2 Objectives of the research**

The objective of this work was to study the operation and performance of the Saasveld solar kiln when drying high density hardwoods by utilising natural dehumidification. The first aim was to assess the drying quality of the wood by means of a recognised method after it has been dried in the Saasveld solar kiln. The results would indicate whether the claims of the good drying quality were valid. The next step was to demonstrate the operation of this solar hardwood drying kiln which utilises natural dehumidification. Temperature and humidity data was continuously collected at five positions inside and outside the kiln while the moisture content of the timber (MC) was measured continuously.

This data was processed to investigate the drying conditions inside the kiln, the timber drying rate and the amount of dehumidification occurring during the full 24-hour day at different stages of drying. The internal kiln conditions were also compared with the external conditions to investigate the degree to which the kiln protected timber against extreme climatic conditions. It must be stressed that the reason for the collection of temperature and humidity data was to study the kiln operation and not to control the atmospheric conditions inside the kiln.

The drying conditions in the Saasveld solar kiln were compared with other recognised drying schedules. The processed data will clarify the operation of this solar kiln and will examine solutions to improve the kiln layout and operation.

### 1.3 Definition of concepts

**Dry bulb temperature ( $T_d$ ):** It is the temperature of the air (Van Wylen & Sonntag, 1985).

**Wet bulb temperature ( $T_w$ ):** It is the temperature of the air as measured by a thermometer where the bulb is covered with a cotton wick that is kept saturated with water. It is approximately equal to the adiabatic saturation temperature (Van Wylen & Sonntag, 1985). Unlike dry bulb temperature, wet bulb temperature is an indication of the amount of moisture in the air.

**Humidity:** Humidity is a measurement of the water in the air. Humidity can be expressed in various ways:

- Relative humidity (RH):
- Absolute humidity (AH)
- Equilibrium moisture content (EMC)
- Dew-point temperature (DP)

**Relative humidity:** The ratio of the mole fraction of water vapour in moist air to the mole fraction of water vapour in saturated air at the same pressure and temperature, expressed as a percentage (Stoecker & Jones, 1982).

**Absolute humidity:** It is the ratio of the mass of water vapour to the mass of dry air in an air-water vapour mixture (Van Wylen & Sonntag, 1985). Absolute humidity is also known as the humidity ratio and is usually expressed as g water per kg dry air.

**Equilibrium moisture content (EMC):** It is a balanced state of moisture content attained by the wood throughout its entire dimension when exposed for a sufficiently long period to a specific and

constant air temperature and relative humidity (Koch, 1972). Upon attaining equilibrium moisture content (EMC), the wood neither gains nor loses moisture, nor does any change in moisture content occur within different parts of the wood piece, as the moisture content is the same value throughout the wood piece (Panshin & de Zeeuw, 1980). The term EMC is also used to describe an air property, consisting of a specific combination of temperature and relative humidity.

**Condensation:** The process whereby a fluid in a gas phase changes into a liquid. If the temperature of a surface is below the saturation temperature of a condensable vapour, condensate will form on the surface and under the action of gravity it will flow down the surface (Holman, 1992). In the context of this study, it is the change from water vapour into liquid water by cooling the vapour below its saturation temperature.

**Dew-point temperature:** The temperature, to which humid air must be cooled, under constant pressure, for saturation to occur (Holman, 1992). The saturation is recognised whereby some vapour in an enclosed air-vapour mixture will condense to liquid, called dew.

**Natural dehumidification:** It is the process whereby the water vapour in the air (humidity) is reduced by means of the condensation of the water vapour in contact with a surface below the dew-point temperature of the air. The surface is naturally cooled by cold exterior temperatures. This principle was phrased as “condensation” and only briefly described in the literature available (Lumley and Choong, 1979). Condensation is also a process in electrical dehumidifiers where the condensing surface is the evaporator coil of a refrigeration cycle (Stoecker & Jones, 1982). This technology is used in timber drying kilns and is known as a dehumidifier kiln (Simpson, 1991). The term “natural dehumidification” was created to prevent confusion.

**Collector ratio:** It is the ratio of the radiation surface to timber volume, also expressed as the wood volume in  $\text{m}^3$  / collector area in  $\text{m}^2$  (Steinmann, 1989).

**Fibre saturation point (FSP):** The moisture content at which the cell walls are completely saturated with bound water, but all the free water is gone from the cell cavities (Koch, 1972).

**Bergwind:** It is a well known warm dry wind which occurs during mid-autumn to mid-spring. This wind results in severe drying defects like end cracks, surface cracks and even cell collapse.

**Refractory timber species:** Species that is difficult to dry and especially prone to check formation or cell or collapse readily (Australian Hardwood Drying Best Practice Manuel, 2010)

**ZA Dry Q:** It is a South African system to ensure that the dried quality of softwood complies as closely as possible with the specifications of a customer. The purpose was not to try to achieve the specification, but to assess the drying quality with a recognised assessment technique. (SALMA, 2003a)

## **2 LITERATURE REVIEW**

Since the 1960's, much research and development has been conducted into the use of solar kilns for drying timber. A recent update of the 31 different designs of research and industrial solar kilns has been documented by Wengert (2010). Two categories distinguish these kilns, namely: solar kilns with external collectors and greenhouse type solar kilns

According to Banks (1969) solar kilns have been proved to have the following advantages:

- 1) Solar drying is faster than air-drying.
- 2) Timber can be dried to moisture content (MC) lower than 10 per cent (%). The MC is not limited to the equilibrium moisture content (EMC) during air-drying.
- 3) The drying quality is better than air-drying, provided that there is a good control system.
- 4) The drying costs are competitive.

A major drawback is the lower operating temperatures that can be attained by solar kilns, compared to commercial kilns. However, the successful drying of high density hardwoods is achieved by low temperatures above fibre saturation point (Vermaas, 1995) and hence the potential use of solar kilns for this purpose.

This literature review covers drying using solar heat. The drying of timber in direct radiation, or greenhouse type solar kilns is examined although humidity control by venting is normally used. Studies that explored solar drying in combination with electrical dehumidifiers were done, although it is not a popular method. A literature study was conducted on the general drying of hardwoods, specifically the drying of high density hardwoods and *Eucalyptus* species. The chapter is concluded by looking at a method to do a drying quality assessment.

### **2.1 Solar drying by natural dehumidification**

Natural dehumidification is the process whereby the water vapour in the air (humidity) is reduced by means of the condensation of the water vapour in contact with a surface below the dew-point



temperature of the air. The surface is naturally cooled by cold exterior temperatures. This principle was phrased as “condensation” and only briefly described in the literature available. Condensation is also a process in electrical dehumidifiers where the condensing surface is the evaporator coil of a refrigeration cycle (Stoecker & Jones, 1982). This technology is used in timber drying kilns and is known as a dehumidifier kiln (Simpson, 1991). The term “natural dehumidification” was created to prevent confusion.

Although Wengert (2010) described the double plastic or glazing layers to reduce conduction heat losses, none of the 31 kilns as described by him use the humidity control method of natural dehumidification at night which is in use at the Saasveld solar kiln. However, it is mentioned by Wengert (2010) that inadequate venting may result in very high humidity which may result in slow drying.

Sattar (1993) described a number of solar kilns, one of which was mentioned as a “self-dehumidifier”. This kiln is described as a “Solar dry wood kiln” by the Solar Kiln Company (Solar Kiln Company, 1983).

Lumley and Choong (1979) performed an economical comparison between two kiln designs, based primarily on the shape of two collectors: a greenhouse type solar heat collector and an enclosed drying chamber with an external solar heat collector. Greenhouse type kilns have the advantage of being inexpensive, are easy to design and build, and simple to operate; however tend to have radical diurnal temperature fluctuations, due to substantial night losses (Lumley and Choong, 1979). These kilns proved to be successful in developing countries, but have a major drawback of practical size limitations. In such structures the timber volume increases faster than the surface area needed to collect the necessary solar energy. Further, the diurnal temperature fluctuations in greenhouse type solar kilns create the problem that venting at night brings greater heat losses.

Lumley and Choong (1979) mentioned the possibility of using a greenhouse type solar kiln, with natural self-dehumidification. The possibility of water removal by condensation could eliminate the need for venting and have the following advantages:

- heat loss during venting could be eliminated
- part of the heat of evaporation may be recovered
- reduction in heat losses could allow heat build-up in the structure so final drying could take place at higher temperatures

Apart from this publication, there are no other descriptions or studies of this natural dehumidification type kiln.

Steinmann (1989) investigated the solar kiln drying of wood. Although *Pinus radiata* was dried in a solar kiln with a collector and vents, there were important conclusions made that can be compared to this study. The experimental solar kiln discussed by Steinmann experienced a few short periods of natural condensation. The possibility of drying refractory hardwoods by this means might prove effective, since they require slow drying. The author referred to the simplicity of this method; however, it could result in a slow drying rate that cannot be optimised.

## **2.2 Direct radiation solar kilns**

Apart from the publication by Lumley and Choong (1981), all the direct radiation or greenhouse type solar kilns discussed in literature managed humidity control by means of venting humid air via venting flaps with venting fans. These vents were opened with micro-processors or programmable logic controllers (PLC's).

Bauer (2003) described a schedule for a biomass furnace-assisted greenhouse-type solar dryer with a 100 - 240m<sup>3</sup> stacking capacity. A microprocessor with six input parameters and seven output parameters controlled the air temperatures and the humidity via supplemental heat exchangers, ventilators and water sprays. The 27mm thick boards dried in 27 days.

The performance of an industrial solar kiln, at Boral Timber in New South Wales, Australia, with a 120m<sup>3</sup> stacking capacity, is described by Haque and Langrish (2006) to dry 43mm thick *Eucalyptus pilularis*. The authors used a technique of intermittent drying. This will be further discussed in Section 4.4.4.

## **2.3 Solar dehumidifier kilns**

Electrical dehumidifiers are described in various publications from 1960 to 1980. An example is described by Chen, Helmer, Rosen, and Barton (1982). They seem to have become unpopular, probably due to the long operational hours and the resulting drying cost per unit.

## **2.4 The drying of hardwoods**

Timber drying is normally performed either by means of natural air-drying or by artificial drying in kilns. Three control parameters, air temperature, air humidity and the air movement over the timber influence the drying time and quality of timber, whether drying occurs naturally or in kilns. The

incorrect use of one of these parameters will result in slow drying or in drying defects. It is impossible to control these parameters with air-drying with the result that kiln drying became popular, despite its high capital costs. The development of the modern kiln aimed at optimising the pay-back of the capital cost (Lumley and Choong, 1981). The effect is that the drying time must be minimised against a specified drying quality - these are often two indirectly related outputs that need to be compromised. The result is the development of schedules for different timber dimensions and species. Most schedules consist of a variation in air temperature and humidity at various stages of the drying process. The air velocity is seldom used in a schedule; if so, it will be for softwood schedules (Culpepper, 1990).

Drying stresses are related to the difference between the surface and interior MC's, or moisture gradient (MG). The development of drying stresses is a limiting factor for the selection of a drying schedule. Kiln schedules must be developed so that drying stresses remain smaller than the timber strength, to prevent any cracks and collapse in the timber (Cech & Pfaff, 1980). Timber becomes stronger as the MC is reduced, and to a lesser extent, becomes weaker as the temperature increases (Simpson, 1981). Temperatures are selected to increase the drying rate, but must be low enough not only to prevent the abovementioned formation of cracks, but also cell collapse (Vermaas, 1995) and drying stains (Cech & Pfaff, 1980). These drying defects are related to the MC of the timber. As the timber dries, and becomes stronger, it can be subjected to higher temperatures and a lower humidity (Simpson, 1991). The MG, and therefore, the stresses are set up by the drying rate and is a result of the kiln temperature, humidity, the air velocity over the timber and the timber specie characteristics (Bauer, 2003).

Most drying schedules start with a period of medium temperatures and a high humidity. The idea is to have a 100 per cent (%) relative humidity until the wood core reaches the wet bulb temperature setting. Once this point has been reached, the humidity drops gradually until fibre saturation point (FSP) has been reached, while the temperature remains constant. Thereafter, the temperature will gradually be raised as the timber is dried further, while the humidity will remain low. When the desired MC has been reached, the timber will be subjected to an equalising period of higher humidity and the same final drying temperature. The equalising period aims at having an equilibrium moisture content (EMC) of about two per cent (%) lower than the desired final MC. In order to relieve the residual drying stresses, this period is followed by a conditioning phase at a slightly higher temperature and a high humidity (an EMC of 2-3 per cent (%) higher than the desired final MC) (Simpson, 1991).

#### 2.4.1 Problems when drying high density hardwoods

The anatomical structure of hardwoods makes it prone to drying defects, especially if the wood has a high density, resulting in defects due to excessive shrinkage. These defects include surface and end checks, internal checks (honeycomb), cell collapse, case-hardening and a large MC variation (Vermaas, 1995).

Density is directly related to cell wall thickness. The higher the density of the wood, the larger is the mass of bound water per volume of wood. Therefore, a higher density wood will have more bound water removed from it and the shrinkage will thus be more. Most drying defects are connected to shrinkage (Cech & Pfaff, 1980).

Hardwoods differ from softwoods in the sense that they are usually denser. Furthermore they have characteristics of slow drying due to an impermeable structure. This impermeable structure is the result of thick cell walls, small cell lumens, small pit openings, aspirated border pits, tylosis in some timbers and an accumulation of extractives in the heartwood (Koch, 1972). This wood structure makes the drying of hardwoods extremely slow. The danger exists that the timber dryer can create conditions that are too harsh for drying. This action may dry the surfaces but not the core of the wood resulting in steep MGs which cause drying stresses to develop (Cech & Pfaff, 1980).

The MG is influenced by the speed at which the water vapour in the wood can be transferred to the surface. The transfusion of bound water is attained by diffusion. The diffusion coefficient is bigger for high density hardwoods. Haque and Langrish (2006) described the drying of 43mm thick *Eucalyptus pilularis* in a solar kiln. Diffusion is seen as the general mechanism for the drying of impermeable hardwoods such as *Eucalyptus*. The authors cited Doe, Oliver & Booker (1994), who gave an equation for the diffusion coefficient of bound water transport within Australian hardwoods:

$$D = D_r e^{-D_E/T}$$

Where,

D = diffusion coefficient, m/s<sup>2</sup>

D<sub>r</sub> = reference diffusion coefficient = 1.15 x 10<sup>-5</sup> m/s<sup>2</sup>

D<sub>E</sub> = activation energy = 3730 K

T = temperature of medium, K

(Haque & Langrish, 2006)

The importance of temperature on the rate of diffusion will be discussed in Section 4.3.4.2.

If the drying stress is greater than the timber strength, then cracks, or checks, in the timber can be expected. Checks are in the form of surface checks, internal checks and end checks. These checks will form if tensile stresses in a specific region of the board are higher than the tensile strength across the grain. This tensile strength across the grain is lowest at the intersection of ray and longitudinal cells. Tangentially cut boards are renowned for formation of these checks, as the higher tangential shrinkage will cause a greater total shrinkage across the width of the board, especially on the side furthest from the pith. The rays stretch across the surface causing a weak plane across this tangentially aligned width of the board (Cech and Pfaff, 1980). Hardwoods usually have wider rays, which create a weak plane in the timber. Checks usually propagate along these rays (Cech & Pfaff, 1980).

Surface checks form during the initial drying period when the surface layers dry to below the fibre saturation point of timber. The surface layers shrink against the rest of the timber core, which is still above fibre saturation point and has not shrunk yet. When the surface layers are exposed to low EMCs, the shrinking surface layers result in severe tension stresses, which culminate in surface checks (Simpson, 1991).

Surface checks are associated with knots where there is grain deviation around the knot. The grain deviation will result in fast evaporation in the areas where the grain exits the surface. Timber density is also higher at knots, resulting in bigger shrinkage and, consequently, more surface checks (Koch, 1972).

Internal checks form when high tensile stresses, owing to excessive case-hardening, are imposed on the core of planks in the final drying stages. End checks propagate through the same mechanisms as surface and internal checks. The problem is exacerbated by growth stresses, especially found in *Eucalyptus*. This necessitates slow and careful drying of high density hardwoods, for which the Saasveld solar kiln can be utilised.

#### 2.4.2 Eucalyptus drying

Vermaas (1995) described the drying of *Eucalyptus* for quality with reference to the material characteristics, pre-drying treatments, drying methods, schedules and optimisation of drying quality. Cell collapse is often aggravated by the thin cell walls of early wood or young trees that contain a big proportion juvenile wood (Vermaas, 1995). *Eucalyptus* timber is prone to end split during handling and end checks are difficult to avoid (Vermaas, 1995).

Various other authors examined *Eucalyptus* drying schedules and general drying in solar kilns: Vermaas (1987), Simpson (1980), Langrish et al. (1992), Neumann & Saavedra (1991), Stöhr & Mackay (1983), Bauer (2003) and Haque and Langrish (2006). These schedules are discussed in Section 4.4.

In order to dry a common globally utilised timber, it was decided to dry the high density local grown karri gum, *Eucalyptus diversicolor*. Karri gum is known as “moderate difficult to difficult to dry”, with major defects of warp, moderate to severe surface checking, moderate honey-combing and collapse and moderate end-splitting (The Wood Explorer Database, 2010). Partial air-drying before kiln-drying is recommended. Kiln drying from green should be done at low temperatures and high humidity (The Wood Explorer Database, 2010). Karri gum has an average air-density of between 849-961 kg/m<sup>3</sup> (Banks, Schoeman & Otto, 1977).

## 2.5 Specific heat capacity of timber

In conventional kiln drying, the temperature drop across the load (TDAL) denotes the air temperature change as it passes over the timber. In conventional drying, the timber load reaches a temperature equal to the air wet bulb within the first few hours. The timber acts as a wet bulb wick as there is evaporation of free water from the timber surface. The wood temperature will gradually drift towards the dry bulb temperature as the evaporative surface, or wet line, recedes into the timber (Culpepper, 1990). Apart from schedule changes, there are no fluctuating temperatures in conventional kilns as the temperature is usually kept at a specified level by a controller. In the Saasveld solar kiln however, diurnal temperature fluctuations caused the kiln to heat and cool on a daily basis. The timber will heat up during the day and cool off during the night. The alternating heating and cooling of the timber (heat transfer) is influenced by the specific heat capacity of the wood. The specific heat capacity depends mostly on the moisture content and temperature of the wood, but is practically independent on the specie or density (Simpson, 1991). The relationship with the MC is evident from the specific heat capacity equation, in BTU/lb. °F, by Simpson (1991):

$$\text{Specific heat capacity} = \frac{0.25+0.0006T+m}{1+m} \text{ (BTU/lb. °F)}$$

Where,

T = Temperature, °F

m = moisture content as a fraction =  $\frac{MC}{100}$

(Simpson, 1991)

## **2.6 Drying quality assessment**

Drying quality in this work was assessed according the ZA Dry Q method. The ZA Dry Q is a South African system to ensure that the dried quality of softwood complies as closely as possible with the specifications by a customer. It is a “patented trademark of a kiln drying management system, which assures the customer that the final dried products comply with the customer’s specifications” (SALMA, 2003a; page 2). A board of technical experts and sawmill representatives manage this system. The board operated under the auspices of the South African Lumber Millers Association (SALMA), now Sawmilling South Africa (SSA). The ZA DRY Q Assurance System provides the possibility to produce to customers’ desired quality standards. To obtain a ZA Dry Q certificate, the board audits a lumber dryer on drying defects and MC variation. If a lumber dryer passes this audit, then customers know that the drying facility can dry timber to a tight defect and within MC specification. The lumber dryer and the customer can now negotiate the required drying quality on the basis of the ZA Dry Q Audit procedure. The audit serves as a basis for quality control purposes by both the lumber drier and buyer (SALMA, 2003a). Although the ZA Dry Q mark was designed for the management of softwood, the drying quality work instructions is a very good technique to assess the drying quality of any timber.

## **3 MATERIAL AND METHODS**

Various solar kiln designs have been used in the past century. The operation of the Saasveld solar kiln is unique in that evaporated wood moisture will be condensed from the air instead of being vented. Little research has been done on this type of solar kiln. The aim of this work was to study the exact behaviour of the kiln when drying a load of high density hardwood. This was done by positioning temperature and humidity sensors at various critical locations inside and outside the solar kiln. The drying quality was measured to evaluate the effectiveness of the kiln.

### **3.1 Study site**

The study site was at Saasveld, the George Campus of the Nelson Mandela Metropolitan University (NMMU). George is situated in the Southern Cape Region of the Western Cape, South Africa. The global coordinates of the solar kiln at Saasveld were S 33° 58’; E 22° 32’.

### 3.2 Layout and geometry of the Saasveld solar kiln

The Saasveld solar kiln was a modified greenhouse, with an arrangement to facilitate airflow through the stacks.



Figure 3.1: The Saasveld solar kiln

An isometric view of the Saasveld solar kiln can be seen in Figure 3.1. The solar kiln was 9.8m long, 8m wide, with an apex height of 3.5m. The kiln centre line was oriented in a north-south direction. The main cover that stretched over the kiln consisted of an inflated double layer of polyethylene plastic which formed an air jacket. The ends had a single plastic layer. The southern end had a double loading door, and the northern end, at the plenum chamber, had a single entrance door.

The 180 $\mu$ m thick poly-ethylene plastic sheets were attached to the concrete base and steel structure with standard greenhouse clamping rails.

The curved steel ribs that shaped the kiln outline were 2m apart from centre-to-centre. The second last rib formed the position of the fan frame and plenum wall. A transparent plastic plenum wall underneath the second last rib divided the greenhouse tunnel in unequal parts (see Figure 3.2).



The smaller part formed the plenum chamber and the larger main chamber contained the timber stacks.

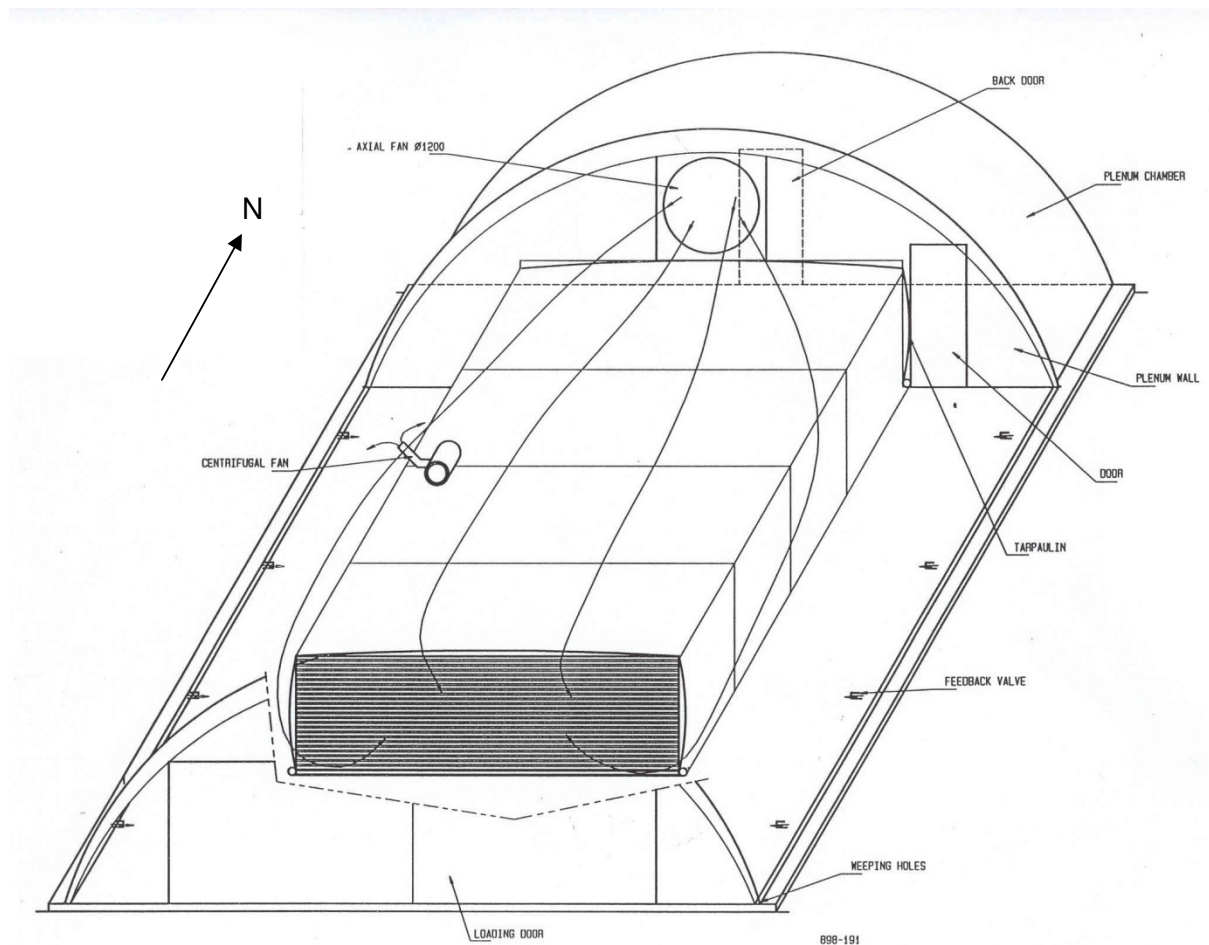


Figure 3.2: Schematic isometric view of the Saasveld solar kiln (Steinmann, 2001)

The plenum wall supported the main fan which circulated the air through the stack. The 380V three phase 3 kW axial flow fan, diameter of 800mm, was situated on top of a steel frame in the plenum wall. The steel frame had an opening which was equal in size to the stack cross-section. From Figure 3.2 it can be seen that the fan created a negative pressure inside the plenum chamber. This will suck air through the stacks and blow it back into the main chamber over the stacks. Air bypass and air short circuiting was prevented by covering all the stacks on the sides and the top with a tarpaulin. The tarpaulin was fixed to the frame, which formed part of the plenum wall. The only openings to the load are at the air inlet side, south, and the plenum chamber, north (see Figure 3.3).



Figure 3.3: Tarpaulin covers the sides and top of the stacks

The only heat source was the solar heat gained from the sun. The 125mm thick 25 MPa strength concrete floor was painted black to increase solar absorbency. The floor surface acted as a heat store.

### 3.3 Humidity control

Kiln air from the main chamber was blown into a 400mm diameter manifold with a 0.15kW radial fan. The fan is driven by a 230V single phase motor. From the pressurised manifold, air enters the double-layered plastic air jacket of the main cover via four 75mm diameter flexible hoses. This kept this air jacket inflated. The blower is situated in the middle and top of the kiln chamber and can be seen in Figure 3.4.



Figure 3.4: Air inlet manifold delivering air into the double skin (jacket)

The air exited the air jacket by feedback valves through which the air re-entered the kiln chamber. Eight feedback valves (see Figure 3.5) were equally spaced inside the kiln on both sides (east and west), 300 mm from the kiln floor. Each feedback valve, with a diameter of 75mm, has a manual setting to control the amount of feedback. The valves in the centre of the kiln were partly closed to release less air. This was done to ensure an even air movement over the entire inflated double plastic layer.

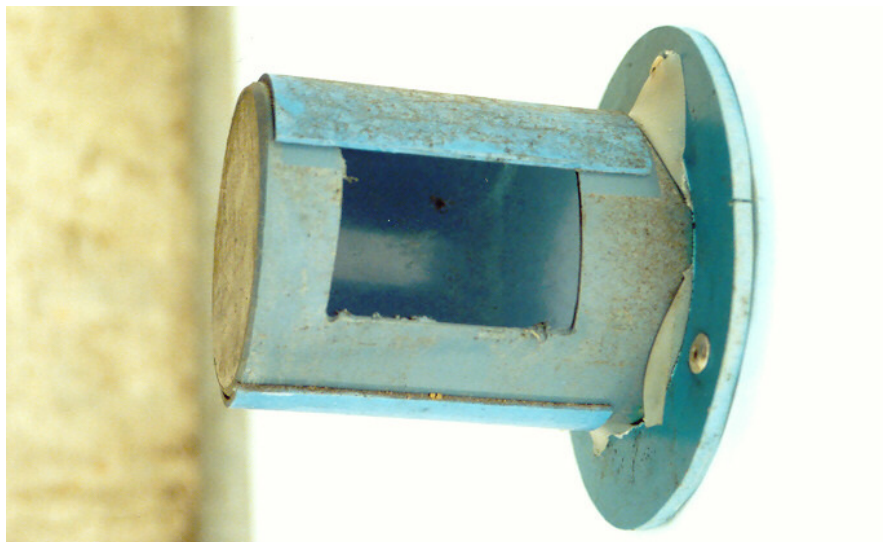


Figure 3.5: Feedback valve for air to exit the jacket

Humidity control was achieved by a process of natural dehumidification at night. As the air from the main kiln chamber was circulated through the inflated double plastic layer, the air came in contact

with the outer plastic sheet. If the temperature of this sheet was less than the dew-point of the air in the solar kiln, then condensation will occur on the inside of the outer sheet. The condensate will flow down and collect at the bottom of the inflated air pocket. The condensate was released via small weeping holes, with a diameter of 0.8mm to 0.9 mm (Figure 3.6). The weeping holes were punched with a straightened paper clip.

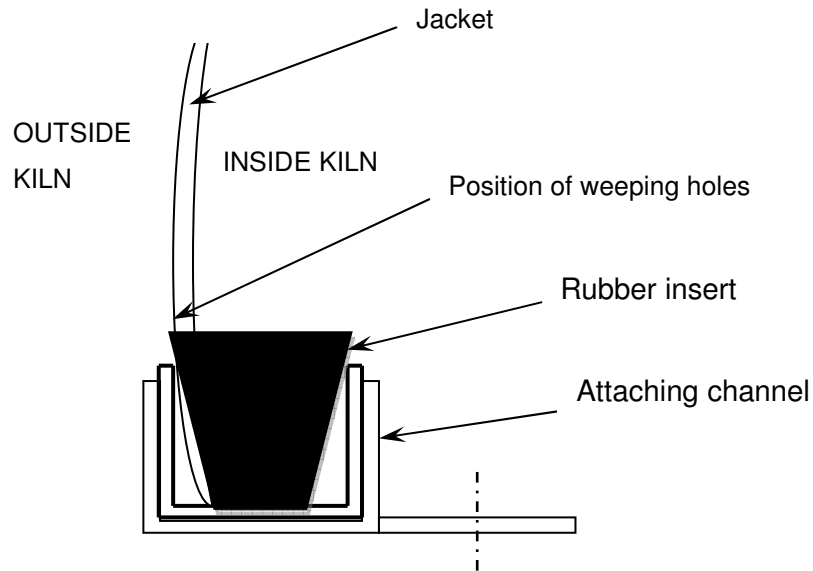


Figure 3.6: Position of weeping holes above the fixing rails

More technical details can be viewed in Annexure A.

### 3.4 Expected climatic conditions inside the Saasveld solar kiln

Qualitative results from many previous performed drying runs in the Saasveld solar kiln, on a range of timber species, were available. The behaviour of the kiln was thus known (Müller, 2008). It was anticipated that the enclosed kiln would protect timber against harsh climatic Bergwind conditions characteristic of a high temperature and low humidity environment.

It was expected that the temperature would consistently be higher inside the kiln than outside. The initial temperature difference should be lower as the higher evaporation rate, due to the availability of free water, will cool the air. The greater temperature difference should occur more towards the end of the drying process (Simpson, 1991).

The humidity inside the kiln is likely to start at a comparatively low AH and reach saturated conditions of 100 per cent (%) relative humidity in the evening as condensation takes place. Since there is no venting of the air-vapour mixture and condensation is expected at night, the belief is that the AH will be very high, especially in the afternoons (Müller, 2008)

In this study, the expectation is that the timber will dry during the day and the vapour will condense during the night, although the exact timing of these occurrences is unknown. It is expected that the night periods of no drying will act as an equalising period and stresses will be small as there will be few moisture gradients (Müller, 2008).

### **3.5 Timber species**

In order to dry a common globally utilised timber, it was decided to dry 20.1 m<sup>3</sup> green dimension, local grown karri gum, *Eucalyptus diversicolor*. The karri gum had an average air-density of 897kg/m<sup>3</sup>.

In preparation for this study, the gum trees, age 55 years, were harvested at the MTO Karatara Plantation. The trees grew in fire belts between pine plantations. No pruning was performed on the trees. The timber was cut by a Woodmizer Band Saw, in a cant cutting pattern. Since boxed heart splits are common with *Eucalyptus* species, it is standard procedure to remove a central square section containing the pith. In this case, a section of 90mm x 90mm was separated and discarded.

For this study, the timber, containing only heartwood, was randomly stacked.

### **3.6 Stacking**

Stacks were placed, as shown in Figure 3.7, in a two-by-four pattern, with the air passing through four stacks on its way to the plenum chamber. In the direction of the air flow, a space of 550mm separated the stacks. The last two stacks in the airflow direction were placed flush with the plenum wall. The space between the two rows of 4 stacks was baffled to prevent by-pass of air. Figures 3.7 and 3.8 indicate the baffling between stacks 1 and 2. It can be seen how these stacks were placed to fill the entire opening in the steel frame, which formed the plenum wall.



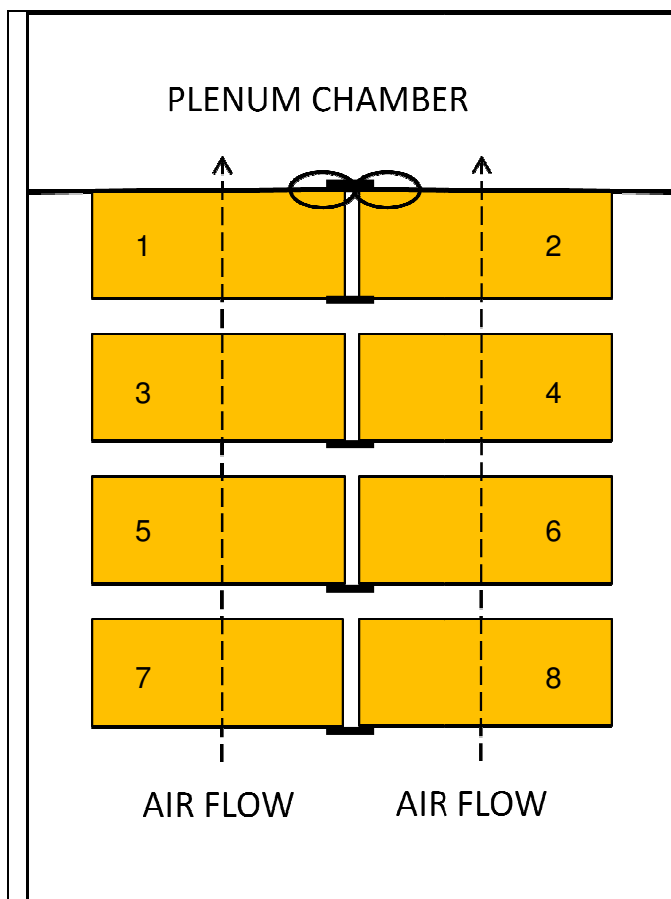


Figure 3.7: Position of the stacks, in brown, in the kiln. Baffles are shown by black lines. Numbers were assigned to each stack



Figure 3.8: Stacking was done to fill the steel frame opening of the plenum wall. Note the baffle between stacks 1 and 2

Overall individual stack dimensions were as follows:

- Length: 2.5m
- Width: 1.2m
- Height: 1.71m
- Layers of boards: 30
- Total timber volume (eight stacks): 20.1 m<sup>3</sup>

Board dimensions (green):

- Length: 2.5m
- Thickness: 30mm
- Width: 124mm or 87mm

Stacks were placed in the kiln and care was taken to align the stickers vertically. A sticker spacing of 400mm was maintained, with double stickers at the ends of the stacks. To prevent sticker stain,

the stickers were made from dried *Eucalyptus diversicolor*. Uniform sticker thickness was used in accordance with good stacking practises. The thickness of the stickers was 27mm, the width 30mm and the length 1.25m.

### 3.7 Sampling procedure

The sampling procedure was aimed at obtaining representative data of the moisture content during drying, the drying quality and accurate values of temperature and humidity.

#### 3.7.1 Sampling of moisture content during drying

Three full length moisture content (MC) sample boards per stack (24 in total) were placed on the air outlet side to the long side of each of the eight stacks, at the height of the 5<sup>th</sup>, 15<sup>th</sup> and 25<sup>th</sup> layer from the top of each stack.. The sample boards could be reached via the 550mm openings indicated in Figure 3.7. MC sample boards were randomly selected, although sample boards with big knots were rejected. Short stickers were wedged in the sticker openings and the MC sample boards were placed on top of these short stickers. The positioning of the short stickers and MC sample boards were placed on top of these short stickers. The positioning of the short stickers and MC sample boards can be seen in Figure 3.9, which represents a sectional side view of a stack. The MC sample boards were selected at intervals during the stacking procedure to ensure representation of the entire kiln load.

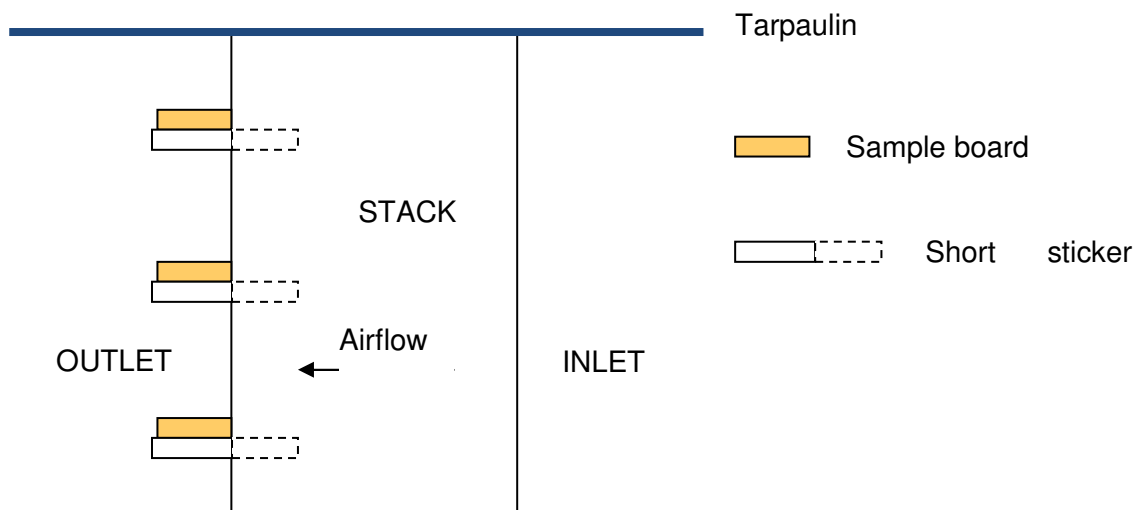


Figure 3.9: Sectional side-view of the MC sample boards in each of the eight stacks; sample boards rested on short stickers wedged in the sticker opening spaces

### 3.7.2 Sampling for drying quality

Drying quality analysis was performed on the basis of a ZA Dry Q Audit. The background is provided in Section 2.6. The sample size depended on the number of stacks in the kiln. Two of the eight stacks were assessed, selecting 20 drying quality (DQ) sample boards from each of stacks number 2 and 7 (see Figure 3.7 for the position of the stacks). DQ sample boards were identified according to the position within the stacks.

According to ZA Dry Q, five board layers must be selected, with the first layer being the second one from the top and last layer being the second from the bottom. The other three layers were evenly distributed over the stack height. Layers 2, 9, 16, 22 and 29 were selected, each yielding four sample boards. DQ sample boards were marked as indicated in Figure 3.10. The four boards in each layer were positioned as shown in Figure 3.10. For the purpose of this study, they will be called position 1, 2, 3 and 4. Moisture content and moisture gradient measurements were taken at six locations on each of the 20 drying quality (DQ) sample boards. The six locations along the 2.5m length of the board were at 0.25m, 0.65m, 1.05m, 1.45m, 1.85m and 2.25m from one end (note that for the purposes of this study it will be called the 0.25-location, 0.65-location, and so forth). Because the stack shown in Figure 3.10 is seen from the side of the load towards the middle of the kiln, the airflow in Stack 2 is from left to right. The airflow in Stack 7 is from right to left.

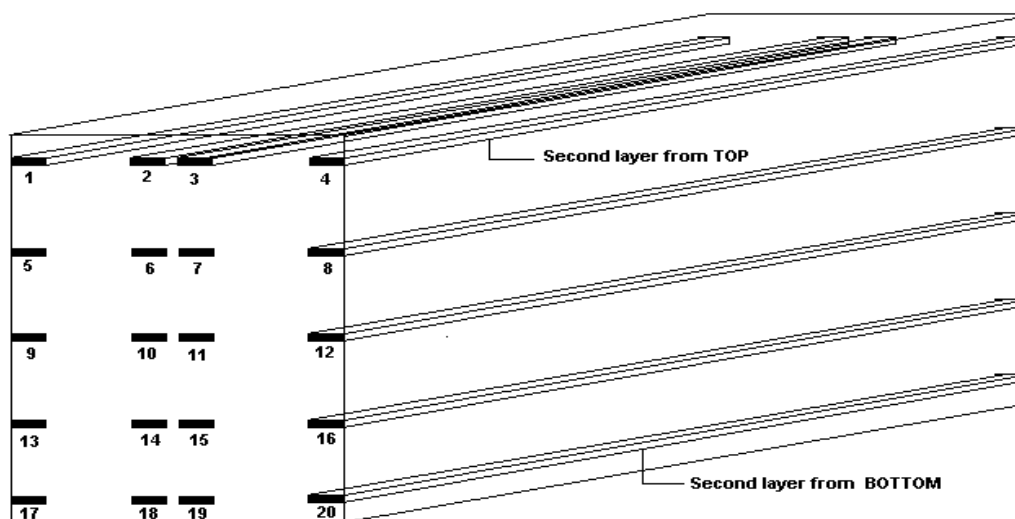


Figure 3.10: ZA Dry Q sample pattern of the stack as seen from the side of the load towards the middle of the kiln (SALMA, 2003b)

To test for surface checks, at least 15 of the 20 DQ sample boards in each stack had to be tangentially sawn.



No moisture readings or samples for testing were taken within 250mm of each end of a board. The area being measured for moisture and case-hardening was free of resinous wood, bark, knots, reaction wood, resin pockets and sticker marks. Both stacks were treated the same way.

### 3.7.3 Temperature and humidity sensors

Dry bulb ( $T_d$ ) and wet bulb ( $T_w$ ) temperatures were collected with nine type K-thermocouples at five positions in the kiln. Further details of the data collection methods can be seen in the discussion on “Positioning and management of sensors” (p.31).

## 3.8 Data collection methods

In this section the methods of collecting data on

- moisture content during drying,
- drying quality
- temperature and humidity values

are discussed.

Note that calibration procedures will be discussed in this section and not under “Results”.

### 3.8.1 Moisture content during drying

The initial or green MC of a sample board was determined from the average of two MC sections cut from each ends of the sample board. In doing so it was accepted that a linear moisture gradient existed along the length of the MC sample board.

The determination of the MC was based on oven dry mass:

$$\text{Moisture content} = \left\{ \frac{\text{wet mass} - \text{oven dry mass}}{\text{oven dry mass}} \right\} \times 100 \%$$

The procedure for preparing each of the 24 MC sample boards was as follows:

- Sample boards, and especially the MC sections, needed to be free from knots, pitch pockets, resin infiltration, wane and wavy grain, and therefore, the selected boards were inspected before cutting.
- a 20 mm section, at least 300mm from each end of a sample board was cut and loose sawdust and slivers were scraped off.
- The sections were weighed as soon as possible after cutting and marked according to the specific MC sample board,  $m_{sect1}$  and  $m_{sect2}$ .
- Both ends of the MC sample boards were end-coated to avoid end-drying. Rubber silicon sealant with an aluminium foil strip was used to cover the ends; this ensured that shorter boards would have the same drying characteristics as full length boards. (Refer to Figure 3.11).

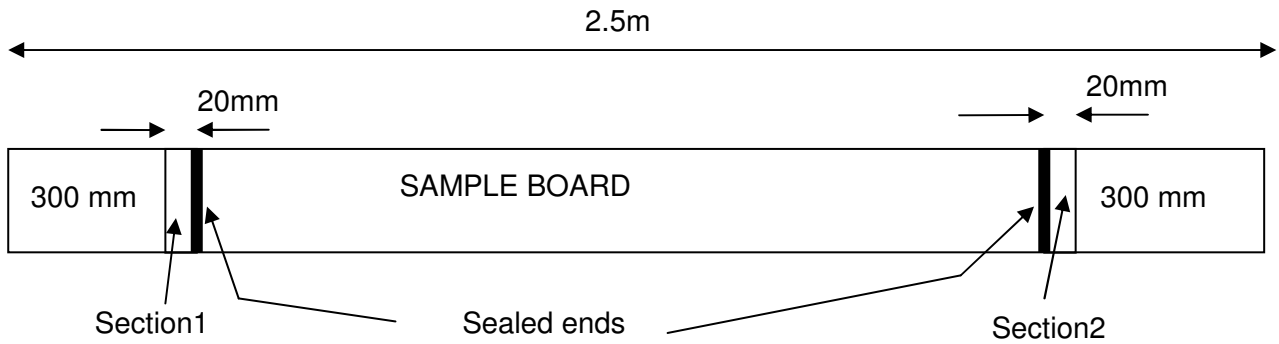


Figure 3.11: Preparation of a MC sample board

- The green mass of the MC sample board (  $m_{SB \text{ green}}$  ) was determined.
- The MC sample boards were positioned on the short stickers along the air exit side of the stacks (Figure 3.9) throughout the drying process. During the drying process, the sample boards were weighed at intervals to determine their mass. After weighing, the boards were returned to the original position on the short stickers.
- The sections were dried in a thermostatically controlled oven at 103°C for at least 24 hours and until they reached a constant mass,  $OD_{sect1}$  and  $OD_{sect2}$ .
- The MC of the sections were determined:

$$MC_{sect1} = (m_{sect1} - OD_{sect1}) / OD_{sect1} \times 100\% ;$$

$$MC_{sect2} = (m_{sect2} - OD_{sect2}) / OD_{sect2} \times 100\%$$

- A linear moisture gradient was assumed to exist along the length of the MC sample board and the MC of the sample board was taken as the average of the adjacent moisture sections:

$$MC_{SB} = (MC_{sect1} + MC_{sect2}) / 2 \%$$

- The oven dry mass of the MC sample board was determined (note that this is an estimation):

$$OD_{SB} = m_{SB \text{ green}} / \left( \frac{MC_{SB}}{100} + 1 \right)$$

- The MC sample board mass at regular intervals during the drying run was used to monitor the MC of the MC sample board at that stage:

$$MC_{SB} = \left\{ \frac{m_{SB} - OD_{SB}}{OD_{SB}} \right\} \times 100 \%$$

The results are given in Table 3.1

Table 3.1: Initial mass, initial MC and calculated oven-dry mass of the MC sample boards

Sample board	Section 1			Section 2			SB average green MC	SB wet mass	SB OD Mass (estimated)
	Green	OD	MC	Green	OD	MC			
	g	g	%	g	g	%	%	[kg]	[kg]
1	246	149	65.1	279	165	69.1	67.1	5.79	3.465
2	297	185	60.5	191	116	64.7	62.6	6.65	4.09
3	180	114	57.9	275	174	58.1	58.0	6.24	3.95
4	184	117	57.3	219	130	68.5	62.9	5.64	3.463
5	287	164	75.0	260	143	81.8	78.4	6.12	3.43
6	297	174	70.7	213	136	56.6	63.7	7.87	4.809
7	225	160	40.6	258	182	41.8	41.2	6.41	4.54
8	228	135	68.9	187	110	70.0	69.4	5.82	3.435
9	225	130	73.1	245	137	78.8	76.0	6	3.41
10	224	144	55.6	179	121	47.9	51.7	6.83	4.501
11	165	93	77.4	184	107	72.0	74.7	6.48	3.709
12	263	161	63.4	240	153	56.9	60.1	5.83	3.641
13	242	141	71.6	170	100	70.0	70.8	6.03	3.53
14	254	139	82.7	243	141	72.3	77.5	6.56	3.695
15	272	151	80.1	305	160	90.6	85.4	7.18	3.873
16	272	149	82.6	242	134	80.6	81.6	6.71	3.695
17	274	170	61.2	281	174	61.5	61.3	6.02	3.731
18	196	135	45.2	242	169	43.2	44.2	7.46	5.174
19	303	210	44.3	308	212	45.3	44.8	7.14	4.931
20	204	133	53.4	203	131	55.0	54.2	7.46	4.839
21	223	136	64.0	196	119	64.7	64.3	7.24	4.406
22	187	121	54.6	202	132	53.0	53.8	6.35	4.129
23	333	177	88.1	343	196	75.0	81.6	7.28	4.009
24	326	191	70.7	319	197	61.9	66.3	7.19	4.323
					Average		64.7		
					St Dev		12.3		

### 3.8.2 Drying quality

The ZA Dry Q Audit procedure was followed to determine the drying quality of the timber dried in the Saasveld Solar Kiln. The sampling design was discussed in Section 3.6.2. The following drying characteristics were examined in the ZA Dry Q Audit procedure:

- Mean MC
- Moisture gradient

- Short bow caused by incorrect stacking
- Case-hardening
- Surface checks
- End checks
- Internal checks
- Discolouration

#### *3.8.2.1 Average moisture content and moisture gradient*

Moisture measurements were taken using a calibrated resistance type moisture meter with pins with insulated shafts. Each of the 20 drying quality (DQ) sample boards in stacks 2 and 7 (Figure 3.7) was measured at six locations along the 2.5m length of the board: 0.25m, 0.65m, 1.05m, 1.45m, 1.85m and 2.25m. At each of these six measuring locations,  $MC_{1/6}$ ,  $MC_{1/3}$  and  $MC_{1/2}$  were measured where;

- $MC_{1/6}$  = MC at one-sixth thickness,
- $MC_{1/3}$  = MC at one-third thickness and,
- $MC_{1/2}$  = MC at half thickness.

Moisture gradient (MG) was obtained by the difference  $MC_{1/2} - MC_{1/6}$ . The average MC was obtained from  $MC_{1/3}$ .

#### *3.8.2.2 Moisture content and moisture gradient variation through the load*

The assessment of the MC and MG variations over the length, width and height of the load does not form a part of the ZA Dry Q assessment. However, the ZA Dry Q assessment method was constructed in such a way that the captured data can be used to analyse the MC and MG variation through the load. The selection of the data-points required by ZA Dry Q, contributed to a sample that represents the entire load. Representative data was obtained as the two stacks identified (stacks 2 and 7) were in opposite corners of the load (see Figure 3.7).

#### *3.8.2.3 End checks*

All the 20 DQ sample boards selected from each of stacks 2 and 7 were visually inspected for end checks.

#### 3.8.2.4 Short bow

A 500mm long straight edge was placed over the concave side of the maximum bow. The maximum deviation between a 500mm long straight edge and the board face was tested with a 1.5mm feeler gauge. If the feeler gauge fitted into this space, the board was defined as having short bow. All 20 DQ sample boards were assessed.

#### 3.8.2.5 Case-hardening

The 10 widest tangentially sawn DQ sample boards were selected for this test. Test slices were prepared according to Figure 3.12 and were taken at least 300mm from either end of the board.

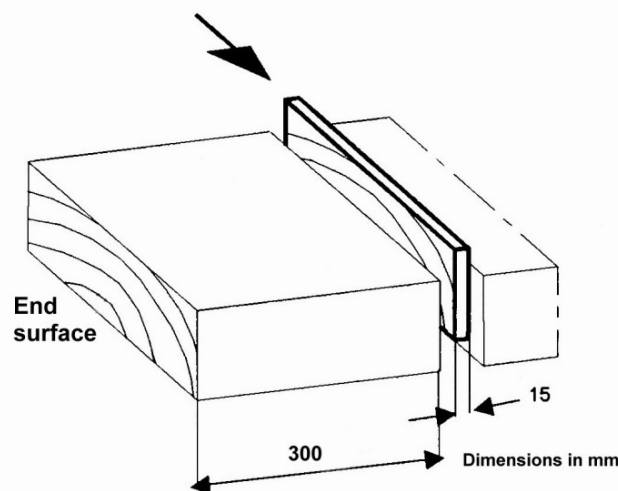


Figure 3.12: Preparation of case-hardening test pieces (SALMA, 2003b)

The test slices were deep-ripped into two equal parts as indicated in Figure 3.13.

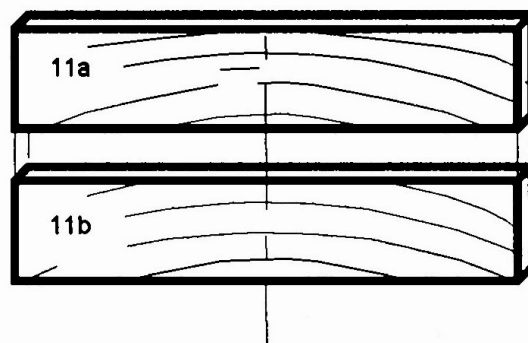


Figure 3.13: Separation and marking of the slices for case-hardening test (SALMA, 2003b)

A test jig with 10mm diameter pins (Figure 3.14) was used to measure the magnitude of case-hardening. The purpose of the 10 mm pins was to enable reverse case-hardening measurements.

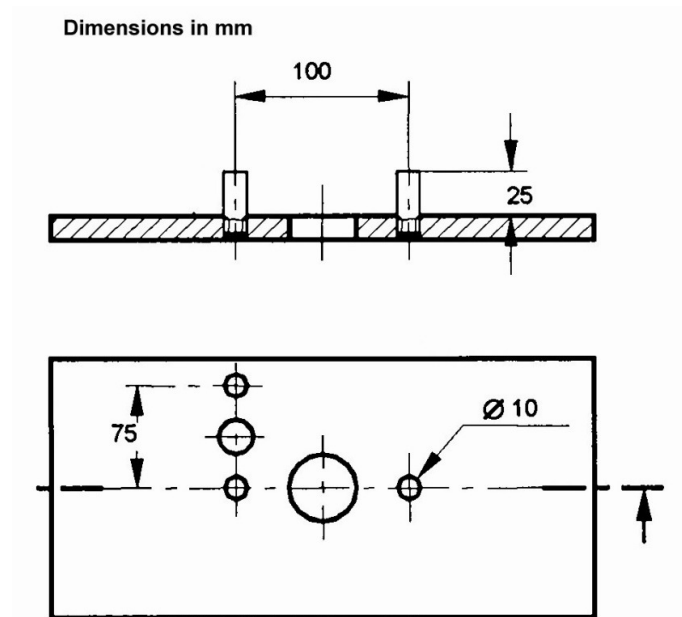


Figure 3.14: Test jig for assessment of case-hardening (SALMA, 2003b)

The parts were placed in the test jig as per Figures 3.15 and 3.16. Note that the parts were placed in their original orientation, with respect to each other, as they occurred in the board. If the original board width was wider than 100mm, the pins 100mm apart were used. If the original board was 75mm - 100mm in width, the pins 75mm apart were used (see Figure 3.15 for the test jig). The calliper was positioned between the two pieces at its widest point, centred across the test rig.

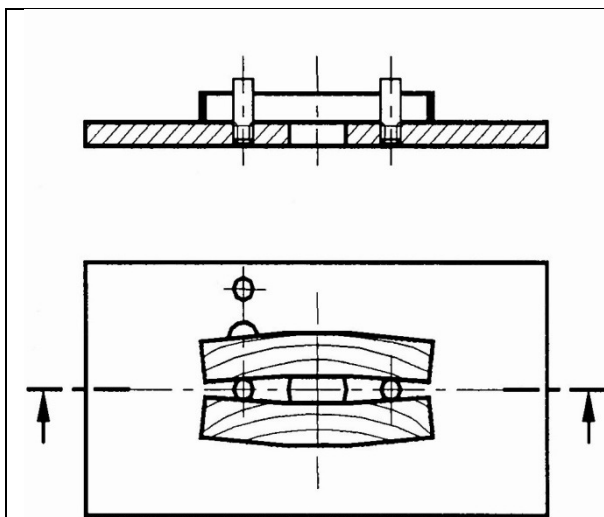


Figure 3.15: Evaluation with the test jig, of case-hardening from a board wider than 100mm (SALMA, 2003b)



Figure 3.16: Case-hardening is measured with a vernier calliper as a distance between the two slices.

The amount of case-hardening as measured over the pins 100mm apart ( $CH_{100}$ ) was determined by:

The measurement gap between the split pieces – the pin diameter,

$$CH_{100} = (\text{read}_{100} - 10)\text{mm}.$$

If the pins 75mm apart had to be used due to the boards being narrower than 100mm, the case-hardening value had to be converted to 100mm pin values. For a case-hardening reading obtained by the 75mm pin setting,  $\text{read}_{75}$ , the deviation due to the case-hardening ( $CH_{75}$ ) equals  $CH_{75} = (\text{read}_{75} - 10)\text{mm}$ . Refer to Figure 3.17.

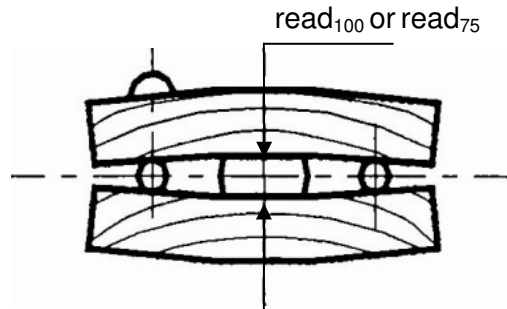


Figure 3.17: Measurement at the 100mm or 75mm spaced pins (SALMA, 2003b)

To simplify the calculations, the profile of the case-hardening test slices will be discussed from the viewpoint that only positive case-hardening was formed. The profile of the curve after deep-ripping a test slice was assumed to be a parabola. The contribution of each test slice was  $\frac{1}{2} \times (\text{read}_{75} - 10) = \frac{1}{2} \times CH_{75}$ , as abbreviated as  $d_{75}$ , indicated on the x-y axis in Figure 3.18. If the test slices were placed over the 100mm pin position, then the contribution of each test slice was  $d_{75} - d_2$ , as shown in Figure 3.18.

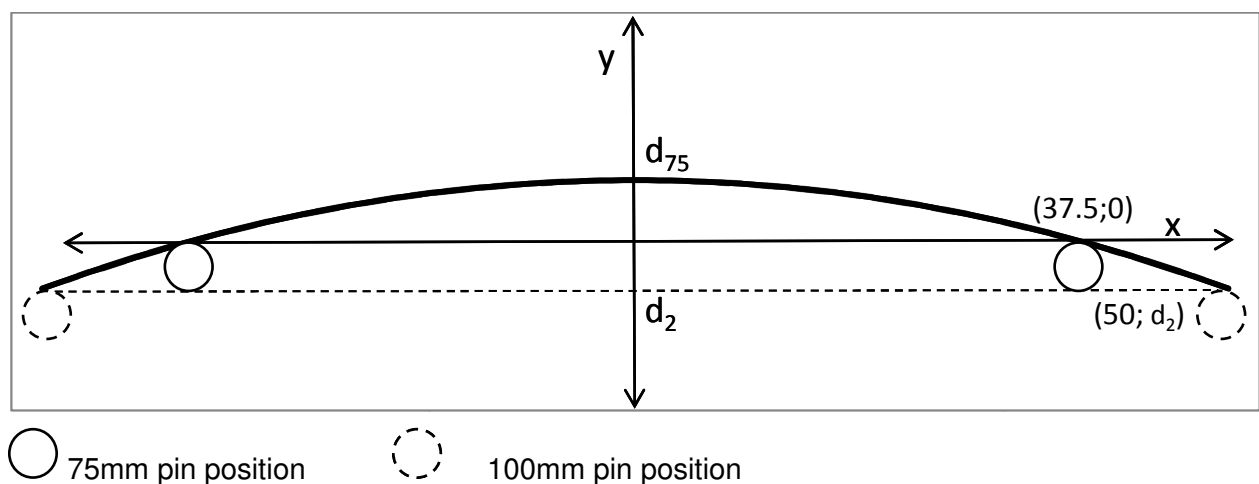


Figure 3.18: Deflection caused by case-hardening of a test piece in a 100mm and 75mm pin position (note that  $d_{75} - d_2 = \frac{1}{2} \times (\text{read}_{100} - 10) = d_{100}$ )



The algebraic equation of the parabola,  $= ax^2 + bx + c$ , was solved by identifying  $c = d_{75}$  and  $b = 0$ , then substituting the point (37.5;0), which is the support position at the 75mm pin position, in order to obtain the value for  $a$ .

$$a = -\frac{d_{75}}{(37.5)^2}$$

The equation therefore becomes:

$$y = -\frac{d_{75}}{(37.5)^2}x^2 + d_{75}$$

The distance  $d_2$ , on the negative y-axis, was solved by substituting the point (50;  $d_2$ ), the 100mm support position, into the equation above:

$$\begin{aligned} d_2 &= -\frac{d_{75}}{(37.5)^2}(50)^2 + d_{75} \\ &= -1.778d_{75} + d_{75} \end{aligned}$$

As discussed, when the test piece was put on the 100mm pin position, then the contribution of each test piece would be  $d_{75} - d_2$ .

Therefore,

$$d_{100} = d_{75} - d_2 = d_{75} - (-1.778d_{75} + d_{75}) = 1.778d_{75}$$

The amount of case-hardening as measured over the pins 100mm

= the measurement gap between the split pieces – the pin diameter

$$= (\text{read}_{100} - 10) = 2 d_{100} = 2(1.778 d_{75}) = 2(1.778 \times \frac{1}{2} (d_{75} - 10)) = 1.778 \times (d_{75} - 10)$$

It is now possible to convert the data from the 75mm pin position to the 100mm pin position by using the formula  $(\text{read}_{75} - 10) \times 1.778\text{mm}$ , where 1.778 is the correction factor to adjust the (75mm spaced pins)-value to the (100mm spaced pins)-value.

### 3.8.2.6 Internal checks and collapse

The ten DQ sample boards, selected for case-hardening, were visually inspected for internal checks and cell collapse on the cross sections that were exposed after cutting the case-hardening samples.

### 3.8.2.7 Surface checks

All ten the DQ sample boards as selected for case-hardening plus five more tangentially sawn boards from the stack were inspected. These 15 boards were planed on the tangential face, away from the pith, to a maximum depth of 2mm to obtain a smooth finish. The planed surfaces were wetted thoroughly with water and then left to soak for 3 to 5 minutes. The wet surfaces were allowed to dry in direct sun for about 2 hrs. Thereafter, the boards were visually inspected for surface checks.

### 3.8.2.8 Surface discolouration

The 15 DQ sample boards used for the surface check test were visually inspected for surface discolouration. Surface discolouration excludes blue stain, but includes kiln brown stain and sticker stains.

### 3.8.3 Positioning and management of sensors

Dry bulb ( $T_d$ ) and wet bulb ( $T_w$ ) temperatures were collected with nine type K-thermocouples at five positions at the kiln as indicated in Table 3.2.

Table 3.2: The position of thermocouple pairs

1.	$T_d$ and $T_w$ temperatures at the air inlet into the timber load	$T_d$ Load In $T_w$ Load In
2.	$T_d$ temperature at the air outlet out of the timber load	$T_d$ Load Out
3.	$T_d$ and $T_w$ temperatures at the air inlet into inflated skin (air jacket)	$T_d$ Jacket In $T_w$ Jacket In
4.	$T_d$ and $T_w$ temperatures at the feedback valve, which is the air outlet out of the inflated skin (air jacket).	$T_d$ Jacket Out $T_w$ Jacket Out
5.	$T_d$ and $T_w$ temperatures of the air outside the kiln	$T_d$ Exterior $T_w$ Exterior

These nine thermocouple values served as data input and were processed to examine the influence of weather conditions (position 5) on the operation of the kiln (positions 1-4). The differences between all the temperature values were critical for this study and special care was taken to ensure accurate readings. The position of the temperature probes can be seen in Figure 3.19.

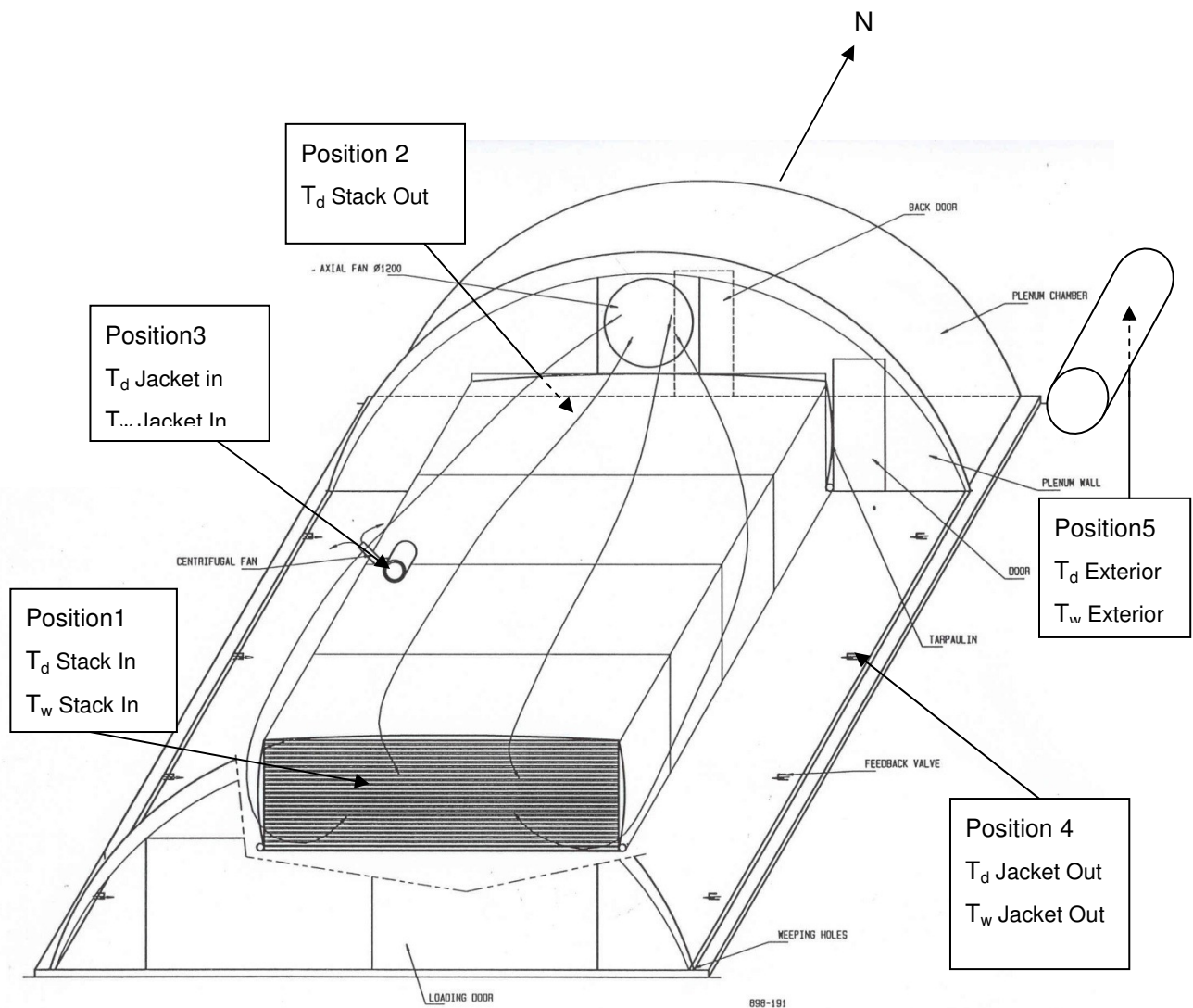


Figure 3.19: Positioning of the thermocouples

#### 3.8.4 Data-logging

Data from the nine thermocouples was logged on a data-logger, manufactured by MC Systems. The data-logger, model MCS 120-04EX, was programmed to temporarily store temperature values once every minute on the RAM. Every ten minutes, the average of the values per thermocouple on the RAM were computed. These averages were then stored in a memory module. This meant that 144 values per day were stored for each of the 9 thermocouples. The data from the memory module was downloaded onto a personal computer (PC) as a text-file and imported into MS Excel.

### 3.8.5 Thermocouple calibration

The results from the thermocouple calibration procedure must not be confused with the results from the primary research study that is covered in Chapter 4. The calibration of thermocouples was seen as part of the methodology to obtain accurate research data.

The thermocouples needed to be calibrated in order to ensure accurate values. Small temperature errors can have a huge effect on humidity values. The calibration was performed by an initial auto-calibrating step with the MCS 120-04EX software (MC Systems, 1998). The accuracy of the thermocouple values was further improved by water calibration, where the thermocouples were subjected to equal temperatures. These two processes are explained and illustrated in Appendix C. Thermocouples with similar temperatures and patterns through the temperature range from 0 °C to 40 °C were paired for data collection purposes. The pairing of the thermocouples is shown in Table 3.3.

Table 3.3: Pairing of the thermocouples

<b><u>CHANNEL</u></b>	<b><u>POSITION</u></b>	
2	$T_d$ Jacket Out	}
1	$T_w$ Jacket Out	
11	$T_d$ Jacket In	}
16	$T_w$ Jacket In	
10	$T_d$ Exterior	}
15	$T_w$ Exterior	
13	$T_d$ Load In	}
12	$T_w$ Load In	
14	$T_d$ Load Out	

#### 3.8.5.1 Operating procedures

In order to achieve accurate wet bulb temperatures, there must be turbulent flow over the wet bulb thermometers. In addition, some sources state that a 3m/s air speed over the temperature probe is required to ensure that the convective heat transfer is large in comparison to the radiant heat transfer (Van Wylen and Sonntag, 1985). To test this, a smouldering piece of canvas was put at

the measuring position and the smoke was observed for turbulent flow. All thermocouples experienced turbulent flow, except for  $T_w$  Load In and  $T_w$  Exterior. As there were doubts about these two wet bulb thermocouples, a small 12V DC fan, typically used to cool the hard drives of computers, was installed at  $T_w$  Load In and  $T_w$  Exterior (see Figure 3.19). This ensured turbulent airflow at the measuring points under discussion.

Accumulation of salts on the wick of the wet bulb was prevented by frequently refilling the reservoir for the wet bulb thermocouples with fresh rain water.

To prevent solar radiation, the exterior thermocouples were installed in the centre of a horizontal concrete pipe, elevated 600mm over a grass lawn. The pipe had an inside diameter of 400mm and a length of 2.5m. The outside of the pipe was wrapped with reflective insulation to protect it from solar heat. The pipe was oriented in the direction of the persisting wind, which is in a north-west to south-east direction. This provided natural flow over and through the pipe, similar to a Stevenson screen. The dry bulb temperature sensor at the north-oriented stack exit position,  $T_d$  Load Out, was positioned 100mm inside the stack to protect it from direct solar radiation.

### **3.9 Data analysis methods**

Dry bulb ( $T_d$ ) and wet bulb ( $T_w$ ) temperatures were collected with the nine type K-thermocouples at five positions at the kiln as discussed in 3.7.3.

The evaporation of water from a wood surface can be compared to the adiabatic saturation process. The wet-bulb temperature and the adiabatic saturation temperature are approximately equal for air-water vapour mixes at atmospheric pressures and temperatures (Van Wylen and Sonntag, 1985). This approximation is valid for temperatures below 60 °C, and air velocities of more than 3m/s. This means that the wet bulb temperature remains almost constant as the air travels through the timber stack while the dry bulb temperature drops, and therefore no wet bulb was needed at the air exit side of the timber stack. The measured  $T_w$  Load In – temperature was, therefore, also used at the air exit side, for calculations.

A number of air properties can be derived from the dry bulb and wet bulb temperatures. These air properties will assist in the analysis of the data:

- Ambient air pressure
- Relative humidity
- Equilibrium moisture content (EMC)
- Absolute humidity (AH) on a mass basis
- Dew-point temperature

The formulas for the above parameters are given in Appendix D. These formulas will be used to determine atmospheric conditions inside and outside the Saasveld solar kiln.

In summary, the  $T_d$  and  $T_w$  were measured at critical chosen positions to generate data to determine other atmospheric parameters. The parameters were: relative humidity, Equilibrium moisture content (EMC), AH on a mass basis and dew-point temperature.

### **3.10 Drying run**

The kiln was stacked on 18 May 2009. Thermocouples and sample boards were prepared and positioned in the stacked kiln as indicated. The tarpaulin was pulled over the eight stacks and all preparations were completed before the fans were switched on. The fans were started on 28 May 2009. For further reference, this was called Day 1 of the drying run.

Two incidents interrupted the drying run. The data-logger was off from 1 June to 3 June 2009 as a result of lightning. The fan was switched off for the duration of this period. Due to motor failure of the main-fan, the fan had to be removed to be repaired from 16 to 26 September 2009.

The drying run ended on 14 October and the timber was de-stacked the next day. Drying quality tests were performed on 15 and 16 October 2009.

## 4 RESULTS, ANALYSES AND DISCUSSION

In this chapter the performance of the Saasveld solar kiln is discussed, to evaluate the validity of the claim that the kiln should offer good drying quality by examining the high density hardwood dried in it. Temperature and humidity data, collected continuously over a 24-hour period over the entire run, provided insight into the internal and external atmospheric conditions during different stages of drying. Analysis of this data afforded a better understanding of how this kiln operated and explained the concept of its drying abilities. The parameter of MC, rather than that of time, defined the stages of drying.

It must be stressed that the collection of temperature and humidity data was to enable a study of kiln operation and *not* to control the atmospheric conditions inside the kiln.

The average air velocity through the stacks was 1.52 m/s.

### 4.1 Drying quality evaluation according to ZA Dry Q

Sampling and data collection methods of the ZA Dry Q drying quality audit were discussed in 3.6.2 and 3.7.2. Stacks 7 and 2 were evaluated. In Section 3.5 (Stacking) the position of the stacks was discussed and the full results are shown in Table E.1 and E.2 of Appendix E.

#### 4.1.1 MC and MG variation through the load

In order to observe whether unequal drying had occurred, an assessment of the MC and MG variations over the length, width and height of the stacks 2 and 7 was undertaken (see Appendix F). This does not form a part of the ZA Dry Q assessment. However, the ZA Dry Q assessment method was constructed in such a way that the captured data can be used to analyse the MC and MG variation through the load. The two stacks assessed, stacks 2 and 7, were in diagonally opposite corners of the load (see Figure 3.7) and were therefore representative of the load. Note that the  $\frac{1}{3}$  depth MC value is the average MC of a board only at that specific point on the board where the prongs of the electrical resistance moisture meter were inserted to one-third of the depth. The MGs are determined by the MC at a thickness of  $\frac{1}{2}$  of the board thickness minus the MC at a thickness of  $\frac{1}{6}$  of the board thickness.

#### 4.1.1.1 Summary of average MC and MG results

A summary of the results for the stacks is shown in Table 4.1. Note that “STDEV” means the standard deviation.

Table 4.1: A summary of the results for stack 7 and stack 2

SUMMARY OF MOISTURE CONTENT MEASUREMENTS FOR STACK 7			SUMMARY OF MOISTURE CONTENT MEASUREMENTS FOR STACK 2		
MEASURE POINT	STACK AVERAGE (%)	STACK STDEV (%)	MEASURE POINT	STACK AVERAGE (%)	STACK STDEV (%)
½ depth	12.44	1.01	½ depth	12.13	1.16
⅓ depth	11.71	0.91	⅓ depth	11.38	1.04
⅙ depth	11.05	0.87	⅙ depth	10.53	0.92
MG	1.39	0.50	MG	1.60	0.51

Stacks 7 and 2 had average MCs of 11.7% and 11.4% respectively. The small standard deviation of the MC and MG measurements indicate that the variations within both stacks were very small. This indicates equal climatic conditions in opposite corners of the load. This variation is further investigated in Section 4.1.1.2.

#### 4.1.1.2 Variations over the length, width and height of the load

The results of the MC and MG variation in all three geometric directions can be seen in Appendix E. Wetter and drier MCs and MGs were evenly spread throughout each of stacks 2 and 7. The average MC of the 20 boards of stack 7 and those of stack 2 did not differ much. There were no positions where a portion of a stack could be identified as being too wet or dry. The only observation was that the MC and MG were a fraction lower at the board ends (MC of 0.2% lower). This could be because the measurements were taken 250mm from the end at both ends of the boards. However, the percentage being so small, it could be ignored.

The standard deviation of the values as seen from the top of the stack was generally higher than as seen from the end of the stack. This was to be expected because the measuring points were across different boards; the chances are greater that wood properties vary between boards, rather than within boards.

These results confirm the tight final MC being achieved by the Saasveld solar kiln. The moisture distribution, as seen from all directions, confirmed an equal distribution of temperature, humidity



and airflow. This proved that the air circulation through the stacks was properly baffled, the stacking was good and the geometry of the kiln assured efficient air circulation. The MG was low and the expectation was that the stresses would be small.

#### 4.1.2 Assessing mean MC and MG against ZA Dry Q requirements

The allowable ranges for MC and MG allowable ranges are specified by the ZA Dry Q standards.

##### 4.1.2.1 *MC allowable range*

ZA Dry Q standard requires that 90% of all  $MC_{1/3}$  readings must lie within the upper and lower limits calculated as follows:

Lower limit:  $MC_t \text{ minus } (0.1 \times MC_t) = 11 - 0.1 \times 11 = 9.9\%$

Upper limit:  $MC_t \text{ plus } (0.2 \times MC_t) = 11 + 0.2 \times 11 = 13.2\%$

Where  $MC_t$  = target moisture content = 11%

##### 4.1.2.2 *MG allowable range*

ZA Dry Q standard requires that 90% of all MG values must be smaller than  $(MC_t \times 0.2) = 11 \times 0.2 = 2.2\%$ .

##### 4.1.2.3 *Results and discussion of the mean moisture content and the moisture gradient*

The results of the assessment are shown in Table 4.2:

Table 4.2: Assessing the mean MC and MG against ZA Dry Q standards

	Number values below lower MC specification (9.9%)	Number values above upper MC specification (13.2%)	Number values pass within MC specification	Number values outside MG specification (2.2%)	Number values pass within MG specification
Stack 7 (120 values)	0	7	113	3	117
Stack 2 (120 values)	8	5	107	11	109
Total of 240 values	8	12	220	14	226
Total pass rate			91.7%		94.2%

This is a clear indication of the small variation in MC and moisture gradients of timber being dried in the Saasveld solar kiln. The uniform moisture distribution throughout stacks 2 and 7 and the small difference between these two stacks are proof of the uniform distribution of the drying conditions (temperature, humidity and airspeed) in the solar kiln. As the ZA Dry Q specifications were specifically designed for the assessment of appearance grade softwood, the results achieved with the refractory hardwood confirmed the outstanding drying quality. The results of the moisture gradient assessment are proof of the mild drying conditions as expected.

#### 4.1.3 Other defects

Other defects tested as required by ZA Dry Q included: end checks, short bow, case-hardening, internal checks, surface checks and surface discolouration.

##### *4.1.3.1 Summary of defects for stacks 7 and 2*

The results are tabulated Tables 4.3 and 4.4.

Table 4.3: Summary of drying defects in stack 7 with board dimensions of 30mm x 80mm

Board #	End Checks	Short Bow	Case-hardening (mm)	Internal Checks	Surface Checks	Discolouration
Sample size	20	20	10 tangential	10 tangential	15 tangential	15 tangential
Board #1	None	pass	0.09	none	none	none
Board #2	none	pass	0.98	none	none	none
Board #3	none	pass	0.73	none	none	none
Board #4	none	pass	0.53	none	none	none
Board #5	none	pass	—	—	none	none
Board #6	yes	pass	—	—	—	—
Board #7	yes	pass	—	—	none	none
Board #8	yes	pass	—	—	none	none
Board #9	none	pass	0.94	none	none	none
Board #10	yes	pass	0.84	none	none	none
Board #11	yes	pass	—	—	none	none
Board #12	none	pass	—	—	—	—
Board #13	yes	pass	<b><u>1.03</u></b>	none	none	none
Board #14	none	pass	—	—	—	—
Board #15	none	pass	—	—	none	none
Board #16	none	pass	0.69	none	none	none
Board #17	none	pass	—	—	none	none
Board #18	none	pass	0.94	none	none	none
Board #19	yes	pass	0.20	none	—	—
Board #20	none	pass	—	—	—	—
Total	Yes = 7	Fail = 0	Fail = 1	Yes =0	Yes =0	Yes =0

Table 4.4: Summary of drying defects in stack 2 with board dimensions of 30mm x 120mm

Board #	End Checks	Short Bow	Case-hardening	Internal checks	Surface checks	Discolouration
Sample size	20	20	10 tangential	10 tangential	15 tangential	15 tangential
Board #1	yes	pass	—	—	—	—
Board #2	none	pass	0.48	none	none	none
Board #3	none	pass	—	—	—	—
Board #4	none	pass	0.90	none	none	none
Board #5	yes	pass	—	—	—	—
Board #6	yes	pass	—	—	1 surface check	none
Board #7	none	pass	—	—	none	none
Board #8	none	pass	0.84	none	none	none
Board #9	none	pass	0.78	none	none	none
Board #10	yes	pass	—	—	none	none
Board #11	none	pass	0.69	none	none	none
Board #12	yes	pass	—	—	none	none
Board #13	yes	pass	0.89	none	none	none
Board #14	yes	pass	0.97	none	none	none
Board #15	none	pass	—	—	none	none
Board #16	none	pass	0.65	none	none	none
Board #17	yes	pass	—	—	—	—
Board #18	yes	pass	0.37	none	none	none
Board #19	none	pass	—	—	—	—
Board #20	none	pass	0.52	none	none	none
Total	Yes = 9	Fail = 0	Fail = 0	Yes =0	Yes =1	Yes =0

#### 4.1.3.2 End checks

With end checks, it was difficult to differentiate between those caused by drying and those caused by growth stresses. The end checks were mostly a result of the wide wood rays present. The

massive growth stresses in gums were another contributing factor. Some boards already had end cracks when the stacking was done.

The end-check count was conducted after de-stacking and separation of these boards. It would have been better to assess end checks before de-stacking, as *Eucalyptus* timber is prone to end split during handling.

A more accurate tally would have been achieved had these stacks of 20 boards each been painted with regular PVA paint to cover the cracks that formed prior to drying. These cracks would then have been excluded from the final end-check score. The ZA Dry Q specification of only one board per stack was specified for softwoods, with end splitting at a much reduced rate. The suggestion is that all hardwoods should be end coated before drying and/or the ZA Dry Q specification should be revised to include *Eucalyptus* standards. The fact is that end checks in *Eucalyptus* are difficult to avoid (Vermaas, 1995).

#### 4.1.3.3 *Short bow*

No short bow was found in either of the stacks. Proper stacking is part of the drying process. Short bow can be avoided by proper stacking and therefore is regarded as a drying defect. Other warp defects (such as twist, crook and cup) can only be reduced, not avoided, during drying, and are therefore excluded from the ZA Dry Q drying defects.

The argument could be made that end cracks, discussed above, indicate both a drying and a wood material defect. Future research could investigate the influence of coating the ends of boards and the resultant effect on end checking in the Saasveld solar kiln. A suggestion would be to cover the end with a rubberized paint. Traces of paint inside an end crack will be conclusive evidence of cracks existing before drying.

#### 4.1.3.4 *Case-hardening*

The data displayed in Tables 4.3 and 4.4 shows the case-hardening deflection with the 10 mm subtracted from the vernier calliper readings, as discussed in Section 3.7.2.5. The 80mm samples of stack 7 were converted to a value over the 100 mm pin position as described in Section 3.7.2.5.

The ZA Dry Q specification allowed only one of the 10 sample boards per stack to have case-hardening deflection of more than 1mm. Stack 7 had one incident of case-hardening more than

1mm and stack 2 had none. The average case-hardening values for stacks 7 and 2 were 0.7mm (standard deviation = 0.33mm) and 0.71mm (standard deviation = 0.2mm) respectively.

Drying stress causes case-hardening and is the result of the moisture gradient that develops when drying timber. The impermeable structure of hardwoods will promote greater moisture gradients, which result in more severe case-hardening. The ZA Dry Q specifications were designed for drying quality in softwood for furniture and remanufacturing applications. Although just inside the specifications, the results were excellent since the possibility of case-hardening is more likely in hardwoods than softwoods, suggesting that drying stresses were limited in the Saasveld solar kiln. This implies that the case-hardening was definitely under control.

#### *4.1.3.5 Internal checks and surface checks,*

Reasons for the formation of surface and internal checks are discussed in Section 2.4.1. The best way to avoid it is to maintain small MGs, and therefore small drying stresses, throughout the drying process.

Surface checks form in the initial drying period when the surface layers dry to below the fibre saturation point of the timber. Two aspects reduced the likelihood of surface checks in the present work:

- Initially, the timber was exposed to mild conditions and this meant that the surface layers remained relatively wet, which ensured that the MG remained small. Final MGs are discussed in Section 4.1.1 and Appendix F proved this correct.
- The air in the kiln at night should have a high RH due to cooling in the jacket. Moisture loss at night at a lower temperature and high RH should be slow, allowing the hot inside of the wood to move water to the wood surface to reduce the MG.

Section 4.3 will investigate the atmospheric conditions that are discussed above.

Six of the 30 DQ sample boards had surface checks, five of which were across the knot faces and were not treated as surface checks (see Figure 4.1). This means that there was only one true surface check, in the two stacks that were evaluated. The drying assessment criteria were achieved for surface checks as ZA Dry Q allows only one board of a stack to have a surface check.



Figure 4.1: The only surface check encountered

Since there was little case-hardening, few or no internal checks were expected in this drying run. The ZA Dry Q assessment indicated no internal checks.

#### *4.1.3.6 Surface discolouration*

As the timber specie is not known to have thermal discolouration and the air temperatures were well below 40 °C in the drying period prior to fibre saturation, there was no surface discolouration. There were no sticker stains as the stickers were clean and already dry at the time of stacking.

#### *4.1.3.7 Cell collapse*

Cell collapse is not a drying defect that is assessed in the ZA Dry Q. The reason for this is that ZA Dry Q is aimed at assessing softwood drying. Since hardwoods are more prone to cell collapse, it is necessary to discuss the presence of this drying defect. However, cell-collapse will inherently be found in the case-hardening and internal check assessment. No cell collapse was observed in the 40 boards tested during the ZA Dry Q assessment as well as during the destacking of the 20.1 m<sup>3</sup> load. It can be stated that there was no cell collapse.

## **4.2 Moisture content during drying**

Using values of the oven-dry mass (OD) shown in Table 3.1, the MC of each sample board was calculated from its wet mass and current mass on successive dates and is given in Table 4.5.

Table 4.5: Recorded % MC of all sample boards in the load

Date	19-May	04-Jun	22-Jun	13-Jul	31-Jul	26-Aug	15-Sep	30-Sep	16-Oct
Day	-9	8	24	45	63	89	109	114	130
Starting day	28-May								
Sample Board									
1	67.1	50.9	46.0	31.3	22.1	17.2	15.4	14.0	14.3
2	62.6	48.9	45.2	32.0	22.7	17.1	15.2	13.5	12.2
3	58.0	40.5	37.7	29.1	22.0	17.2	16.0	13.9	13.9
4	62.9	44.7	41.8	31.1	21.3	16.7	15.5	12.6	11.5
5	78.4	46.4	40.2	27.1	17.2	13.1	12.5	9.6	8.2
6	63.7	49.5	40.8	32.9	23.3	17.5	15.0	11.7	9.4
7	41.2	39.4	39.0	30.0	23.4	18.7	15.0	15.4	15.4
8	69.4	55.8	50.8	35.4	25.5	20.2	16.5	16.7	16.7
9	76.0	49.6	44.0	32.0	23.2	18.5	14.1	14.7	13.5
10	51.7	40.6	38.2	27.3	17.8	13.5	10.4	10.0	9.5
11	74.7	47.5	41.0	25.9	17.6	13.2	10.8	10.3	8.9
12	60.1	34.6	30.7	24.1	16.7	13.4	10.7	9.9	8.8
13	70.8	56.4	51.0	33.4	21.3	15.6	15.3	11.6	9.6
14	77.5	57.8	51.8	34.2	22.9	16.4	16.1	12.3	10.4
15	85.4	58.5	52.6	34.8	23.4	15.2	14.6	10.5	8.4
16	81.6	57.5	52.1	35.3	23.1	15.3	11.8	10.7	8.8
17	61.3	39.9	35.4	23.0	15.5	11.5	9.1	8.3	6.9
18	44.2	32.2	31.6	25.8	19.3	14.6	12.1	10.8	9.0
19	44.8	35.7	34.5	26.1	19.7	15.4	13.2	11.5	10.1
20	54.2	41.1	37.8	26.5	18.2	13.5	11.2	9.9	7.9
21	64.3	39.6	35.5	25.1	16.4	10.8	8.0	6.7	5.1
22	53.8	42.7	38.8	26.4	18.9	14.6	12.6	11.4	9.5
23	81.6	60.6	51.2	33.0	21.5	14.7	11.5	10.0	8.3
24	66.3	43.7	39.0	27.2	18.0	12.9	10.3	8.7	7.3
Load average	64.6	46.4	41.9	29.5	20.4	15.3	13.0	11.4	10.2
Load Standard Deviation	12.3	8.2	6.7	3.8	2.8	2.3	2.4	2.4	2.9

It is clear that the MC followed the classical pattern of fast initial drying and slower drying towards the end, as described in Simpson (1991). An important result of this study is the variation of MC. It is clear from the gradual decrease in the standard deviation of the moisture distribution in the load that the Saasveld solar kiln contributes greatly towards equalising the moisture in the load, as



initially expected. This important feature was confirmed in the results from the ZA Dry Q audit in Sections 4.1.1 and 4.1.2.

A concern was that the initial MC might influence the final MC. A scatter plot as shown in Figure 4.2 was constructed to compare the initial green MC and the final MC.

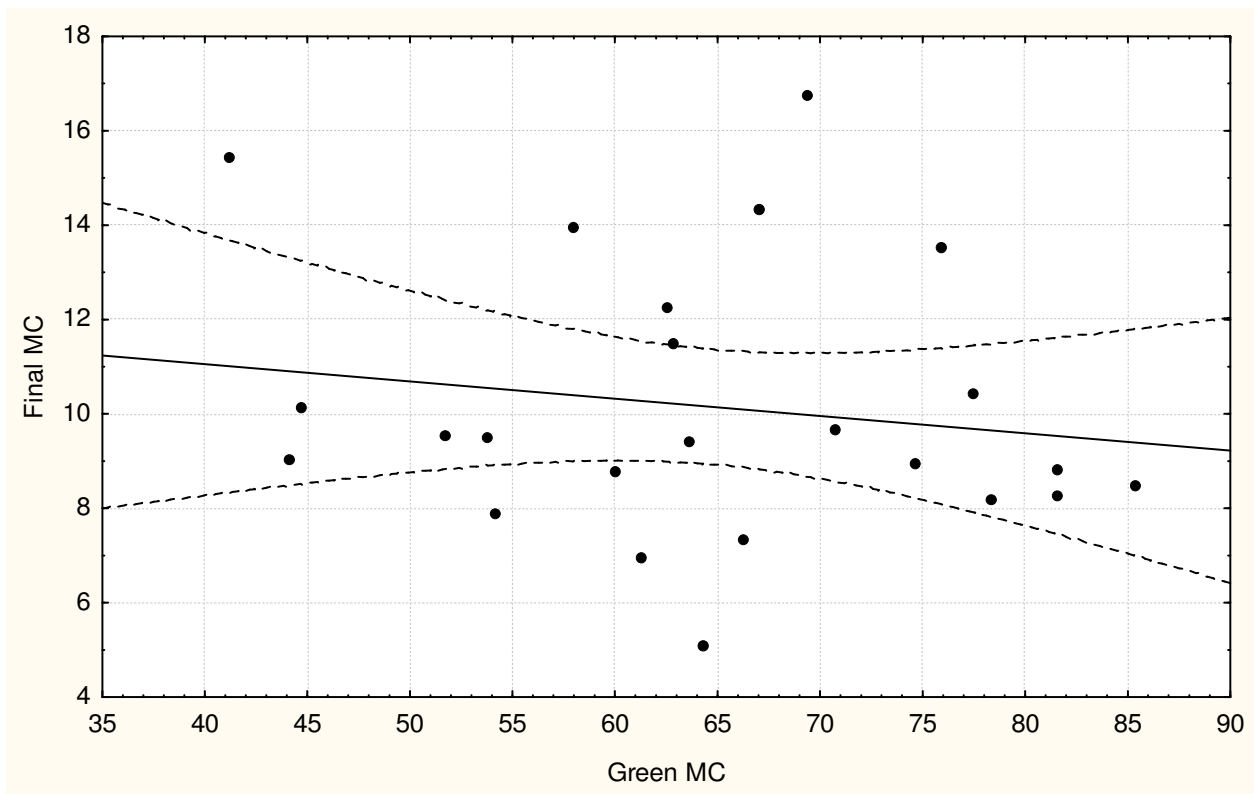


Figure 4.2: Scatter plot of final MC against green MC of the 24 sample boards

It appeared that there was no correlation between the green MC and the final MCs. To test this apparent lack in correlation, a product-moment correlation matrix was computed with Statistica Version 9. The green and dry MC of each sample board was used to compute the correlation matrix. The correlation matrix resulted in a correlation coefficient ( $r$ ) of -0.16 on a 95% confidence interval. This value indicated that the correlation between the green MC and final MC of the 24 sample boards was not significant.

The final load average MC of 10.2% was a little lower than the results from the ZA Dry Q test of 11.4% and 11.7%. There could be some reasons for this:

- The MC sample boards relied on an estimation of the oven-dry mass
- The sections did not represent the sample board

A concern was that the sample boards would be exposed to higher radiation from the tarpaulin that heats up during the day.

The position of the sample boards, in terms of its position in the stacks, was investigated in Figure 4.3.

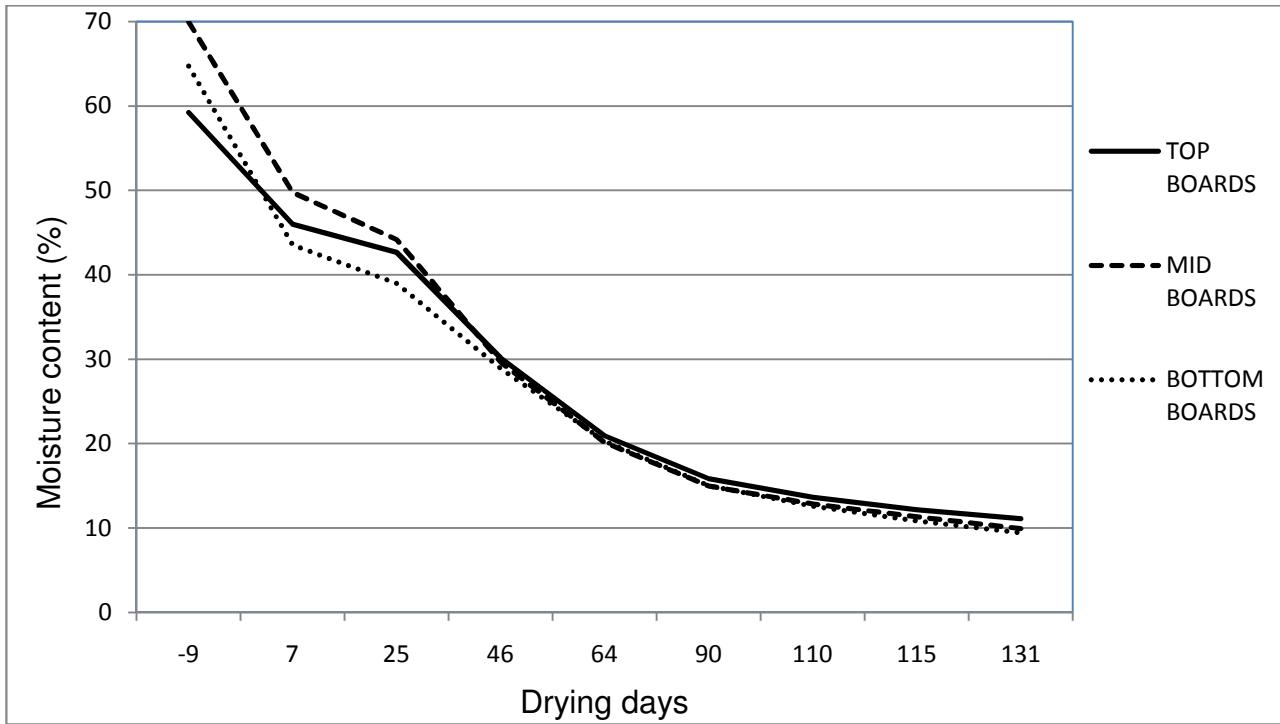


Figure 4.3: Comparison of the drying of sample boards at different heights in the stacks

From Figure 4.3, it is clear that the radiation from the tarpaulin had no influence. It might be that the concrete at the inlet into the stacks would have heated up the air. The bottom sample boards had a lower final MC, especially the boards at the in-feed side (boards 24 and 21), with an MC of 7.33% and 5.08% respectively. Boards 15 and 18 were also low at 8.44% and 9.01%.

However, it must be mentioned that the sample board method is based on an estimated oven dry mass of the sample board, and there are other smaller mistakes that can influence specific readings.

### 4.3 Internal and external atmospheric conditions

The aim of this section was to compare both temperature and humidity values of the air inside and outside (external) the solar kiln in order to establish the kiln conditions and the resulting drying conditions. Data of the dry bulb ( $T_d$ ) and wet bulb ( $T_w$ ) temperatures were measured at carefully chosen positions to generate data to compute other atmospheric parameters. The parameters

were: relative humidity, equilibrium moisture content (EMC), AH on a mass basis, and dew-point temperature. Humidity values were expressed in terms of these parameters.

All dry bulb temperatures values ( $T_{ds}$ ) were consistently reliable and continuous observations were made over the entire drying run. It should be noted again that the temperature and humidity measurements were used for analyses, and not to control the kiln.

The external wet bulbs (outside the kiln) worked without trouble. As the wet bulb wicks inside the kiln at the outlet of the air jacket and especially at the inlet of the air jacket occasionally dried out between weekly services, only the values recorded during the first three days after each service were used to analyse the kiln climate. The wet bulb temperature services included cleaning of the wicks and filling of the reservoirs. The reason for the dry wicks at the inlet of the air jacket was that the main fan was positioned in front of the temperature probe. This proved to be a problem in only the last drying stage, when the wood MC was below 15%. Fortunately, many readings were taken. A total number of 168 480 temperature values were logged over the 130 days, allowing an accurate analysis of climatic conditions. The fact that incorrect data was occasionally collected, when some wet bulbs became dry, had no influence on the progress of the drying.

The data was analysed in two ways:

Firstly, as the amount of data collected over the 130 days of drying was huge, the drying time was divided into five drying stages, as indicated in the Table 4.6:

Table 4.6: The five drying stages of the drying run

Range of the drying stage (days)	Wood MC range (%)
-9 - 24	64 - 42
25 – 45	42 – 29.5
46 - 63	29.5 – 20.4
64 - 89	20.4 – 15.3
90 - 130	15.3 – 10.15

Data or parameters were presented over the course of a typical day in each of the five drying stages. The value for the data or parameter was the average over the number of days at a specific time in that stage. The recorded time incidents were separated by 10 minutes. An example will clarify this when Figure 4.6 of Section 4.3.2 is discussed.

Secondly, six measuring periods of three consecutive days each, evenly distributed over the drying run, were selected. Each period started just after the wet bulb had been serviced for reliability of wet bulb data (Table 4.7). The selected measuring periods were:

Table 4.7: The six measuring periods during the drying run

Day range	Date	Wood MC (%)
1 - 4	28-31 May	50
18-21	16-19 June	43
39-42	7-10 July	30
63-66	31 July – 3 August	20.5
90 - 93	27-30 August	15.3
120-123	5-8 October	10.5

The measuring periods were chosen with the wood MC in mind: green, intermediate MC (free water) range, FSP, intermediate MC (bound water) range and dry. The data collected during these six periods was used to analyse various parameters.

#### 4.3.1 Load Inlet temperatures

The air properties at the load inlet were an indication of the drying conditions that the timber was subjected to. The dry bulb temperature is one of the parameters by which a drying schedule is described, the other being the humidity. This section will discuss the temperature at inlet to the load.

Temperature data was captured every ten minutes of each day, thus 144 readings per day. The average of the internal temperature,  $T_d$  Load In, for every day, over the 130 day drying run is shown in Figure 4.4.

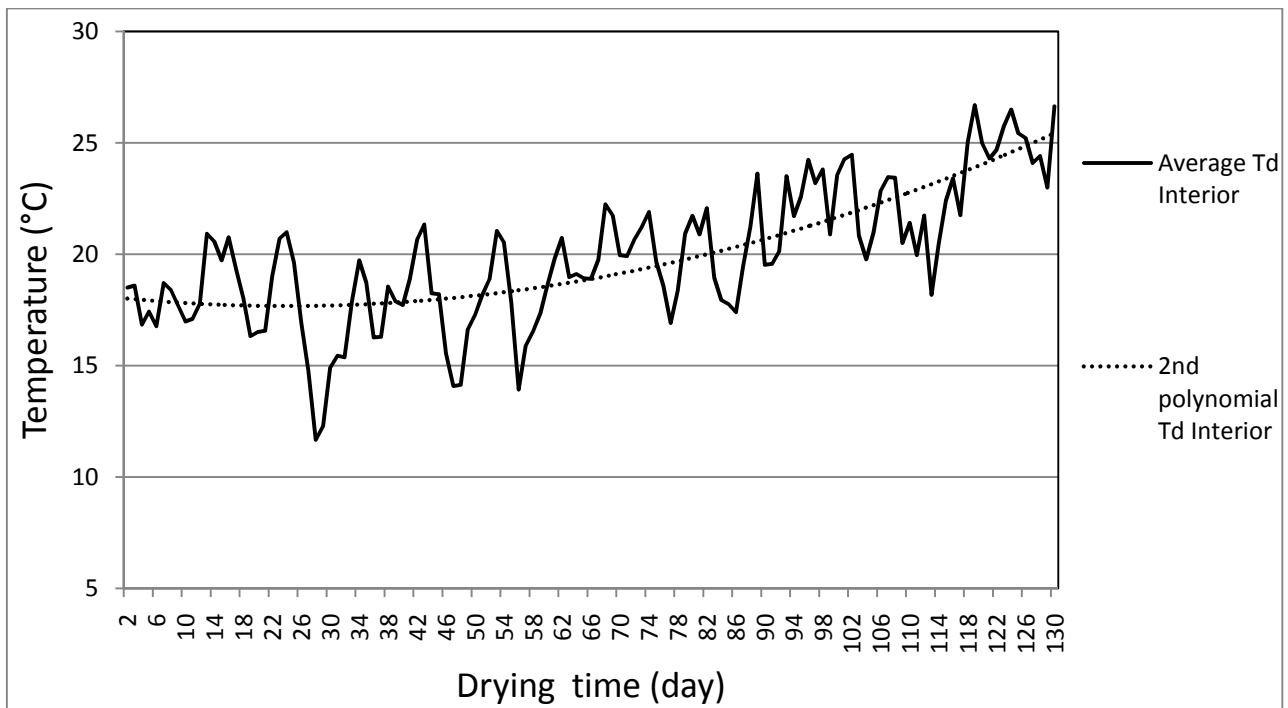


Figure 4.4: Daily average of  $T_d$  Load In against the drying days

The average of the daily kiln temperature increased from 18.0°C initially to 25.7°C at the end. These values were obtained from a second order polynomial trend line as indicated in Figure 4.4. An average of 19.9°C was achieved over the entire drying run. It is evident that the daily average internal temperature increased throughout the drying run. To confirm this, a product-moment correlation matrix was compiled on the daily average  $T_d$  Load In over the 130 days. The correlation coefficient on a 0.05 level was  $r = 0.71$ . This indicates that there was a strong significant correlation between the day of drying and the average daily air inlet temperature at the load. In Section 4.3.6, it was proved that the external temperature had no influence in this rise in temperature.

The maximum internal temperature,  $T_d$  Load In, for each day, over the 130 day drying run is shown in Figure 4.5. The average maximum internal temperature was 26.1 °C

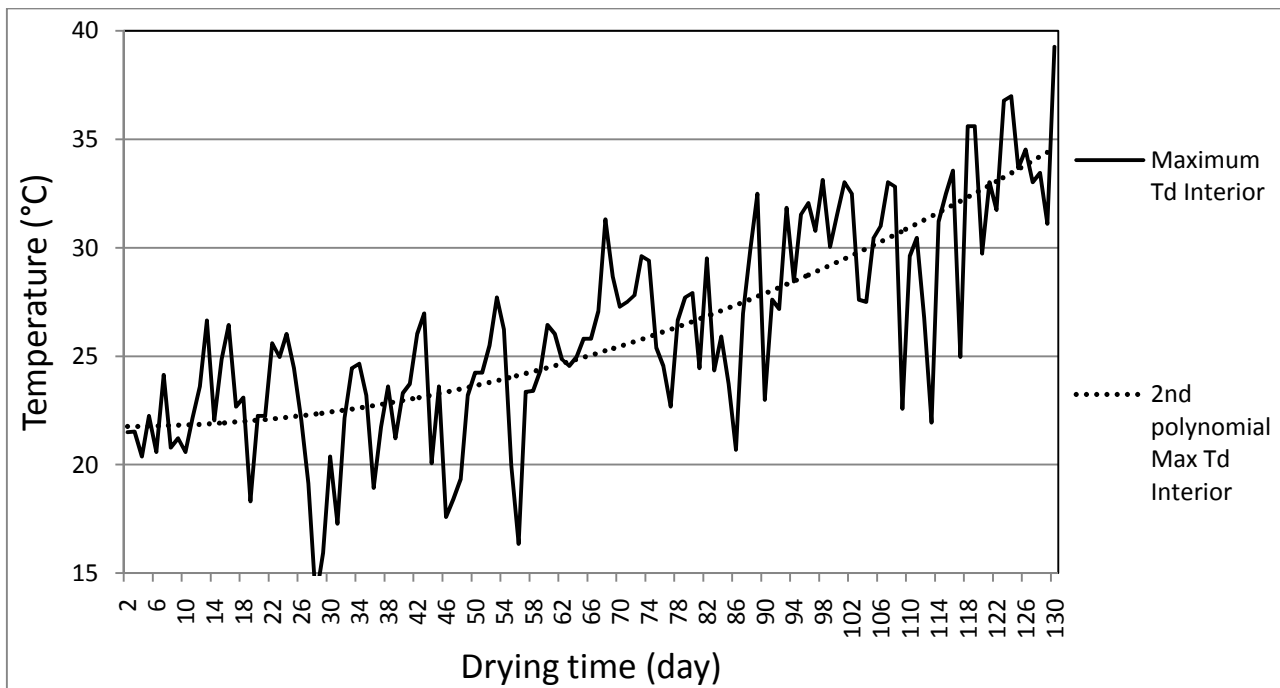


Figure 4.5: Daily maximum  $T_d$  Load In against the drying days

This graph is similar to Figure 4.4 where the average daily temperature is shown. It displays the same pattern of a steady increase as the wood MC decreased. The daily maximum temperatures stayed below 30°C, when the MC was above FSP. Thereafter it increased to a maximum temperature of 38.1 °C that was recorded at the end of drying. It should be noted that much higher maxima have been recorded at other locations and weather conditions. This required reduction of the solar radiation on the kiln by covering it with shade cloth as long as the wood was above FSP to prevent cell collapse.

The low value of the maximum internal temperature while the wood was still above FSP prevented the formation of cell collapse. Haque and Langrish (2006) suggested an initial dry bulb temperature as low as 25°C for the drying of *Eucalyptus pilularis*, while other authors suggested an initial temperature around 40°C.

The internal kiln temperature and the prevention of cell collapse is discussed further in Section 4.3.3, when the change in air temperature as it travels over the timber ( $T_d$  Load In -  $T_d$  Load Out), is considered.

#### Summary:

- The average and maximum temperature inside the kiln increased as the wood dried.
- The average internal temperature was 19.9 °C and a maximum temperature of 38.1 °C was recorded at the end of drying.

- The low value of internal temperature with wood MCs above FSP prevented the formation of cell collapse.

#### 4.3.2 Load Inlet EMC's

Humidity is the second parameter that is used to describe a drying schedule. The humidity at the load inlet will be discussed in terms of the EMC (calculated as per Appendix D3. The graph shown in Figure 4.6 is a summary of the average daily EMC for each of the five defined drying stages as the air entered the timber load. Data is presented for a typical day for each of the five drying stages. An example will be used to clarify the graph. The point indicated by "X" on the graph, represents an EMC of 18.87% at 07h50 for the first drying stage, from days 1-24. This meant that at 07h50 on the 24 days of the first drying stage the average EMC was 18.87%. Similarly, the average of the 24 EMC values that was calculated covering days 1-24 at 08h00 was 18.63%. The same procedure was performed for all the 10-minute intervals covering days 1-24, and likewise for the other four drying stages.

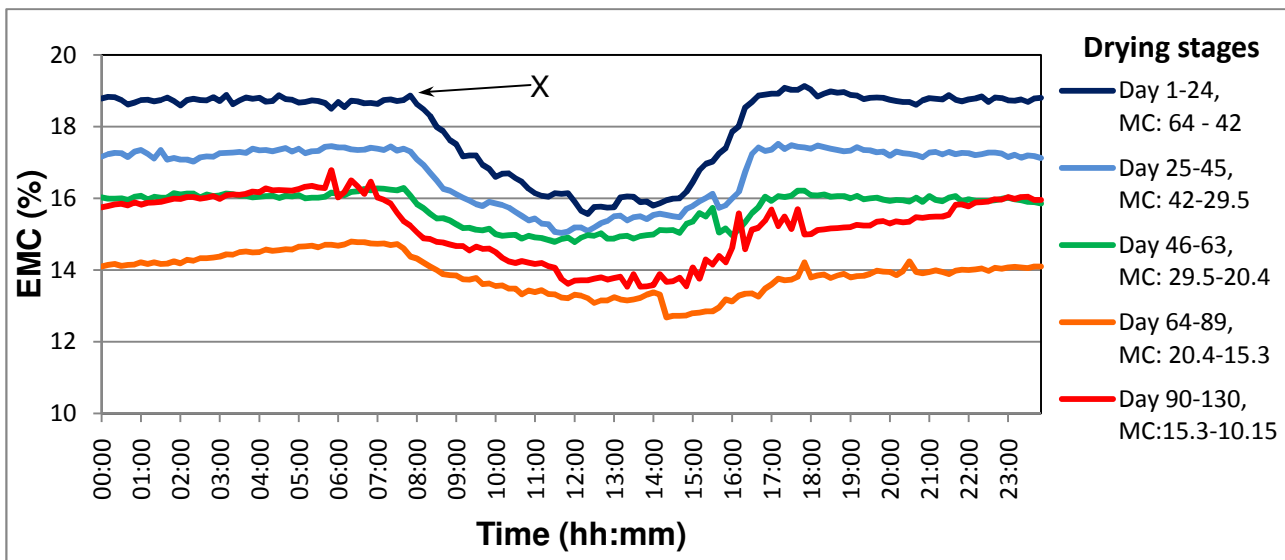


Figure 4.6: Average load inlet EMC at various stages of drying seen over the course of a typical day

It is clear that the calculated average EMC values of the last stage (days 90-130) were not quite as expected since the lowest average EMC value was recorded as 12.7%. This value should be less as the MC analysis of two kiln stacks resulted in 11.4% and 11.7% MC. However, it should be noted that these EMCs are average values. Furthermore, the occurrence of the occasional dried-out wicks in the last drying stage ( $10.15 < MC < 15.3$ ) resulted in a too small wet bulb depression and caused a too high average EMC. The actual graph for the last stage should have been much lower than indicated. With the general trend of reduced EMC lines, the EMC line for days 90-130

should be well below the EMC line covering days 64-89. For the period day 120 to day 123, the actual EMC in the stack was measured to be between 8% and 11% (Figure 4.22).

The data showed that the general trend was towards a decreasing EMC as drying advanced. The EMC stayed relatively even throughout the night and dropped by 2-4% during the daytime (between 08h00 to 17h00). The periods of lower EMC's found during the day, were extended a little as drying progressed. The drop in EMC during the daylight period became progressively smaller as the wood dried. The drop in EMC during the day was initially about 5% and reduced to 2%. It showed that the timber was equalised throughout the drying run by daily periods of high EMC in the initial drying stages and the small daily reduction (2%) at the end of drying. The minimum recorded EMC was 7.3%, indicating that timber was never exposed to extreme dry conditions.

As the wood lost its moisture, the EMC gradually dropped from 18% to 8%, as can be seen in Figures 4.17 to 4.22; a trend similar to all standard drying schedules. This comparison will be discussed further in Section 4.4.6.

#### Summary:

- The EMC decreased automatically from 18% to 8% from the initial MC to the final MC.
- Generally, a lower EMC condition was experienced from 08h00 to 17h00. The variation in EMC became smaller from 5% to 2% as drying advanced.
- Equalizing of timber was promoted throughout the drying run by the longer periods of high EMC at night in the initial drying stages and the low variation during the last drying stages. EMC was never below 7.3%.

#### 4.3.3 Load inlet and outlet air temperatures

The temperature drop across the load (TDAL) is a result of the heat transfer between the air and the timber in convention kiln drying. Once the timber is at temperature, the heat is used to evaporate the moisture in the wood. In conventional kiln drying, the kiln temperature during any given drying stage is kept constant, which is not the case in solar drying.

In the Saasveld solar kiln, heat was transferred between the timber and the surrounding air due to both the evaporation of moisture as described above, as well as the diurnal temperature fluctuations in the kiln. The TDAL in the Saasveld solar kiln is shown in Figures 4.45 to 4.48. The timber was heated up during the day and cooled off during the night. The heating and cooling of



the timber was influenced by the heat capacity of the wood. The relationship is evident from the specific heat capacity equation, in BTU/lb. °F, by Simpson (1991), as discussed in Section 2.5.

The relationship between specific heat capacity and MC can be seen in Figure 4.9 for two typical limiting temperatures in the Saasveld solar kiln. The MC has clearly the major influence on the heat capacity.

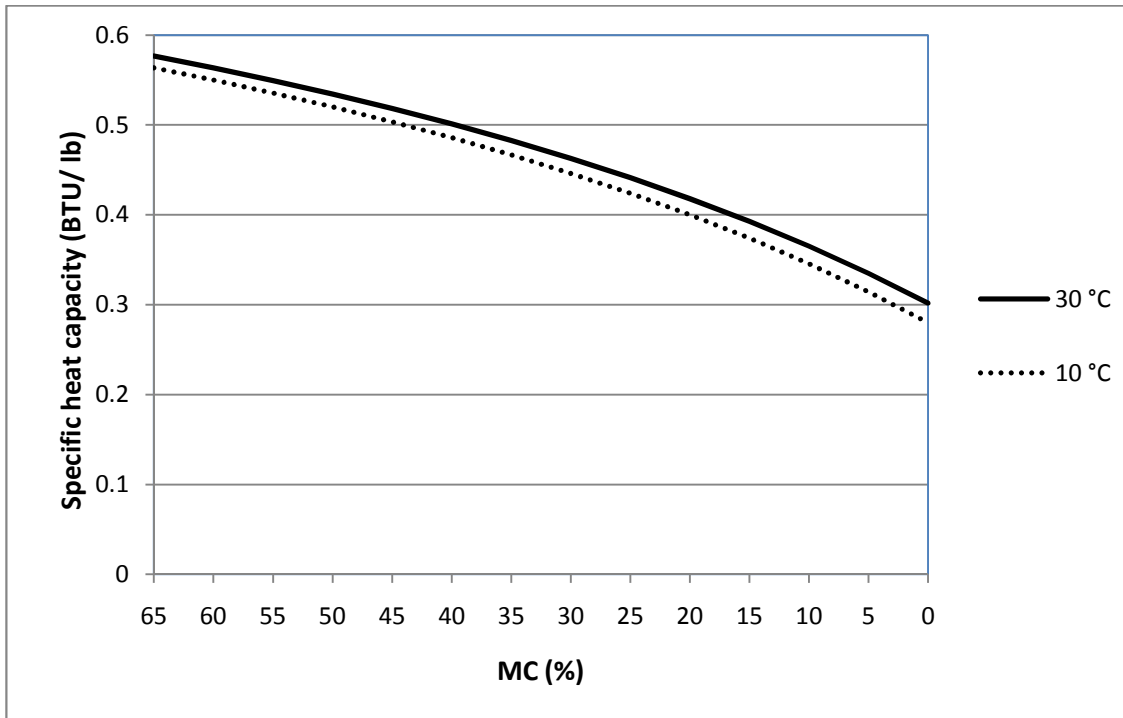


Figure 4.7: The specific heat capacity in BTU/lb. °F against MC for two temperatures.

The implication is that during the mornings until noon, the temperature drop across the load is not only due to evaporation, but also due to the possible cooling of the air by the cold timber. Warm timber, being heated up during the daytime, transferred heat to the air at night, as it passes over it, and resulted in a rise in air temperature. Alternatively, air can be cooled due to evaporation. The net-effect will be determined by the biggest influence.

Initially at high MCs, when the wood was green, the TDAL took place right through the day and night. This is evident from the graph taken over a three-day measuring period covering days 1 - 4 (28 – 31 May), when the timber had an average MC of 50%. Refer to Figure 4.8. The night TDAL was lower than day TDAL due to lower  $T_d$  Load In and less evaporation of water.

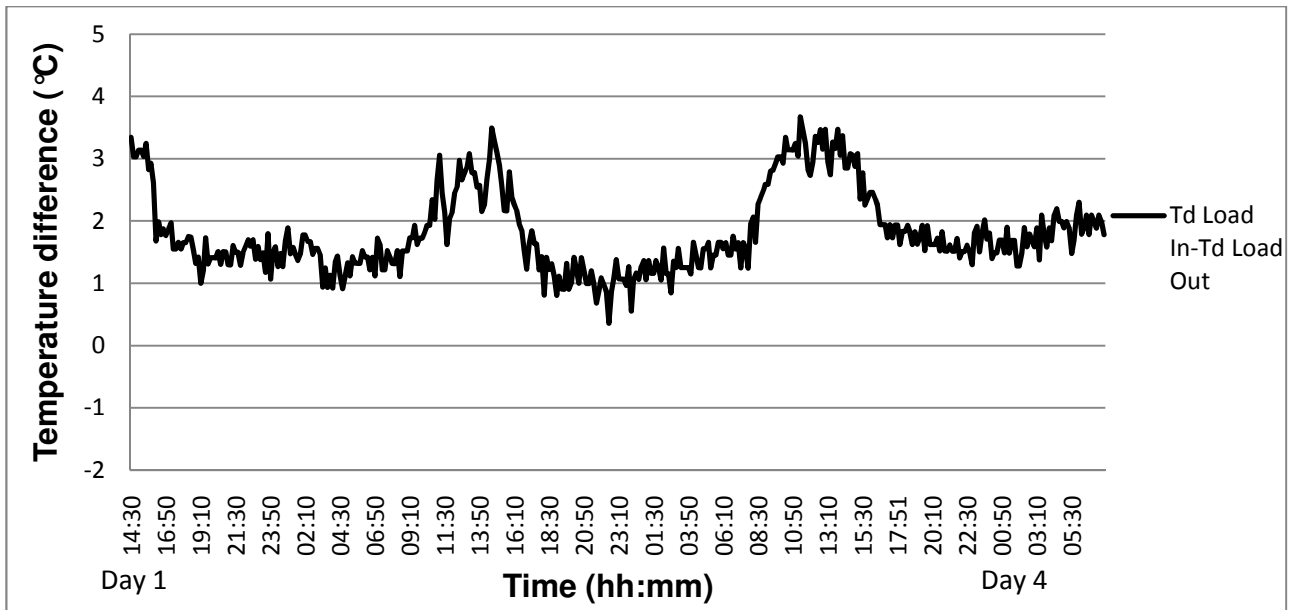


Figure 4.8: TDAL ( $T_d$  Load In- $T_d$  Load Out) against time covering days 1 - 4; MC = 50%

When wood moisture content dropped below 45%, the temperature drop of the air through the load occurred only during the day time. During the night, the air temperature increased as it passed through the load, as indicated by the negative values in Figure 4.9. This means that the nocturnal airflow actually cooled the load.

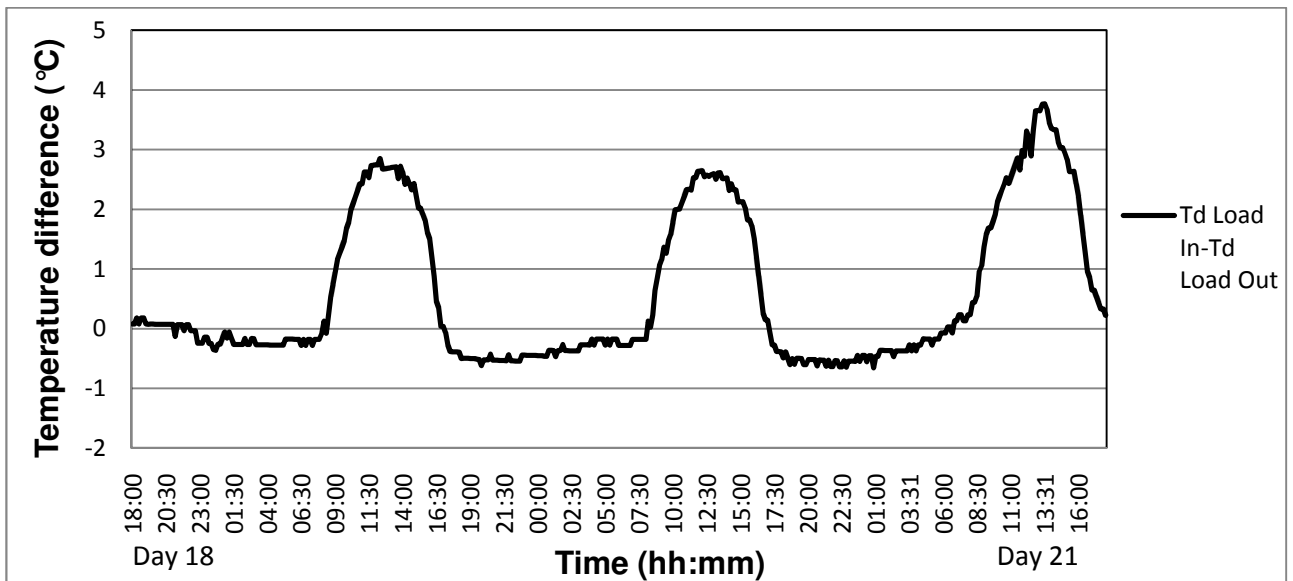


Figure 4.9: TDAL ( $T_d$  Load In- $T_d$  Load Out) against time covering days 18 - 21; MC = 43%

If TDAL=0, the heating gained from warm wood was equal to the heat loss through evaporation of water from wood. If TDAL is negative, heat gain from warm wood was more than losses. This was due to little evaporation or there was no evaporation of water as the air was saturated due to cooling in jacket.

This pattern was repeated throughout the drying period until the end of drying. As expected, the TDAL during the day became smaller, since there was less evaporation, and therefore less cooling of the air. This is supported by the findings of Culpepper (1990). As most of the free water was evaporated, the difference between timber MC and air EMC will be small and the vapour pressure difference between wood and air will be small.

The last measuring period (day 120 – 123; MC = 10.5 %) is shown in Figure 4.10.

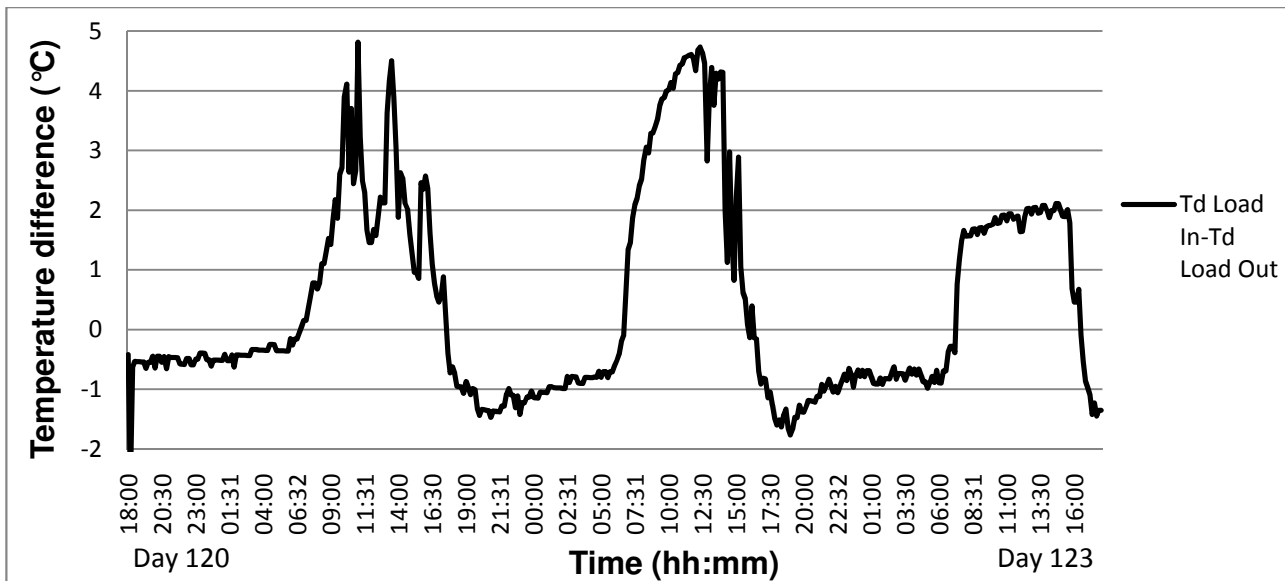


Figure 4.10: TDAL ( $T_d$  Load In- $T_d$  Load Out) against time covering days 120 - 123; MC = 10.5%

From Figure 4.9 and Figure 4.10, it is clear that during the night, the value of ( $T_d$  Load Out -  $T_d$  Load In), or temperature rise across the load (TRAL), increased with a decrease in wood MC. It seems that it was possible for the timber to adsorb water vapour that resulted in a temperature rise.

Two opposing factors were involved in the nocturnal air temperature change as it passed through the stack, the net-effect being caused by the biggest influence:

- TDAL became smaller due to little or no evaporation of water, therefore, less cooling of the air, and
- Timber has a heat capacity and can, depending on the temperature difference, heat or cool the air. The scenario here was that warm timber, being heated up during the daytime, transferred heat to the air at night, as it passed over it, and resulted in a rise in air temperature. At night, the air was heated by the hot stack and absorbed heat.

The results in this study showed that initially the evaporation at night had the biggest influence on TDAL. Towards the end of drying, the heat stored in the timber dominated the in-kiln temperature

at night. The possibility of adsorbed moisture meant that the MG was reduced and it conditioned the wood. However, a better analysis of the evaporation and adsorption can be obtained by the change in AH across the load. This will be analysed in Section 4.3.4.1.

During the mornings until noon, the air temperature drop across the load was not only due to evaporation, but there was also cooling of the air by the cold timber.

Summary:

- TDAL occurred during the full 24-hour day initially. When wood MC dropped below 45%, TDAL occurred only in daylight hours, and the air was heated by the load during night hours.
- Timber has a heat capacity and can supply heat to or absorb heat from the air in the Saasveld solar kiln. This occurred simultaneously with the TDAL and should be considered in drying characterised with diurnal fluctuations, such as the Saasveld solar kiln.

#### 4.3.4 Evaporation of wood moisture from the load inlet to the load outlet

The evaporation of moisture from the timber and the subsequent absorption of vapour by the air as it travelled through the timber stack will be discussed in the following sections investigated. The change in AH is first investigated and thereafter the change in EMC. The effect of the stack width is then examined to see whether the air was saturated with vapour as it travelled through the stack. Lastly, the amount of evaporation that occurred is calculated.

##### 4.3.4.1 *Absolute humidity (AH) at the load inlet and outlet*

The AH at the load inlet and outlet was calculated, to investigate the amount of evaporation that took place during the five stages of the drying run. Data is presented as a typical day in each of the five drying stages. Figure 4.11 provides an overview of the average change in AH of the air as it flows through the timber stacks,  $\Delta AH_{Load} = AH_{Load\ Out} - AH_{Load\ In}$ . When  $\Delta AH_{Load}$  is positive, the timber lost moisture, and when negative, the timber adsorbed moisture from the air.

It is clear from Figure 4.11 that evaporation started around 07h30 and stopped around 16h45.

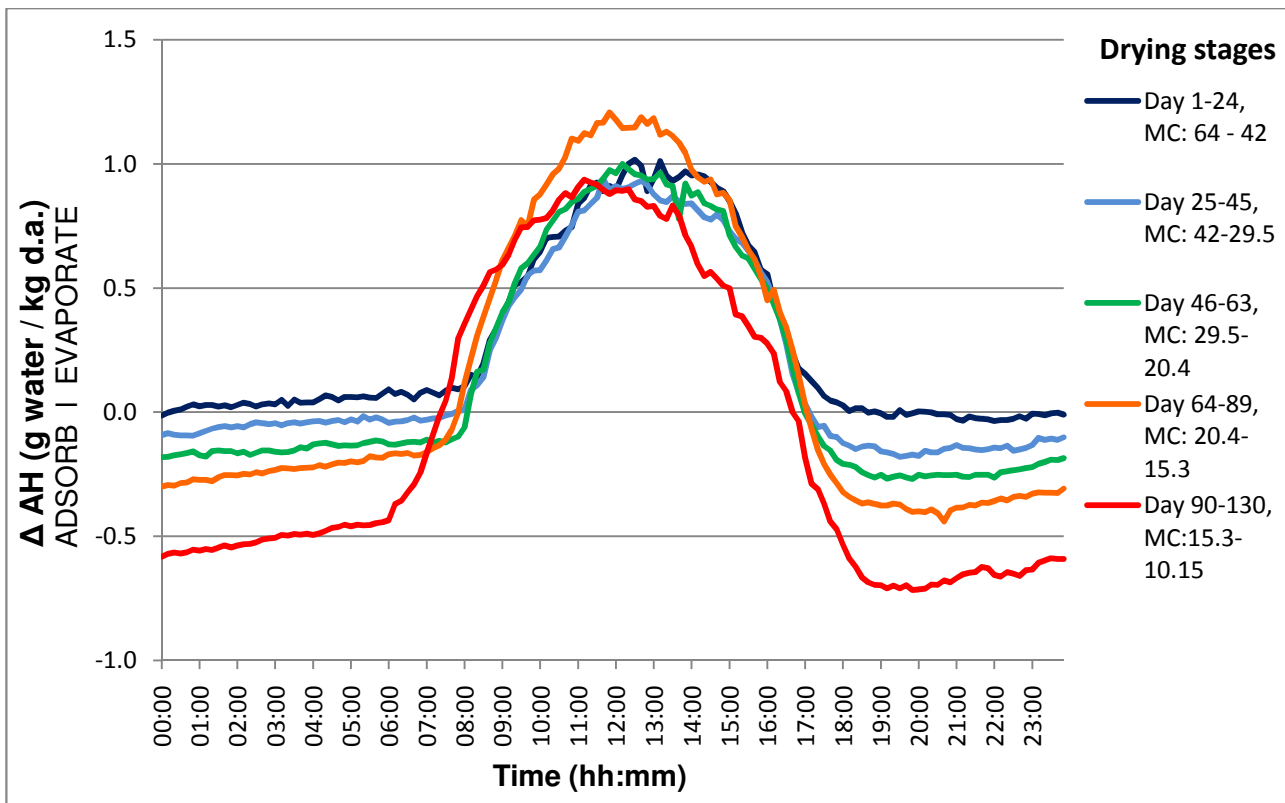


Figure 4.11: Difference in AH between load outlet and load inlet (or  $\Delta AH_{Load}$ ) during the five stages of drying

During the first drying stage, days 1-24, there was very little evaporation between 01h00 and 08h00, since it occurred mainly from 08h00 – 18h00. During the subsequent four drying stages, evaporation only occurred from about 07h30 until 16h45. During the nocturnal hours, from 16h45 to 07h30, the  $AH_{Load Out}$  was smaller than  $AH_{Load In}$ . This means that water was carried to the stack by the airflow. This resultant adsorption of moisture by the load at night benefits the release of drying stresses as it is adsorbed on the wood surface. This adsorption increased as drying progressed.

The main circulating fan could be switched off during the night once the timber reached 45% MC since there is little evaporation. This action will use less electricity. Also, with no airflow, there is less heat transfer through convection from timber to air and the load will stay at a higher temperature for a longer time. This may promote diffusion to the surface layers of the timber and will result in smaller moisture gradients. The evaporation during the following day may be faster as the moisture is closer to the surface and will have a shorter transfusion path to the air stream. The influence of the temperature on the diffusion coefficient will be examined further in Section 4.3.4.2 where the evaporation rate is discussed. This zero airflow at night would cause less cooling of the load and the resulting higher wood temperatures would promote diffusion of moisture to the wood

surface. This also promoted the equalising of MGs in the timber. More research is required on the airflow through the load at different times of the day and different MCs.

A very interesting observation was the maximum negative values for  $\Delta AH_{Load}$ . A maximum negative value means maximum moisture adsorption by the load. The times of maximum adsorption is displayed in Table 4.8.

Table 4.8: Maximum negative values for  $\Delta AH_{Load}$  for the five drying stages

Drying stage (Day)	Wood MC range (%)	Time of maximum adsorption
1 - 24	64 - 42	22h00
25 - 45	42 - 29.5	20h00
46 - 63	29.5 - 20.4	19h50
64 - 89	20.4 - 15.3	19h50*
90 - 130	15.3 - 10.15	19h50

\* One outlier was recorded at 20h40.

It is clear that the time when maximum negative  $\Delta AH_{Load}$  was reached, occurred earlier at each stage, until approximately FSP was reached. The time of maximum adsorption proved to be at 19h50. A probable reason for this time is that in the early evenings, there was still a moisture gradient in the timber from the day's evaporation. The timber was the most receptive for moisture adsorption before the MG was relieved by vapour transfusion from the wood core. Note that moisture adsorption proceeded until the next morning at about 07h30.

The question arises as to whether the fans should be switched off some time after the minimum  $\Delta AH_{Load}$  has been reached, for example at 21h00, in order to allow moisture to be adsorbed by the wood surface. However, if the fans are switched off at 17h00, there will be electricity savings, the timber core temperature will drop slower and the MG will be relieved during the night by moisture migration from the core to the surface, and this moisture will be readily available for evaporation during the next day. More studies need to be conducted into the airflow practices in this type of solar kiln to maximise positive effects.

The real values of  $\Delta AH_{Load}$  can be seen in Figures 4.12 – 4.16, where the five graphs of the respective three-day measuring periods are shown. The evaporation ( $\Delta AH_{Load} > 0$ ) and adsorption ( $\Delta AH_{Load} < 0$ ) that took place during the drying periods of three consecutive days are visible in these figures.

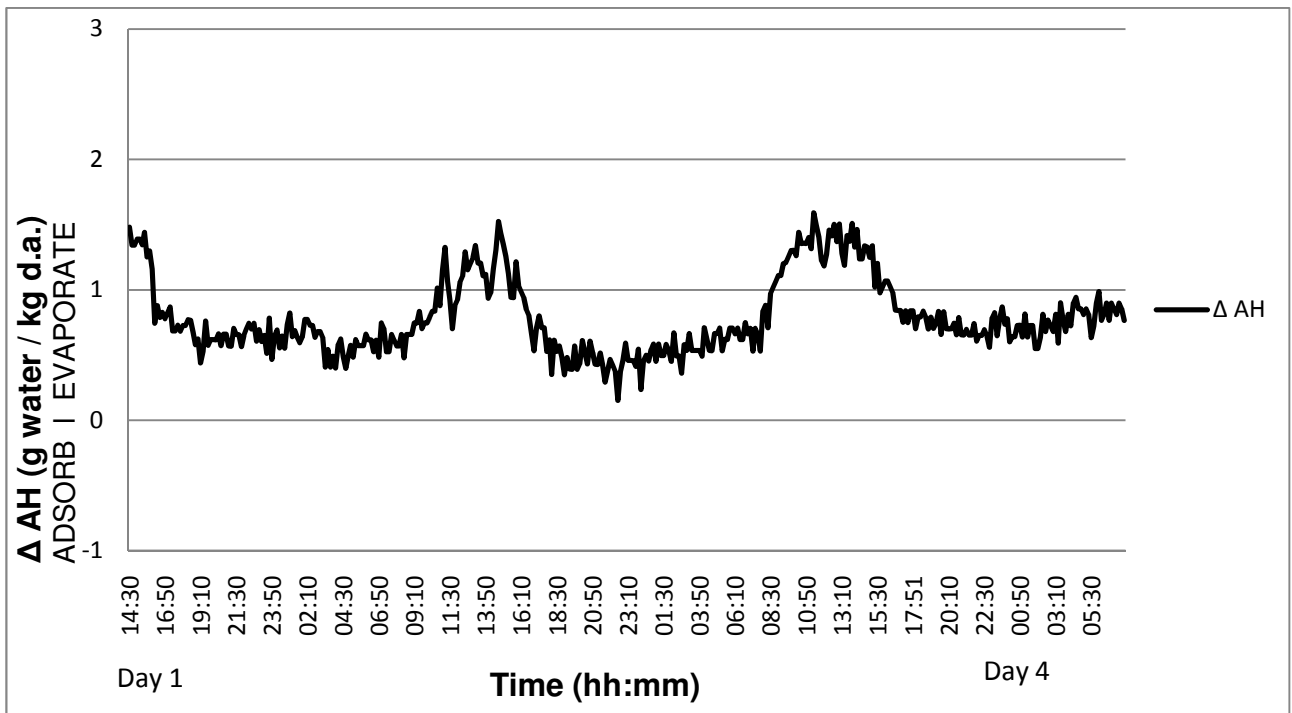


Figure 4.12:  $\Delta AH_{load}$  against time for the measuring period of days 1 - 4; MC = 50%

The initial drying was characterised by continuous evaporation as  $\Delta AH_{load}$  remained positive throughout the 24-hour day. As the MC reached 45%, periods of  $\Delta AH_{load} < 0$  g water/kg dry air were seen during the night hours. The nocturnal  $\Delta AH_{load}$  values became progressively more negative (thus more adsorption) from Figure 4.13 to 4.16 (i.e. when the MC dropped from approximately 45% to 15%).

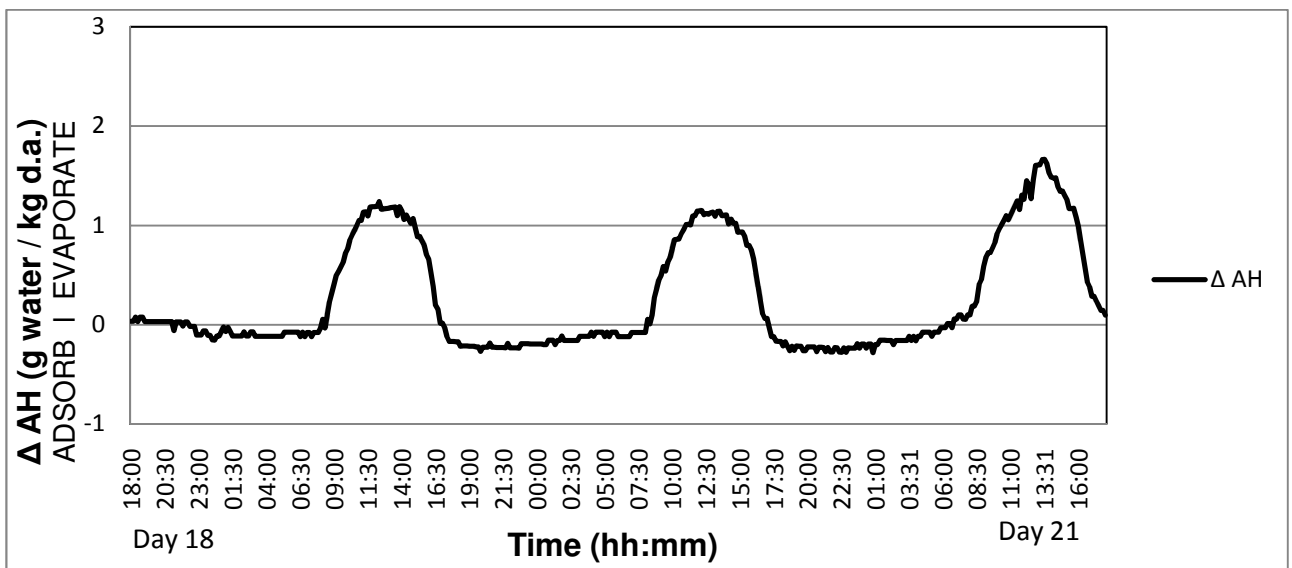


Figure 4.13:  $\Delta AH_{load}$  against time for the measuring period of days 18 - 21; MC = 42%

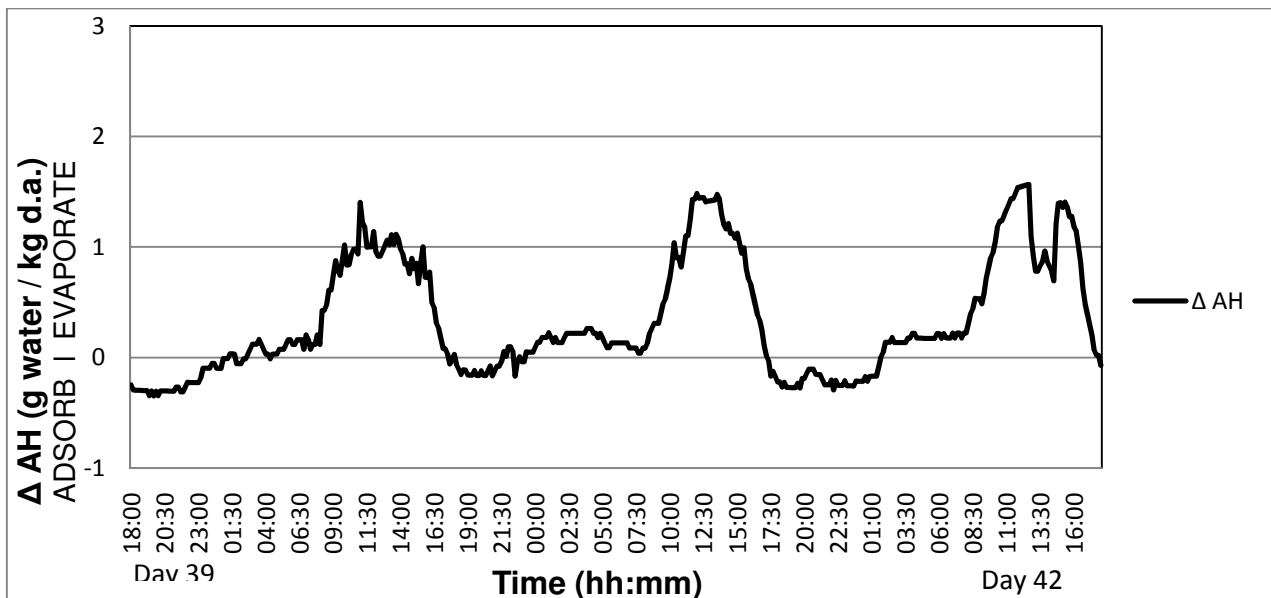


Figure 4.14:  $\Delta AH_{load}$  against time for the measuring period of days 39 - 42; MC = 29%

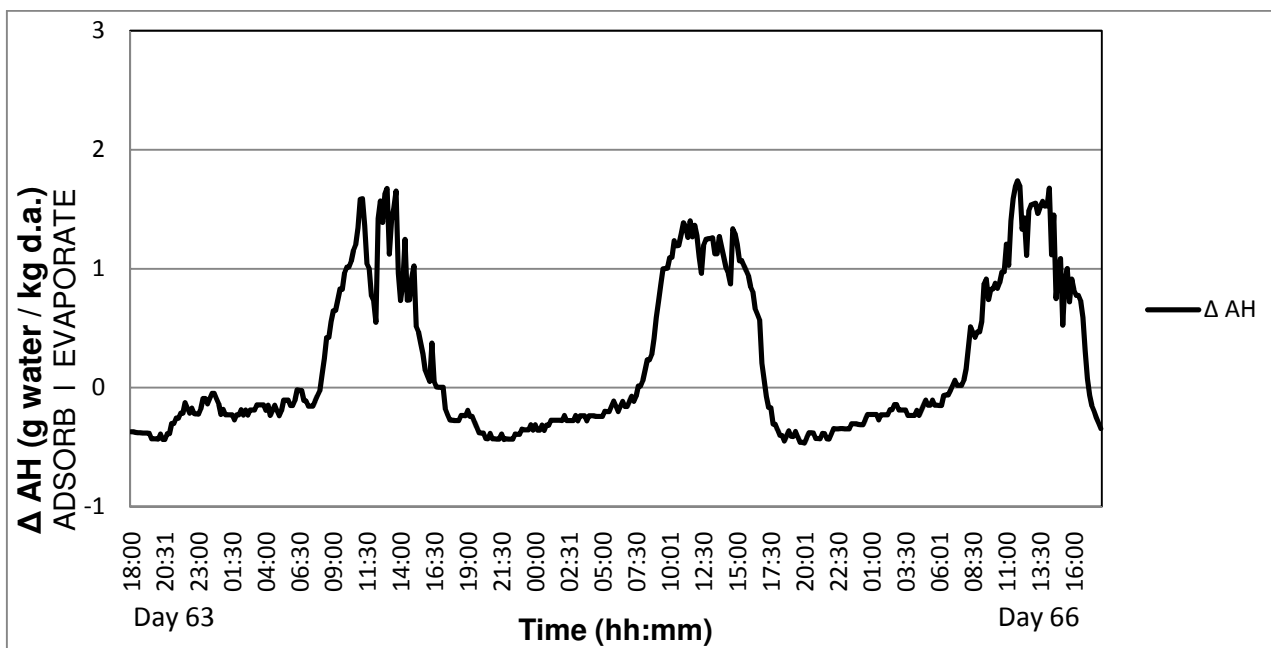


Figure 4.15:  $\Delta AH_{load}$  against time for the measuring period of days 63 - 66; MC = 20.5%



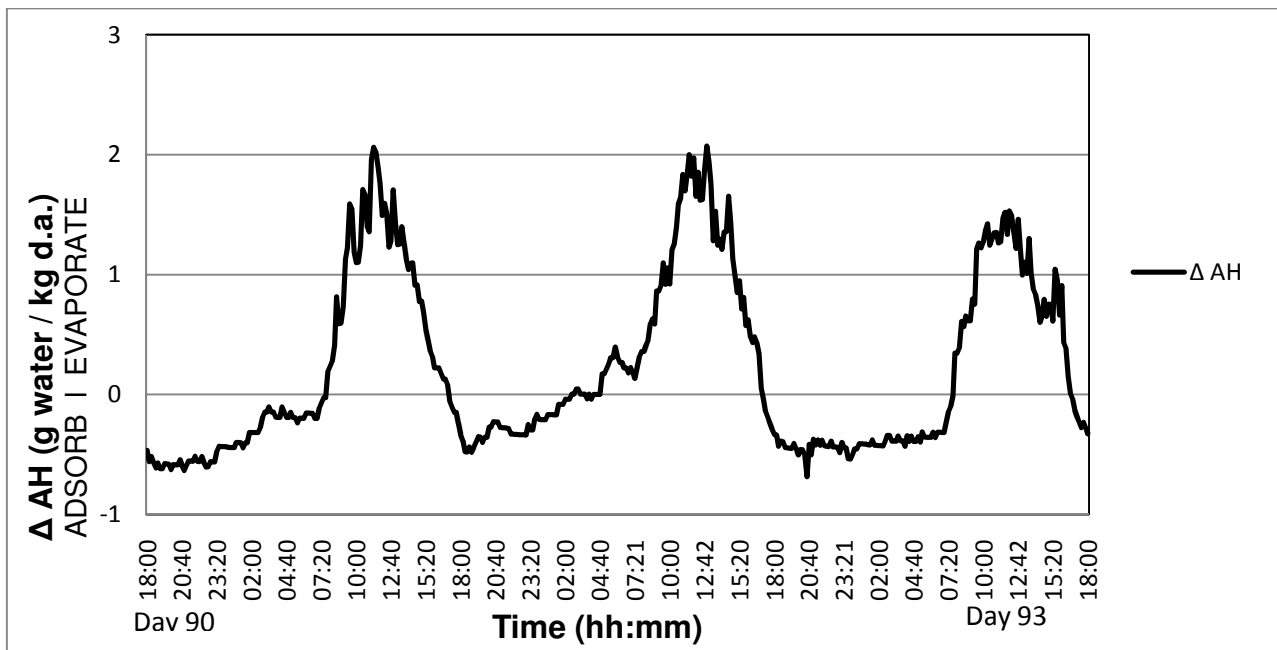


Figure 4.16:  $\Delta AH_{load}$  against time for the measuring period of days 90 - 93; MC = 15.3%

The increased nocturnal negative  $\Delta AH_{load}$  values from Figure 4.13 to 4.16 indicate an increased adsorption of moisture on the wood surface at night as the timber dried.

#### Summary:

- Evaporation definitely occurred at night when the wood MC was higher than 45%, although not throughout the entire night.
- Evaporation generally started around 07h30 and stopped around 16h45 when the MC was below 45%.
- The timber load adsorbed moisture during the night which benefited the release of the MG and therefore the drying stresses. This adsorption increased as drying progressed.
- The maximum adsorption initially occurred at 22h00. When the MC approached FSP, the maximum adsorption occurred constantly at 19h50.
- Nocturnal adsorption of moisture on the wood surface increased as the timber became dryer.
- A general pattern of evaporation during the day and a little moisture adsorption at night existed when the MC was below 45% MC.
- The suggested time to switch off the main circulating fan is from 17h00 to 07h30, once the timber reaches 45% MC. This fan could run up to 21h00, for example, to supply water vapour for adsorption by the wood, though the benefits from the electricity savings, slower cooling of the timber core and automatic relieve of MG by transfusion of water from the wood core, may outweigh the advantages of adsorption of water on the surface.

#### 4.3.4.2 Load Inlet and outlet EMC conditions on selected days

The EMC Load In measurements were discussed in 4.3.2. The change in EMC as air travelled through the timber load will be discussed here in order to examine the change in drying conditions.

Measuring periods of three consecutive days were analysed by comparing selected days after the wet bulb wicks were cleaned and water reservoirs filled. The results from these periods will be accurate.

The initial drying period (days 1-4), indicated in Figure 4.17, was dominated by a high evaporation rate during the day and a smaller one by night. EMC Load Out was consistently higher than EMC Load In for both day and night. Note the constant behaviour of the EMC Load In. It had an average EMC of 15.03%, with a standard deviation of 0.76%. This pattern was soon to change as drying progressed.

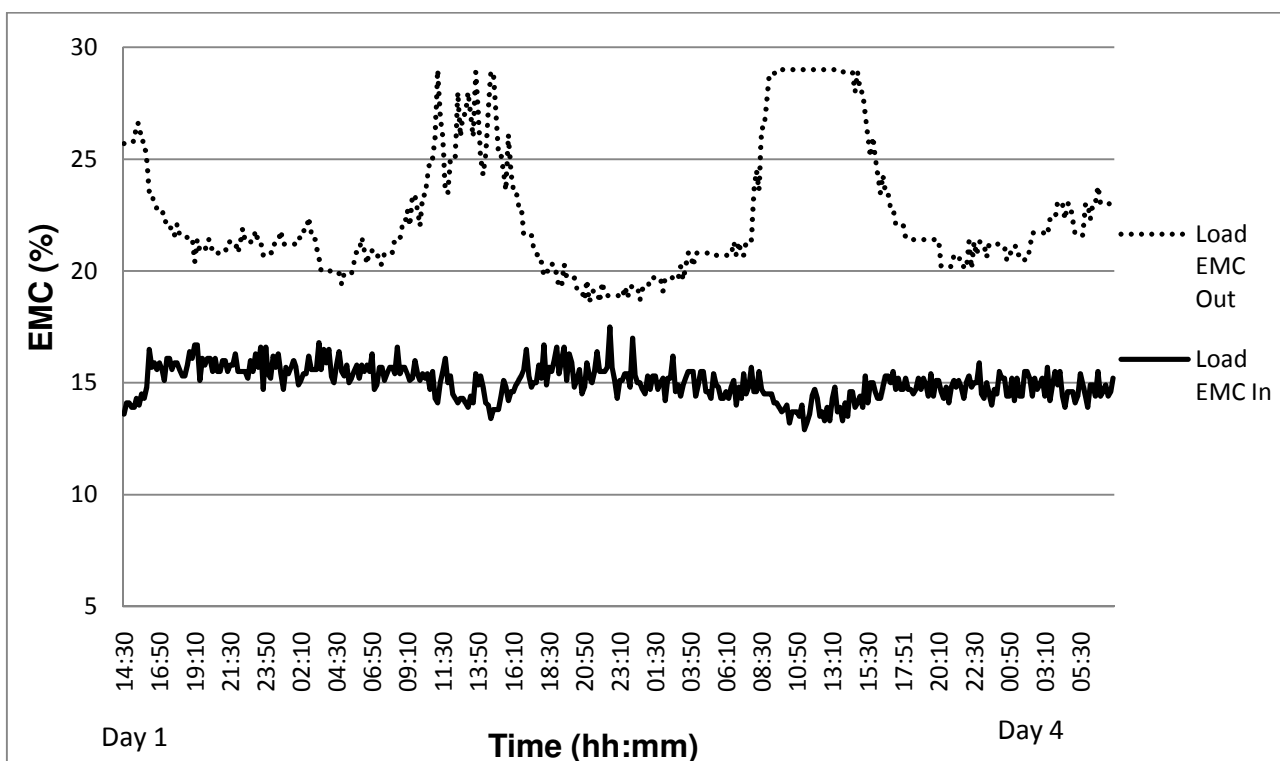


Figure 4.17: Load inlet and outlet EMC against time for days 1 - 4; MC = 50%

Whenever the EMC reached a figure close to 28% (approximately FSP), it can be interpreted as conditions favourable for the air to be saturated with vapour ( $RH \approx 100\%$ ). This can be seen at the air exit from the load for brief periods on day 2 and for some time on day 3 (Figure 4.17). This period on day 3 had a relative humidity of more than 95% for 5½ hours. The saturation due to the effect of stack width is discussed in Section 4.3.4.3.

The EMC Load Out easily reached approximate saturation during the day during this initial period. The higher temperatures in the day and the availability of free water increased the evaporation rate and therefore the air reached saturation rather easily as it travelled through the load. The saturation is visible for brief periods during days 18-21 in Figures 4.17 and 4.18. The saturation appears to only have occurred during the initial stage of drying when the MCs were above FSP. This behaviour already stopped when FSP was reached on day 39.

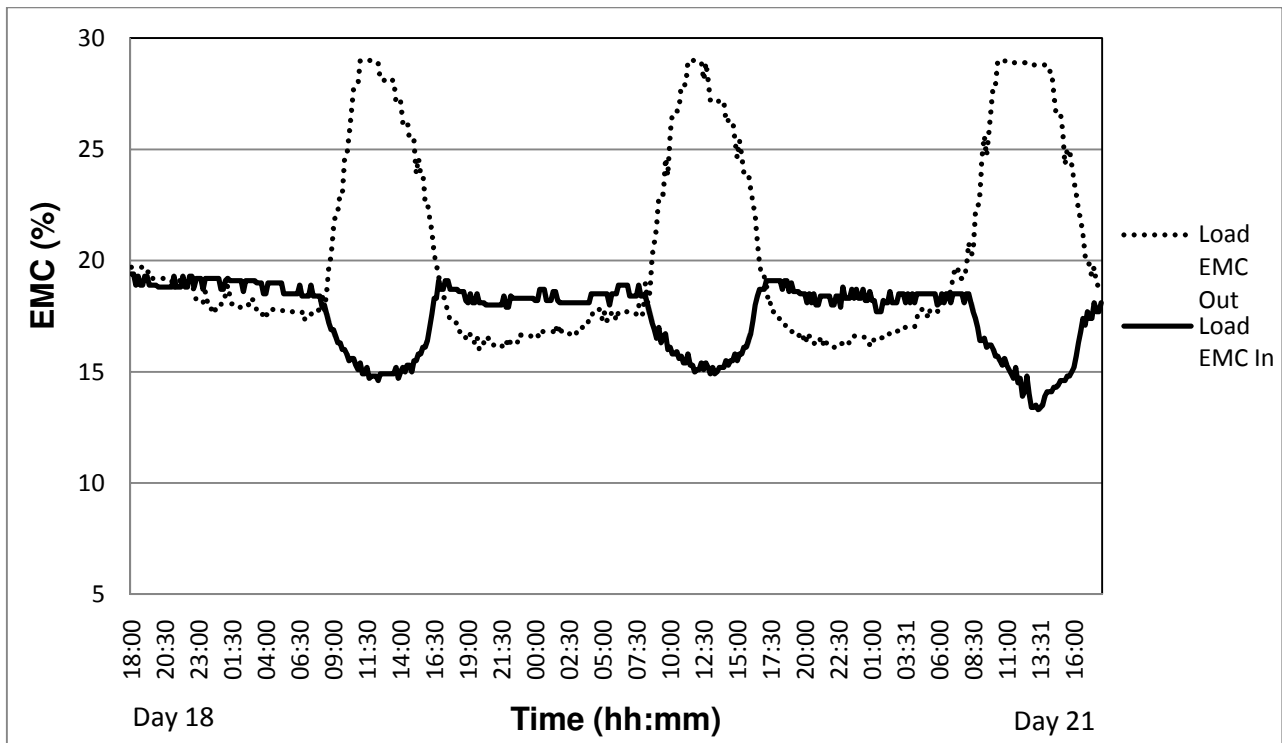


Figure 4.18: Load inlet and outlet EMC against time for days 18 - 21; MC = 43%

Day 21 (19 June) was a warm day, and was dominated by Bergwind conditions as previously discussed. The result was that saturated conditions existed for a longer time. The protection offered by the kiln is evident by the saturation inside the load.

From Figures 4.18 - 4.22, it can be seen that EMC Load Out was only greater than EMC Load In during the day when the MC dropped below  $\approx 45\%$ . The difference between day and night became smaller as drying progressed, due to the water in the timber that became less available as the MC decreased. At night there was a drop in  $EMC_{in}$  due to:

- the air being heated by the warm timber
- the moisture that was deposited on the wood surface

Days 39-42 were also characterised by a Bergwind spell, and EMC conditions in the kiln are displayed in Figure 4.19 together with external EMC.

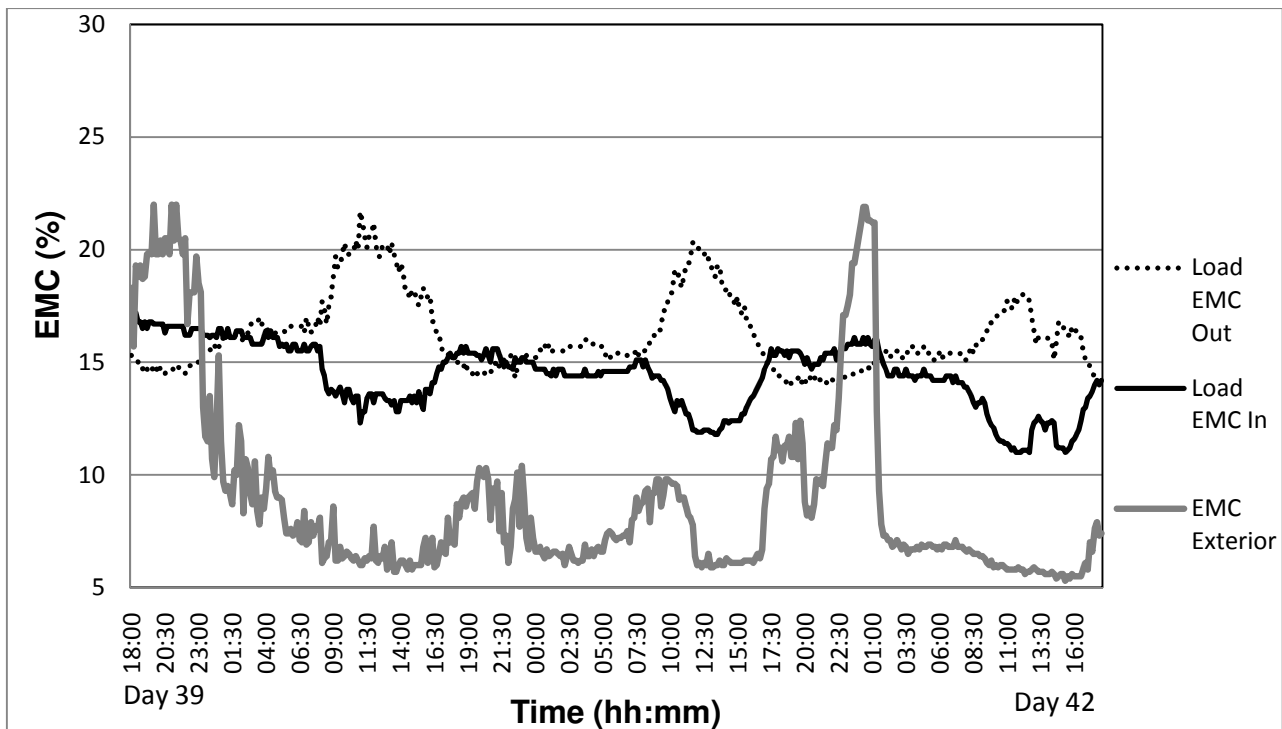


Figure 4.19: Load inlet and outlet and external EMC against time for days 39 - 42; MC = 30%

The exterior EMC had no influence on the conditions inside the kiln as there was no air exchanged between the kiln air and external air. A maximum temperature of 27.5°C and a minimum EMC of 5.4% were recorded outside the kiln. Previously, Bergwind conditions with an EMC as low as 1.9%, together with a temperature of 38°C, had been recorded. Timber above FSP would suffer severe drying defects if it was exposed to these conditions. The EMC Load In was limited to 11%. It is evident that the temperatures inside the kiln and especially the EMC did not respond to these harsh external conditions. When the MC dropped below FSP, and wood can withstand higher temperatures, it was found that maximum temperatures inside the kiln rose as indicated in Figure 4.5 (p.51).

The following three figures (Figure 4.20 to 4.22) indicate the consistent decrease in EMC Load In, and that the difference between the EMC Load In and EMC Load Out were getting smaller.

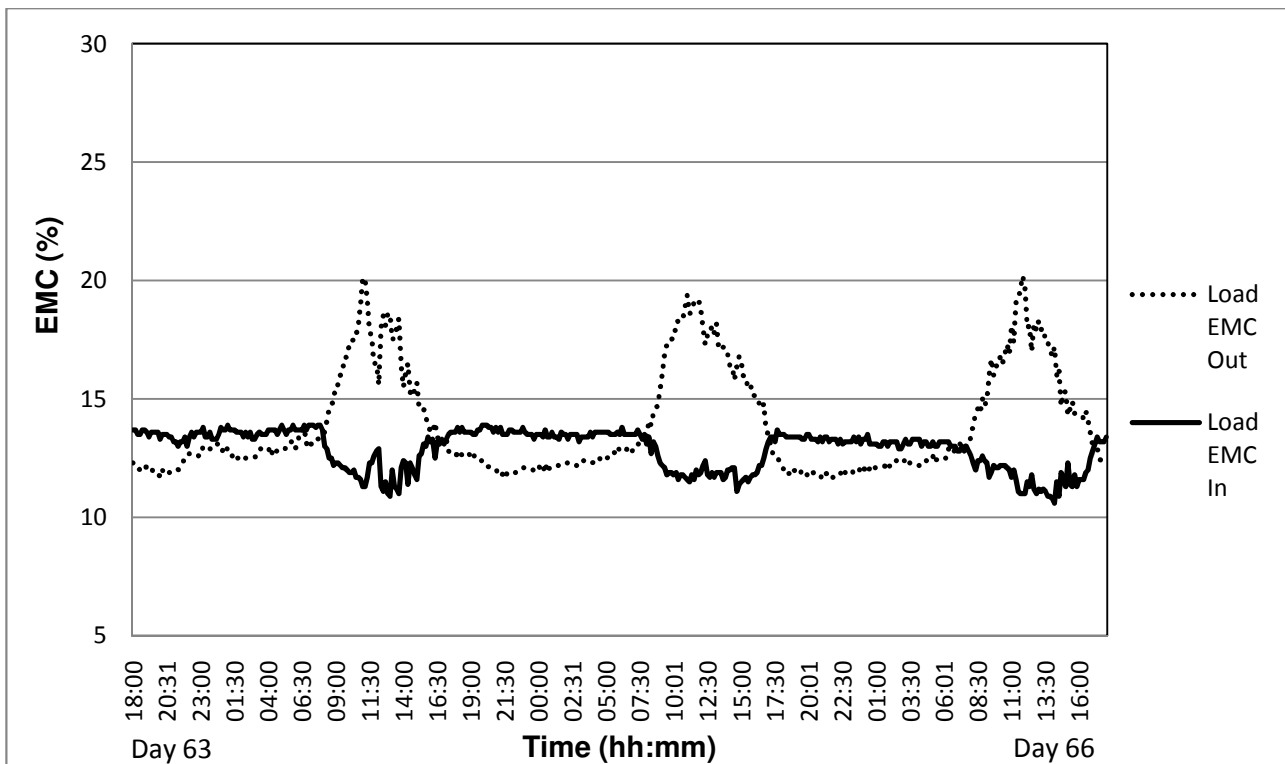


Figure 4.20: Load inlet and outlet EMC against time for days 63 - 66; MC = 20.5%

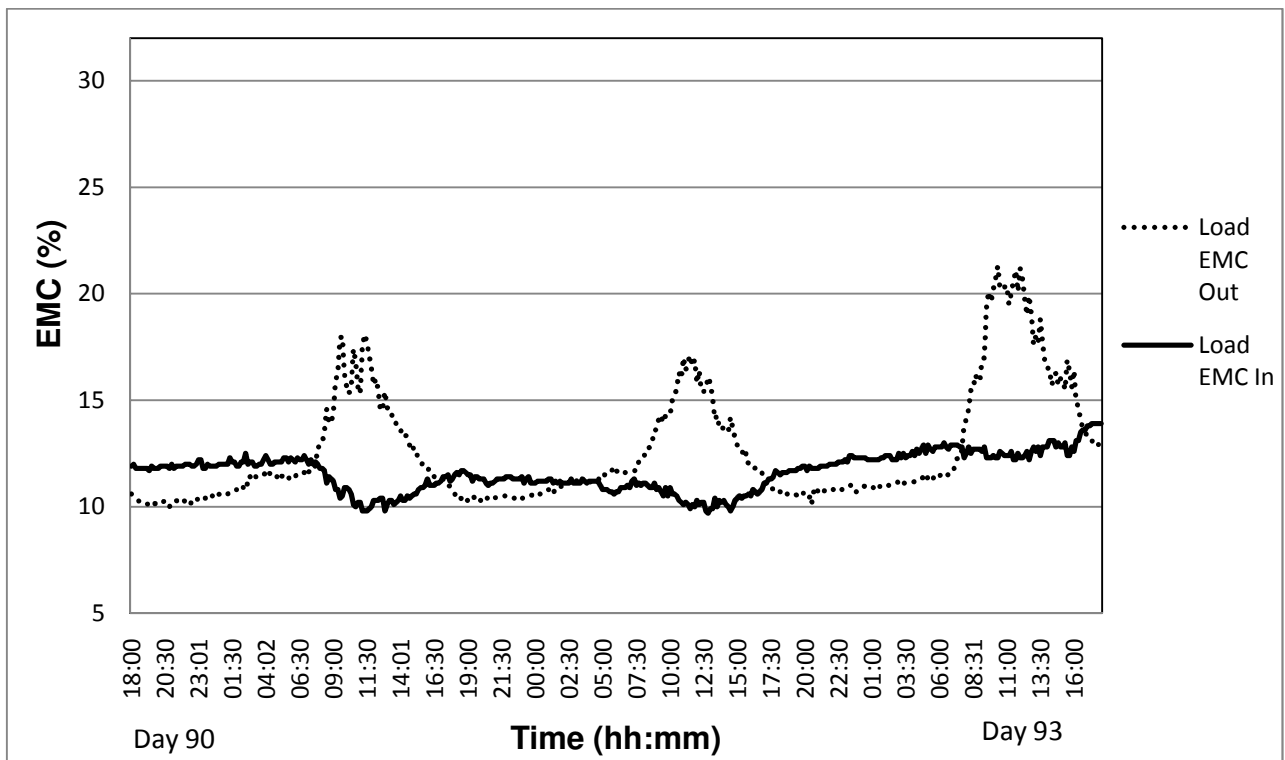


Figure 4.21: Load inlet and outlet EMC against time for days 90 - 93; MC = 15.3%

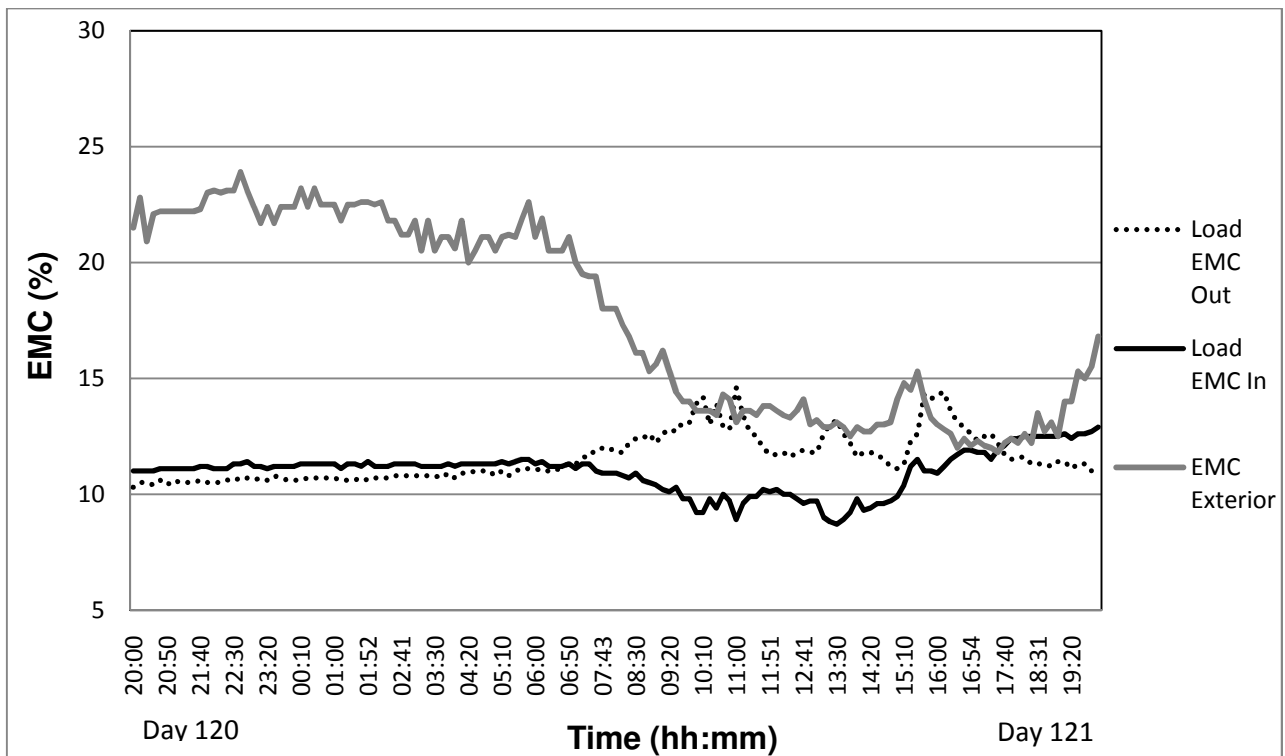


Figure 4.22: Load inlet and outlet and external EMC against time for days 120 - 123; MC=10.3%

Figure 4.23 indicates the temperatures as measured at the air inlet, air outlet and the kiln exterior. The time of evaporation in Figure 4.22 is easily identified by the TDAL in Figure 4.23. The kiln temperature remained consistently higher than the kiln exterior temperature.

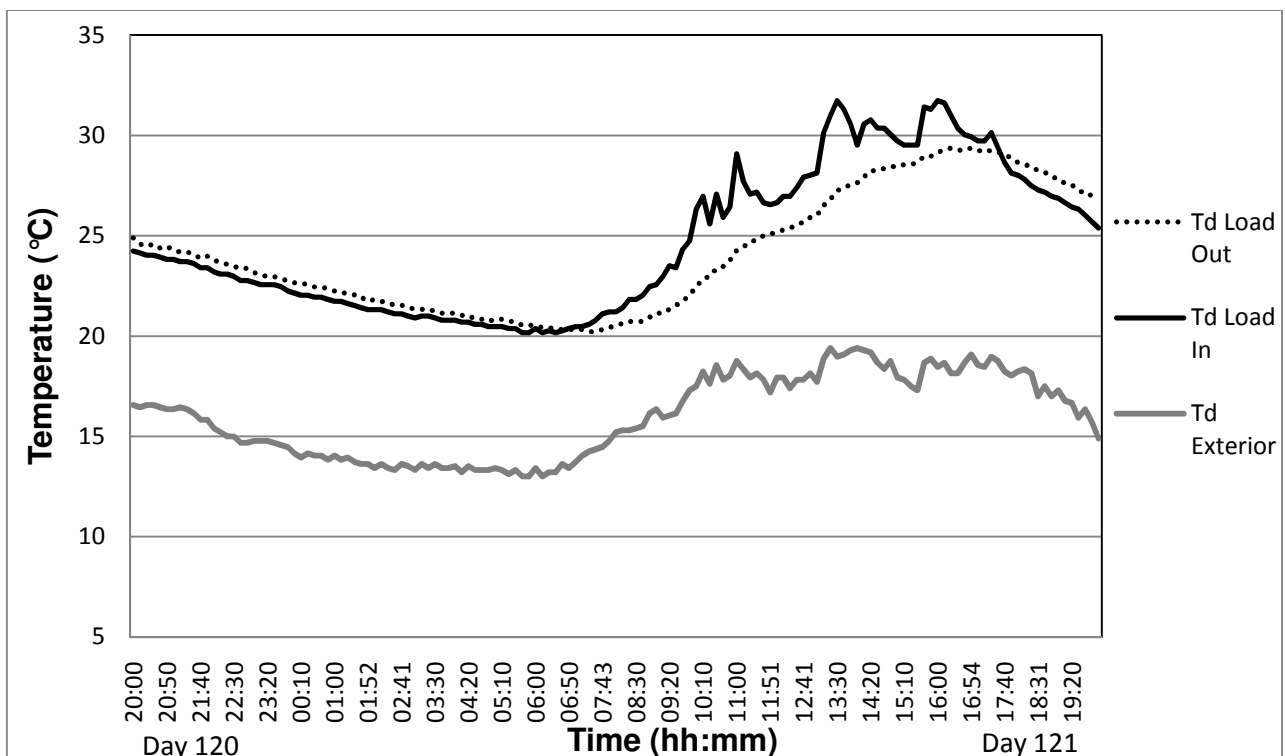


Figure 4.23: Load inlet and outlet and external  $T_d$  against time for days 120 - 123; MC = 10.3%

The {Load EMC Out – Load EMC In} values during the day became progressively smaller as the timber dried. The negative values of {Load EMC Out – Load EMC} In at night were the result of the small rise in air temperature through the load at night and re-adsorption of moisture into the wood surface, as previously discussed. The small rise in air temperature at night, and, therefore, a lower EMC Out, was due to the timber being heated up during the daytime and cooling off at night. The graph of days 1-4 (Figure 4.17) did not indicate this – probably due to the high amount of evaporation that cooled the load, while the evaporated moisture increased the EMC. From this stage on, the exiting EMC was lower than entering EMC for most of the night hours.

These results again indicated that the entire timber load was never exposed to periods of low EMCs. This resulted in small moisture gradients throughout the entire drying period, evident in the measured ZA Dry Q results of the MG. Consequently, the drying stresses formed during drying remained small, and this was affirmed by the excellent drying quality in terms of practically no checks and little case-hardening forming in the timber.

The surface layers soon dried to below FSP and started to shrink. Diffusion from inside the boards was responsible for the transfer of moisture to these dry surface layers. The diffusion was thus critical to achieve a low MG, small drying stresses and no surface checks. During the night, the bound water continued to migrate to the surface as the core temperature of the timber was still high. Diffusion is a function of the temperature of the medium, with diffusion being faster through a heated medium. This relationship is documented in Section 2.4.1 where Haque and Langrish (2006) described the diffusion coefficient of bound water transport within Australian hardwoods. As an example, the diffusion coefficient at 30°C was determined as  $5.1 \times 10^{-11} \text{ m/s}^2$ , about 1.5 times greater than that at 20°C ( $3.3 \times 10^{-11} \text{ m/s}^2$ ).

More clarity on the phenomenon of diffusion at night with regard to its equalising effect was obtained when the nocturnal kiln temperature ( $T_d$  Load In) from 17h00 to 07h30, was investigated for the five drying stages. The calculated diffusion coefficient inside the kiln was compared with the diffusion coefficient outside the kiln for each of the five stages (see Table 4.9). The temperature values used were the average  $T_d$  Load In and the average  $T_d$  External. The external temperature was used to indicate the advantage gained by using the solar kiln. A better analysis of the diffusion would have been possible if the wood core temperature was available. The internal and external kiln temperatures will be thoroughly discussed in Section 4.3.6. The values here will only be used to evaluate the effect on the diffusion in the solar kiln.

Table 4.9: Calculated diffusion coefficients for the nocturnal hours inside and outside the kiln as obtained from the average temperatures in each drying stage

Day range of drying stages	MC range (%)	Nocturnal average $T_d$ Load In ( $^{\circ}\text{C}$ )	Nocturnal D Inside ( $\text{m/s}^2$ )	Nocturnal average $T_d$ External ( $^{\circ}\text{C}$ )	Nocturnal D External ( $\text{m/s}^2$ )	% Increase in D from external to inside ( $^{\circ}\text{C}$ )
1 - 24	64 - 42	17.7	3.1E-11	12.7	2.5E-11	125.3
25 - 45	42 - 29.5	16.1	2.9E-11	12.0	2.4E-11	120.4
46 - 63	29.5 - 20.4	16.6	2.9E-11	10.3	2.2E-11	133.2
64 - 89	20.4 - 15.3	18.5	3.2E-11	10.7	2.2E-11	142.3
90 - 130	15.3 - 10.15	20.9	3.5E-11	11.9	2.4E-11	149.5
Total 1 - 130	Average	18.4	3.2E-11	11.6	2.3E-11	136.1

It is clear that the higher nocturnal temperatures inside the kiln increased the diffusion coefficient inside the kiln on average by a factor 1.36 compared to the diffusion coefficient outside the kiln. It is also clear that the nocturnal temperature between the inside and outside of the kiln, increased towards the end of drying. The nocturnal diffusion coefficient inside the kiln increased by 1.5 times compared to the outside the kiln, assuming the wood core temperature equalled the temperature that the timber was exposed to. This is an ideal situation for the last drying stage before the kiln is de-stacked. The kiln load was exposed to 40 days of this improved diffusion. The results with the Saasveld solar kiln showed a state where the MG that formed during the day, was equalised at night. When the sun heated the kiln the next morning, the EMC in the kiln dropped and drying was continued.

The combined slower surface drying that occurred during the night and the vapour transfusion experienced under the influence of a higher wood core temperature could have been instrumental in obtaining the small MGs produced throughout the entire drying period, and the resulting lower occurrence of case-hardening and check-free timber.

A suggestion for further possible research would be to measure wood core temperatures during a drying cycle. This should confirm the levels of heat collection and heat loss during diurnal drying cycles.



As discussed in Section 3.8, the evaporation of water from the wood surface can be compared to the adiabatic saturation process which results in the wet-bulb temperature and the adiabatic saturation temperature being approximately equal. It was, therefore, standard practice to use only one properly working wet-bulb temperature probe. The wet-bulb temperature stayed constant under these drying conditions. However, the diurnal temperature fluctuations in the solar kiln differed from the constant conditions in a standard kiln. There was a constantly varying heat transfer between the timber and the air, as temperatures fluctuated between the day and night. This affected the wet bulb temperatures and it is, therefore, suggested that future research in a solar kiln should employ a wet bulb at the exit side of the load to investigate this phenomenon.

#### Summary:

- There was an EMC increase across the load only during the day. This EMC increase became smaller as the MC decreased.
- At night there was a drop in EMC of the air as it moved across the load, due to moisture deposited on the wood surface. Furthermore, the air was heated by the warm timber, while there was very little evaporation, also causing the EMC to drop.
- The exiting EMC occasionally reached saturation during the day when the MC > FSP.
- The difference between the inlet EMC and exit EMC became smaller as the MC decreased - a sign of a reduced evaporation rate due to a smaller availability of free moisture in the timber.
- Because of higher wood temperatures at night inside the kiln compared to temperatures outside, the diffusion coefficient was 1.5 times higher than for wood outside the kiln.
- The results indicated that the entire timber load was never exposed to periods of low EMCs. This, together with the elevated diffusion coefficient, resulted in small MGs throughout the entire drying period, evident in the measured ZA Dry Q results of the MG.
- Future research should also measure the wood core temperature and the wet bulb temperature at the exit of the load.

#### 4.3.4.3 *The effect of stack width in the Saasveld solar kiln*

The purpose of this investigation was to determine whether the air that travelled through the kiln load became saturated with vapour before leaving the stack. This is known as the effect of stack width. Air, which is saturated with vapour, results in timber with a higher moisture content towards the outlet of the load. If saturated conditions occurred for some time, then it means that the length of air travel was too long or the air velocity was too low. The load exit dry bulb temperature minus dew-point temperature of the exit air,  $\Delta DP_{load} = \{T_d \text{ Load Out} - DP \text{ Load Out}\}$  was compared for the same drying stages used before. It must be noted that the movement through the timber is

assumed as an adiabatic saturation process, where the wet-bulb stays constant as the air moved through the load. This was not exactly the case as the diurnal influence in the solar kiln proved in Sections 4.3.3 and 4.3.4. Wet-bulb measurements on the air exit of the load would provide a more accurate indication of the effect of stack width. The DP Load Out values were calculated assuming  $T_w \text{ Load In} = T_w \text{ Load Out}$ .

A zero  $\Delta DP_{\text{load}}$ -value meant that the air was saturated and was on the point of condensation, thus having a relative humidity of 100%. This indicated whether favourable conditions existed for vapour saturation. It should be noted that it is impossible to have a negative value. Data of a typical day in each of the five drying stages is presented in Figure 4.24.

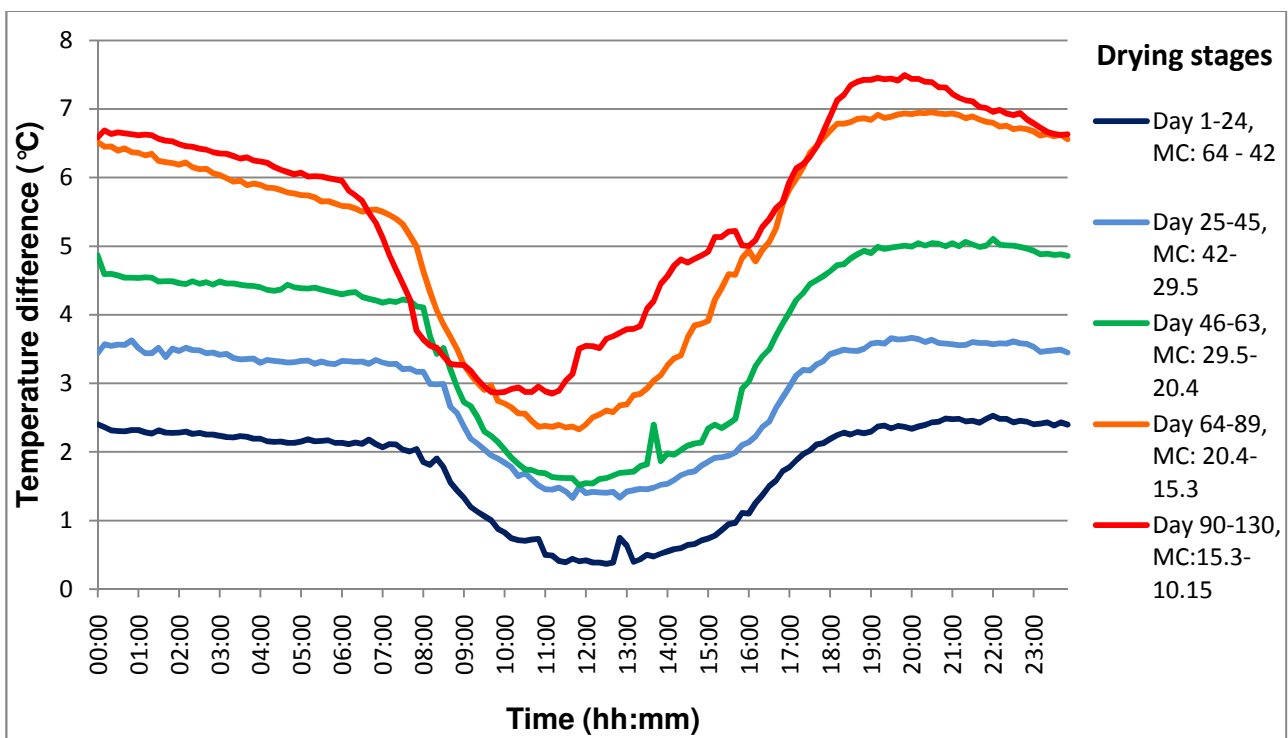


Figure 4.24:  $\Delta DP_{\text{load}} = \{T_d \text{ Load Out} - DP \text{ Load Out}\}$  temperature at various stages of drying

Figure 4.24 indicates that because average values were used, the air that passed through the load was not saturated when it reached the exit of the load and that the air could absorb more vapour. However, there were a number of individual incidences when vapour saturation was reached in the initial drying stage. As drying proceeded, the chances of saturation became less. The trend of the general evaporation time from 07h30 to 16h45, as discussed in Section 4.3.4.1, is clearly visible by the drop in  $\Delta DP_{\text{load}}$  values.

The individual incidences of saturation can be seen in the following six figures (Figures 4.25 to 4.29) of the six three-day drying measuring periods. The data is presented by  $\Delta DP_{\text{load}} = \{T_d \text{ Load Out} - DP \text{ Load Out}\}$ . If  $\Delta DP_{\text{load}} = 0$  then the air was saturated.

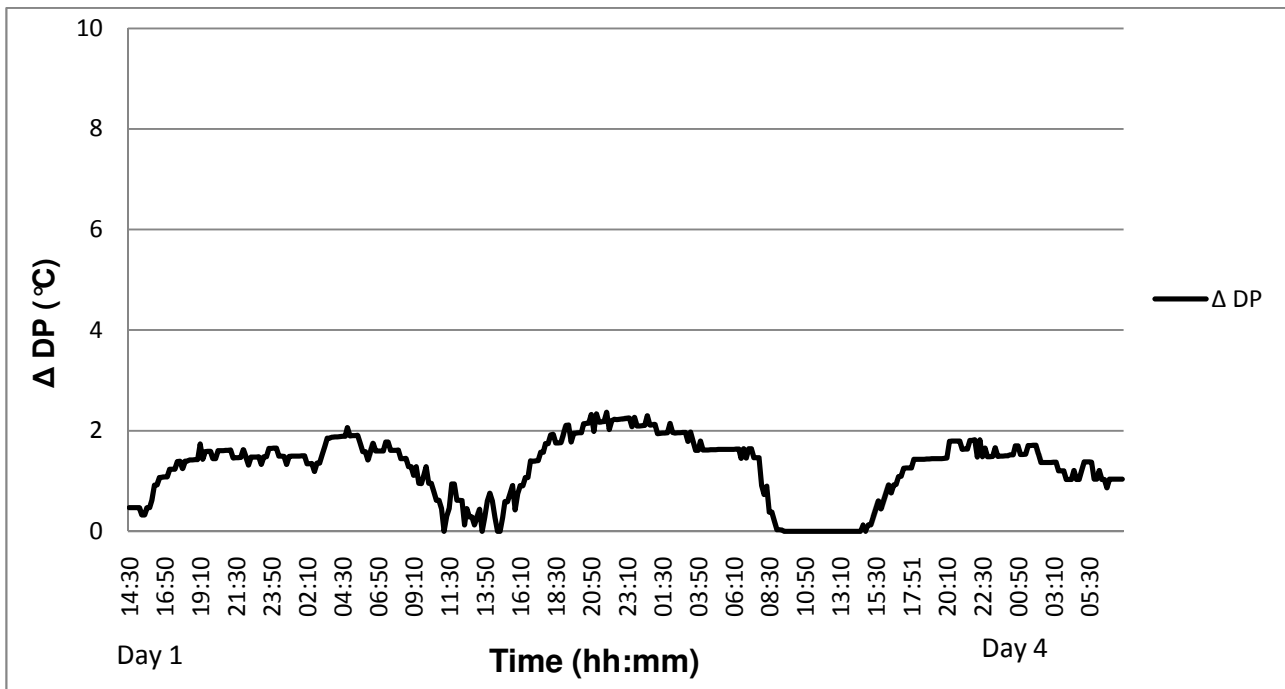


Figure 4.25:  $\Delta DP_{load}$  against time for the measuring period of days 1 - 4; MC= 50%

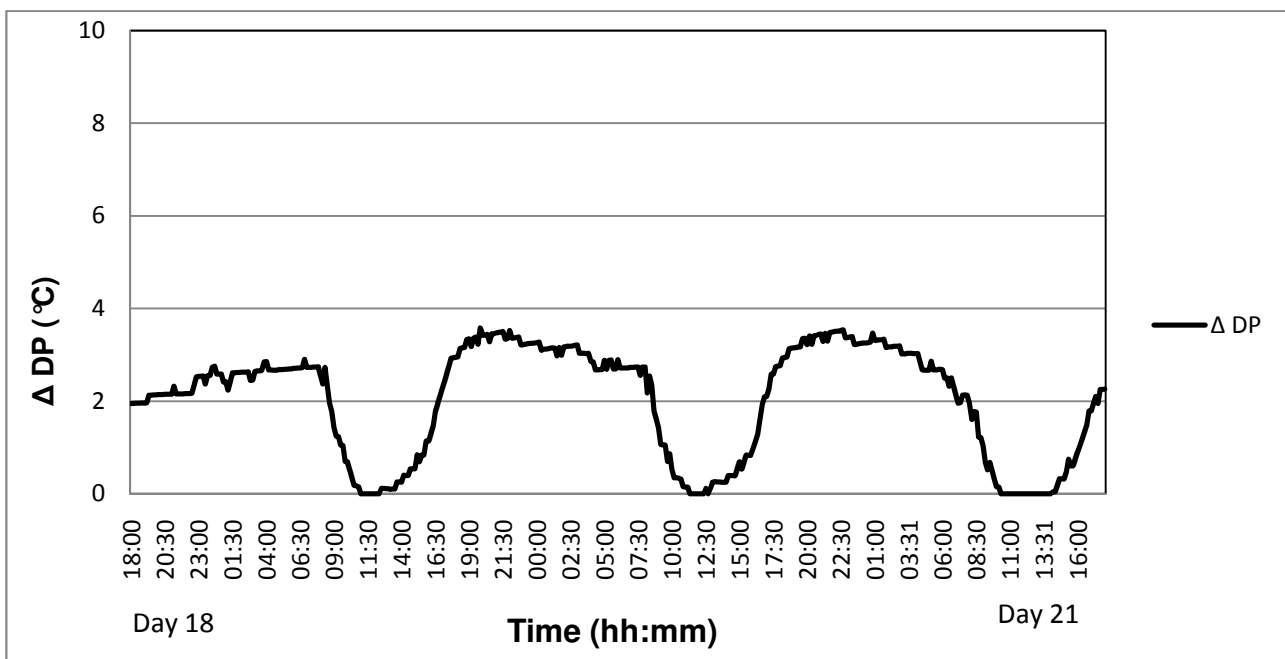


Figure 4.26:  $\Delta DP_{load}$  against time for the measuring period of days 18 - 21; MC = 42%

Since the real value were used and not averages, the individual incidences when saturation was reached, can be seen in the initial drying stage (see Figures 4.25 and 4.26). Vapour saturation could be seen for brief periods on day 2 and for some time on day 3. This period on day 3 had a relative humidity of more than 95% for 5½ hours. Both these periods occurred during daylight

hours. The drying continued with no incidence of vapour saturation when the MC dropped to below 42%.

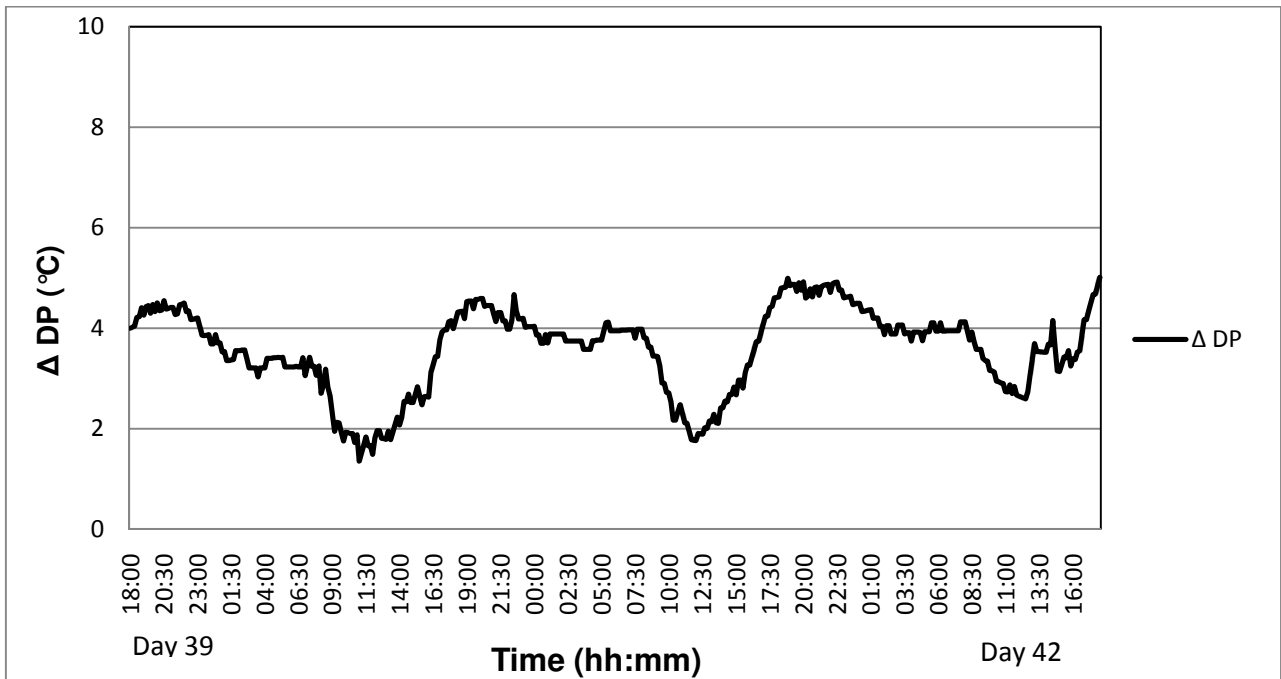


Figure 4.27:  $\Delta DP_{load}$  against time for the measuring period of days 39 - 42; MC = 29%

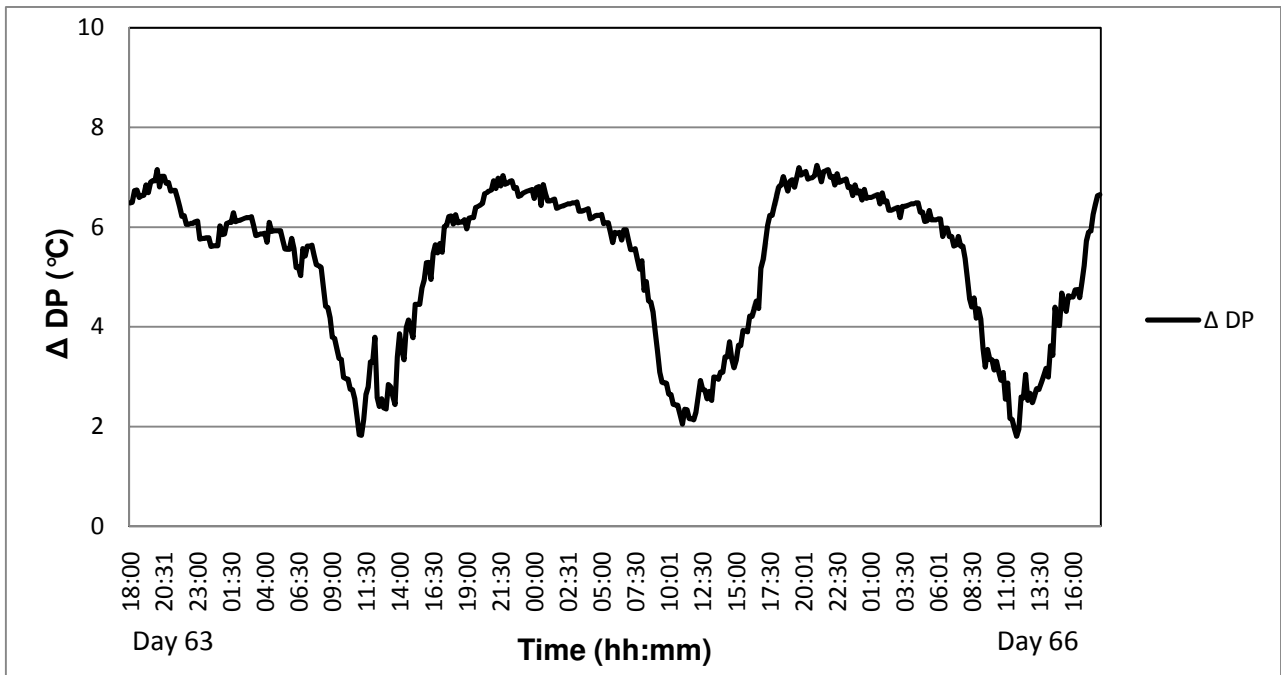


Figure 4.28:  $\Delta DP_{load}$  against time for the measuring period of days 63 - 66; MC = 20.5%

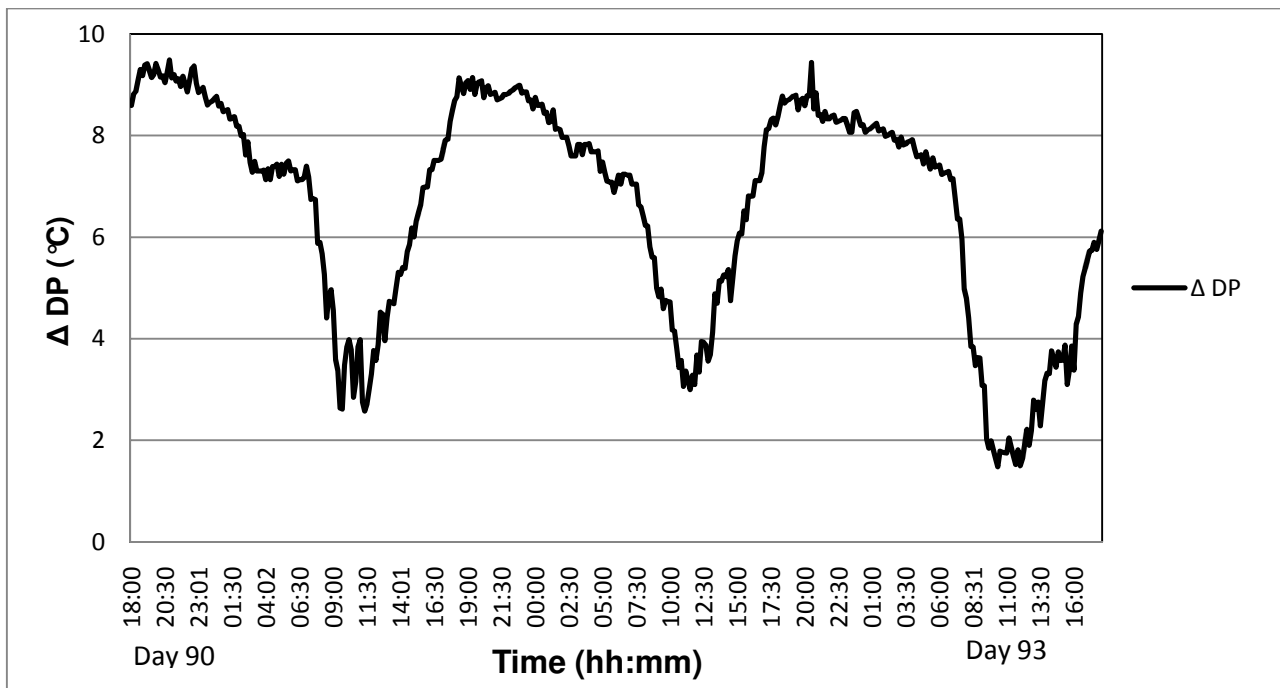


Figure 4.29:  $\Delta DP_{load}$  against time for the measuring period of days 90 - 93; MC = 15.3%

As drying proceeded, the chances of reaching saturation became less. The trend of the general evaporation time from 07h30 to 16h45, as discussed in Section 4.3.4.1, is clearly visible by the rise in  $\Delta DP_{load}$  values during each of the measuring periods.

The brief initial periods of vapour saturation at the exit side of the load had no influence on the wood quality in terms of the MC distribution through the load, as confirmed by the ZA Dry Q audit. However, the length of the air path should be kept in mind for the design of a similar kiln. The air path had a length of 4.8m in the Saasveld solar kiln. A longer air path will mean a better chance of saturation at the load exit. Haque and Langrish (2001) studied the effect of stack width in a greenhouse type solar kiln. Australian ironbark (*Eucalyptus paniculata*) was dried at  $T_d = 60^\circ\text{C}$  and  $T_w = 50^\circ\text{C}$  (EMC = 9%), with an air path of 6.6m, 1.8m longer than the Saasveld solar kiln. The conclusion was that the effect of stack width was insignificant and can be ignored. According to Haque and Langrish (2001), the steady drying conditions in solar kilns makes drying over ten times longer than in conventional drying and the drying rate is correspondingly lower. The required air path length can thus be longer in solar kilns. The equalising at night in the Saasveld solar kiln further reduced the effect of stack width.

#### Summary:

- Vapour saturation at the exit side of the load due to the effect of stack width was negligible in the drying run. A few incidences occurred when the MC was still above 42%.

#### 4.3.5 Dehumidification in the jacket

As expected in Section 2.7, the humidity control, or rather auto-regulation, was achieved by a process of natural dehumidification at night. This type of humidity control is extremely simple as colder night temperatures are a certainty, with no control system and no human intervention necessary in this type of kiln.

The air from the main kiln chamber was circulated through the inflated double plastic layer (the air jacket) where the air came into contact with the outer plastic sheet. When the temperature of this outer sheet was lower than the dew-point of the air in the solar kiln, condensation occurred on the inside of the outer plastic sheet. The condensation collected at the bottom of the inflated air jacket and was released by the weeping holes at the bottom.

The dehumidifying effect was analysed below in Sections 4.3.5.1 and 4.3.5.2 by looking at the properties of the air entering the air jacket, the air exiting the air jacket and the external air. The air properties investigated were the dry bulb temperature, the absolute humidity (AH) in g water per kg dry air, and the dew-point (DP). The difference in entering and exiting AH in the jacket indicated the amount of dehumidification that took place.

The position of the temperature probes in relation to the layout of the kiln is shown in Section 3.7.3 (p.32). It is important to note that the probes at the jacket exit were positioned at the eastern side of the kiln, resulting in a rapid rise in temperatures in the mornings.

The kiln was also not perfectly air-tight; therefore, it exchanged minute amounts of air with the ambient air, resulting in a lower humidity inside the kiln. These openings are mostly at the double back door and small holes, left by a troop of curious baboons. A solution is provided in Annexure A. These small holes were covered with transparent “Nitto” greenhouse repair tape, provided by Rhino Plastics. The chances of small holes to the outside may still be possible.

Since the outlet temperature probes were on the eastern side of the jacket, the morning temperatures were higher at the eastern feedback valves, compared to the western feedback valves. The probes were also influenced by radiation during the day, and the values were not exact, although trends in the climatic pattern at the jacket were observed.

Throughout the drying run, the temperature inside the kiln followed a pattern similar to the load inlet temperatures shown in Section 4.3.1.

#### 4.3.5.1 Comparison of the temperature at the jacket exit and the dew-point during the six measuring periods

The three-day drying measuring periods described at the beginning of Section 4.3 were used to analyse the change in air properties in the air jacket. Two graphs (Figures 4.30 and 4.31) show the results of each measuring period indicating:

- The AH difference,  $\Delta AH_{\text{jact}}$ , between the jacket inlet and outlet [ $\Delta AH_{\text{jact}} = [AH \text{ Jacket in} - AH \text{ Jacket out}]$ ; see Figure 4.31]
- Dew-point temperature of the air leaving the jacket (DP Jacket out) and the temperature on both sides of the condensation surface ( $T_d \text{ Jacket out}$  and  $T_d \text{ Exterior}$ ) were recorded (see Figure 4.30). Saturated conditions were possible when  $DP \text{ Jacket out} = T_d \text{ Jacket out}$  (this analysis was preferred as the wick of  $T_w \text{ Jacket In}$  was prone to dry-out)

**Day 1-4, MC = 50%:**

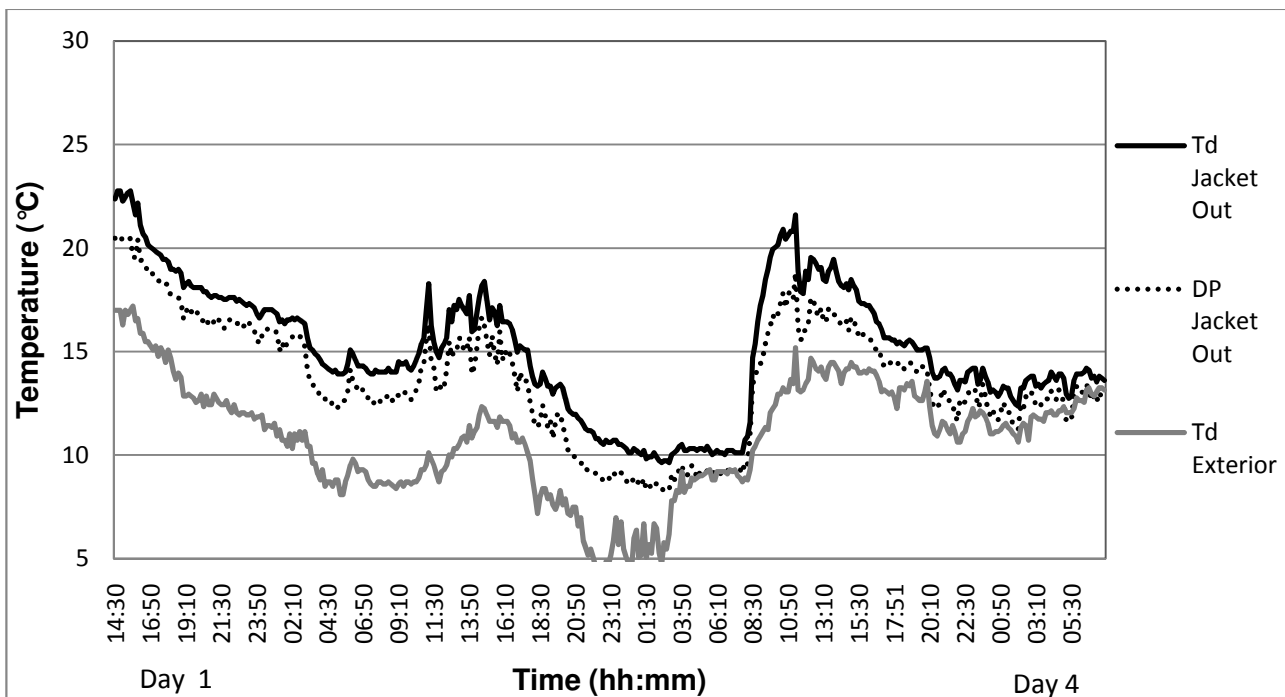


Figure 4.30: DP Jacket Out,  $T_d$  Jacket out and  $T_d$  Exterior during the measuring period of days 1 - 4; MC = 50%

Although DP Jacket out was not exactly equal to  $T_d$  Jacket out, it was possible that condensation occurred at the air film in contact with the outer plastic sheet. The outer plastic sheet was cooled by the external air as  $T_d \text{ Exterior} < T_d \text{ Jacket out}$ . Further,  $T_d \text{ Exterior}$  was mostly below the DP Jacket out, which therefore allowed condensation. This was possible throughout the measuring

period from day 1 to day 4. During this measuring period, a damp layer was visible on the inner surface of the kiln cover. As drying proceed, this situation changed to a state where condensation occurred only at night. This will be shown when the measuring period between days 18-21 is discussed.

The positive temperature gradient from  $T_d$  Jacket out to  $T_d$  Exterior at night indicated a constant heat loss to the environment. This was the situation for most of the drying period, as will be discussed when the internal and external temperatures are compared in Section 4.3.6.

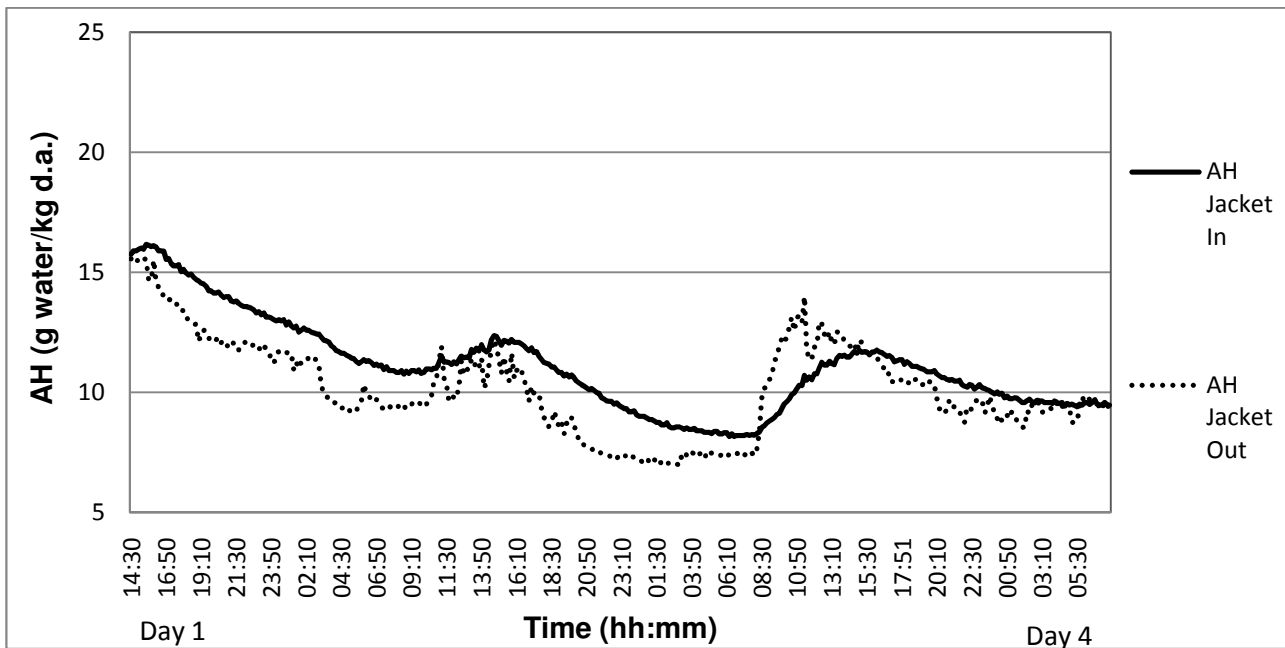


Figure 4.31: AH Jacket In and AH Jacket Out during the measuring period of days 1 - 4; MC = 50%

The AH was mostly higher at the air inlet to the jacket than the air outlet from the jacket, see Figure 4.31. This implies that condensation took place in this measuring period when free water was easily available and is evidence of a fast evaporation rate, as proven in Section 4.3.3.

The AH was mostly higher at the jacket air inlet than the jacket air outlet, except for a short period on 30 May, from 09h00 to 15h00. This means that there was evaporation of water collected in the jacket during this short period in time. This seemed impossible. A likely explanation was that some condensation was left in the jacket and which evaporated. A damp layer was visible as previously mentioned and could be a source of water that evaporated. Also, condensate collected between the plastic sheets, where small ponds formed at ridges on top of the inner plastic sheet. The problem increased as the collected water caused the inner plastic layer to sag. This was the case at the three 8mm tension cables, used for lateral stiffness and also at the two 25mm diameter structural members. This can be seen in the sectional drawing of half the kiln (see Figure 4.32).



The top cables, running on top of the rib-structure, offered by far the biggest problem. When this was realised, all three the cables were refitted to run underneath the rib structure. The water that collected after this interruption was much less. Not much could be done with the small diameter structural members, though the water collected was not much.

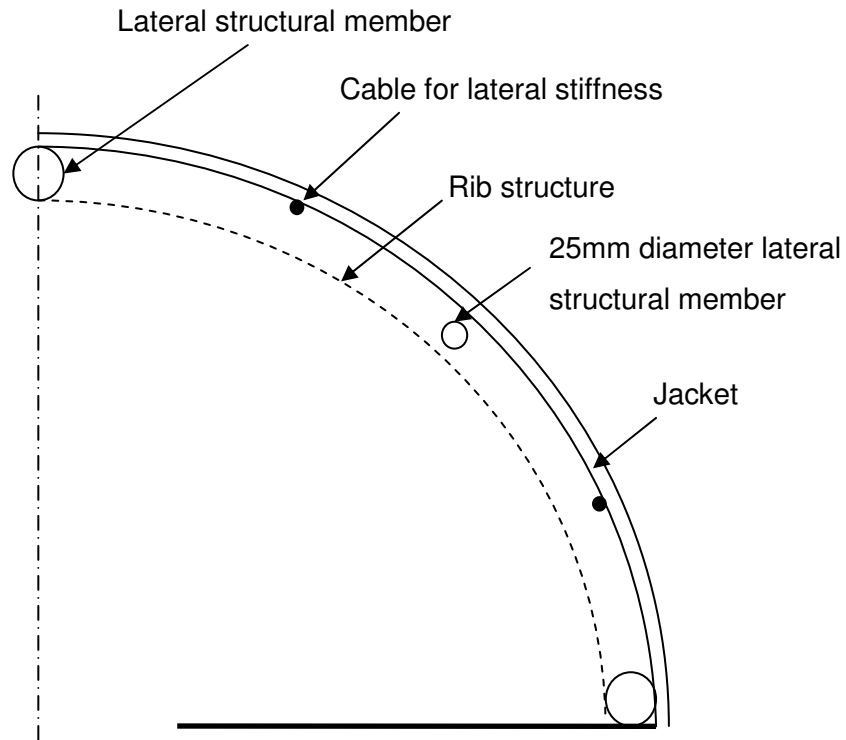


Figure 4.32: Sectional drawing of the possible catchments of condensate.

**Day 18-21. MC = 43%:**

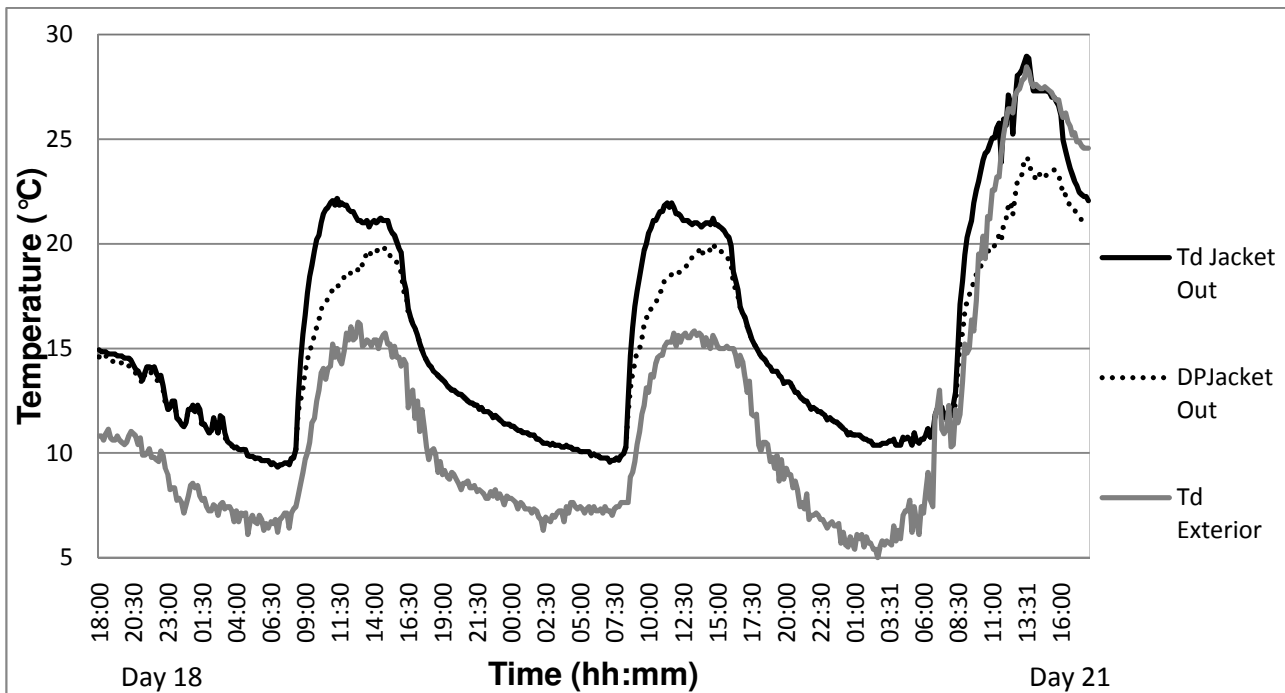


Figure 4.33: DP Jacket Out,  $T_d$  Jacket Out and  $T_d$  Exterior during the measuring period of days 18 - 21; MC = 43%

In Figure 4.33, the probable saturated conditions were clearly visible at night from 16h30 until 08h00, when the  $T_d$  Jacket Out = DP Jacket out. This indicated that the mix of the air was of such a nature that the entire volume of air that moved through the jacket cooled down to dew-point temperature. The ambient temperature was well below the kiln temperature, although not on the last day, which was a warm day with a high  $T_d$  Exterior, probably caused by a Bergwind.

The external temperature was well below the dew-point temperature during the night hours, indicating a possibility of condensation, although the plastic layer will have offered thermal resistance and caused a temperature drop between the jacket air and the external air.

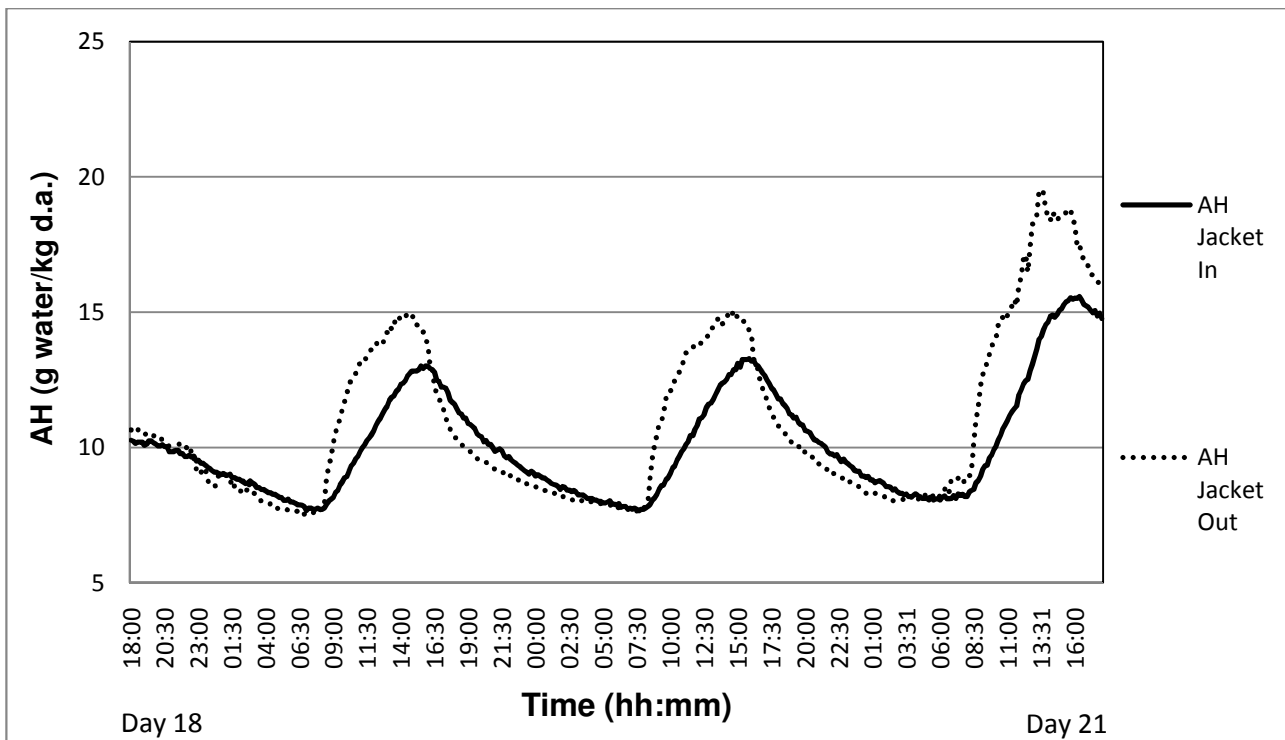


Figure 4.34: AH Jacket In and AH Jacket Out during the measuring period of days 18 - 21;  
MC = 43%.

Between 16h30 and 08h00, the AH for the Jacket Out was lower than at the inlet (Figure 4.34) and with the saturated conditions described above, the prospect of condensation was excellent. The AH Jacket In was less than AH Jacket Out during daylight hours, and it directs towards evaporation in the jacket. Although it was of a short duration, the difference in AH seems abnormally high. The abnormality could be due to the radiation on bare thermocouples during the day. The thermocouples at the stack were protected against radiation. Another important influence could have been evaporation of residual water inside the jacket. The water came from the small ponds described above or from the damp surface on the inside of the outer sheet.

Day 39 - 42: MC = 30%:

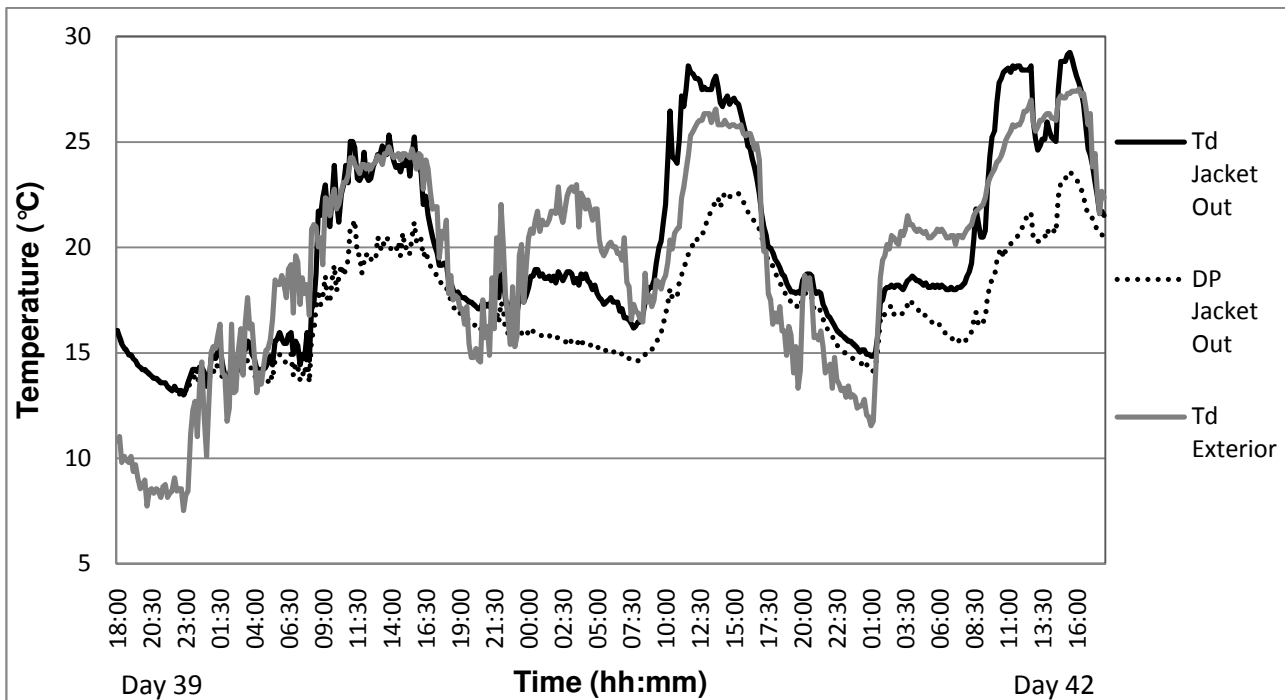


Figure 4.35: DP Jacket Out,  $T_d$  Jacket Out and  $T_d$  Exterior during the measuring period of days 39 - 42; MC = 30%

The measuring period from day 39-42 (Figure 4.35) is recognised as being dominated by Bergwind conditions, starting at 01h00 on day 40. Temperatures remained high even during the night of day 40/41. Saturated conditions inside the jacket existed initially, but when the Bergwind situation set in at 01h00 on day 40, the  $T_d$  Jacket Out was mostly higher than DP Jacket Out, except for a brief period from 17h30 to 24h00 on day 41. This means that condensation at night was not possible in the jacket during Bergwind conditions. The importance of this result is that a similar solar kiln that works on natural dehumidification must be ideally installed in an area with a diurnal temperature range that is not too small. From the results in Section 4.3.6.1 it was found that the average  $T_d$  Exterior at the Saasveld solar kiln was 11.8 °C, with a standard deviation of 6.5 °C.

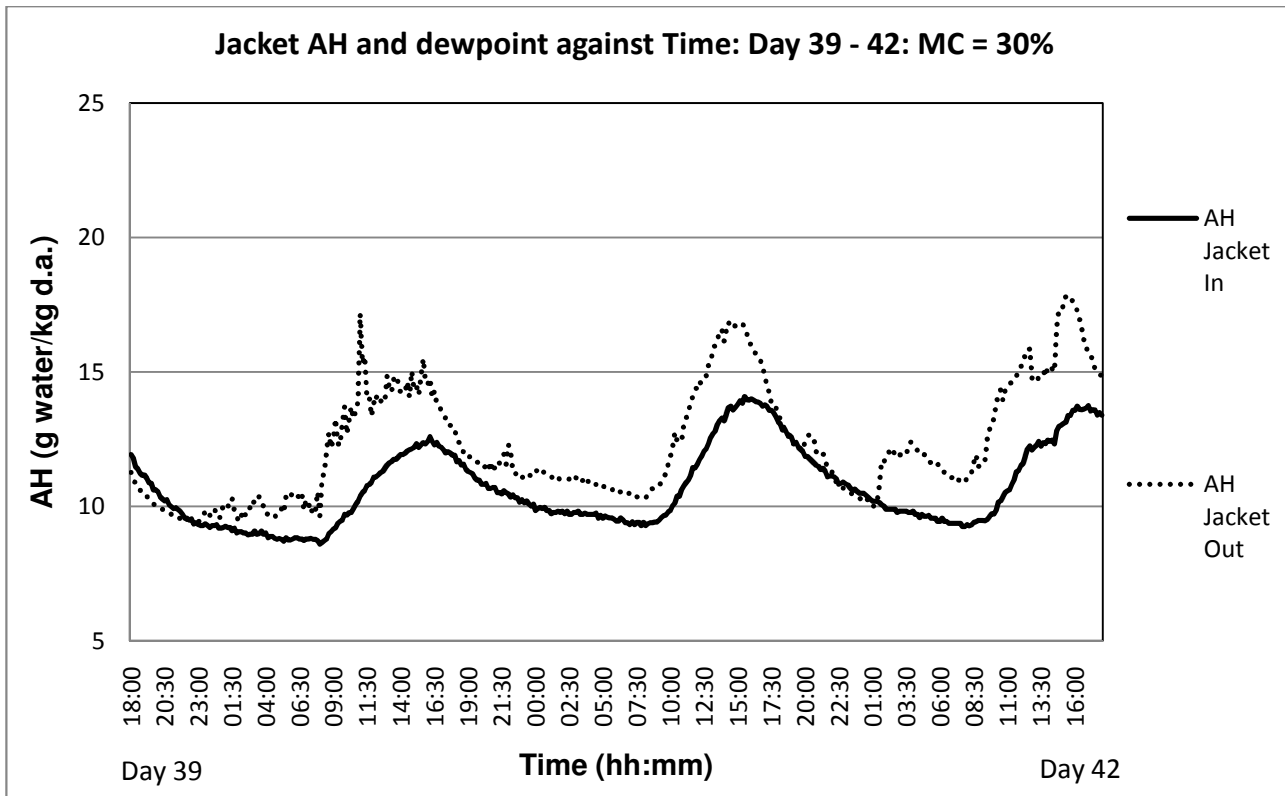


Figure 4.36: AH Jacket In and AH Jacket Out during the measuring period of days 39 - 42; MC = 30%.

The external temperature stayed predominantly above both the inlet and outlet dew-points during the Bergwind state, with no condensation as the outcome. The outlet AH was higher than the inlet AH for most of the time, which proved that there was no condensation, except for the brief period from 17h30 to 24h00 on day 41 (see Figure 4.36). The abnormal high AH Jacket Out was thus again observed.

#### Day 63 - 66: MC = 20.5%:

The external temperature,  $T_d$  Exterior, was lower than DP Jacket Out and  $T_d$  Jacket Out. The pattern was similar to the days 18-21; MC = 43%, and will not be shown below. The  $T_d$  Jacket In is shown in Figure 4.37 instead of  $T_d$  Exterior to visualise the interaction between  $T_d$  Jacket In and  $T_d$  Jacket Out.

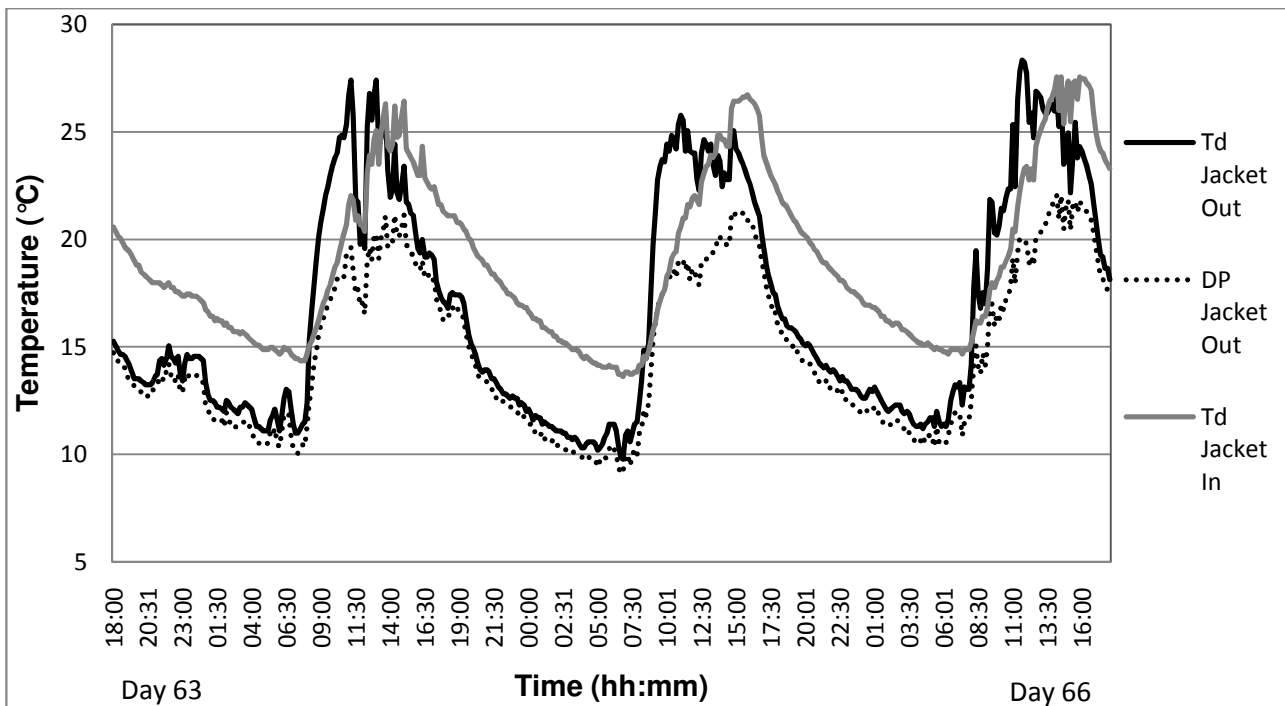


Figure 4.37:  $T_d$  Jacket In,  $T_d$  Jacket Out and DP Jacket Out during the measuring period of days 63 - 66; MC = 20.5%

The possibility of saturation in the jacket was again visible when the DP Jacket out =  $T_d$  Jacket Out, during the time period of 16h30 until 08h00. At the inlet side at night, the air was far from being saturated, as  $T_d$  Jacket In > DP Jacket In. Also,  $T_d$  Jacket In >>  $T_d$  Jacket Out at night indicated that the air cooled progressively until dew-point temperature was reached and after which condensation was expected.

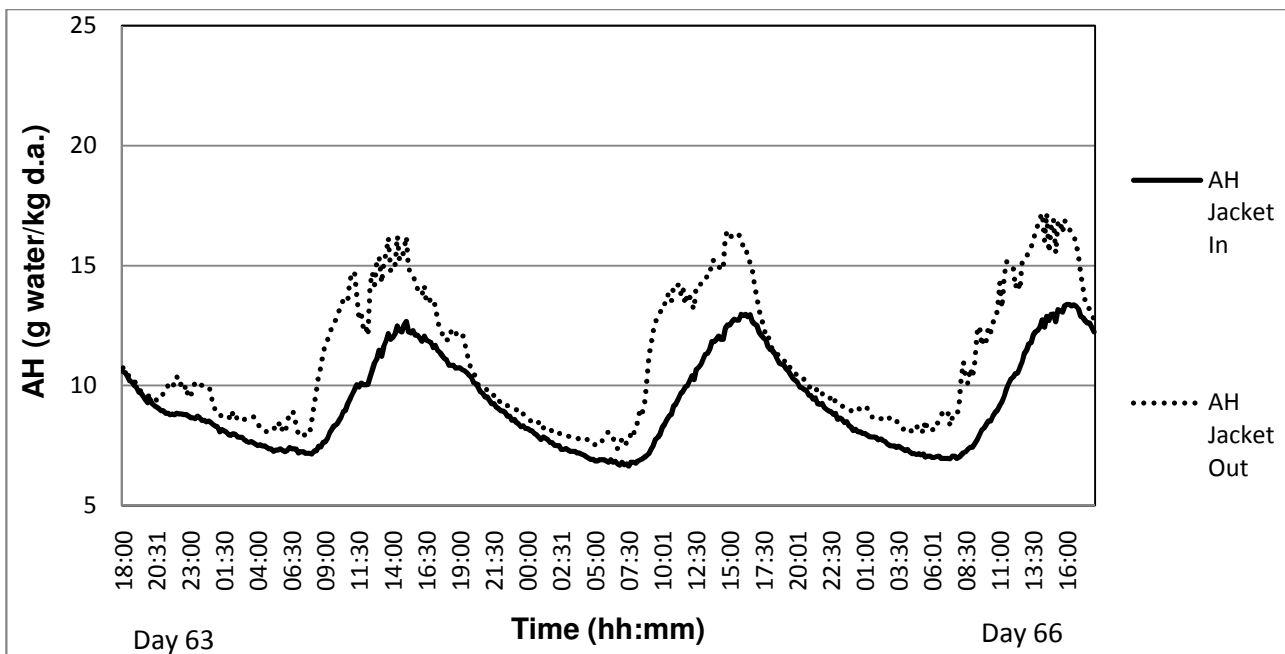


Figure 4.38: AH Jacket In and AH Jacket Out during the measuring period of days 63 - 66; MC = 20.5%

The times that the AH Jacket In  $\approx$  AH Jacket Out, occurred during the night hours (Figure 4.38). It can be concluded that a little condensation was possible inside the jacket during the night.

#### Day 90 - 93: MC= 15.3%:

The period of saturation in the jacket became shorter. When the  $T_d$  Jacket Out was compared to the  $T_d$  Jacket Out below (Figure 4.39), then it was clearly visible that condensation occurred.

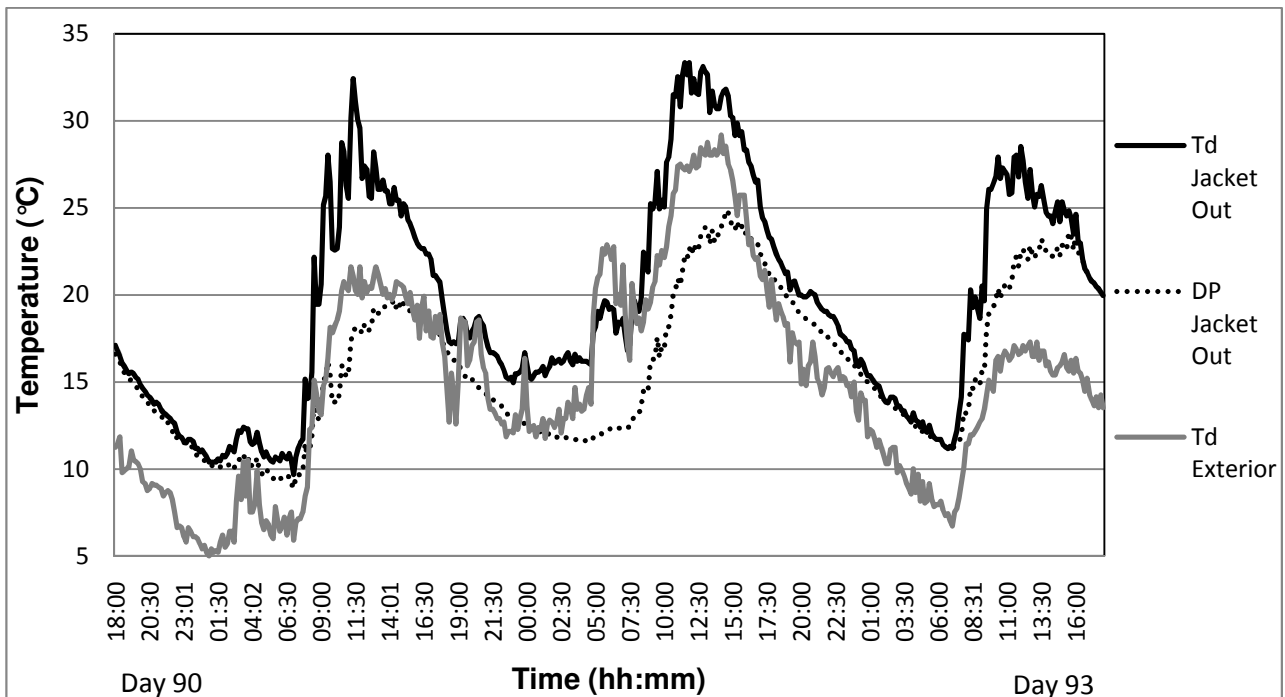


Figure 4.39: DP Jacket Out,  $T_d$  Jacket Out and  $T_d$  Exterior during the measuring period of days 90 - 93; MC = 15.3%

Figure 4.39 appears to have fewer saturated conditions where DP Jacket out =  $T_d$  Jacket Out. Dew-point temperature seemed to be just a little off the  $T_d$  Jacket Out temperature. However, DP Jacket Out =  $T_d$  Jacket out, at the night of day 90 and then again on day 93 from 16h00. The night of day 91/92 was a warm night around 15°C and on the night of day 92/93 the DP Jacket Out and  $T_d$  Jacket Out temperatures came close to be equal. An analysis on the three days following, indicated that the saturation in the air jacket still occurred during the same time period on a daily basis from 16h30 until 08h00, except for the night of day 95/96 when the night temperature rose between 20h00 and 02h00.

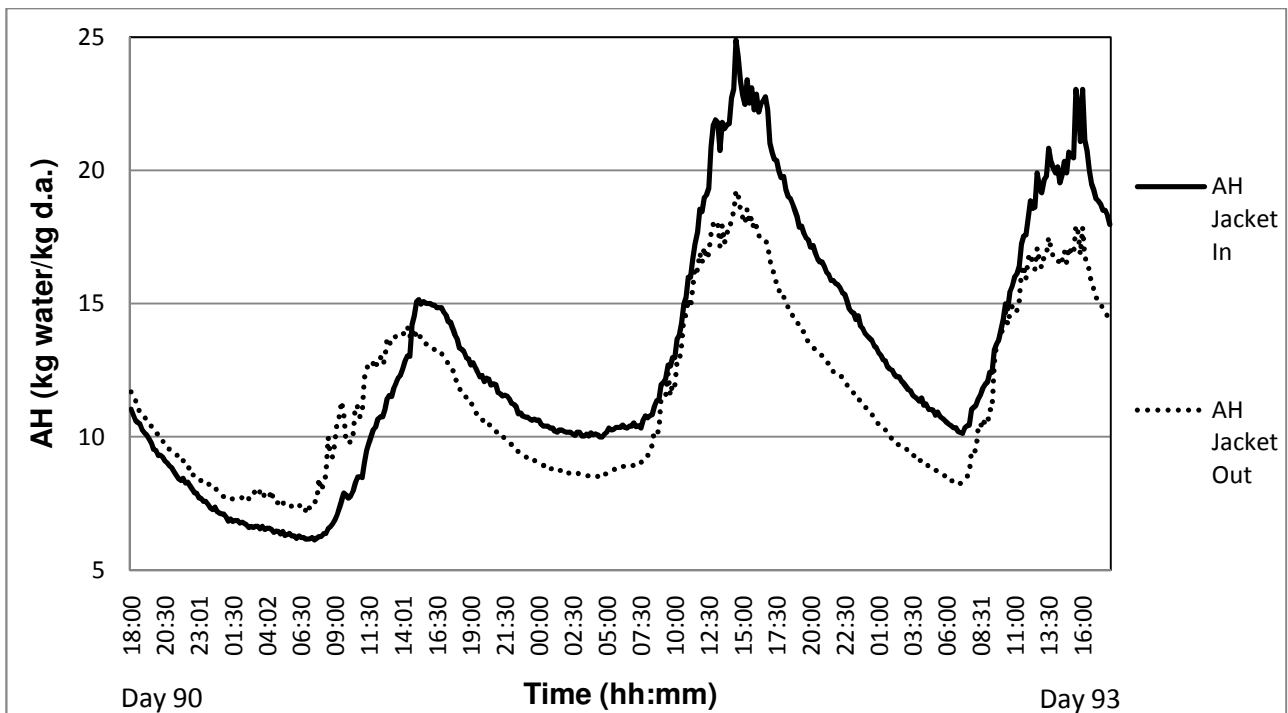


Figure 4.40: AH Jacket In and AH Jacket Out during the measuring period of days 90 - 93;  
MC = 15.3%.

From Figure 4.40, the times that AH Jacket In > AH Jacket Out, was during the night hours of the second and third day, although the inlet wet bulb wick was suspicious. Temperature values at day were probably influenced by radiation during the day.

#### Day 120 - 123, MC=10.3%

As previously noted, the dry-out problem of the wet bulb wicks became bigger towards the end, especially at the jacket inlet. The reservoirs were filled to the top and wicks were cleaned on day 120 at 18h00. Within 40 minutes, the wet bulb wick of the jacket inlet became dry. The results given above at MC of 15.3% will have to be sufficient, since it is close enough to the final MC.

The unfortunate occurrence of the wet bulb wicks drying out resulted in this section being difficult to analyse. However, the measuring periods selected assisted greatly in analysing the extraction of humidity from the kiln.

Humidity is mostly removed by dehumidification at night, although there were minute amounts of venting through small openings; however they were too small to cause drying defects. For future studies, there is the possibility of carrying out some manual venting after FSP has been reached to increase the drying rate, without sacrificing the drying quality.



### Summary:

- The temperature at the jacket inlet side was well above the dew-point at night,  $T_d \text{ Jacket In} > DP \text{ Jacket In}$ , indicating that the air cooled progressively until dew-point temperature was reached and thereafter condensation was expected.
- A comparison of the dew-point and the temperature at the jacket exit can be used to determine the exact point of condensation. Probable condensation was possible at night from 16h30 until 08h00, when the  $T_d \text{ Jacket Out} = DP \text{ Jacket out}$ .
- $T_d \text{ Exterior}$  was mostly below the  $DP \text{ Jacket out}$  at night, which therefore allowed condensation.
- The outer plastic sheet was mostly cooled by the external air as  $T_d \text{ Exterior} < T_d \text{ Jacket out}$ , indicating a constant heat loss to the environment.
- Some vapour was expelled from the kiln through very small openings at the door attachments and possible small holes in the plastic cover. The openings were too small to cause drying defects
- Not all the condensation left the weeping holes at once as there was some evaporation of residual water inside the jacket.
- A solar kiln that works on natural dehumidification must be installed in an area with a diurnal temperature range that is big enough to produce condensation at night. The diurnal temperature range at the Saasveld solar kiln was 11.8 °C, with a standard deviation of 6.5 °C.
- No condensation occurred at night when Bergwind conditions dominated.
- The possibility is there to do some manual venting after FSP has been reached to increase the drying rate, without sacrificing the drying quality
- Interventions:
  - The wet bulb temperature wicks, especially  $T_w \text{ Jacket In}$  occasionally ran dry, due to high air velocities.
  - Jacket exit was positioned at the eastern side of the kiln, resulting in a rapid rise in temperatures in the mornings.
  - The kiln was not perfectly air tight,
  - The probes at the jacket outlet were also influenced by radiation during the day, and the values were not exact. Trends in the climatic pattern at the jacket were observed.

#### 4.3.5.2 Comparison of the dew-point and the temperature at the jacket exit during the five drying stages

The 130 days of drying is again divided into the same five drying stages, spanning the 130 days. The average daily difference between the dew-point and the dry bulb temperatures at the jacket exit,  $\{T_d \text{ Jacket Out} - DP \text{ Jacket Out}\}$  at a specific time is presented in Figure 4.41 for a typical day in each of the five drying stages.

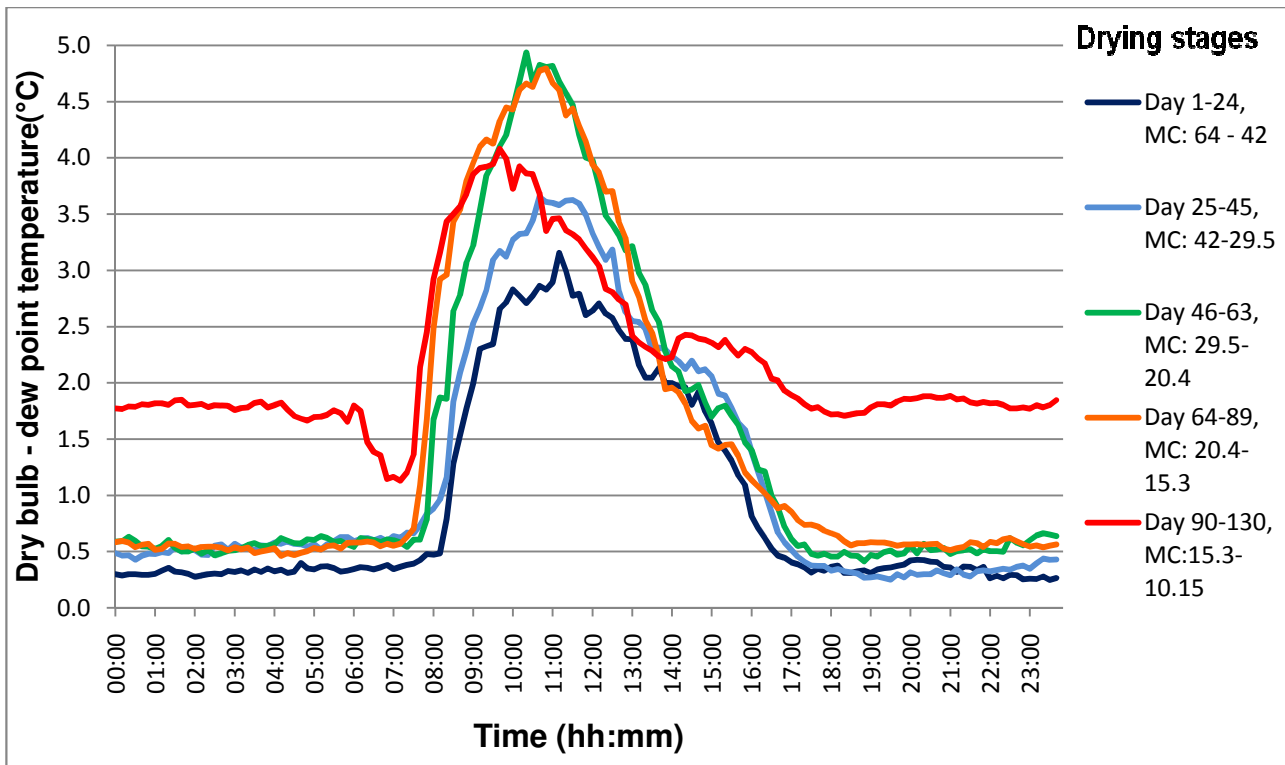


Figure 4.41: Difference between dry bulb and dew-point temperatures at the jacket outlet,  $\{T_d \text{ Jacket Out} - DP \text{ Jacket Out}\}$  at various stages of drying

Note that these are average values, and it is impossible to have values below 0°C. The resultant average value took the occasional warm nights into account where there was no condensation.

It is clear from this chart that the condensation occurred mostly from 17h00 to 07h30, with a leeway of 30 minutes on either side. The time of 07h30 is used, although it seems that, with each progressing measuring period, condensation stopped a few minutes earlier. In the case of days 64-89, the condensation stopped at 07h00; this could be due to an earlier rising of the sun since the drying period moves away from winter solstice. As drying progressed, condensation occurred less: either due to condensation taking place on fewer nights or for shorter durations at night. The drying stage from days 64-89, with MCs dropping from 20.4% to 15.3%, indicates that condensation did not start as abruptly as the previous measuring periods, but rather evened out when the

condensation phase started at 20h00. The drying stage from days 90-130 was clearly influenced by a dried-out wick, although the general pattern can still be observed. The trend of the start of condensation on days 64-89, as discussed above, can also be observed on the drying stage of days 90-120.

A random night time of 02h00 was chosen to see how see the frequency of condensation on the surface where  $\{T_d \text{ Jacket Out} = DP \text{ Jacket Out}\}$ . A histogram of  $\{T_d \text{ Jacket Out} - DP \text{ Jacket Out}\}$  -values were assembled at 02h00 in each of the drying stages. A summary of the results is shown in the Table 4.10. The percentage frequency of  $(T_d \text{ Jacket Out} - DP \text{ Jacket Out})$  is indicated in the ranges 0-0.2; 0.2-0.4 and >0.4.

Table 4.10: Percentage frequency of  $(T_d \text{ Jacket Out} - DP \text{ Jacket Out})$  for the ranges 0-0.2; 0.2-0.4 and >0.4 for the different drying stages at 02h00

<b>Ranges of Td Jacket Out – DP Jacket Out</b>	<b>% Frequency Day 1-24, MC: 64 - 42</b>	<b>%Frequency Day 25-45, MC: 42-30</b>	<b>% Frequency Day 46-63, MC: 30-20</b>	<b>% Frequency Day 64-89, MC: 20-15</b>	<b>% Frequency Day 90-130, MC:15-10</b>
0-0.2	52.2*	33.3	16.7	46.2	22.0
0.2-0.4	30.4	19.0	44.4	3.8	0.0
>0.4	17.4	47.6	38.9	50.0	78.0

\*As a matter of interest, during the measuring period of Day 1 to Day 24 at 02h00, 41% of these difference-values were smaller than 0.1 °C.

Small leaks in the jacket and low average wood MC during days 90-130 resulted in little vapour being available for condensation as the MC of the kiln load dropped only by 5.15%.

Summary:

- Condensation occurred mostly from 17h00 to 07h30, with a leeway of 30 minutes on either side
- The possibility for condensation became progressively less as the MC of the wood reduced.

#### 4.3.6 Comparison between temperatures inside the kiln and external temperatures

Since external temperature would influence the climate inside the kiln, the kiln would presumably have heated up during the day as the temperature outside increased as well as because of heat transfer from the sun's radiation. The kiln radiated heat to the outside environment at night. This section will report on the interaction between the external and internal temperatures.

#### 4.3.6.1 Differences between kiln temperature and exterior temperature based on daily averages

The air entering the stacks inside the kiln was for 93.5% of the time at a higher temperature than the external temperature. The average recorded difference between these temperatures was 6.45°C, with a standard deviation of 3.65°C. The range for the temperature difference was between minus 4.58°C and 18.28°C. Bergwind conditions and warm days contributed to high external temperatures – higher than the internal temperatures (6.5% of the time). A Bergwind is a warm dry wind occurring during mid-autumn to mid-spring. EMCs as low as 1.9% at an average wind velocity of 6 m/s have been recorded before at the solar kiln. These conditions would result in severe drying defects like end cracks, surface cracks and even cell collapse in timber air-dried. The results from the ZA Dry Q audit indicated that there were no such defects for the timber dried in the Saasveld solar kiln. The kiln enclosure shielded the timber during Bergwind periods from external drying conditions that were too harsh. This was one of the reasons for the small amount of surface checking found in the load.

The difference between internal and external temperatures,  $\{T_d \text{ Load In} - T_d \text{ External}\}$ , is expressed as  $\Delta T$ . The daily average of  $\Delta T$  over the 130 day drying run, expressed as  $\Delta T_{\text{day}}$ , and is shown in Figure 4.42.

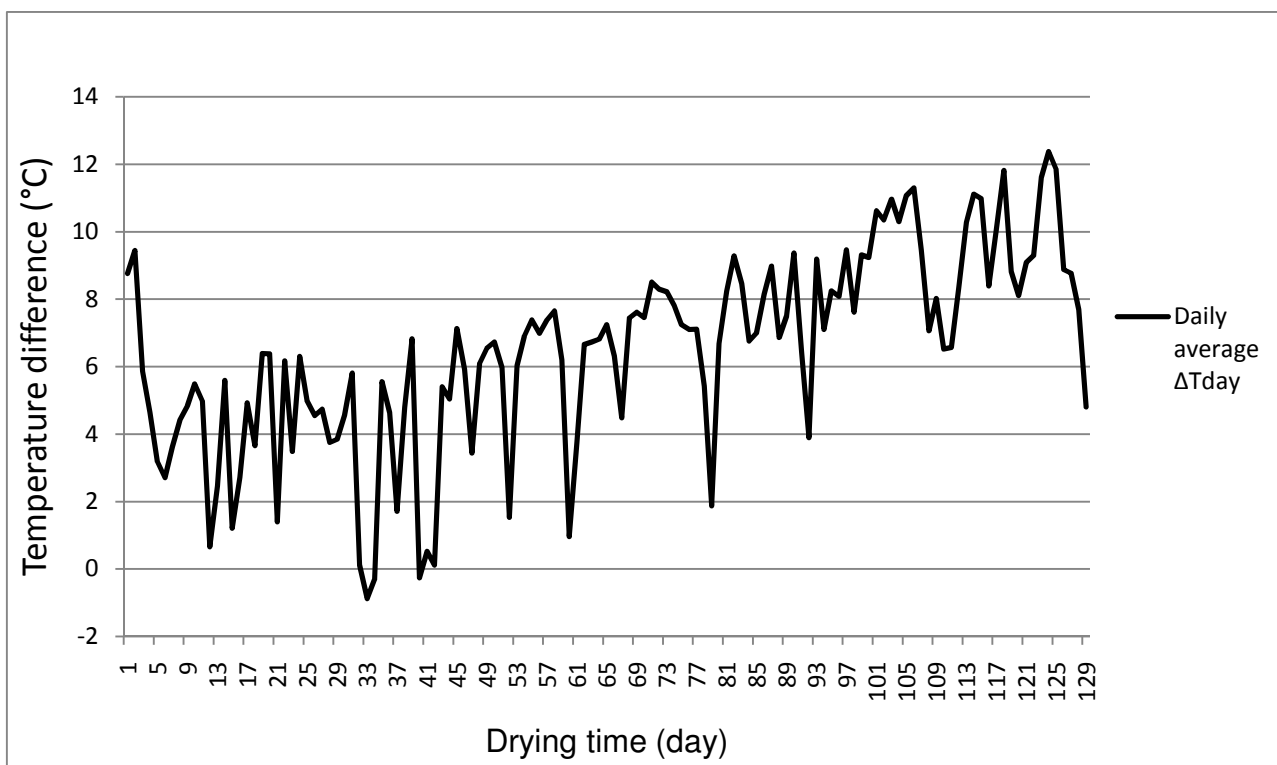


Figure 4.42: Daily average of the difference between internal and external temperature ( $\Delta T_{\text{day}}$ )

More clarity on this difference was obtained when the average  $\Delta T$  as well as the average internal ( $T_d$  Load in) and external temperature ( $T_d$  External) was separated into the five drying stages. The results are displayed in Table 4.11.

Table 4.11: Average  $T_d$  Load in,  $T_d$  External and  $\Delta T_{day}$  for the five drying stages

Day range of drying stages	MC range (%)	Daily average $T_d$ Load In ( $^{\circ}\text{C}$ )	Daily average $T_d$ External ( $^{\circ}\text{C}$ )	$\Delta T_{day}$ ( $^{\circ}\text{C}$ )	St deviation $\Delta T_{day}$ ( $^{\circ}\text{C}$ )
1 - 24	64 - 42	18.57	14.13	4.44	2.98
25 - 45	42 - 29.5	17.02	13.55	3.46	3.31
46 - 63	29.5 - 20.4	17.76	12.04	5.72	2.71
64 - 89	20.4 - 15.3	20.01	12.82	7.19	2.79
90 - 130	15.3 - 10.15	23.04	13.95	9.08	2.89
<b>Total 1 - 130</b>	<b>Weighted Average</b>	<b>19.9</b>	<b>13.43</b>	<b>6.45</b>	<b>2.92</b>

From Table 4.11 and Figure 4.42 it can be seen that, except for the second stage,  $\Delta T_{day}$  increased as the drying progressed. This pattern can be explained by a smaller availability of moisture as drying proceeded and, therefore, less evaporation to the circulating air. The internal temperatures were thus higher during the later stages of drying. A lower MC of the wood in the kiln increased the difference between internal and external temperatures.

A product-moment correlation matrix was performed and is summarised in Table 4.12. A good correlation is observed between the day of the drying run, thus the wood MC, and average  $\Delta T_{day}$  ( $r=0.678$ ). This confirms the pattern of increasing temperature difference with increasing drying days. It can be concluded that the difference between internal and external temperatures,  $\Delta T_{day}$ , increased with a reduction of wood moisture.

i. Seasonal influence

The influence of the season of drying could be considered as a counter argument to the increase in temperature difference between the internal and external temperatures. The influence of the season on the average external temperature ( $T_d$  External) will first be investigated and secondly the seasonal influence on the fluctuation between maximum and minimum daily exterior temperatures, Exterior ( $T_{d \max} - T_{d \min}$ ).

To assist these investigations, a product-moment correlation matrix, on a 0.05% level, is summarised in the Table 4.12, with the highly significant correlation indicated in bold. The independent variables included the day of drying, the daily fluctuation of external temperature [Exterior ( $T_{d \max} - T_{d \min}$ )], and the daily average difference between internal and external temperature [ $\Delta T_{\text{day}}$  = daily average of  $T_d$  Load In –  $T_d$  External].

Table 4.12: Correlation coefficients for the day of drying, Exterior ( $T_{d \max} - T_{d \min}$ ) and  $\Delta T_{\text{day}}$  for the five drying stages

Variables	Day of drying run	Exterior ( $T_{d \max} - T_{d \min}$ )	$\Delta T_{\text{day}}$
Day of drying run	1.000	0.102	<b>0.678</b>
Exterior ( $T_{d \max} - T_{d \min}$ )	0.102	1.000	<b>-0.185</b>
$\Delta T_{\text{day}}$	<b>0.678</b>	<b>-0.185</b>	1.000

ii. Average external temperature ( $T_d$  External)

Higher external temperatures should lead to more solar heat being collected by the kiln which in turn should increase the temperature difference between internal and external temperatures. It was expected in this study that the external temperature ( $T_d$  External) should rise as the drying run progressed into spring. However, the climate in the Garden Route of South Africa is known to exhibit little seasonal fluctuation. The average external temperature (Daily average  $T_d$  External) for the various drying stages is summarised in Table 4.11.

From the results, it is evident that the daily average external temperature did not rise as expected, but remained relatively constant throughout the drying run. To confirm this, a product-moment correlation matrix was compiled on the daily average  $T_d$  External over the 130 days. The correlation coefficient on a 0.05 level was  $r = 0.018$ . This indicated that there was a strong non-significant correlation between the day of drying and the external air temperature, suggesting that

the external temperatures were purely random. In Section 4.3.1, it was shown that there was a significant correlation between the day of drying and the daily average internal temperature ( $r = 0.71$  on a 0.05 level). The strong correlation between the MC and  $\Delta T_{\text{day}}$  ( $r = 0.678$ ), was, therefore, only influenced by the temperature inside the kiln and not the temperature outside. This proved that the season had no influence on the daily average difference between internal and external temperature.

### iii. Fluctuation between maximum and minimum daily exterior temperatures

The seasonal influence of the external day-night temperature fluctuation, Exterior ( $T_{d \text{ max}} - T_{d \text{ min}}$ ) was investigated since the big difference between day (maximum) and night (minimum) temperatures could possibly affect the difference between external and internal temperatures. The difference between the maximum and minimum diurnal external temperatures, or external fluctuations, for each day of the drying run was plotted in Figure 4.43 below. The average was 11.8°C, with a standard deviation of 6.5°C.

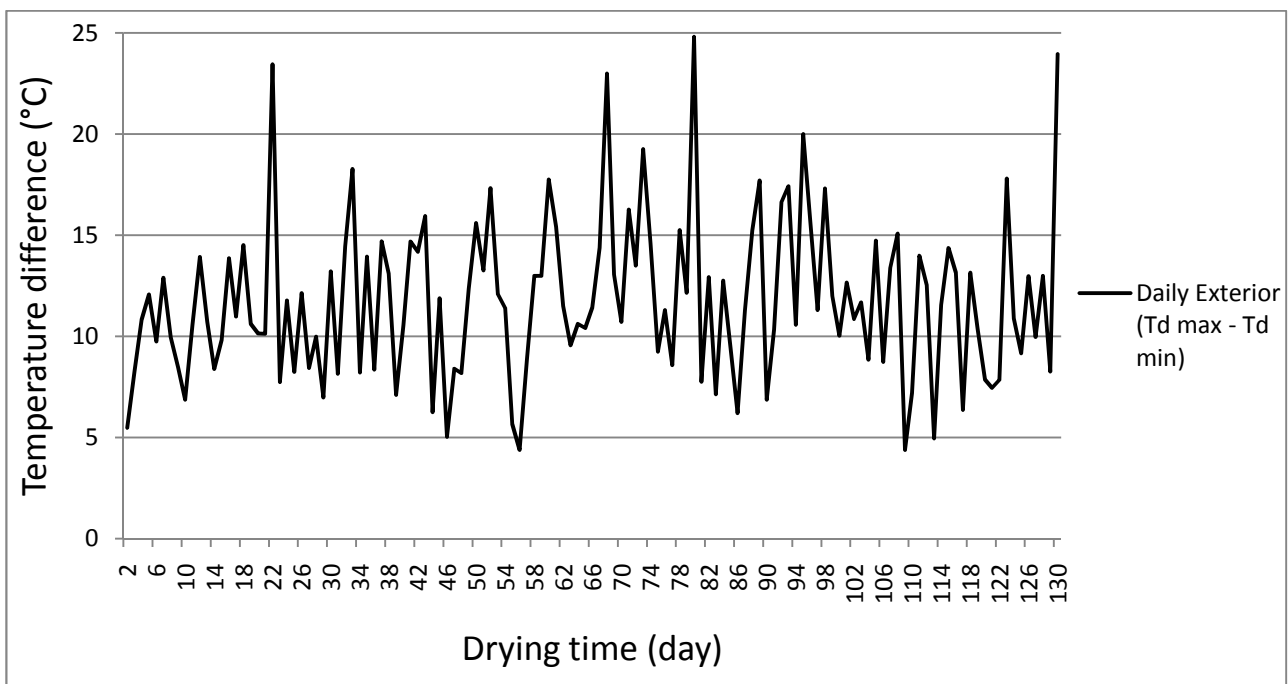


Figure 4.43: Fluctuation of diurnal exterior temperature, Exterior ( $T_{d \text{ max}} - T_{d \text{ min}}$ )

It is clear that the pattern of Exterior ( $T_{d \text{ max}} - T_{d \text{ min}}$ ) was randomly distributed, with no seasonal influence during the drying run. The product-moment correlation matrix performed later will prove this.

A similar graph of internal day-night temperature fluctuation, Interior ( $T_{d \max} - T_{d \min}$ ), was drawn together with the values for Exterior ( $T_{d \max} - T_{d \min}$ ). The interior temperature values were measured at the load inlet. To clarify the results between the two graphs, fourth order polynomial trend lines were derived from the two graphs and are shown in Figure 4.44.

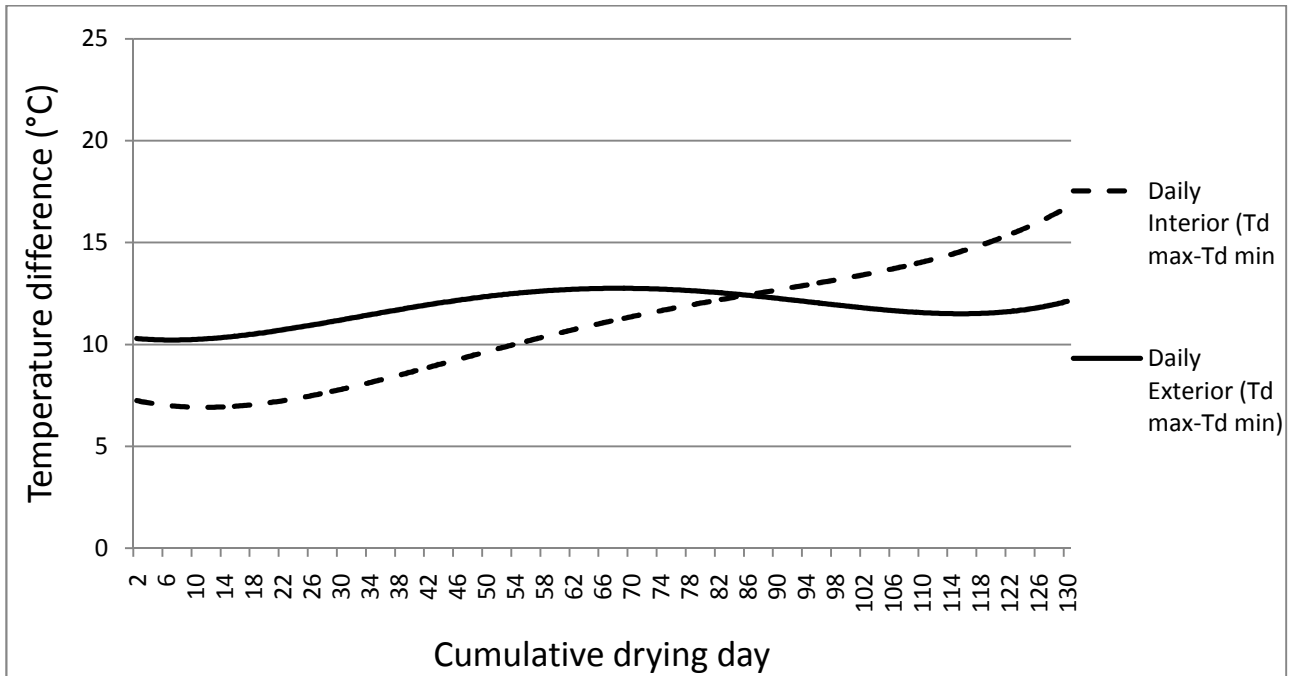


Figure 4.44: Trend lines of the fluctuation of diurnal interior and exterior temperatures, {Interior ( $T_{d \max} - T_{d \min}$ )} and {Exterior ( $T_{d \max} - T_{d \min}$ )}

The difference between the maximum and minimum diurnal internal temperatures, or internal temperature fluctuation, for each day of the drying run was similar to the daily average of the difference between internal and external temperature ( $\Delta T_{\text{day}}$ ).

The product-moment correlation matrix, on a 0.05% level, is summarised in Table 4.12. The random distribution of the Exterior ( $T_{d \max} - T_{d \min}$ ) is confirmed by the insignificant correlation between the day of drying and the Exterior ( $T_{d \max} - T_{d \min}$ ), ( $r=0.102$ ). A greater significance is observed between the day of the drying run and average  $\Delta T_{\text{day}}$  ( $r=0.678$ ). This confirms the pattern of increasing temperature difference correlating with an increase in drying days.

It is now clear that firstly the lower MC of the wood in the kiln caused the increase in the difference between internal and external temperatures, and secondly, increased the internal temperature fluctuation. The season had no influence on the above two phenomena.



#### Summary:

- The kiln air temperature was higher than the external temperature for 93.5% of the time. The average difference was 6.45°C, with a standard deviation of 3.65°C. Bergwind conditions and warm days contributed to lower internal temperatures than external temperatures for 6.5% of the time.
- The daily average external temperature did not rise as the drying run proceeded into spring/summer, but remained relatively constant with no significant correlation between the day of drying and the daily average of external temperatures ( $r = 0.018$ ).
- The difference between internal and external temperatures,  $\Delta T_{\text{day}}$ , increased at a lower MC, with a positive significance ( $r=0.678$ ) and without seasonal influence.
- The daily internal temperature fluctuation, Interior ( $T_{d \text{ max}} - T_{d \text{ min}}$ ), increased at a lower MC, similar to  $\Delta T_{\text{day}}$ , and also occurred without seasonal influence.
- The daily external temperature fluctuation, Exterior ( $T_{d \text{ max}} - T_{d \text{ min}}$ ) was randomly distributed over the drying run ( $r=0.102$ ), with no seasonal influence during the time of the drying run.
- The kiln enclosure shielded the timber during Bergwind periods from harsh external drying conditions. This was one of the reasons for the small amount of surface checking found in the load.

#### *4.3.6.2 Differences between internal and external temperatures at selected measuring periods during the day for the five drying stages*

The discussion in Section 4.3.6.1 considered average temperature differences on a daily basis, and did not report on temperature differences at specific times of the day.

##### i. Kiln behaviour during different measuring periods

The results showed that the difference between internal and external temperatures,  $\{T_d \text{ Load In} - T_d \text{ External}\}$ , or  $\Delta T$ , was more dependent on the diurnal variation of the outside temperature than the inside temperature, which was stabilised by moisture in the wood and the heat capacity of the wood and the concrete floor. From Figures 4.45 to 4.49, it can be seen that during the afternoons and into the night, the temperature inside the kiln did not drop as quickly as the external temperature. This delay in temperature drop inside the kiln was due to heat stored during the day in the timber, the kiln internal structure and mostly to the concrete floor. At night, the stack and concrete in the kiln were a source of heat for the kiln air.

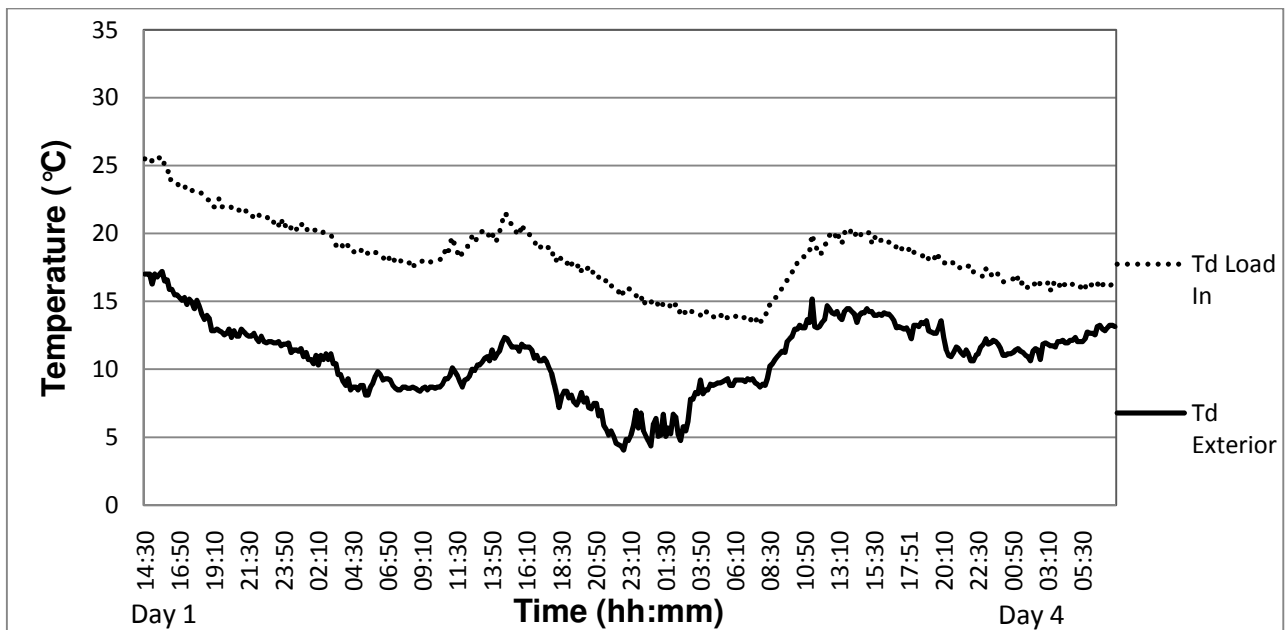


Figure 4.45:  $T_d$  Load In and  $T_d$  Exterior against time covering days 1 - 4; MC = 50%

Day 21 was a warm day and the protection offered by the kiln is evident. This is shown in Figure 4.46.

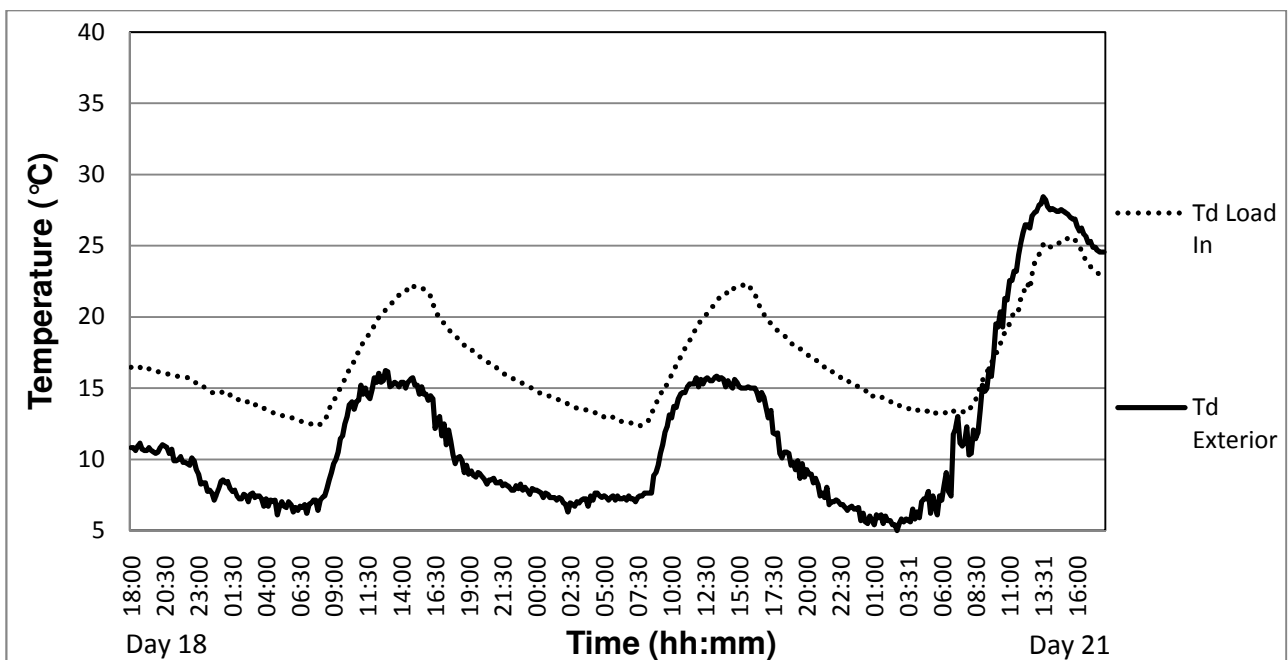


Figure 4.46:  $T_d$  Load In and  $T_d$  Exterior against time covering days 18 - 21; MC = 43%

Bergwind conditions were experienced on days 42-45 as can be seen in Figure 4.47.

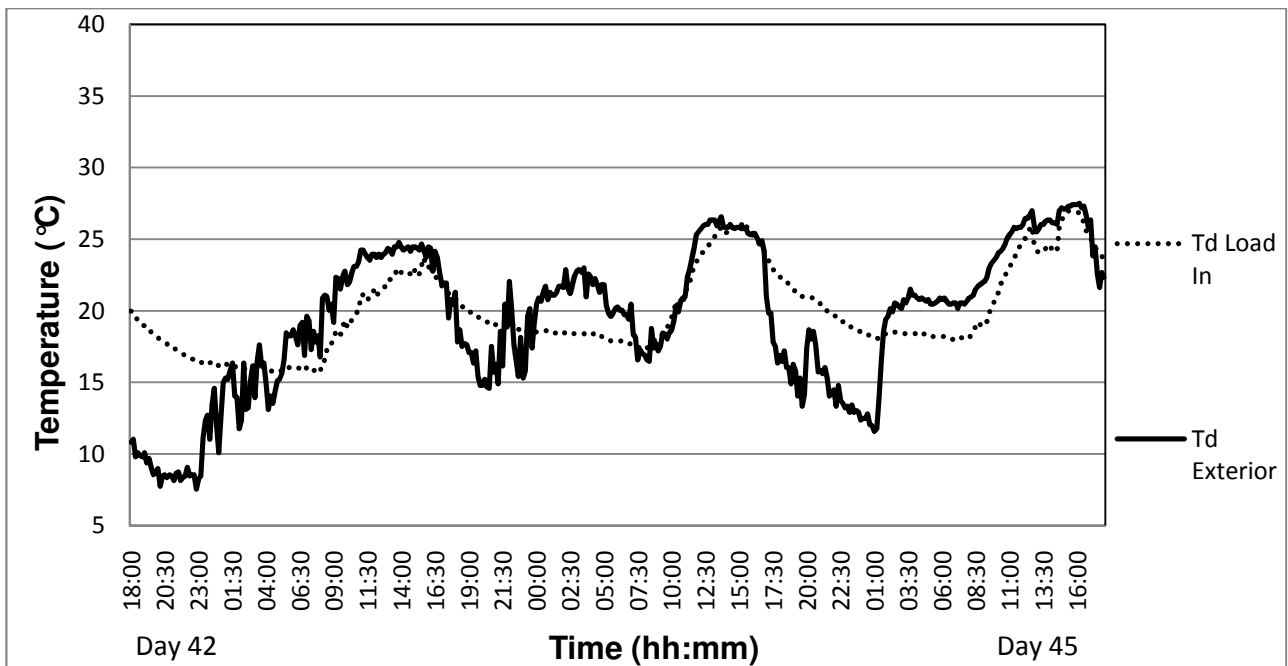


Figure 4.47:  $T_d$  Load In and  $T_d$  Exterior against time covering days 42 - 45; MC = 29%

The graphs in Figure 4.47 indicate a rare occasion where the external air temperature was higher than the kiln temperature. As the wood MC dropped below FSP, an increase in  $\Delta T$  was experienced, as previously shown. This pattern of  $\Delta T$  was repeated throughout the drying period until the end of drying. The last measuring period (days 120 – 123; MC = 10.5 %) is shown in Figure 4.48.

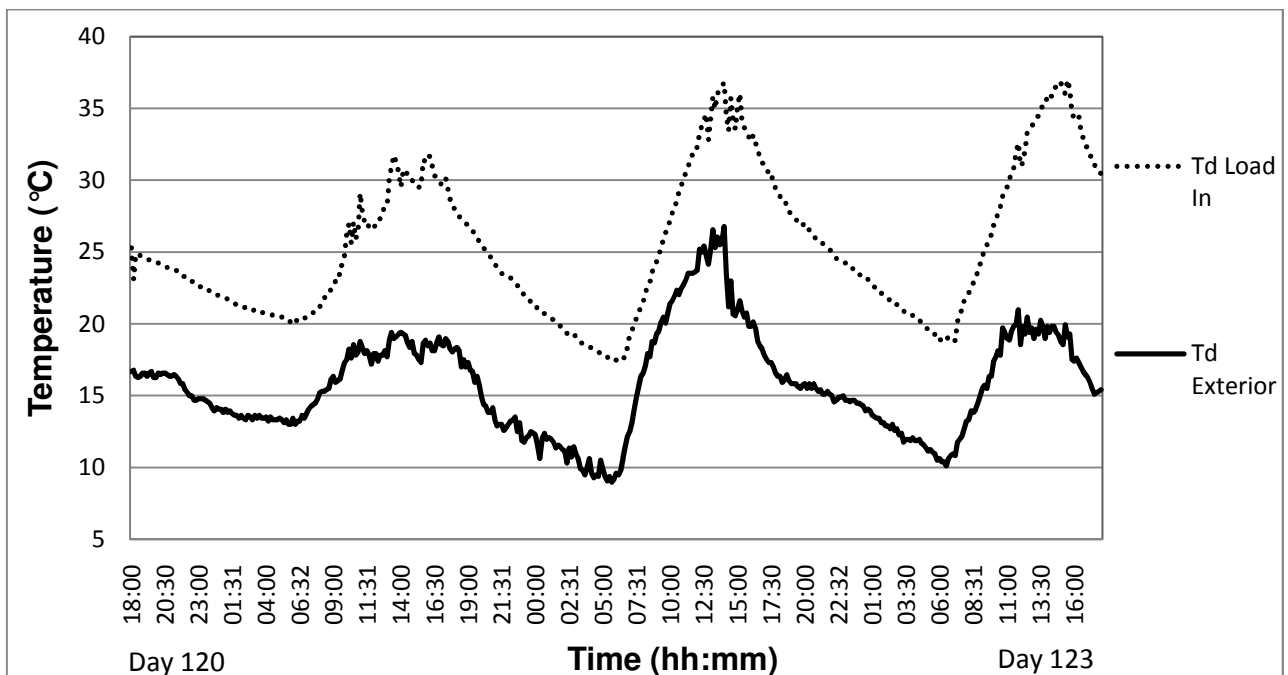


Figure 4.48:  $T_d$  Load In and  $T_d$  Exterior against time covering days 120 - 123;  
MC = 10.15%

It was noted in the initial drying stage that the internal temperature was at a lower level when high external temperatures prevailed. In the later drying stages below FSP, the kiln offered less protection against warm external conditions, as there was less cooling by evaporation from the load. The  $T_d$  Load In temperature increased to rise up to a maximum temperature of 38 °C. Protection was strictly not necessary since the danger of check formation was less and there was no more chance of cell collapse.

ii. Kiln behaviour during the time of the day for the five drying stages.

The 130 days of drying was again divided into the same five drying stages, as used before. The average daily difference between internal and external temperatures at a specific time, or average  $\Delta T_{\text{time}} = \text{average of } (T_d \text{ Load In} - T_d \text{ Exterior})$ , is presented in Figure 4.49 as a typical day in each of the five drying stages.

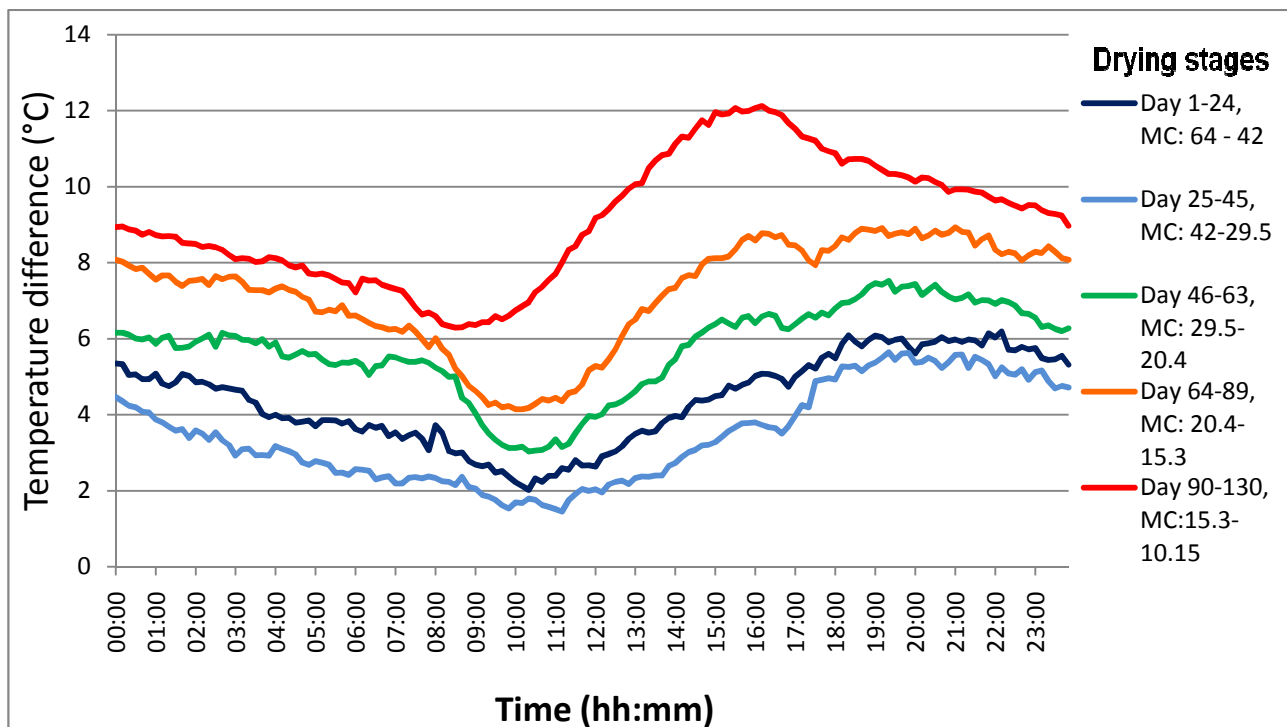


Figure 4.49: Typical average daily difference between internal and external temperature, average  $\Delta T_{\text{time}}$ , at various stages of drying

Again, it is clear that the difference between internal and external temperatures increased towards the end of drying. An interesting pattern is the maximum  $\Delta T_{\text{time}}$  which initially occurred at 21h00 and then gradually shifted towards 16h00 in the final drying period. The minimum  $\Delta T_{\text{time}}$  which initially occurred at 11h00 gradually shifted towards 08h00 in the final drying period. The most likely explanation for this is that the specific heat capacity of the material inside the kiln was much

less since most of the water in the timber had been evaporated. As the drying run proceeded, the kiln stored its heat for a longer time at night and heated up quicker in the mornings.

Summary:

- At MCs above FSP, the kiln temperature was at a lower level when high external temperatures prevailed. This protected the timber against drying defects such as checks and collapse.
- In the later drying stages, the kiln offered less protection against warm external conditions, and the kiln temperatures increased as the timber dried and reached a maximum of 38°C. Here protection was not necessary any more since the danger of check formation was less and there was no chance of cell collapse.
- During the afternoons and into the night, the stack and concrete in the kiln were a source of heat for the kiln air. The temperature inside the kiln did not drop as quickly as the external temperature.
- The difference between internal and external temperatures increased towards the end of drying.
- The maximum  $\Delta T_{\text{time}}$  gradually moved from 21h00 towards 16h00 as drying progressed.
- The minimum  $\Delta T_{\text{time}}$  gradually moved from 11h00 towards 08h00 as drying progressed.

#### 4.3.7 Comparison between EMC inside and outside the kiln

This section will look at the comparison between the EMC inside and the EMC outside the kiln to simulate the conditions as if the timber was air dried under external conditions as experienced during the drying run.

The difference between internal and external EMCs can be obtained when the 130 days of drying is divided into the same five drying stages as used in Section 4.3.6.2 and Figure 4.49. The difference between internal and external EMCs,  $\{EMC_{\text{Load In}} - EMC_{\text{External}}\}$ , is expressed as  $\Delta EMC$ . The MC was obtained from the 24 sample boards and EMC was calculated using the Hailwood-Harrobin equation in Appendix D3.

Table 4.13: MC, Average  $\Delta T_{\text{day}}$ , Average  $\Delta \text{EMC}$  and standard deviation for  $\Delta \text{EMC}$  for the five drying stages.

Day range	MC range (%)	Average $\Delta T$ ( $^{\circ}\text{C}$ )	Average $\Delta \text{EMC}$ (%)	St dev. $\Delta \text{EMC}$ (%)
1 - 24	64 - 42	4.44	3.61	4.34
25 - 45	42 - 29.5	3.46	2.99	4.82
46 - 63	29.5 - 20.4	5.72	0.69	4.49
64 - 89	20.4 - 15.3	7.19	-1.99	5.29
90 - 130	15.3 - 10.15	9.08	-1.65	6.03
<b>Total 1 - 130</b>	<b>64 - 10.15</b>	<b>6.45</b>	<b>0.33</b>	<b>5.70</b>

As is evident from Table 4.13, the average EMC was initially higher inside the kiln and gradually reversed to an EMC lower inside than outside. This pattern can be explained by the greater temperature difference between the internal and external air, and the smaller availability of moisture from the timber. The internal EMC will thus be lower during the latter stages of drying.

To observe the EMC difference at different times during the day, the 130 days of drying was again divided into the same five drying stages. The average difference between internal and external EMCs, at a specific time, average  $\Delta \text{EMC} = \text{average} (\text{EMC}_{\text{Load In}} - \text{EMC}_{\text{External}})$ , is presented in Figures 4.50 – 4.54 as a typical day in each of the five drying stages.

Note how the internal EMC progressively became more evenly spread throughout the 24-hour day, with a small drop during the daylight hours. The problem experienced with the dried-out wet bulb wick inside the kiln towards the end of drying must be kept in mind when observing the average internal EMC values. This will not give exact values, but rather give the general trend.

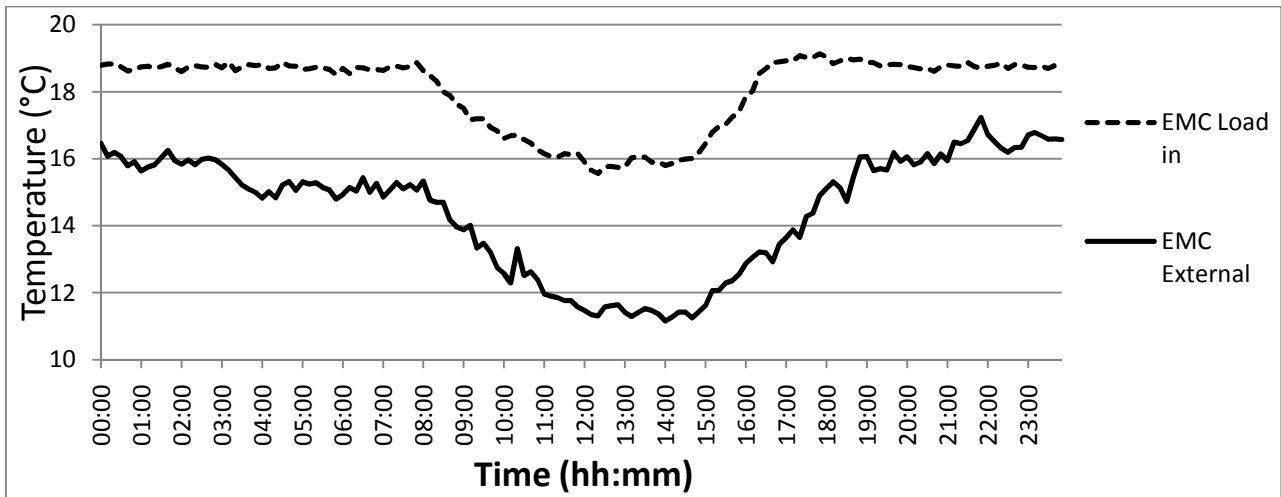


Figure 4.50: Average  $\Delta$ EMC from days 1 - 24; MC = 64% - 42%

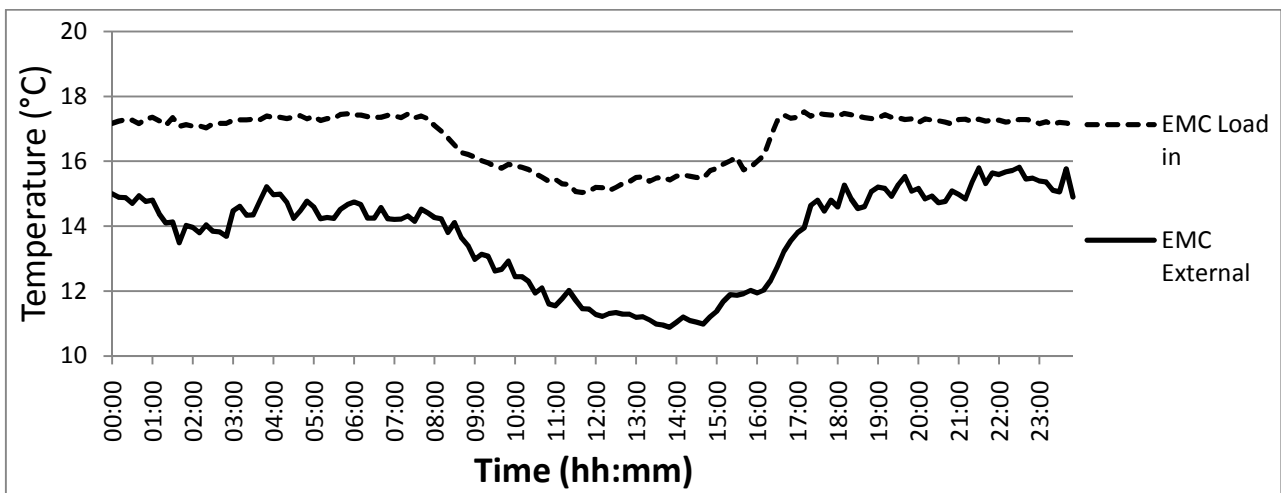


Figure 4.51: Average  $\Delta$ EMC from days 25 - 45; MC = 42% - 29.5%

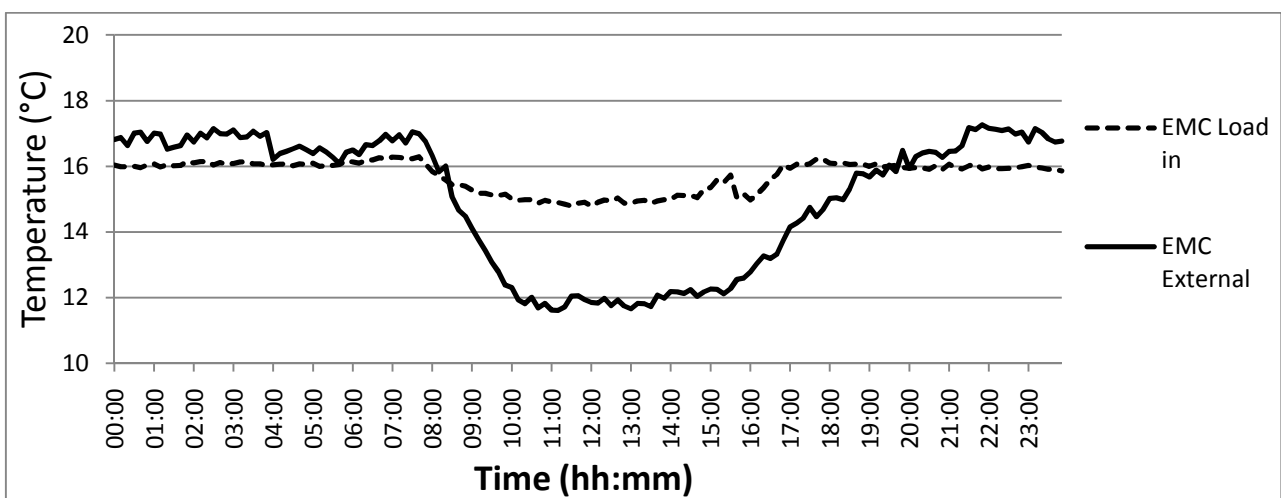


Figure 4.52: Average  $\Delta$ EMC from days 46 - 63; MC = 29.5% - 20.4%

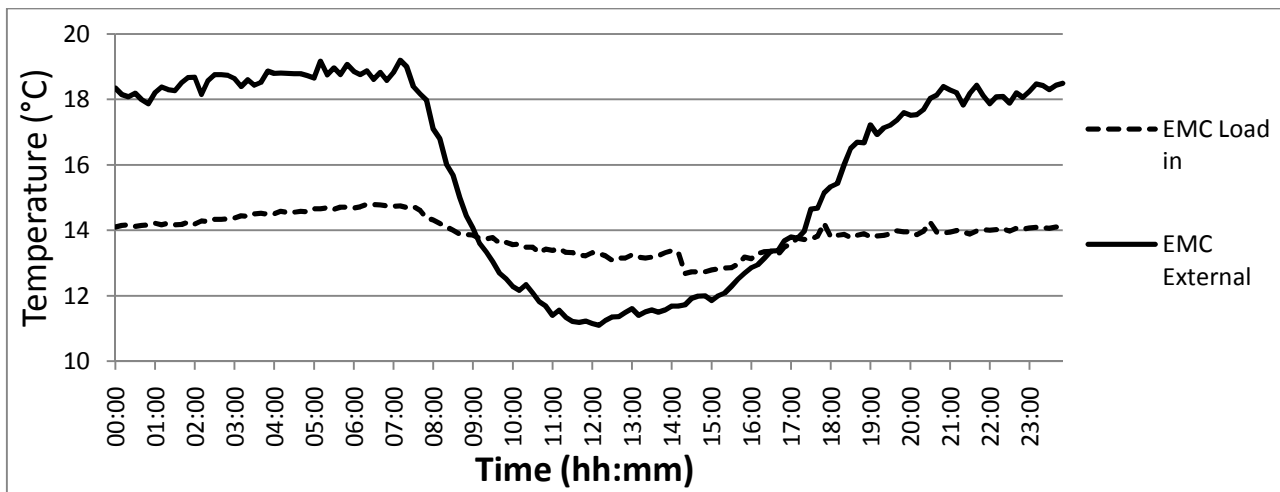


Figure 4.53: Average  $\Delta$ EMC from days 64 - 89; MC = 20.4% - 15.3%

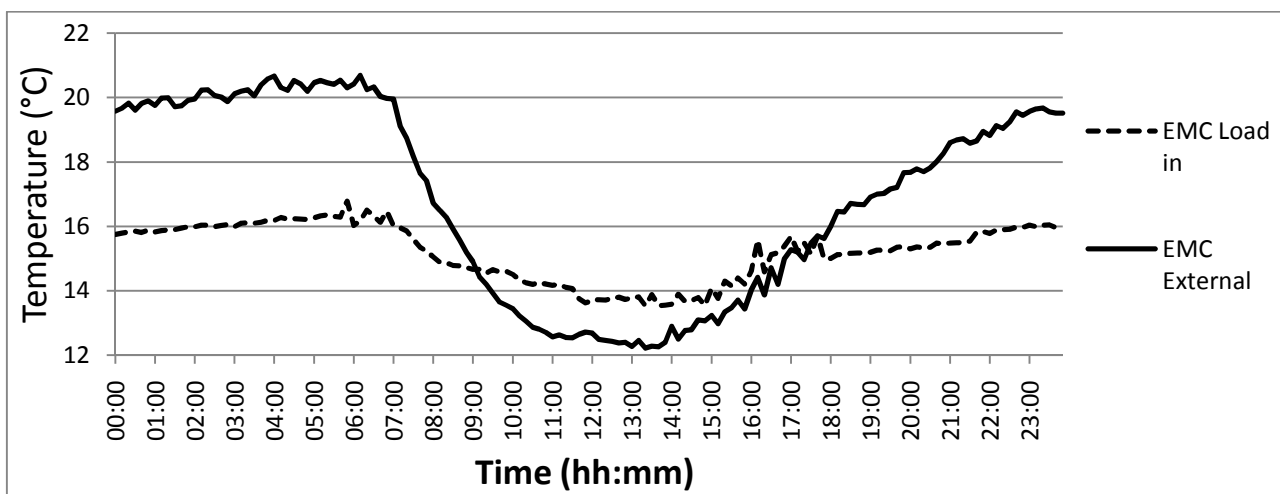


Figure 4.54: Average  $\Delta$ EMC from days 90 - 130; MC = 15.3% - 10.15%

From Figures 4.50 - 4.54, it is again clear that the EMC was initially higher inside the kiln and gradually reversed to an EMC lower inside than outside. Towards the end, there was a pattern during daylight hours where the EMC inside did not drop as much as the EMC outside. The result is that the EMC inside the kiln remained fairly constant compared to the more variable EMC outside.

Previously it was explained how the kiln offered protection against periods of high external temperatures, especially in the initial drying phase. It is now also clear that the timber was protected from dry atmospheric conditions, again in the initial drying phase. Towards the end, with less danger of drying defects, the EMC dropped to below the ambient EMC which resulted in a greater drying potential. This scenario of a gradual decreasing EMC and a gradual increase in temperature is typically found in drying schedules used in climatically controlled kilns. This will be compared with acknowledged drying schedules in Section 4.4.6.



Summary:

- Initially, the EMC inside the kiln was higher than the EMC outside. This condition gradually reversed to a lower EMC inside than EMC outside.
- The internal EMC progressively became more evenly spread throughout the 24-hour day, with a small drop during the daylight hours.
- The timber was protected from dry atmospheric conditions in the initial drying phase. Towards the end, with fewer dangers of drying defects, the EMC dropped to below the ambient EMC which resulted in a greater drying potential.
- The gradual decrease in EMC and gradual temperature increase is typically found in drying schedules used in climatically controlled kilns.

#### 4.3.8 Comparison between AH in the kiln and external AH's

The comparison between the AH inside and the AH outside the kiln is given here. The reason for this comparison was to investigate the feasibility of disposing of humid kiln air by means of traditional venting. This will require a control system of some sort, which was not used in this drying run.

The three-day drying measuring periods described at the beginning of Section 4.3 will now be used to compare the internal and external AHs, in Figures 4.55 to Figure 4.59. The kiln AH was calculated from the inlet temperature conditions to the load.

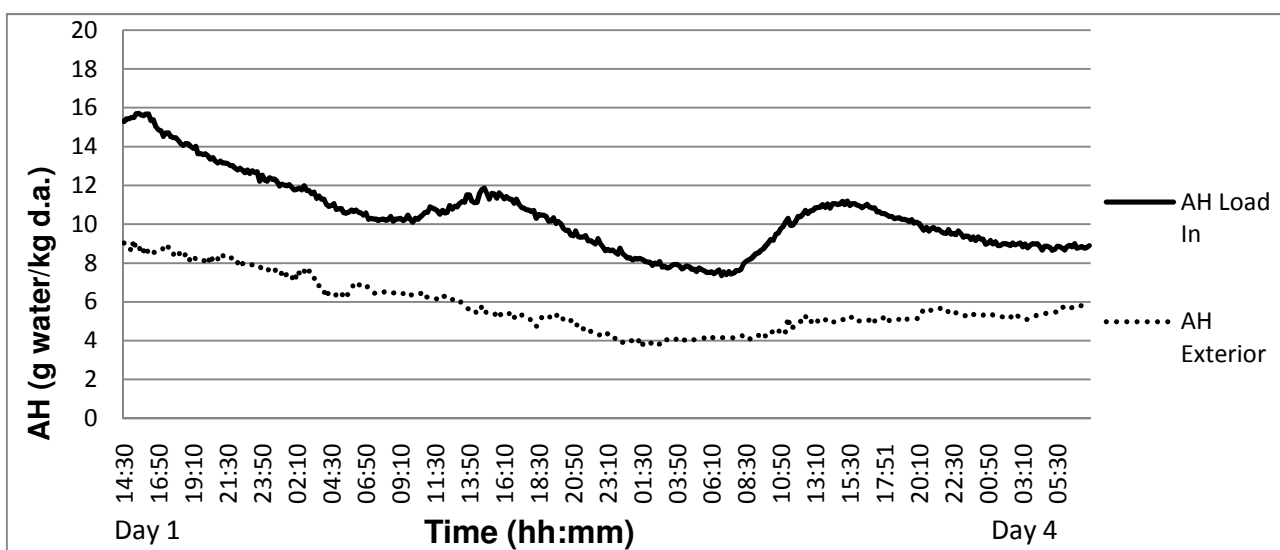


Figure 4.55: Comparison between AH Load In the kiln and AH Exterior during the measuring period of days 1 - 4; MC = 50%

The AH inside the kiln was consistently higher than the exterior AH. This was found during all five measuring periods. During the initial drying stages, the difference between AH Load In the kiln and AH Exterior was fairly constant. When the timber reached a MC of 43%, the trend changed where the AH Load In was at a maximum during noon. This trend continued to the end of drying as will be shown in Figures.4.56 – 4.59.

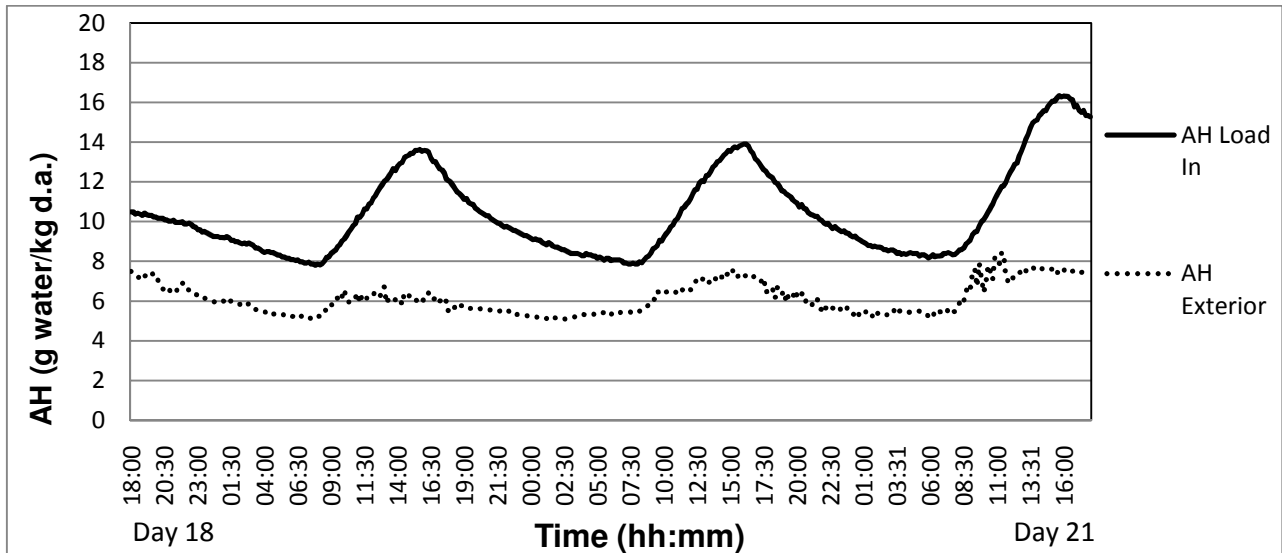


Figure 4.56: Comparison between AH Load In the kiln and AH Exterior during the measuring period of days 18 - 21; MC = 43%

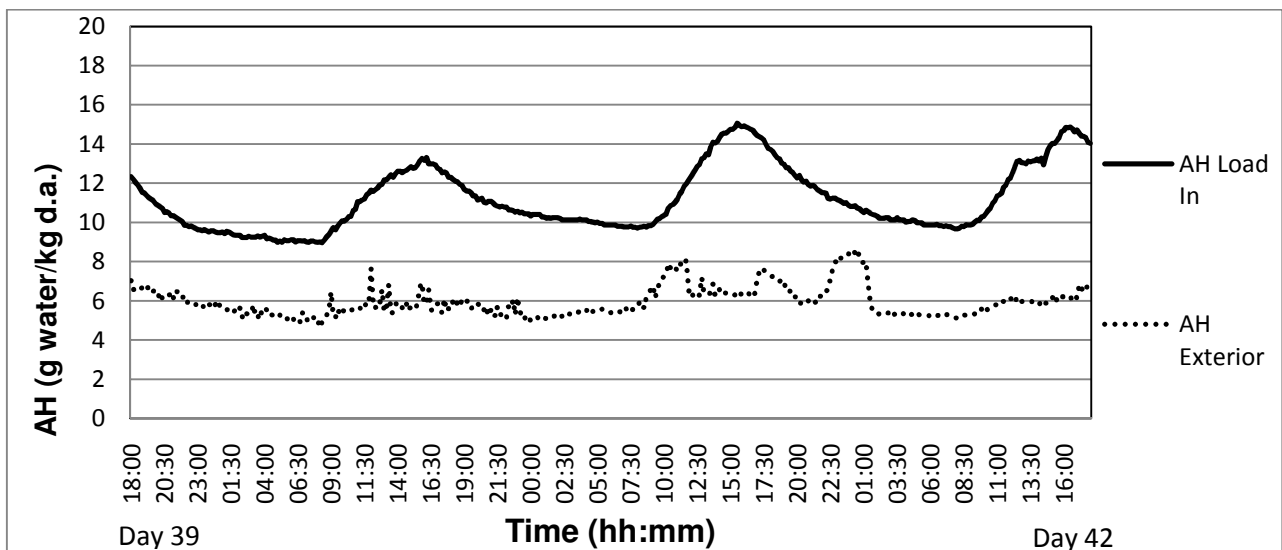


Figure 4.57: Comparison between AH Load In the kiln and AH Exterior during the measuring period of days 39 - 42; MC = 30%

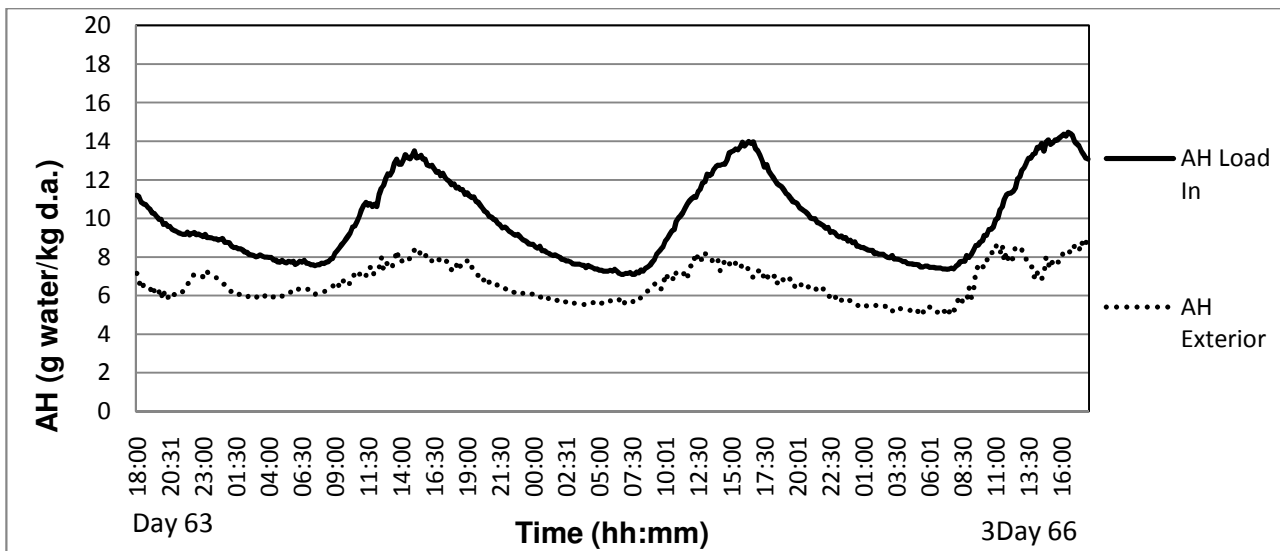


Figure 4.58: Comparison between AH Load In the kiln and AH Exterior during the measuring period of days 63 - 66; MC = 20.5%

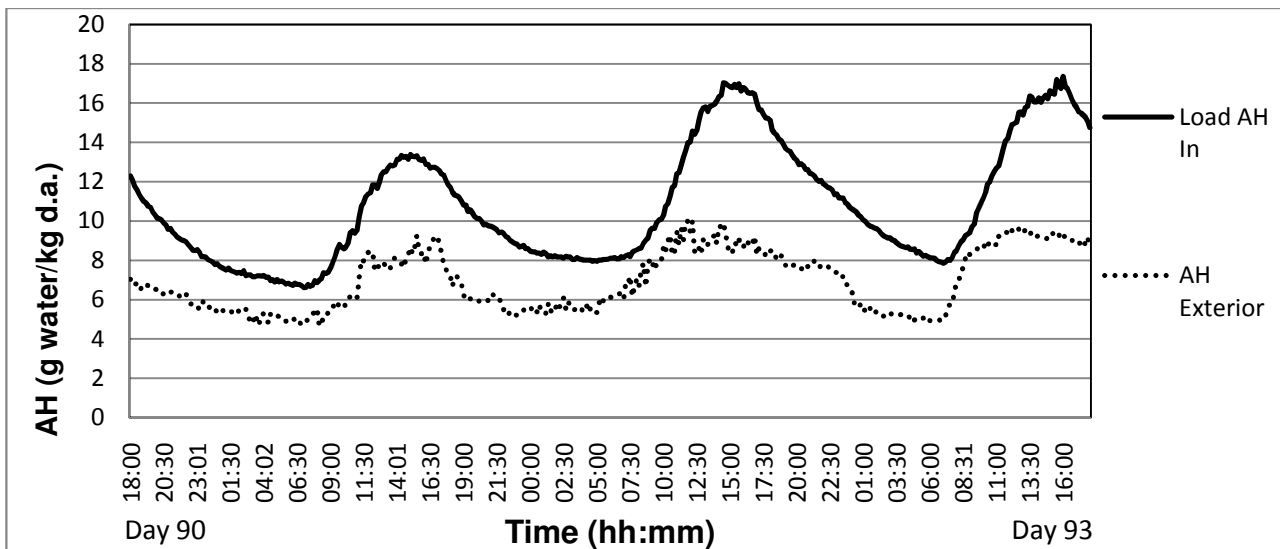


Figure 4.59: Comparison between AH Load In the kiln and AH Exterior during the measuring period of days 90 - 93; MC = 15.3%

Although only selected days are shown, there is a clear indication that during the entire drying run, the AH inside the kiln was constantly at a higher value than outside the kiln. This means that theoretically faster drying was possible by venting throughout the drying run. As venting at night would also reduce the AH inside the kiln, it is not advised as it would cause a substantial heat loss. Previous discussions emphasised the benefit of retaining the heat at night. Once the timber was below 43% MC, the best time of the day for venting would be during noon when the difference between interior and exterior AHs was at its maximum.

A simple form of venting could be applied by either allowing continuous venting with a very small opening or venting by opening the doors to the kiln for an hour during noon. Apart from the maximum difference in AH, venting at noon seem sensible, as there will be enough time left in the day to make up the heat losses from venting. The fresh dry air will promote faster drying as the vapour pressure of the air in the kiln will be lower. However, surface checks are prevalent when drying high density hardwoods too fast at MCs above FSP. Therefore, venting should be performed only once the timber has reached FSP. In this study, the heat lost by venting at noon would have been less since the maximum difference between internal and external temperatures gradually moved from 21h00 towards 16h00 as drying progressed. This difference was much less at noon.

Summary:

- The AH inside the kiln was consistently higher than outside the kiln, making it feasible to vent.
- The difference between interior and exterior AHs was at its maximum at noon when the MC was below 43%. This would be the best time of the day to vent.
- A simple form venting can be applied when the timber reach FSP.

#### **4.4 Comparison with other drying schedules**

The drying “schedule” that evolved over the drying run in the Saasveld solar kiln will be compared with schedules applied in a conventional kiln, where the climate can be controlled following a drying schedule. The drying schedules were obtained from the results and from the literature study performed in Chapter Two.

The temperature and EMC conditions that were evolved in the Saasveld solar kiln will be displayed on the same graph and compared with:

- Temperature and EMC conditions that were experienced outside the Saasveld solar kiln; and
- *Eucalyptus diversicolor* schedule suggested by Boone, Kozlik, Bois & Wengert (1993).

The comparison could provide the ideal schedule in a controlled kiln and will also indicate how closely the ideal kiln climate is to the climate that was experienced inside the Saasveld solar kiln, under auto-control. The benefits of the Saasveld solar kiln compared to air-drying are also shown.

Vermaas (1995) described the drying of *Eucalyptus* for quality by investigating various drying methods and schedules. In other publications, Vermaas (1987), Simpson (1980), Langrish, Keey & Kumar (1992), Neumann & Saavedra (1991), Stöhr & Mackay (1983), Bauer (2003), and Haque & Langrish (2006), discussed different techniques to dry hardwoods. The techniques of the authors above will be discussed and compared with the drying behaviour in the Saasveld solar kiln.

#### 4.4.1 Combined air-and-kiln seasoning

One specific drying technique in use for hardwoods is a combined air-and-kiln seasoning. Refractory timber species are air dried to below FSP in order to avoid cell collapse. The timber is then dried in medium to high temperature kilns, since the danger of collapse is absent below FSP. However, air-drying above FSP is not a safe method. It is only cheaper, but produces more defects. It was shown that the conditions in the Saasveld solar kiln were not as harsh as the conditions during air seasoning. The result was an improved timber quality in terms of drying defects and moisture distribution.

#### 4.4.2 Pre-drying in a solar kiln

The aim of pre-drying in a solar kiln is to have better control than in air seasoning during the drying above FSP. The drying is faster in a solar kiln than in air as there is drying over the full 24-hour day and the weather has no or little influence on the drying. The result is that most air-drying is replaced with pre-driers when drying above FSP (Wengert, 1985).

Vermaas (1995) citing Brennan *et al.* (1966), who used steam heated pre-driers, for the drying of *Eucalyptus* timber, with typical dry bulb temperature of 38-43°C, wet bulb depression of 4-8°C (EMC of 9.7%-14 %) and air velocities of 1.25-2 m/s. The temperature in the Saasveld solar kiln was lower, although with similar EMC and air velocity values.

The drying time from green to FSP in the Saasveld solar kiln was 45 days compared to 20 days in a conventional pre-drier at Northern Timbers in South Africa for 25 mm *Eucalyptus grandis* (Personal communication: S.V. Mogale, 2005). Note that the *Eucalyptus grandis* has a lower air-dry density (570kg/m<sup>3</sup> to 660kg/m<sup>3</sup>, depending on the age (Banks, Schoeman & Otto, 1977)), compared to density of 897kg/m<sup>3</sup> of the *Eucalyptus diversicolor* used in the Saasveld solar kiln.

#### 4.4.3 Smoothed schedules

Simpson (1980) found that relatively large abrupt changes in EMC in a conventional kiln will generate an abrupt MG in red oak. This MG increased the risk of surface checks. The timber experienced stress concentrations at the tip of small micro cracks on the surface layer of the lumber. He added that the stress concentration was magnified by the notch sensitivity of the timber and cracks formed and grew in length. A gradual change in both temperature and humidity improved the drying quality of the timber.

However, the timber in the Saasveld solar kiln was never exposed to conditions of abrupt temperature or EMC changes over the full drying run.

#### 4.4.4 Intermittent schedules

Studies by Langrish, Keey and Kumar (1992) showed the effect when drying high density red beech, while the kiln conditions were cycled over time. Samples were either continuously dried at  $T_d=45^{\circ}\text{C}$ , EMC = 8.6% (wet bulb depression =  $10^{\circ}\text{C}$ ) or intermittent dried from 09h00 to 16h00 each day at the same drying conditions. The samples that were intermittently dried took longer to dry, but the quality in terms of case-hardening and internal checks was better than continuous drying. It should be noted that red beech is a high density specie, known for high drying degradation. This intermittent schedules and the drying quality achieved, compared well with the cyclical nature of the drying inside the Saasveld solar kiln.

Vermaas (1995) dried *E. grandis* with good results by alternating the drying phase with periods of closing all the vents and switching off the heaters. These conditions occurred naturally during most nights in the Saasveld solar kiln, despite a lower average temperature.

Neumann & Saavedra (1992) investigated the use of high humidity treatments on check formation in *E. globulus*. Checks were significantly lower when initial drying temperatures were kept below  $30^{\circ}\text{C}$  and were followed by a 30-minute exposure to high humidity treatments of  $50^{\circ}\text{C}$ , EMC of 18.2% four times a day.

Stöhr & Mackay (1983) evaluated drying schedules for 25mm thick *E. grandis* and developed advanced drying schedules for *Eucalyptus* species. The schedule started with a dry bulb temperature of  $45^{\circ}\text{C}$  and EMC of 18.2% up to 35% MC. Intermittent high humidity treatments were performed for 30 minutes every 24 hours.

The conditions of higher EMCs experienced each night in the solar kiln simulate the controlled EMCs of the intermittent schedules described above. However, it was at lower temperatures in the Saasveld solar kiln. Therefore it supports the excellent drying quality of the Saasveld solar kiln as described in Section 4.1.

#### 4.4.5 Solar drying

Bauer (2003) described an optimised schedule for a biomass furnace assisted solar dryer (see Section 2.3) to dry *E. grandis* timber. Boards, 27mm thick, were dried. The drying schedule to dry 27 mm thick boards in 27 days is shown in Figure 4.60. The air temperature inside the solar kiln oscillated during the whole drying process. The temperatures were higher during the day than at night, depending on the ambient air temperature. The schedule ramped up from  $T_d = 40^\circ\text{C}$ , RH = 70% initially, to  $T_d = 50^\circ\text{C}$ , RH = 25% at the end. In terms of EMC: Initial  $T_d = 40^\circ\text{C}$ , EMC = 12.2%; final  $T_d = 50^\circ\text{C}$ , EMC = 4.7%. Re-humidifying cycles for three hours at 90% RH were run every second day to reduce drying stress.

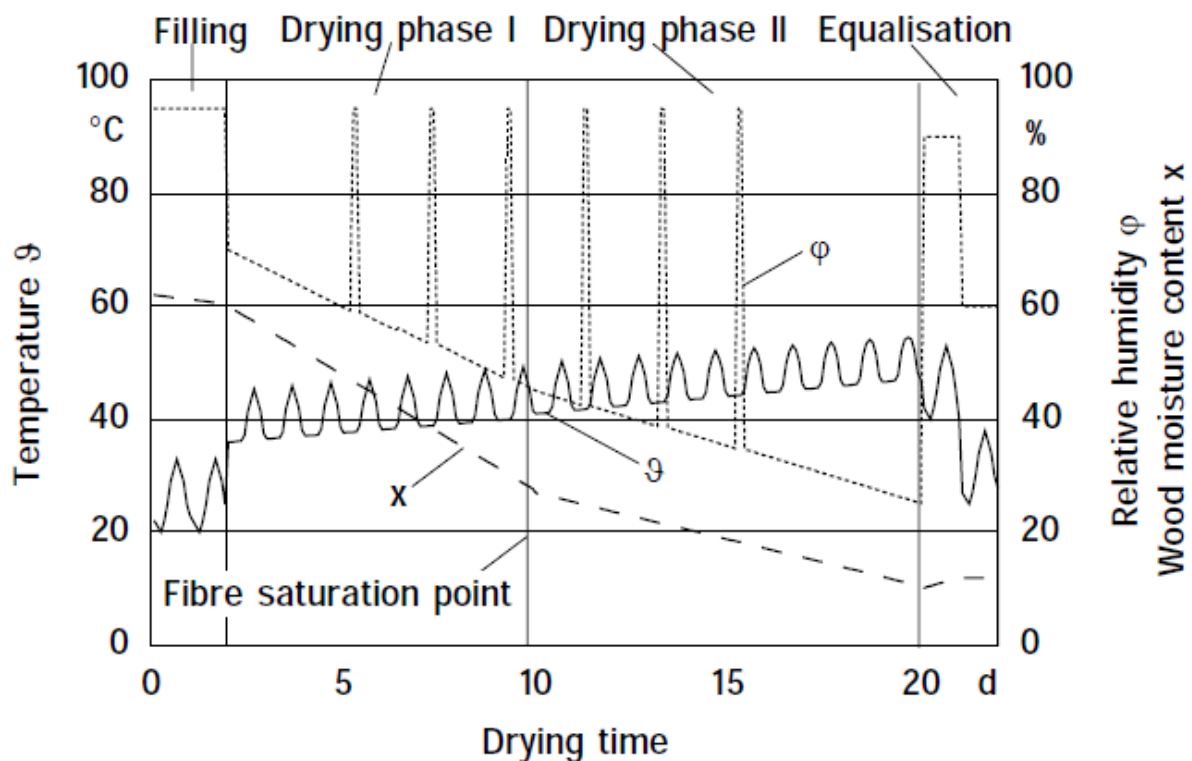


Figure 4.60: Presentation of a drying schedule by Bauer (2003) for sensitive eucalypt timber in the furnace assisted solar dryer

Bauer (2003) reported that the results indicated that the drying quality was excellent, however, the final timber quality was negatively influenced by the low quality of the available raw material, which included shrinkage and growth stresses.

The timber in the Saasveld solar kiln was dried with a similar “schedule” including the auto-execution of high humidity cycles at night, although at lower temperatures. The drying was performed without control systems and additional heating systems and produced excellent drying quality. Equalising and conditioning at the end of drying was not required in the Saasveld solar kiln.

Haque and Langrish (2006) investigated a solar kiln that dried 43mm thick *Eucalyptus pilularis* in five drying runs. The wood MC ranges and average values (in parenthesis) are as follows:

- Initial MC: 43%-62% (53%)
- Final MC: 12%-22% (18%)
- Drying days: 42 - 119 days (69 days)

The temperature gradually increased and the EMC gradually decreased in the 12-step drying schedule used (see Table 4.14). The last step was started when the wood MC was at 10%, although the final wood MC was always higher than 12%. The only reference to the drying quality was the average final MC that was achieved by using the schedule of Table 4.14 below.

Table 4.14: Typical moisture-content based schedule for drying 43 mm thick blackbutt boards  
(Haque and Langrish, 2006)

Initial MC (%)	Dry bulb temperature (°C)	Wet bulb temperature (°C)	Relative humidity (%)	EMC (%)
70	25	24	85	18.0
60	25	23	80	16.0
45	30	27	75	14.0
35	35	30	70	12.5
30	35	29	65	11.3
25	35	28	55	9.5
20	40	29	45	7.8
15	45	29	30	5.7
14	45	26	22	4.0
13	55	26	15	2.0
10	55	25	12	1.5
Recondition	45	40	75	12.8



This final climate would dry out the wood surface and would need a final equalisation and conditioning treatment. Equalising and conditioning requires extra hardware and scheduling, which was not necessary at the Saasveld solar kiln. This schedule compared well with the conditions inside the Saasveld solar kiln, except that the EMC did not drop as low. The drying time in the Saasveld solar kiln was 90 days to get to 15.3% wood moisture content, which appears to be similar to what was obtained by Haque and Langrish (2006).

#### 4.4.6 Comparison with an approved schedule

The average temperature and EMC conditions that were experienced by the Saasveld solar kiln and external drying conditions outside the kiln during the six measuring periods were compared to the *Eucalyptus diversicolor*, or karri gum, schedule suggested by Boone, Kozlik, Bois, and Wengert (1993). This comparison can be seen in Figures 4.61 and 4.62. The schedule by Boone *et al.* (1993) is defined as the moisture content schedule T3C2.

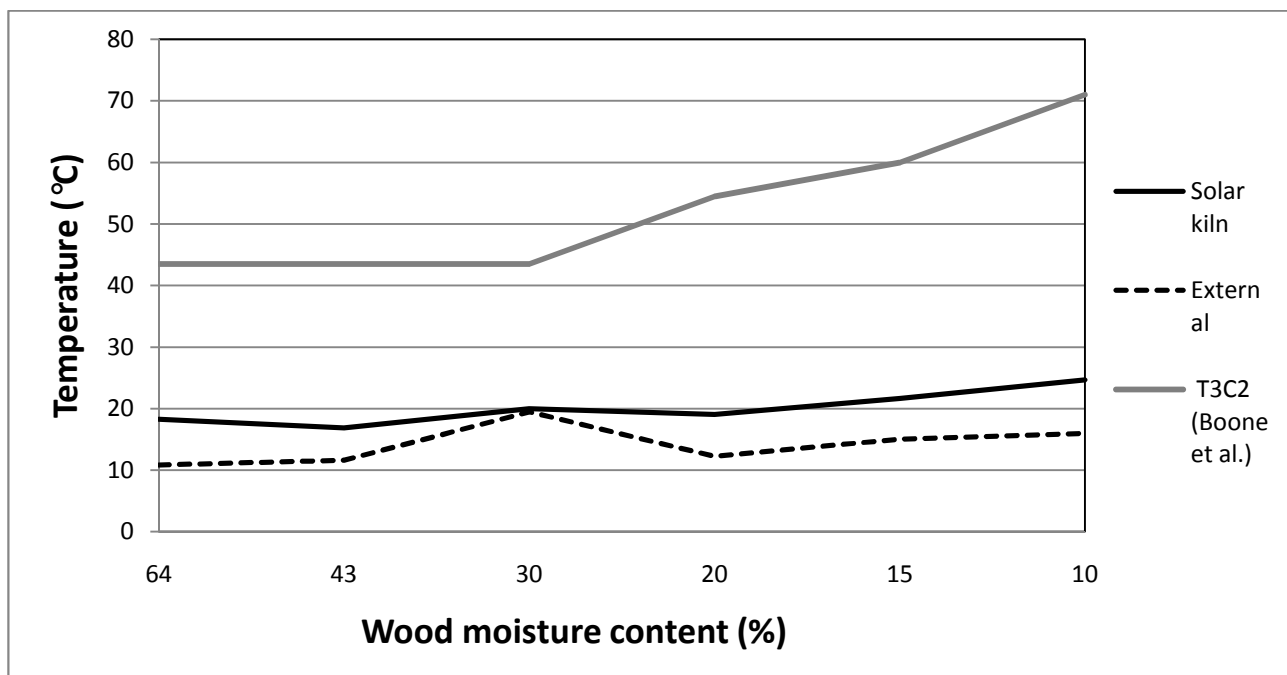


Figure 4.61: Comparison between the T3C2- schedule and the temperature experienced inside and outside the Saasveld solar kiln



Figure 4.62: Comparison between the T3C2- schedule and the EMC experienced inside and outside the Saasveld solar kiln

The temperature in the Saasveld solar kiln showed an increase, similar to all drying schedules. However, the rise was very small and temperatures were not as high as the T3C2- schedule, especially when the MC was below FSP. The solar kiln protected timber against high external temperatures and assisted in the prevention of cell collapse. Cell collapse can occur in air-drying.

The air-drying (external) “schedule” as indicated in Figures 4.60 and 4.61 was purely incidental. This is far from the ideal conditions of T3C2 as set out by Boone *et al.* (1993). The extra-ordinary Bergwind period experienced, when the MC was at 30%, could have occurred when the timber was green and could have caused disastrous drying defects.

The EMC in the solar kiln stayed very close to that of the T3C2 schedule for the critical period above FSP. The Saasveld solar kiln could not reach the lower allowable EMC of the T3C2 schedule, as the temperature in the kiln was limited by the solar radiation and the EMC limited by the natural dehumidification. These lower temperatures and higher EMCs in the solar kiln had the result that the timber dried slower in the solar kiln when the MC was below FSP, compared to conventional drying methods. No equalising and conditioning was needed for the solar kiln, but was required for the T3C2 schedule.

The drying below FSP in the solar kiln was much slower than the industry standard. This suggests that the Saasveld solar kiln could be used as a pre-drier. Timber could be pre-dried to FSP in the solar kiln and thereafter transferred to a conventional kiln if a faster drying rate is required and a

greater MC variation is tolerated. The even MC distribution found in the solar kiln will definitely deteriorate in this combined drying method. There is also a bigger probability that other drying defects would arise. The pre-drying would not be recommended as the advantage of simplicity of operation of the Saasveld solar kiln is lost.

#### 4.5 Configuration of the Saasveld solar kiln for future research on natural dehumidification

As the Saasveld solar kiln operated on a completely different mechanism and taking into account that virtually no previous research was conducted on this type of solar kiln, a basis needs to be set to serve as a benchmark against which to compare solar kilns utilising natural dehumidification.

The specific kiln geometry has to accommodate the timber volume in mind. Too little timber will create conditions that are too dry especially in the initial drying phases, which may introduce drying defects, especially surface checks. In the present work, this problem was experienced during a drying run of ironwood (*Olea capensis*) which had an average density of 1000 kg/m<sup>3</sup>. Only 0.25m<sup>3</sup> of the ironwood was stacked together with 8m<sup>3</sup> of *Pinus taeda*. The *Pinus taeda* dried quickly whereas the ironwood took longer to dry. The conditions were too dry for the wet ironwood and resulted in some surface checks. For the purpose of future research, some unique ratios for this specific drying run at the Saasveld solar kiln are provided in Table 4.15.

Table 4.15: Geometric parameters of the Saasveld solar kiln

Internal air volume (stacked kiln)	196.35 m <sup>3</sup>
Floor area	8 x 9.8 = 78.4 m <sup>2</sup>
Timber volume	20.155 m <sup>3</sup>
Total board surface area	1,711.7 m <sup>2</sup>
Condensation area	115.5 m <sup>2</sup>
Total length of air travel	4.8m
Air volume to timber volume	196.35 / 20.155 = 9.74 m <sup>3</sup> /m <sup>3</sup>
Condensation area to timber volume	115.5 / 20.155 = 5.73 m <sup>2</sup> /m <sup>3</sup>
Wood surface area to air volume	1711.7 / 196.35 = 8.72 m <sup>2</sup> /m <sup>3</sup>
Collector ratio, based on the floor plan area	78.4 / 20.155 = 3.89 m <sup>2</sup> /m <sup>3</sup>

The air volume to timber volume ratio ( $9.74 \text{ m}^3/\text{m}^3$ ) could become a benchmark for deciding the kiln geometry for any solar kiln that works on the natural dehumidification principle of the Saasveld solar kiln, where no vent control was done. A small air volume to timber volume ratio could result in drying that is too slow resulting in fungal growth. A large ratio could result in a climate too severe as discussed with the ironwood example. The condensation area to timber volume could become a benchmark for assessing the natural dehumidification (condensation) potential.

The more wood in a given size kiln, the more water is present to regulate the climate in the solar kiln. Higher initial EMC values will be maintained for a longer period. Fungal growth on most high density hardwoods is not a problem.

Future investigations should be conducted to provide more on the interaction between the air volume to timber volume ratio, the condensation area to timber volume and the influence of the board thickness and timber specie.

## **5 CONCLUSIONS AND RECOMMENDATIONS**

The overall results of the drying run were discussed in Chapter Four. This chapter provides recommendations for the future operation of such kilns as well as suggestions for further research on solar kilns that utilise natural dehumidification. The study will conclude by discussing the most important results that explain the operation and performance of a solar drying kiln that dries high density hardwoods by utilising natural dehumidification.

### **5.1 Conclusions**

The purpose of this thesis was to study the operation and performance of a solar drying kiln drying high density hardwoods by utilising natural dehumidification. The Saasveld solar kiln load consisted of  $20.1 \text{ m}^3$  of a high density hardwood, *Eucalyptus diversicolor*, with an average air-dry density of  $893 \text{ kg}/\text{m}^3$ . The timber dried from 50% moisture content (MC) to an average MC of 11.5% in 130 days. It reached 15.3% MC in 90 days.

The performance of the kiln in terms of drying quality of the wood was assessed by means of a recognised method, ZA Dry Q. The results indicated that the claims of the good drying quality were

valid. The ZA Dry Q drying quality assessment showed outstanding moisture distribution with little drying stress, a few surface checks and no internal checks, collapse, short bow or surface discolouration. The results easily met the ZA Dry Q softwood appearance grade specification, except for end checks, – remarkable for the drying of any high density hardwood. The final average MC of 11.5% (standard deviation 0.97%) and the average MG of 1.49%, (standard deviation 0.5%) are excellent. All MC and MG values were equally distributed in all three geometric directions throughout the load which confirmed uniform drying throughout the load.

It was expected that the temperature and humidity would be auto-regulated as the sun heated the kiln and natural dehumidification would happen at night. This auto regulation was confirmed by temperature and humidity data that was continuously collected inside and outside the kiln, simultaneously with the MC of the load. The parameters derived from the data provided the drying “schedule” that was automatically followed in the kiln. This drying schedule followed the trend of the T3C2 –schedule for *Eucalyptus diversicolor* (Boone, *et al.* (1993)), and explained the excellent drying quality of the load.

The average daily kiln temperature increased from 18.0°C initially to 25.7°C at the end. Initially, there was plenty of moisture available from the timber and this resulted in cooling of the air as evaporation took place. As the timber dried out, there was less moisture; therefore less energy was required for evaporation, causing the temperature inside the kiln to increase. The equilibrium moisture content (EMC) decreased automatically from a daily average of 18.1% to 8% from the initial MC to the final MC. The EMC dropped as there was less moisture available as the evaporation rate decreased. The measured EMC was never below 7.3%.

Evaporation in the kiln was determined by examining the absolute humidity (AH) of the air as it entered and exited the timber load. Evaporation occurred throughout the day and portions of the night when the wood MC was above 45%. When wood MC dropped below 45%, evaporation generally started around 07h30 and stopped around 16h45. Vapour saturation did occur a few times at the wood MC above 42%. However, the stack wide effect was negligible in this drying run.

Humidity control, or rather auto-regulation, was achieved by a unique process of natural dehumidification at night. This type of humidity control is extremely simple as colder night temperatures was a certainty, with no control system and no human intervention necessary. Condensation was expected at night from 17h00 to 07h30.

Nocturnal equalising and conditioning, comparable to intermittent schedules, resulted from

- no evaporation at night below 45% MC
- improved moisture diffusion in heated timber, highest at the end of drying.
- adsorption of moisture on the wood surface that increased as the drying progressed and reduced the moisture gradient.
- The long drying time with mild climatic conditions

Careful drying in the solar kiln persisted over the full drying run. The timber was never exposed to conditions of abrupt temperature or EMC changes. Apart from the mild drying conditions and nocturnal equalising cycles, the protection offered by the kiln was one of the reasons for the small amount of surface checking found in the load.

The functioning of the Saasveld solar kiln can be summarised as drying of the timber during the day and the drying of the air (dehumidification) at night.

There are several possibilities to improve the operation of this solar kiln. Further investigations need to be conducted, including a design where the air-flow is conventional over-the-top, venting strategies, stopping the fan/s at night and the air volume to timber volume ratio. Care should be taken that modifications to the kiln do not complicate the operation of the solar kiln.

The kiln operation is extremely simple with no vents, no controllers or electronics. The operator has to stack the load, put the baffles in place, and start the kiln fan. The fan is switched off when the timber is at the target MC.

Timber processors, who need to dry high density hardwoods within a reasonable time to an excellent drying quality, will benefit from solar kilns that utilise natural dehumidification. The operator does not require great technical skills or have the necessary drying expertise. The operating cost is very low as no drying personnel are needed. The only advanced hardware is a three-phase axial fan for air circulation and a single-phase radial fan at the jacket. The simplicity together with the low cost of the kiln, estimated at US\$ 10,000 (R 70,000), makes it ideal for less economically developed countries, individuals who have little drying expertise or areas where technical back-up is not readily available.

## 5.2 Recommendations

The kiln proved itself by drying high density timber within a reasonable time of 130 days from a MC of 50% to 11.5%. A MC of 15.1% was reached after 90 days.

### 5.2.1 Recommended modifications to the design and operation of a natural dehumidification based green-house solar kiln

It is suggested that the main circulating fan be switched off during the hours from 17h00 to 07h30, once the timber reaches 45% moisture content. This action will save electricity consumption and maintain higher temperatures of the load to promote diffusion. A general purpose digital programmable timer, typically used at swimming pools, can be installed at the Saasveld solar kiln to switch the fan on or off at specific times. It is a simple unit that cost US\$ 35 (R 250). The fan can be set to switch on from 07h30 to 17h00. A manual option can override the automatic settings.

The small fan that is used to inflate the jacket must operate continuously. It is critical for dehumidification at night and during the day it transports air from the jacket into the kiln to promote heating of the wood.

There is the possibility of doing some manual venting after FSP has been reached to increase the drying rate, without sacrificing the drying quality. A small vent can stay open all the time or it can be opened once FSP has been reached when drying hardwoods. This will result in some heat loss due to venting at night. A better approach would be to open the front and back door daily during noon for 30 minutes, once FSP has been reached. As discussed, the maximum difference between AH inside and AH outside occurs at noon and enough time is left in the day to make up the heat losses from venting. This will work well if the kiln is situated at a processing setup where a general worker can be assigned to open and close the doors at the start and end of the lunch period. The effect of venting on the other drying parameters and the drying quality should be further investigated.

Solar kilns operating on natural dehumidification must be installed in locations with a distinct diurnal temperature range, probably more than 10 °C.

The Saasveld solar kiln could be used as a pre-drier to carefully dry the timber to below FSP. The rest of the drying process could be completed faster in a conventional kiln as the wood can now

tolerate higher temperatures and lower EMC conditions. Double handling would be the main disadvantage as well as possible lower overall quality.

A kiln design, with a different airflow was suggested by Steinmann (Steinmann, personal communication, 28 February 2001). The design uses the conventional over-the-top airflow pattern as used in conventional kilns. See Figure 5.1.

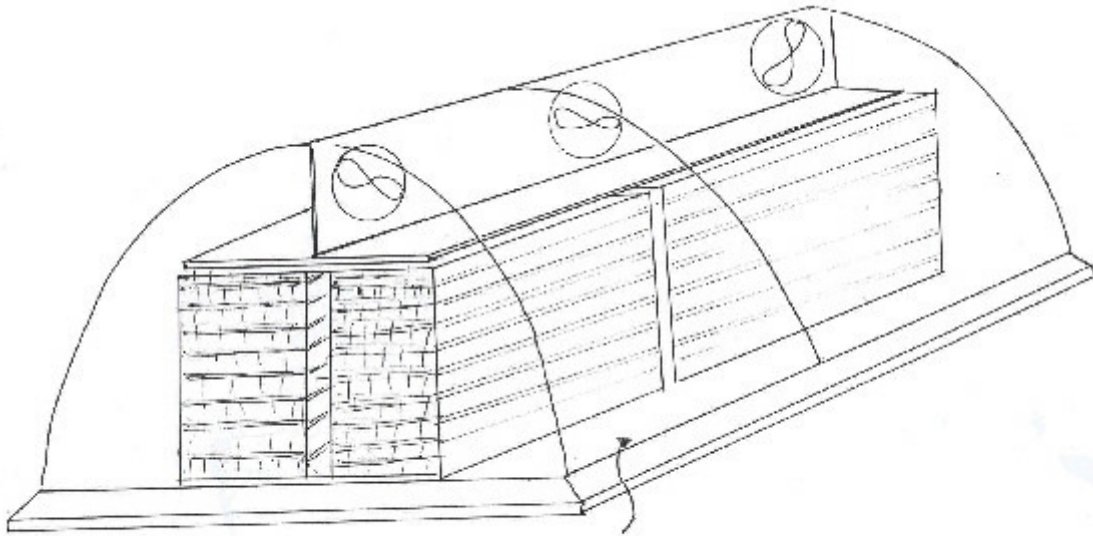


Figure 5.1: Alternative to the Saasveld solar kiln (Steinmann, 2001)

This kiln has the following advantages:

- simple construction
- easier stacking against a solid central frame (on the symmetry-line) as the wood is carried in length-wise and stacked length-wise
- the kiln can be operated with a smaller load if necessary
- no separate canvas is necessary
- the fans can be smaller as the system pressure drop is smaller
- kiln capacity is increased
- stacks can be built outside the kiln and moved into the kiln via rails. Loading will be much faster.
- more and smaller fans, driven by photovoltaic cells, can be used instead of one big fan.

The smaller fans will allow the use of single-phase motors. The use of photovoltaic cells to run the fans will be possible. The current single fan at the Saasveld solar kiln needs a three-phase fan to overcome the system pressure drop and still maintain a 1.5m/s air velocity through the stack. When there are more fans, one or two fans can be switched off once the load reaches FSP as the required air velocity is less below FSP. This will reduce the electric consumption. Lower airspeed will allow the use of photovoltaic cells.



### 5.2.2 Suggested research in solar kilns that utilise natural dehumidification

Care should be taken to avoid the following when research is done on a similar solar kiln:

- The wet bulb temperature probes, especially  $T_d$  Jacket In occasionally ran dry. There was a high air velocity at this probe making it easy to dry out.
- The probes at the jacket inlet and outlet should be protected against radiation, similar to the probes at the load inlet and outlet during this drying run.
- Jacket exit thermocouples were positioned at the eastern side of the kiln, resulting in a rapid rise in temperatures in the mornings. There should be thermocouples situated at the western jacket exit as well.
- As the kiln will probably never be perfectly air tight, this should be taken into account in the analysis.

Wood core temperature in future research should be measured at the inlet and exit of the load to determine the exact levels of heat collected and heat lost during diurnal drying cycles. The precise diffusion coefficient can also be determined during the various times of the day.

Future research should measure the wet bulb temperature at the exit of the load. The diurnal temperature fluctuations in a solar kiln differ from the constant conditions in a conventional kiln. An investigation into the diurnal heat transfer between the timber and the air in the kiln is recommended.

The effect of lower air speeds should be investigated as this will provide answers to the use of smaller fans that can be operated by photovoltaic cells. The fans could operate continuously throughout the night, should the cells store enough ampere-hours during the day. If not, then the fans would stop automatically during the night, which is no problem as no evaporation took place from 16h45 to 07h30.

The specific kiln geometry will influence the air volume to timber volume ratio. The ratio ( $9.74\text{m}^3/\text{m}^3$ ) could become a benchmark for deciding the kiln geometry for any solar kiln that works on the natural dehumidification principle, where no vent control is done. More research is needed on the air volume to timber volume ratio and its effect on the evaporation rate as the condensation area to timber volume is also affected. These ratios should be optimised.

Utilising the solar kiln to allow boron diffusion can be investigated. The boron diffusion process involves a concentrated solution of the preservative being applied to the exterior surfaces of fresh sawn timber, usually by dipping. The timber is then close-stacked while still wet, covered to restrict drying, and left to allow the borate to diffuse to the centre of the timber, a process which takes several weeks. Although the timber is not closed stacked in the Saasveld solar kiln, it is inside an enclosed space, and the fans should not run. It is suggested that no drying take place during the treatment period; the load must be covered with the tarpaulin as it is normally done. The opening at the back can be covered if the tarpaulin is longer, or a separate tarpaulin can be used. The opening at the plenum chamber can easily be covered. The higher kiln temperatures will allow the diffusion to accelerate, and drying could start sooner. Another benefit is that this minimise the handling between the separate processes. The practicality of this process should be investigated.

Examining the effect and practicality of carrying out simple venting by either allowing continuous venting with a very small opening or venting by opening the doors of the kiln for a specified time during the day, is recommended. The venting policy will need to take the MC into consideration.

ZA Dry Q standards for hardwoods should be developed. The lack of standards is problematic especially for end checks, which are much more prevalent in hardwood than in softwood.

## REFERENCE LIST

- Australian Government: Forest and Wood Product Research and Development Corporation, (2010). *Australian hardwood drying best practice manual*, part 2 [Online]. Retrieved January 18, 2009: [http://www.timberbuilding.arch.utas.edu.au/tbia/view\\_article.asp?articleID=318](http://www.timberbuilding.arch.utas.edu.au/tbia/view_article.asp?articleID=318).
- Banks, C.H. (1969). *Solar drying of timber – a development study*. O/Hout 10. Pretoria: CSIR.
- Banks, C.H., Schoeman, J.P. & Otto, K.P. (1977). The mechanical properties of timbers with particular reference to South Africa. *South African Forestry Research Institute Bulletin* 48.
- Bauer, K. (2003). *Development and optimisation of a low-temperature drying schedule for Eucalyptus grandis (hill) ex maiden in a solar-assisted timber dryer*. Unpublished doctoral dissertation, University of Höhenheim.
- Boone, R.S., Kozlik, C.J., Bois, P.J. & Wengert, E.M. (1993). *Dry kiln schedules for commercial woods: Temperature and tropical*. United States of America: Forest Products Society.
- Brice, T. (2010). *Relative humidity and dewpoint temperature from temperature and wet bulb temperature* [Online]. Retrieved August 13, 2010: <http://www.srh.noaa.gov/images/epz/wxcalc/rhTdFromWetBulb.pdf>.
- Cech, M.Y. & Pfaff, F. (1980). *Kiln operator's manual for Eastern Canada* [Special Publication SP504ER]. Ottawa: Forintek Canada Corp.
- Chen, P.Y.S., Helmer, W.A., Rosen, H.N. & Barton, D.J. (1982). Experimental solar dehumidifier kiln for drying lumber. *Forest Products Journal*, 32 (9), 35-41.
- Culpepper, L. (1990). *High temperature drying: Enhancing kiln operations*. San Francisco: Miller Freeman Publications.
- Doe, P.E., Oliver, A.R., & Booker, J.D. (1994). A non-linear strain and moisture content model of various hardwood drying schedules. Published paper in *Proceedings 4<sup>th</sup> IUFRO International Wood Drying Conference*, August 9-13, 1994; Rotorua, New Zealand: Forest Products Association Limited.

- Haque, M.N. & Langrish, T.A.G. (2001). Stack-wide effects in the modelling of solar kilns for drying timber. *Drying Technology*, 19(1), 99-114.
- Haque, M.N. & Langrish, T.A.G. (2006). Assessment of the actual performance of an industrial solar kiln for drying timber. *Drying Technology*, 23, 1541–1553.
- Holman, J.P. (1992). *Heat Transfer*: 7<sup>th</sup> ed. Singapore: McGraw-Hill.
- ISO 2533:1975. [S.a.][Online]. Retrieved, August 14, 2010:  
[http://www.iso.org/iso/iso\\_catalogue/catalogue\\_tc/catalogue\\_detail.htm?csnumber=7472](http://www.iso.org/iso/iso_catalogue/catalogue_tc/catalogue_detail.htm?csnumber=7472)
- Koch, P. (1972). *Utilisation of the Southern pines: Agriculture Handbook No. 420*. Washington: United States Department of Agriculture.
- Langrish, T.A.G., Keey, R.B. & Kumar, M. (1992). Improving the quality of timber from Red Beech (*N. fusca*) by intermittent drying. *Drying Technology*, 10(4), 947-960.
- Le Roux, N.J. (1991). *Statistiek vir Wetenskaplikes 314* Unpublished class notes. Department of Statistics. Stellenbosch: University of Stellenbosch.
- Lumley, T.G. & Choong, E.T. (1979). Technical and economic characteristics of two solar kiln designs. *Forest Products Journal*, 29(7), 49-56.
- MC Systems, (1998). *MCS 120-04EX 20 channel data logger software version 4.121: Users manual* [Unpublished document]. Cape Town: South Africa.
- Mogale, S.V. (2005). *Combined air and kiln seasoning of Eucalyptus grandis at Northern Timbers*. [Personal communication: conversation]. 28 February 2001.
- Müller, R.B. (2008) *Low cost solar drying of hardwoods*. Unpublished paper delivered at South African Lumber Driers Educational Association (SALDEA) Convention, Johannesburg. October, 16-17 2008.
- Neumann, R.J. & Saavedra, A. (1991). Check formation during the during of *Eucalyptus Globulus*. *Holz als Röh- und Werkstoff*, 50, 106-110.

- Panshin, A.J. & de Zeeuw, C. (1980). *Textbook of Wood Technology*: 4<sup>th</sup> ed. New York: McGraw-Hill.
- Paroscientific, (2010). *MET4 and MET4A calculation of dew point* [S.a] [Online]. Retrieved August 13, 2010: <http://www.paroscientific.com/dewpoint.htm>.
- Sattar, M.A. (1993). Solar drying of timber - a review. *Holz als Röh- und Werkstoff*, 51, 409-416.
- Simpson, W.T. (1980). *Accelerating the kiln drying of oak*. Forest Products Library Research Paper FPL 378: Madison, USA.
- Simpson, W.T. (1991). *Dry kiln operator's manual: Agriculture handbook No. 188*. Madison, Wisconsin: United States Department of Agriculture.
- Solar Kiln Company Inc. (1983). *Solar dry wood kiln: A technical note*. Mazomanie: USA.
- South African Lumber Millers Association (SALMA), (2003a). *Awareness campaign for ZA Dry Q System*. Johannesburg: SALMA [unpublished document].
- South African Lumber Millers Association (SALMA), (2003b). *ZA Dry Q Work Instructions for assessing dried board quality*, ZW 03 (2003), Johannesburg: SALMA [unpublished document].
- Steinmann, D.E. (1989). *Solar kiln drying of wood*. Unpublished doctoral dissertation, University of Stellenbosch.
- Steinmann, D.E. (2001). *Solar kiln design*. [Personal communication: conversation]. 28 February 2001.
- Stoecker, W.F. & Jones, J.W. (1982). *Refrigeration and air conditioning*. 2<sup>nd</sup> ed. Singapore: McGraw-Hill.
- Stöhr, H.P. & Mackay, D. (1983). *Drying schedule evaluation of 25mm E. grandis*. Hout 320. Pretoria: CSIR.
- The Wood Explorer Database (2010) [S.a] [Online]. Retrieved August 13, 2010: [http://www.thewoodexplorer.com/maindata/we500.html#Scientific\\_Name](http://www.thewoodexplorer.com/maindata/we500.html#Scientific_Name)

- Van Wylen, G. & Sonntag, R. (1985). *Fundamentals of classic thermodynamics*. 3<sup>rd</sup> ed. New York: John Wiley & Sons.
- Vermaas, H.F. (1987). Case for the low temperature kiln drying of *Eucalyptus grandis*, *South African Forestry Journal*, 140, 72 - 77.
- Vermaas, H.F. (1990). *Wood Physics 214* Unpublished class notes. Department of Wood Science. Stellenbosch: University of Stellenbosch.
- Vermaas, H.F. (1995). Drying eucalypts for quality: material characteristics, pre-drying treatments, drying methods, schedules and optimisation of drying quality. *South African Forestry Journal*, 174, 41 - 49.
- Vömel, H. (2010). *Saturation vapor pressure formulations* [Online]. Retrieved August 13, 2010: <http://cires.colorado.edu/~voemel/vp.html>.
- Wengert, E.G. (1985). New drying technology in the USA. Published paper in *Symposium proceedings: Forest products research international* (3, pp.1-13), April, 22-26, 1985. Pretoria: South Africa.
- Wengert, E.G & Oliviera, L.C.(2010) , *Solar heated, lumber dry kiln designs* [Online]. Available at <http://www.woodweb.com> [Accessed 13 August 2010].

## APPENDICES

## **APPENDIX A: KILN HARDWARE**

### **A.1 Plastic cover:**

All plastic sheets are of the same material. The plastic used here had a thickness of 180  $\mu\text{m}$ . Anti-drip additives raise the surface tension of the film to prevent dripping. It is used in greenhouses to prevent water droplets from falling onto plants, thus reducing the incidence of disease. It is important that the double skinned plastic covers should not have this feature. The water should rather run down the plastic sheet as a film of water. The plastic cover at the Saasveld Solar kiln was the Suntherm TM, obtained from Vegtech 2000 and STANDEX, obtained from Rhino Plastics.

### **A.2 Fastening of plastic cover:**

The plastic sheets were attached to the concrete base by a single clamping rail. The plastic sheet was clamped between a rubber strip and a high density polyethylene (HDPE) profile. The plastic sheet was placed in position and the rubber strip was hammered with a rubber mallet into the HDPE profile. The HDPE profile fitted into an aluminium rail (see Figure A.2). The aluminium rail is fastened to the concrete by nail plugs, also known as “Hilti’s”.

The plastic sheets were attached to the frame using the same type of rail system. These offered problems at the first and last curved ribs at the edges of the main cover. Here the rail has to keep three plastic sheets: two from the main cover and one from the end cover. The installation was difficult and the plastic sheets were not held tight, with the result of wind damage to the kiln (see Figure A.1). These were removed and replaced by a superior double rail system, supplied by Rhino Plastics. One of the rails fastened the double plastic sheets of the main cover and the other rail is used for the side wall plastic of the greenhouse tunnel. Here the plastic sheet is positioned in-between the aluminium rail and a HDPE profile. The HDPE profile is pressed into position to keep the sheet momentarily fastened. This allows easy movement during installation as the plastic sheet is not tightly clamped. To ensure a firm connection, a final HDPE wedge shape strip is hammered with a rubber mallet into the initial HDPE profile (See Figure A.3). This initial profile expands sideways, and pinches the sheet. Two HDPE profiles fitted into a double aluminium rail. Both rail systems were fastened to the frames by self-tapping “text” screws.





Figure A.1: Damage from the Bergwind.



Figure A.2: Original rail system. The plastic sheet fits in-between the HDPE profile and the rubber strip.

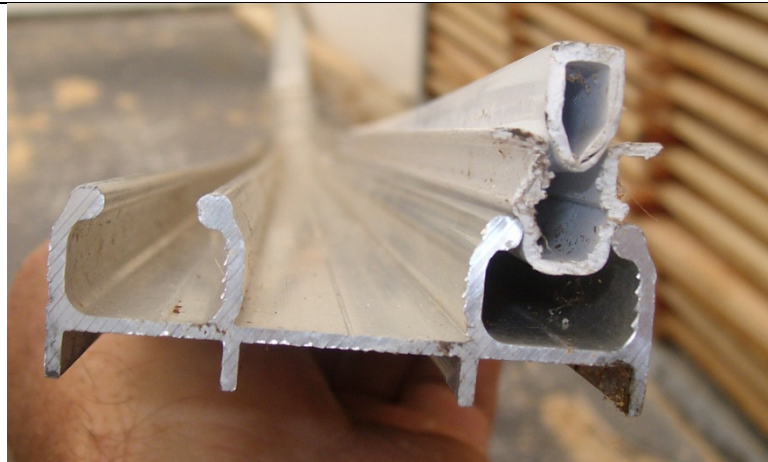


Figure A.3: The double rail system used at the leading edges of the Saasveld Solar kiln. The plastic sheet fits in-between the HDPE profile and the HDPE wedge strip.

All plastic sheets are of the same material. The plastic had a thickness of 180  $\mu\text{m}$ .

### **A.3. Main fan for air circulation**

The 380V three phase 3kW axial flow fan, diameter of 800mm, is situated on top of a steel frame in the plenum wall.

### **A.4 Heating of the kiln**

The only heat source was the solar heat gain from the sun. The 125mm thick 25 MPa strength concrete floor was painted black to increase solar absorbency. The floor surface acted as a heat store.

### **A.5 Small fan for humidity control**

Kiln air from the main chamber was blown with a 0.15kW forward curved radial fan into a 400mm diameter manifold. The fan was driven by a 230V single phase motor. The air was directed to the jacket via four 75mm diameter flexible aluminium foil tubes.

### **A.6 Stacking**

Eight stacks, each 2.5m long, 1.71m high and 1.2m wide, were prepared with timber of the following wet (green) dimensions:

Length: 2.5m

Thickness: 30mm

Width: Six stacks had 124mm wide boards, with nine boards in a row, and two stacks had 87mm wide boards, with 13 boards in a row.

### **A.7 Circuit board**

The entire electrical circuit board is shown in Figure A.4. Included was the following:

- Main isolator switch
- 20 Amp three phase isolator switch
- 10 Amp isolator switch to the lights
- 10 Amp isolator switch to the plugs

- Earth leakage protection
- Electric impulse fencing to fend off baboons
- Transformer to supply 12V to the electrical impulse fencing unit

The electric impulse fencing, for fending off troublesome baboons, had the following specifications:

- Maximum stored energy: 1.0 J
- Maximum output voltage: 10,000 V
- 12V battery at 85 mV

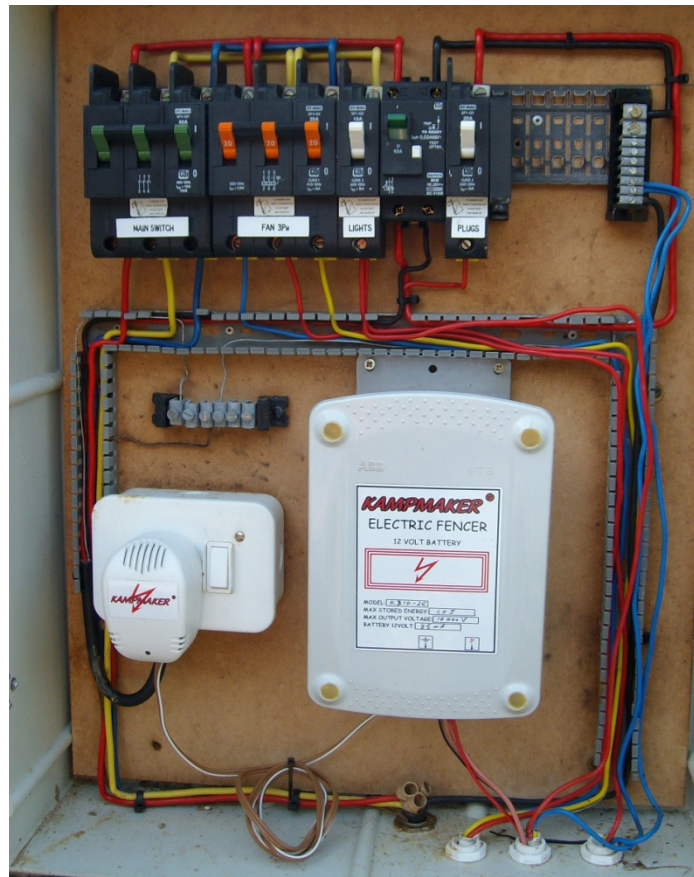


Figure A.4: Saasveld solar kiln electrical circuit board

A motor protection unit was inside the kiln.

## **APPENDIX B: DEFINITIONS OF DRYING DEFECTS AS DESCRIBED BY ZA DRY Q**

**Target moisture content:** The desired moisture content of all boards in a pack, stack or kiln load after drying is completed.

**Case-hardening:** The residual drying stresses in boards, which are caused by the drying process. It does not include stresses at the end of drying caused by inherent growth stresses or by the inclusion of reaction wood in a board.

**Surface checks:** – Separation of the fibres on the board surfaces shows up as cracks in the direction of the wood fibres.

**Internal checks:** – The lengthwise separation of the fibres inside the board that do not penetrate the board surface.

**End checks:** – Separation of the fibres at the end of boards, not stretching across the full thickness of the board and exceeding 30mm in length.

**Short bow caused by incorrect stacking:** – A deviation of the flat surface of the board of more than 1.5mm measured over a distance of 500mm along the board.

**Discolouration:** – An abrupt colour deviation along a board length from the general board colour and specifically at sticker positions.

## **APPENDIX C: THERMOCOUPLE CALIBRATION**

The calibration was performed by an initial auto-calibrating step with the MCS 120-04EX software (MC Systems, 1998). The accuracy of the thermocouple values was further improved by a water calibration, where the thermocouples were subjected to equal temperatures.

### **C.1 Auto calibration and pairing**

The MC Systems data logger had an internal programme that allowed the user to auto-calibrate probes by generating offset and multiplier values to suit the linear output from thermocouples. The input parameters were generated by setting the output sensor to a low known temperature like ice water. This value was entered in a low end register. The sensor was then set to a known temperature of water, close to 60 °C, and this value entered into the upper limit value, or “high end register”. The logger then calculated the appropriate offset and multiplier, and replaced any previous values with the new calculated values (MC Systems, 1998).

An initial data logging exercise was conducted after the auto-calibration to examine the behaviour of the thermocouples. The following method exposed thermocouples to equal temperatures ranging from 0 °C to 40 °C:

A small enclosed water reservoir of 200mm x 150mm x 100mm was prepared inside the solar kiln. The nine thermocouples were bundled together and positioned inside the reservoir. The reservoir was filled with ice water and the thermocouples were immersed into the ice water. A small water pump ensured that the water was constantly flowing over the bundle of thermocouples. The exit of the water pump was 15mm from the thermocouples. Since the thermocouples were exposed to a turbulent stream of water, they should give the same temperature reading. Temperature recordings started in the early morning immediately after the ice water and some ice cubes were poured into the reservoir. The data logger was set to record temperatures every minute for the entire day. The temperature of the water gradually increased during the day to a maximum of 40 °C.

The results indicated that measurements showed a small variation, though it could be improved. It also showed that some thermocouples followed similar patterns. Since the thermocouples were employed in pairs of a dry bulb and wet bulb, the ideal would be that the temperature values from each pair of thermocouples behave identically. It was thus decided that thermocouples with similar patterns should be paired, so that error values will be similar, and will ultimately have a smaller effect.

The nine sets of temperature values were they were plotted on MS Excel. Thermocouples were named according to the channel where it was connected. Thermocouples with similar temperatures and patterns through the temperature range from 0 °C to 40 °C were paired:

Table C.1: Pairing of thermocouples.

<u>CHANNEL</u>	<u>POSITION</u>	
2	$T_d$ Jacket Out	}
1	$T_w$ Jacket Out	
11	$T_d$ Jacket In	}
16	$T_w$ Jacket In	
10	$T_d$ Exterior	}
15	$T_w$ Exterior	
13	$T_d$ Load In	}
12	$T_w$ Load In	
14	$T_d$ Load Out	

## C.2 Improved calibration

Further care was taken, by means of a further water calibration, to ensure that the temperature values were accurate. The set-up for the water calibration was identical to the pairing exercise described in Section C.1. It was performed right after the kiln load was removed from the kiln, with the thermocouples still connected to the data logger.

The nine temperature values were plotted on MS Excel. Since the thermocouples were exposed to a turbulent stream of water, they should indicate the same temperature value, which was not the case. The variation, especially at higher temperatures, is evident from the graph in Figure C.1.

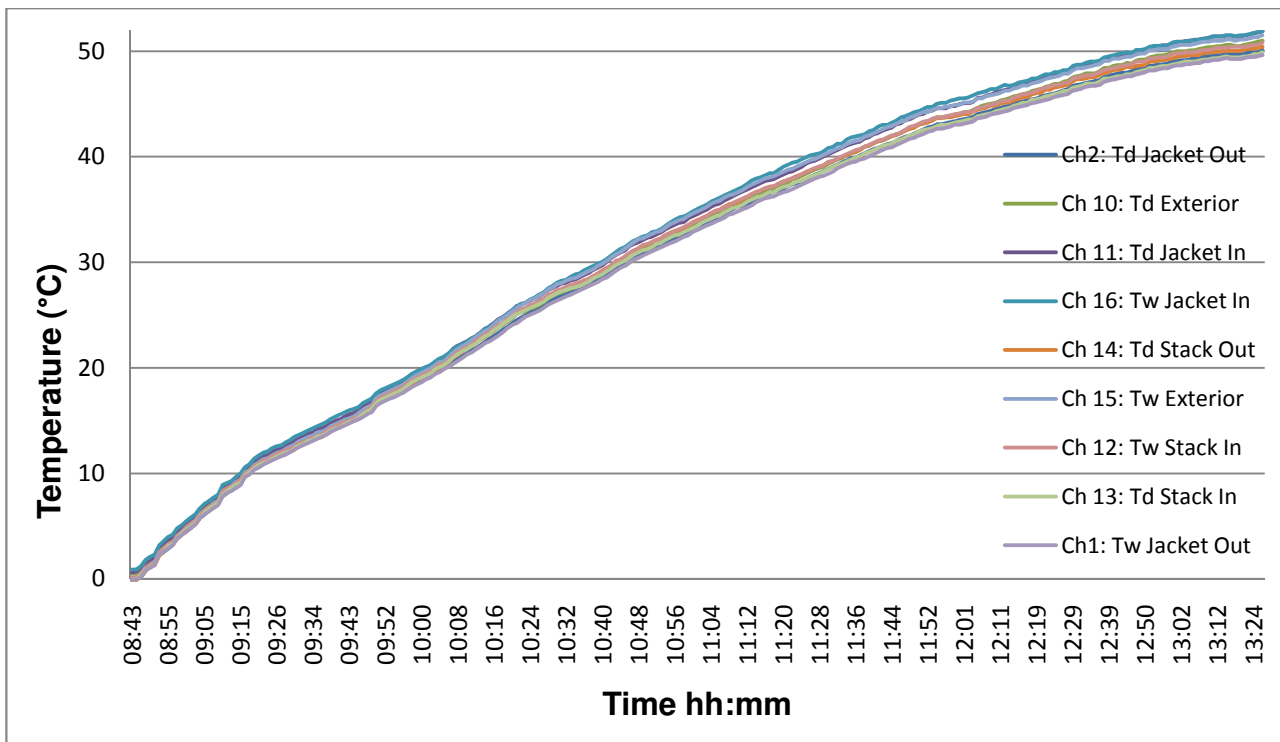


Figure C.1: The temperature variation during the water calibration procedure

Temperature values from the thermocouple connected to Channel 15 correlated the best with an independent digital thermometer, a TES-1310. It was decided to use the temperature value from Channel 15 as a reference value to improve the accuracy of the other thermocouples.

Each of the other eight thermocouples went through the procedure explained below. For clarity, the procedure to improve the accuracy for Channel 10 will be discussed.

Since the thermocouples were held at the same temperature, a difference will expose an error value. The initial thermocouple values for Ch 10 were subtracted from the reference thermocouple Ch 15 (See Table C.2. column 3). This difference, or correction value, was plotted against the Ch 10 temperature on MS Excel. An effort was then made to derive an equation, by means of a regression line, that represents this correction value:

$$\text{Correction} = \text{Ch 15} - \text{Ch 10} \cong f(\text{Ch 10})$$

Improved values for Ch 10 can then be obtained by:

$$\text{Ch 10} + f(\text{Ch 10}) = \text{Improved Ch 10 value.}$$

The linear, second order polynomial, third order polynomial and fourth order polynomial equations of  $\text{Ch 15} - \text{Ch 10} \cong f(\text{Ch 10})$  were derived by the trend-line function of MS Excel. These equations and trend-lines are shown in Figure C.2. The equations for these regression lines are shown along with their  $R^2$  values. The  $R^2$  value, also known as the coefficient of determination, is a number from



0 to 1 that reveals how closely the estimated values for the trend-line correspond to actual data. A trend-line is more reliable when its R-squared value is at or near 1 (Le Roux, 1991). This will give an indication of which polynomial function to use, although this will be discussed later.

Previous measurements indicated that the kiln temperatures and external temperatures varied in the range from 3°C up to 38°C. The calibration was performed for temperatures from 0°C to 38 °C.

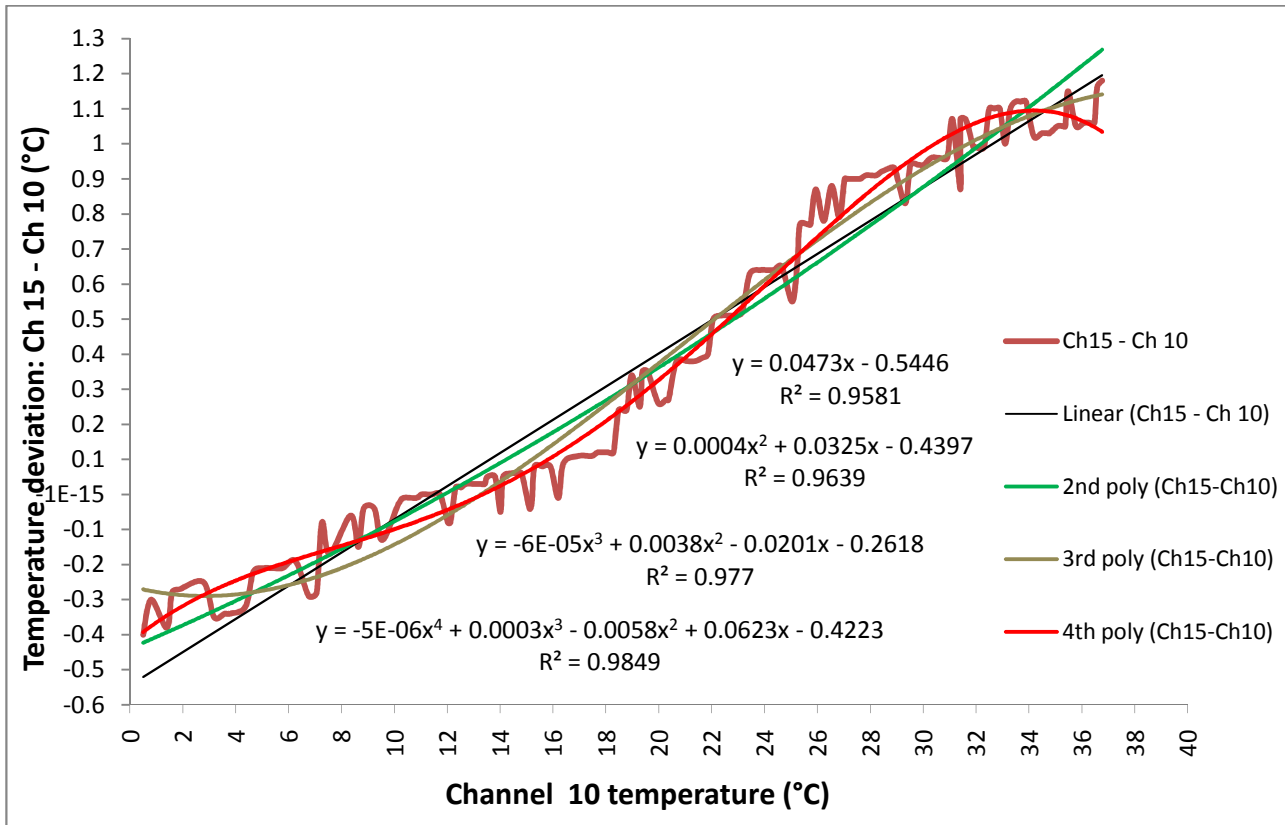


Figure C.2: Establishment of an algebraic equation of the correction in temperature

A portion of the calibration results are indicated in Table C.2 for the Channel 15-temperature range from 0°C to 5.16 °C and then towards the end from 35.52°C to 37.95 °C



Table C.2: A portion of the table for the initial calculations of polynomial functions to improve temperature values

		Correcti on	Ch15- 10	<u>Improve</u>	Ch15- 10	<u>Improve</u>	Ch15- 10	<u>Improve</u>	Ch15- 10	<u>Improve</u>
Ch 15	Ch 10	Ch15- 10	Trend	<u>Ch 10 (lin)</u>	Trend	<u>Ch 10 (2nd)</u>	Trend	<u>Ch 10 (3rd)</u>	Trend	<u>Ch 10 (4th)</u>
			1 Poly	1 Poly	2 Poly	2 Poly	3 Poly	3 Poly	4 Poly	4 Poly
0.10	0.50	-0.40	-0.52	-0.02	-0.42	0.08	-0.27	0.23	-0.39	0.11
0.10	0.50	-0.40	-0.52	-0.02	-0.42	0.08	-0.27	0.23	-0.39	0.11
0.50	0.80	-0.30	-0.51	0.29	-0.41	0.39	-0.28	0.52	-0.38	0.42
1.01	1.39	-0.38	-0.48	0.91	-0.39	1.00	-0.28	1.11	-0.35	1.04
1.31	1.59	-0.28	-0.47	1.12	-0.39	1.20	-0.28	1.31	-0.34	1.25
1.62	1.89	-0.27	-0.46	1.43	-0.38	1.51	-0.29	1.60	-0.32	1.57
2.53	2.78	-0.25	-0.41	2.37	-0.35	2.43	-0.29	2.49	-0.29	2.49
2.83	3.18	-0.35	-0.39	2.79	-0.33	2.85	-0.29	2.89	-0.27	2.91
3.24	3.58	-0.34	-0.38	3.20	-0.32	3.26	-0.29	3.29	-0.26	3.32
3.44	3.78	-0.34	-0.37	3.41	-0.31	3.47	-0.29	3.49	-0.25	3.53
4.05	4.37	-0.32	-0.34	4.03	-0.29	4.08	-0.28	4.09	-0.24	4.13
4.45	4.67	-0.22	-0.32	4.35	-0.28	4.39	-0.28	4.39	-0.23	4.44
4.86	5.07	-0.21	-0.30	4.77	-0.26	4.81	-0.27	4.80	-0.22	4.85
5.16	5.37	-0.21	-0.29	5.08	-0.25	5.12	-0.27	5.10	-0.21	5.16
etc	etc	etc	etc	etc	etc	etc	etc	etc	etc	etc
etc	etc	etc	etc	etc	etc	etc	etc	etc	etc	etc
etc	etc	etc	etc	etc	etc	etc	etc	etc	etc	etc
etc	etc	etc	etc	etc	etc	etc	etc	etc	etc	etc
etc	etc	etc	etc	etc	etc	etc	etc	etc	etc	etc
35.52	34.49	1.03	1.09	35.58	1.16	35.65	1.10	35.59	0.06	34.55
35.72	34.69	1.03	1.10	35.79	1.17	35.86	1.11	35.80	0.04	34.73
35.82	34.79	1.03	1.10	35.89	1.18	35.97	1.11	35.90	0.03	34.82
36.13	35.08	1.05	1.11	36.19	1.19	36.27	1.12	36.20	0.00	35.08
36.33	35.28	1.05	1.12	36.40	1.20	36.48	1.12	36.40	-0.02	35.26
36.43	35.38	1.05	1.13	36.51	1.21	36.59	1.13	36.51	-0.03	35.35
36.63	35.48	1.15	1.13	36.61	1.22	36.70	1.13	36.61	-0.04	35.44
36.83	35.78	1.05	1.15	36.93	1.24	37.02	1.14	36.92	-0.07	35.71
37.14	36.08	1.06	1.16	37.24	1.25	37.33	1.14	37.22	-0.11	35.97
37.34	36.28	1.06	1.17	37.45	1.27	37.55	1.15	37.43	-0.13	36.15
37.54	36.48	1.06	1.18	37.66	1.28	37.76	1.15	37.63	-0.16	36.32
37.74	36.58	1.16	1.19	37.77	1.28	37.86	1.15	37.73	-0.17	36.41
37.95	36.77	1.18	1.19	37.96	1.30	38.07	1.15	37.92	-0.20	36.57

The improvement in accuracy is clearly visible in Figure C.3. Note the inaccurate old Channel 10 values. The improvement is evident from the small difference between Channel 15 temperatures and the second and third polynomial Channel 10 temperatures.

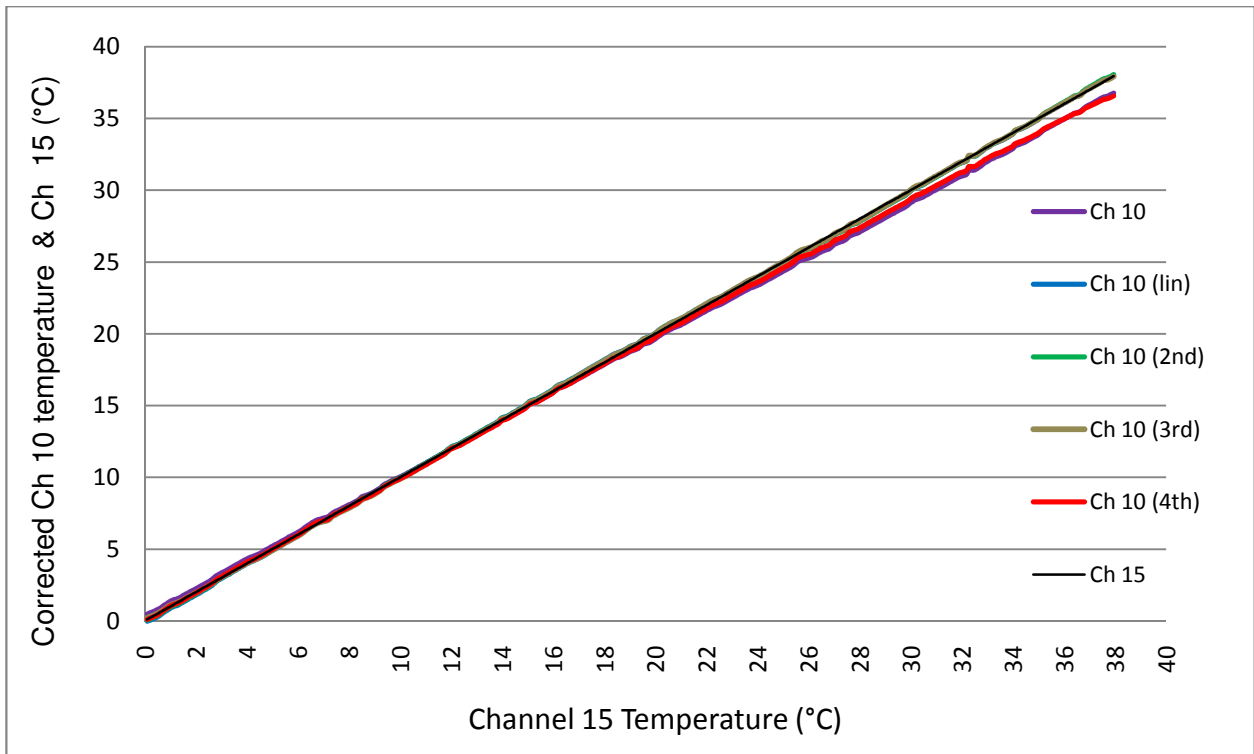


Figure C.3: Improved thermocouple values

The next step was a decision of which polynomial function to apply to each thermocouple. Once again, it will be described by using the Channel 10 thermocouple.

Previously it was described that  $\text{Ch 10} + f(\text{Ch 10}) = \text{Improved Ch 10 value}$ . It should be kept in mind that all thermocouples were kept at the same temperature throughout the water calibration process. The improved Ch 10 values are much closer to Ch 15, as can be seen in Figure C.3. However, there was a small difference, and the aim was to see which of these polynomial functions had the smallest difference. New correction values for each of the four polynomial functions described in Figure C.2 were obtained by:

$\text{Ch 15} - \text{Improved Ch 10} = \text{new correction value}$

The absolute values of the new correction values were obtained and the sum of all these values was compared. The polynomial function with the minimum sum was selected. Therefore the goal was to determine:

$$f(x) = \min \sum_{i=1}^n \{ |\text{Ch 15}_i - \text{Improved Ch 10}_i| \} = \min \sum_{i=1}^n \{ |\text{new correction value}_i| \}$$

A portion of the new correction values and the corresponding absolute values are displayed in Table C.3. Again, it is displayed for the Channel 15-temperature range from 0°C to 5.16°C and then to the end from 35.52°C to 37.95°C

Table C.3: A portion of the table for the new correction values (note that the sum and average at the bottom is for the entire table, and not for the values displayed).

New correction values				Absolute values of New correction values			
Ch15 - Improved Ch10 (lin)	Ch15- Improved Ch10 (2nd)	Ch15- Improved Ch10 (3rd)	Ch15- Improved Ch10 (4th)	Ch15 - Improved Ch10 (lin)	Ch15- Improved Ch10 (2nd)	Ch15- Improved Ch10 (3rd)	Ch15- Improved Ch10 (4th)
0.12	0.02	-0.13	-0.01	0.12	0.02	0.13	0.01
0.12	0.02	-0.13	-0.01	0.12	0.02	0.13	0.01
0.21	0.11	-0.02	0.08	0.21	0.11	0.02	0.08
0.10	0.01	-0.10	-0.03	0.10	0.01	0.10	0.03
0.19	0.11	0.00	0.06	0.19	0.11	0.00	0.06
0.19	0.11	0.02	0.05	0.19	0.11	0.02	0.05
0.16	0.10	0.04	0.04	0.16	0.10	0.04	0.04
0.04	-0.02	-0.06	-0.08	0.04	0.02	0.06	0.08
0.04	-0.02	-0.05	-0.08	0.04	0.02	0.05	0.08
0.03	-0.03	-0.05	-0.09	0.03	0.03	0.05	0.09
0.02	-0.03	-0.04	-0.08	0.02	0.03	0.04	0.08
0.10	0.06	0.06	0.01	0.10	0.06	0.06	0.01
0.09	0.05	0.06	0.01	0.09	0.05	0.06	0.01
0.08	0.04	0.06	0.00	0.08	0.04	0.06	0.00
etc	etc	etc	etc	etc	etc	etc	etc
etc	etc	etc	etc	etc	etc	etc	etc
etc	etc	etc	etc	etc	etc	etc	etc
etc	etc	etc	etc	etc	etc	etc	etc
-0.06	-0.13	-0.07	0.97	0.06	0.13	0.07	0.97
-0.07	-0.14	-0.08	0.99	0.07	0.14	0.08	0.99
-0.07	-0.15	-0.08	1.00	0.07	0.15	0.08	1.00
-0.06	-0.14	-0.07	1.05	0.06	0.14	0.07	1.05
-0.07	-0.15	-0.07	1.07	0.07	0.15	0.07	1.07
-0.08	-0.16	-0.08	1.08	0.08	0.16	0.08	1.08
0.02	-0.07	0.02	1.19	0.02	0.07	0.02	1.19
-0.10	-0.19	-0.09	1.12	0.10	0.19	0.09	1.12
-0.10	-0.19	-0.08	1.17	0.10	0.19	0.08	1.17
-0.11	-0.21	-0.09	1.19	0.11	0.21	0.09	1.19
-0.12	-0.22	-0.09	1.22	0.12	0.22	0.09	1.22
-0.03	-0.12	0.01	1.33	0.03	0.12	0.01	1.33
-0.01	-0.12	0.03	1.38	0.01	0.12	0.03	1.38
			<b>Sum</b>	<b>12.12</b>	<b>11.00</b>	<b>8.99</b>	<b>55.58</b>
			<b>Ave</b>	<b>0.09</b>	<b>0.08</b>	<b>0.06</b>	<b>0.39</b>

It was, therefore, decided to use the third order polynomial function for Channel 10, since the sum of the corrections was the minimum.

Therefore:

$$\text{Correction} = f(\text{Ch10}) = -6\text{E-}05 * (\text{Ch10})^3 + 0.00388(\text{Ch10})^2 - 0.0201 * (\text{Ch10}) - 0.2618;$$

Then,

$$\begin{aligned} T_d \text{ Exterior} &= \text{Ch10} + f(\text{Ch10}) \\ &= \text{Ch10} - [6\text{E-}05 * (\text{Ch10})^3 + 0.00388(\text{Ch10})^2 - 0.0201 * (\text{Ch10}) - 0.2618]. \end{aligned}$$

Similarly, the correction functions were calculated for the other thermocouples and are indicated in Table C.4.

Table C.4: Regression functions of the correction for the different thermocouples

Thermocouple	Correction function
$T_w$ Jacket Out	$f(\text{Ch1}) = -6\text{E-}05 * (\text{Ch1})^3 + 0.0039 * (\text{Ch1})^2 - 0.0207 * (\text{Ch1}) + 0.29$
$T_d$ Jacket Out	$f(\text{Ch2}) = -5\text{E-}05 * (\text{Ch2})^3 + 0.0032 * (\text{Ch2})^2 - 0.0181 * (\text{Ch2}) + 0.2918$
$T_d$ Jacket In	$f(\text{Ch 11}) = 0.0005 * (\text{Ch 11})^2 + 0.0053 * (\text{Ch 11}) - 0.5221$
$T_w$ Jacket In	$f(\text{Ch16}) = -0.0004 * (\text{Ch16})^2 + 0.0329 * (\text{Ch16}) - 0.8837$
$T_d$ Exterior	$f(\text{Ch10}) = -6\text{E-}05 * (\text{Ch10})^3 + 0.0038 * (\text{Ch10})^2 - 0.0201 * (\text{Ch10}) - 0.2618$
$T_w$ Exterior	Reference thermocouple, $f(\text{Ch15}) = 0$
$T_d$ Load In	$f(\text{Ch13}) = 0.0013 * (\text{Ch13})^2 - 0.0118 * (\text{Ch13}) + 0.2388$
$T_w$ Load In	$f(\text{Ch12}) = 9\text{E-}06 * (\text{Ch12})^3 + 8\text{E-}05 * (\text{Ch12})^2 + 0.0125 * (\text{Ch12}) - 0.0386$
$T_d$ Load Out	$f(\text{Ch14}) = 0.0003 * (\text{Ch14})^2 + 0.0048 * (\text{Ch14}) + 0.2837$

Using these correction functions, it was now possible to obtain accurate temperatures at the different locations inside and outside the solar kiln.

## APPENDIX D: DATA ANALYSIS METHODS

### D.1 Ambient air pressure

The solar kiln was situated at an altitude of 220m above sea level. This has an influence of the average atmospheric pressure. The atmospheric pressure was required for a number of psychrometric equations. The average atmospheric pressure was determined by the International Standard Atmosphere values:

$$P_t = P_0 \cdot \left(1 - \frac{L \cdot h}{T_0}\right)^{g \cdot M / R \cdot L} \text{ Pa}$$

where:

$P_t$  = total atmospheric pressure, Pa ,

$P_0$  = sea level atmospheric pressure = 101325 Pa ,

$T_0$  = sea level standard temperature = 288.15 K

$g$  = earth-surface gravitational acceleration = 9.80665 m/s<sup>-2</sup>

$L$  = temperature-lapse rate = 0.0065 K/m

$R$  = universal gas constant = 8.31447 J/mol. K

$M$  = molar mass of dry air = 0.0289644 kg/mol

$h$  = metres above sea level,  $m$  = 220m for the Solar kiln in George, South Africa  
(ISO 2533:1975)

Put into the equation,  $P_t = 98,709.92 \text{ Pa}$ .

### D.2 Relative humidity

Relative humidity (RH) is the ratio of the partial vapour pressure to the saturated vapour pressure of the air-vapour mixture at the same temperature, expressed as a percentage:

$$RH = \frac{p_{vap}}{p_{sat \text{ vap}}} \times 100 \%$$

The saturated vapour pressure  $p_{sat \text{ vap}}$  must first be calculated. Then, a vapour pressure corresponding to the wet bulb temperature needs to be calculated in order to determine the actual vapour pressure. There are various ways to calculate the vapour pressure (Vömel, 2010). Vömel (2010) cited the work of the Buck Research Manual of 1996 where it was suggested the initial saturated vapour equation of Buck be modified. Both these are an improvement on the original Magnus-Tetens formula (Vömel, 2010). The improved Buck-formula is indicated below:

$$p_{sat\ vap} = 6.1121 \times e^{\left[ \left( \frac{18.678 - t_{db}}{234.5} \right) \times \frac{t_{db}}{(257.14 + t_{db})} \right]} \text{ hPa}$$

where:  $t_{db}$  = dry bulb temperature, °C

The partial vapour pressure corresponding to the wet bulb temperature,  $p_{WB\ sat\ vap}$  was determined in a similar way to the  $p_{sat\ vap}$

$$p_{WB\ sat\ vap} = 6.1121 \times e^{\left[ \left( \frac{18.678 - t_{wb}}{234.5} \right) \times \frac{t_{wb}}{(257.14 + t_{wb})} \right]} \text{ hPa}$$

where:  $t_{wb}$  = wet bulb temperature, °C

The vapour pressure,  $p_{vap}$ , was then determined by using the formula supplied by Vermaas (1990). It is also available from Brice (2010).

$$p_{vap} = p_{WB\ sat\ vap} - P_t \times (t_{db} - t_{wb}) \times 0.00066 \times (1 + 0.00115 \cdot t_{wb}) \text{ hPa}$$

(Brice, 2010)

With all the terms available, the relative humidity could be computed with the input data of the dry bulb temperature,  $t_{db}$ , the wet bulb temperature,  $t_{wb}$ , and the total atmospheric pressure,  $P_t$ .

### D.3 Equilibrium moisture content (EMC)

The EMC at the measure stations was determined using the Hailwood-Harrobin equation:

$$EMC = \frac{1800}{M_p} \left[ \frac{K \cdot h}{1 - K \cdot h} + \frac{K_1 \cdot K \cdot h + 2K_1 \cdot K_2 \cdot K^2 \cdot h^2}{1 + K_1 \cdot K \cdot h + K_1 \cdot K_2 \cdot K^2 \cdot h^2} \right]$$

where:

$$M_p = 349 + 1.29t + 0.0135t^2$$

$$K = 0.805 + 0.000736t - 0.00000273t^2$$

$$K_1 = 6.27 - 0.000938t - 0.000303t^2$$

$$K_2 = 1.91 + 0.0407t - 0.000293 \cdot t^2$$

$$h = \text{Relative vapour pressure} = \frac{RH}{100}$$

RH = Relative humidity, %

$t$  = Dry bulb temperature, °C

(Simpson, 1991)

#### D.4 Absolute humidity (AH) on a mass basis

The absolute humidity (AH) on a mass basis, also known as the humidity ratio, is expressed as the mass of vapour per mass of dry air (Stoecker and Jones, 1982). It is expressed as a function of the partial vapour pressure:

$$AH = \frac{\text{mass of vapour}}{\text{mass of dry air}} = \frac{V \times p_v / R_s \times T}{V \times p_a / R_a \times T} = 0.622 \frac{p_v}{P_t - p_v} \text{ kg water / kg dry air}$$

where:

$V$  = arbitrary volume of air vapour mixture,  $m^3$

$R_a$  = gas constant of dry air = 287 J/kg. K

$R_v$  = gas constant of water vapour 461.5 J/kg. K

$p_v$  = vapour pressure, Pa

$P_t$  = total atmospheric pressure, Pa

$p_a$  = partial pressure of dry air =  $P_t - p_v$ , Pa

$T$  = absolute temperature of air vapour mixture, K

(Stoecker and Jones, 1982)

Normally AH is multiplied by 1000 to convert it to g water / kg dry air, therefore,

$$AH = 622 \frac{p_v}{P_t - p_v} \text{ g water / kg dry air}$$

#### D.5 Dew-point temperature

The Magnus-Tetens equation is based on the August–Roche–Magnus approximation and is described by Paroscientific (2010) in two steps:

$$\alpha = (17.271 \times t_{db} / (237.7 + t_{db})) + \ln h$$

where:

$t_{db}$  = dry bulb temperature, °C

$$h = \text{Relative vapour pressure} = \frac{RH}{100}$$

$$T_{dew} = 237.7 \times \frac{\alpha}{17.271 - \alpha} \text{ °C}$$

## APPENDIX E: ZA DRY Q RESULTS

Table E.1: ZA Dry Q MC (%) record for stack 2, 30mm x 124mm green dimensions

AIR INLET SIDE LEFT (board no 1)

BOARD LAYER FROM THE TOP	BOARD NO. IN LAYER	MEASURE DEPTH	LOCATION ALONG BOARD LENGTH (in meter) TOWARDS MID OF KILN (% MC)					
			0,25	0.65	1.05	1.45	1.85	2.25
2	1	½	14	13.5	14	13.5	13	13
		⅓	13	12.5	13	13	12	12
		⅙	12.5	11.5	11.5	11.5	10.5	11
		Gradient	1.5	2	2.5	2	2.5	2
	2	½	9.5	10	10.5	10	10	10
		⅓	9.5	9	9.5	9.5	9.5	9.5
		⅙	9	9	9	9	9	9
		Gradient	0.5	1	1.5	1	1	1
	3	½	12	12	12	11	11	11
		⅓	11	10.5	11	10	10.5	10.5
		⅙	10	10	9.5	9	9	9.5
		Gradient	2	2	2.5	2	2	1.5
	4	½	12.5	14	13	13.5	12.5	12
		⅓	11	12	12	11.5	11	11.5
		⅙	10.5	11	11	11	10	10.5
		Gradient	2	3	2	2.5	2.5	1.5
9	1	½	12	12	13	14	14	14
		⅓	11.5	11.5	12	12.5	13	13.5
		⅙	11	11	11	12	12.5	12.5
		Gradient	1	1	2	2	1.5	1.5
	2	½	10	10.5	10.5	10.5	11	11
		⅓	9.5	10.5	10	10	10.5	10.5
		⅙	9	9.5	9.5	9.5	9.5	10



		Gradient	1	1	1	1	1.5	1
	3	$\frac{1}{2}$	11.5	11.5	12.5	12	12	12
		$\frac{1}{3}$	11.5	11	11.5	11	11.5	11.5
		$\frac{1}{6}$	10	9.5	11	10	10	10
		Gradient	1.5	2	1.5	2	2	2
	4	$\frac{1}{2}$	10.5	11	11	11	11	11
		$\frac{1}{3}$	10.5	10.5	10	10.5	10.5	10.5
		$\frac{1}{6}$	9.5	9.5	9.5	10	9.5	9.5
		Gradient	1	1.5	1.5	1	1.5	1.5
16	1	$\frac{1}{2}$	11	12	11.5	12	11.5	12
		$\frac{1}{3}$	11	11.5	11	11.5	11	11.5
		$\frac{1}{6}$	10.5	10.5	10.5	10.5	10.5	11
		Gradient	0.5	1.5	1	1.5	1	1
	2	$\frac{1}{2}$	10.5	10.5	11	11	11	11
		$\frac{1}{3}$	9.5	10	10	10.5	10	10
		$\frac{1}{6}$	9	9.5	10	9.5	9.5	10
		Gradient	1.5	1	1	1.5	1.5	1
	3	$\frac{1}{2}$	12	12.5	13	12.5	12.5	12
		$\frac{1}{3}$	11.5	12	12	11.5	12	11.5
		$\frac{1}{6}$	10	11	11	10.5	11	11
		Gradient	2	1.5	2	2	1.5	1
	4	$\frac{1}{2}$	12	13	14	14	14	14
		$\frac{1}{3}$	11.5	12	13	13.5	13.5	13.5
		$\frac{1}{6}$	10	11.5	12	11.5	11.5	12
		Gradient	2	1.5	2	2.5	2.5	2
22	1	$\frac{1}{2}$	11	10.5	11.5	12	11.5	11
		$\frac{1}{3}$	10.5	10.5	11	11	11	11
		$\frac{1}{6}$	10	9.5	10	10.5	10	10.5
		Gradient	1	1	1.5	1.5	1.5	0.5

	2	$\frac{1}{2}$	11.5	12	12	12	12	12
		$\frac{1}{3}$	11	11	11	11	11	11.5
		$\frac{1}{6}$	10	10	10.5	10.5	10.5	10.5
		Gradient	1.5	2	1.5	1.5	1.5	1.5
	3	$\frac{1}{2}$	13	14	14	14	14	13
		$\frac{1}{3}$	12.5	13	12.5	13	12.5	11.5
		$\frac{1}{6}$	11	12	11.5	12	11.5	10.5
		Gradient	2	2	2.5	2	2.5	2.5
	4	$\frac{1}{2}$	11.5	13	13	13	12.5	12.5
		$\frac{1}{3}$	11.5	12	12	12	11.5	11.5
		$\frac{1}{6}$	10.5	11	11	11	10.5	11
		Gradient	1	2	2	2	2	1.5
29	1	$\frac{1}{2}$	12.5	13	12.5	12.5	12.5	12
		$\frac{1}{3}$	11.5	12	11.5	11.5	12	11
		$\frac{1}{6}$	10.5	11	11	11	11	10.5
		Gradient	2	2	1.5	1.5	1.5	1.5
	2	$\frac{1}{2}$	12	12.5	12.5	12.5	13	13
		$\frac{1}{3}$	11.5	12	12	12	12	12
		$\frac{1}{6}$	11	11	11.5	11	11	11
		Gradient	1	1.5	1	1.5	2	2
	3	$\frac{1}{2}$	14	14	14	13.5	13.5	12.5
		$\frac{1}{3}$	13	13	14	13	12.5	12
		$\frac{1}{6}$	12	12	12.5	12.5	12	11.5
		Gradient	2	2	1.5	1	1.5	1
	4	$\frac{1}{2}$	11	11.5	12	11.5	11.5	11.5
		$\frac{1}{3}$	10.5	10.5	11	11	11	11
		$\frac{1}{6}$	10	9.5	11	10.5	9.5	10
		Gradient	1	2	1	1	2	1.5

Table E.2: ZA Dry Q MC (%) record for stack 7; 30mm x 87mm green dimensions

AIR INLET SIDE RIGHT (board no 4)

BOARD LAYER FROM THE TOP	BOARD NO. IN LAYER	MEASURE DEPTH	LOCATION ALONG BOARD LENGTH (in meter) TOWARDS MID OF KILN (% MC)					
			0,25	0.65	1.05	1.45	1.85	2.25
2	1	½	10	12	13	11	11.5	12
		⅓	11	12	12	10.5	11	11.5
		¼	10	10	11	11	10	10
		Gradient	0	2	2	0	1.5	2
	2	½	12	12	12.5	13	12.5	12
		⅓	11.5	12	12	12	12	12
		¼	10.5	11	11	11	11	11
		Gradient	1.5	1	1.5	2	1.5	1
	3	½	10.5	10.5	10.5	11	11	10
		⅓	10	10	10	10.5	10.5	10
		¼	9	9	9	9.5	10	9
		Gradient	1.5	1.5	1.5	1.5	1	1
	4	½	12	12	12	12	12	12
		⅓	11	11.5	11.5	11.5	11.5	11
		¼	11	10.5	11	10.5	11	10.5
		Gradient	1	1.5	1	1.5	1	1.5
9	1	½	15.5	15.5	15	14	15	13.5
		⅓	13	15	15	14	14	13
		¼	13	13.5	13	13	13	12
		Gradient	2.5	2	2	1	2	1.5
	2	½	11	13	13	13	13	13
		⅓	11	12	12.5	13	12.5	12
		¼	10	12	12	12	12	11.5
		Gradient	1	1	1	1	1	1.5
	3	½	11.5	12	12	12	12	11

		$\frac{1}{3}$	11	11	11	11	11	10.5
		$\frac{1}{6}$	10	10	10	10.5	10.5	10
		Gradient	1.5	2	2	1.5	1.5	1
	4	$\frac{1}{2}$	12	12	12	11	12	12
		$\frac{1}{3}$	11.5	11.5	11.5	11	11	11.5
		$\frac{1}{6}$	11	11	11	11	11	11
		Gradient	1	1	1	0	1	1
16	1	$\frac{1}{2}$	13	13	13	13	13	13
		$\frac{1}{3}$	12	12	11.5	12	11.5	12
		$\frac{1}{6}$	11	11	11	11.5	11.5	12
		Gradient	2	2	2	1.5	1.5	1
	2	$\frac{1}{2}$	12	11.5	11	11.5	12	12
		$\frac{1}{3}$	11	11	11	11	11	11
		$\frac{1}{6}$	11	10	10	11	10	10.5
		Gradient	1	1.5	1	0.5	2	1.5
	3	$\frac{1}{2}$	11.5	12	12	12.5	13	13
		$\frac{1}{3}$	11	11	11.5	12	12	12
		$\frac{1}{6}$	10	10.5	11	11.5	11	11
		Gradient	1.5	1.5	1	1	2	2
	4	$\frac{1}{2}$	12.5	13	13	13	13	13
		$\frac{1}{3}$	11.5	11	12	12	12	11.5
		$\frac{1}{6}$	11	10.5	11	11	11	11
		Gradient	1.5	2.5	2	2	2	2
22	1	$\frac{1}{2}$	12	12	12	12	12	12
		$\frac{1}{3}$	11.5	12	12	11.5	11	11.5
		$\frac{1}{6}$	11	11	11	11	10.5	11
		Gradient	1	1	1	1	1.5	1
	2	$\frac{1}{2}$	11.5	12	12	12	12	12
		$\frac{1}{3}$	11	11	11	11	11.5	11

29			½	10	11	10.5	10.5	11	10
			Gradient	1.5	1	1.5	1.5	1	2
		3	½	12.5	13	13	13	13	12
			⅓	11.5	12	12	12	12	11.5
			¼	11	11	11	11	11	10.5
			Gradient	1.5	2	2	2	2	1.5
		4	½	12.5	13	13	13	13	13.5
			⅓	12	12	12.5	12	12	13
			¼	11	11.5	11.5	11.5	12	12
			Gradient	1.5	1.5	1.5	1.5	1	1.5
		1	½	12	12	12	12	12	12
			⅓	11.5	11	11	11.5	11.5	11.5
			¼	11	11	11	11	11	11
			Gradient	1	1	1	1	1	1
		2	½	12.5	12.5	13	12.5	12	13
			⅓	12	11.5	11	11.5	11	11
			¼	11.5	11	11.5	11.5	11.5	11
			Gradient	1	1.5	1.5	1	0.5	2
		3	½	13	13	13	13.5	13	12
			⅓	12	12.5	13	13	12.5	12
			¼	11.5	12	12	12.5	12	11.5
			Gradient	1.5	1	1	1	1	0.5
		4	½	14.5	15	14	14.5	13	14
			⅓	14	14	12	12	13	13.5
			¼	13	13	12.5	12	12	12
			Gradient	1.5	2	1.5	2.5	1	2

## APPENDIX F: MOISTURE CONTENT ANALYSIS

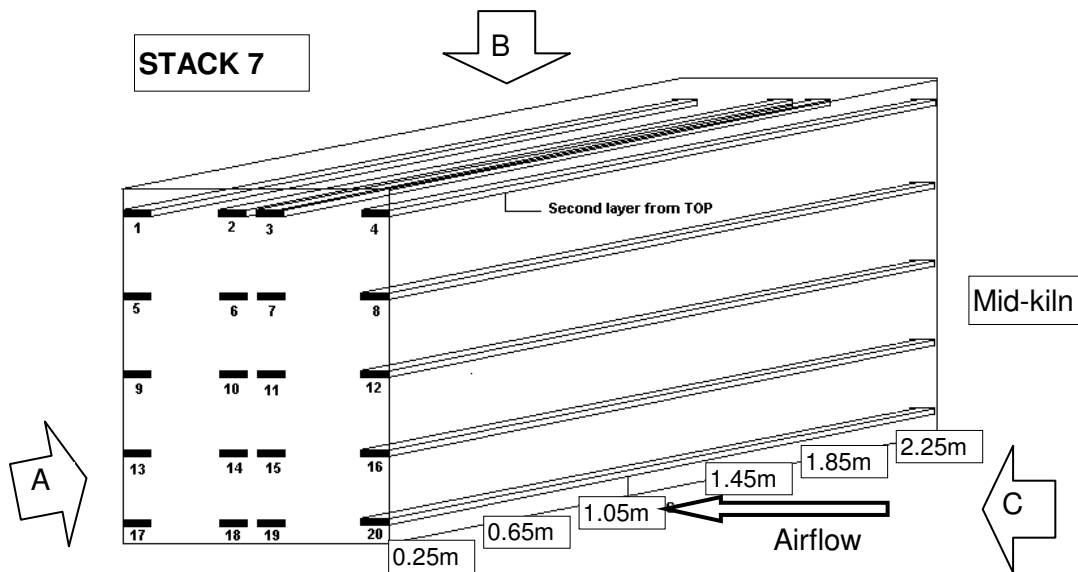


Figure F.1: Observation points to assess the moisture variation in stack 7; the average all  $MC_{\frac{1}{2}}$  measurements were 11.7%

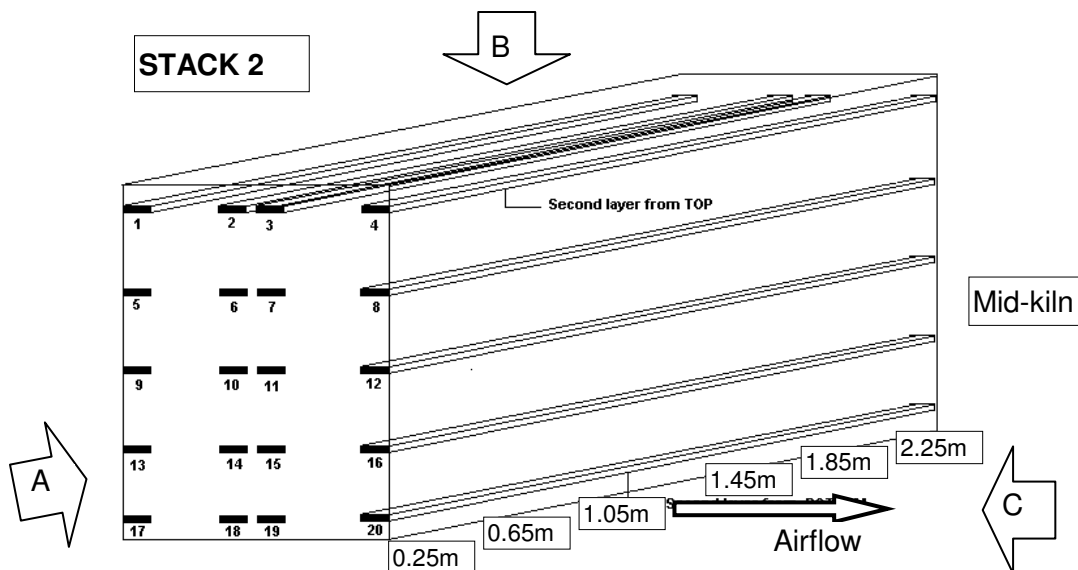


Figure F.2: Observation points to assess the moisture variation in stack 2; the average of all  $MC_{\frac{1}{2}}$  measurements were 11.4%

The following symbols will be used to assist the interpretation of the results:

|A|: Parallel to the face of the stack as indicated by A

|B|: Parallel to the face of the stack as indicated by B

|C|: Parallel to the face of the stack as indicated by C

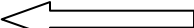
Note that the  $\frac{1}{3}$  depth MC value is the average MC of a board only at that specific point on the board where the prongs of the electrical resistance moisture meter have been inserted to one-third of the depth.

### F.1 MC and MG variation over the width and height of the stacks, as seen from the end of the stack (A)

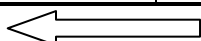
The average of six measurements on each board is shown in Table F.1. Note that the results as seen from A will give the average values of the six  $MC_{\frac{1}{3}}$  measurements that were taken along the six measuring locations on each of the boards. For example, the average MC of the six values taken at the along the length of the sample board in stack 7 in board position 1 in layer number 2, was 11.3%. This was thus the average MC of the board in this position.

Table F.1: Average of six MC values on each board of stack 7 at  $\frac{1}{3}$ -depth, as seen from the end of the stack (Face A)

STACK 7: AVERAGE MC OF 6 VALUES ON EACH BOARD AT ⅓ DEPTH - AS SEEN FROM END (FACE A)						
LAYER NO	BOARD POSITION IN EACH LAYER				LAYER AVERAGE  B	
	1	2	3	4		
TOP	2	11.3	11.9	10.2	11.3	11.2
	9	14.0	12.2	10.9	11.3	12.1
	16	11.8	11.0	11.6	11.7	11.5
BOTTOM	22	11.6	11.1	11.8	12.3	11.7
	29	11.3	11.3	12.5	13.1	12.1
	POSITION AVERAGE  C	12.0	11.5	11.4	11.9	11.7



Airflow


 Airflow

The standard deviation of the six measurements on each board at  $\frac{1}{3}$  of the board depth is shown in Table F.2.

Table F.2: Standard deviation of six MC values on each board of stack 7 at  $\frac{1}{3}$ -depth, as seen from the end of the stack (Face A)

STACK 7: STANDARD DEVIATION OF 6 VALUES ON EACH BOARD AT $\frac{1}{3}$ DEPTH - AS SEEN FROM END (FACE A)					
LAYER NO	BOARD POSITION IN EACH LAYER				LAYER AVERAGE  B
	1	2	3	4	
TOP	2	0.6	0.2	0.3	0.3
	9	0.9	0.7	0.2	0.3
	16	0.3	0.0	0.5	0.4
BOTTOM	22	0.4	0.2	0.3	0.4
	29	0.3	0.4	0.4	0.9
	POSITION AVERAGE  C	0.5	0.3	0.3	0.5

← Airflow

Stack 2 is displayed similarly. Note that the direction of airflow is from board position 1 to 4.

Table F.3: Average of six MC values on each board of stack 2 at  $\frac{1}{3}$ -depth, as seen from the end of the stack (Face A)

STACK 2: AVERAGE MC OF 6 VALUES ON EACH BOARD AT $\frac{1}{3}$ DEPTH - AS SEEN FROM END (FACE A)					
LAYER NO	BOARD POSITION IN EACH LAYER				LAYER AVERAGE  B
	1	2	3	4	
TOP	2	12.6	9.4	10.6	11.5
	9	12.3	10.2	11.3	10.4
	16	11.3	10.0	11.8	12.8
BOTTOM	22	10.8	11.1	12.5	11.8
	29	11.6	11.9	12.9	10.8
	POSITION AVERAGE  C	11.7	10.5	11.8	11.5

→ Airflow

Table F.4: Standard deviation of six MC values on each board of stack 2 at  $\frac{1}{3}$ -depth, as seen from the end of the stack (Face A)

STACK 2: STANDARD DEVIATION OF 6 VALUES ON EACH BOARD AT $\frac{1}{3}$ DEPTH - AS SEEN FROM END (FACE A)					
LAYER NO	BOARD POSITION IN EACH LAYER				LAYER AVERAGE  B
	1	2	3	4	
TOP	2	0.5	0.2	0.4	0.4
	9	0.8	0.4	0.3	0.2
	16	0.3	0.3	0.3	0.9
BOTTOM	22	0.3	0.2	0.5	0.3
	29	0.4	0.2	0.7	0.3
	POSITION AVERAGE  C	0.4	0.3	0.4	0.4

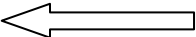
→ Airflow



The average of six MGs on each board is shown in Tables F.5 and F.7 for stacks 7 and 2 respectively, with corresponding standard deviations in Tables F.6 and F.8. This indicates the variation in MG in the direction of airflow and over the stack height.

Table F.5: Average of six MG values on each board of stack 7, as seen from the end of the stack  
(Face A)

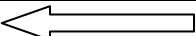
STACK 7: AVERAGE MG OF 6 VALUES ON EACH BOARD - AS SEEN FROM END (FACE A)					
LAYER NO	BOARD POSITION IN EACH LAYER				LAYER AVERAGE  B
	1	2	3	4	
TOP	2	1.3	1.4	1.3	1.3
	9	1.8	1.1	1.6	1.3
	16	1.7	1.3	1.5	1.6
BOTTOM	22	1.1	1.4	1.8	1.4
	29	1.0	1.3	1.0	1.3
	POSITION AVERAGE  C	1.4	1.3	1.5	1.5

 Airflow

The standard deviation of the six MG measurements on each board is shown in Table F.6.

Table F.6: Standard deviation of six MG values on each board of stack 7, as seen from the end of  
the stack (Face A)

STACK 7: STANDARD DEVIATION OF 6 MG VALUES ON EACH BOARD - AS SEEN FROM END (FACE A)					
LAYER NO	BOARD POSITION IN EACH LAYER				LAYER AVERAGE  B
	1	2	3	4	
TOP	2	1.0	0.4	0.3	0.3
	9	0.5	0.2	0.4	0.4
	16	0.4	0.5	0.4	0.3
BOTTOM	22	0.2	0.4	0.3	0.2
	29	0.0	0.5	0.3	0.5
	POSITION AVERAGE  C	0.4	0.4	0.3	0.3

 Airflow

Similarly for stack 2:

Table F.7: Average of six MG values on each board of stack 2, as seen from the end of the stack  
(Face A)

STACK 2: AVERAGE MG OF 6 VALUES ON EACH BOARD - AS SEEN FROM END (FACE A)						
LAYER NO	BOARD POSITION IN EACH LAYER				LAYER AVERAGE  B	
	1	2	3	4		
TOP	2	2.1	1.0	2.0	2.3	1.8
	9	1.5	1.1	1.8	1.3	1.4
	16	1.1	1.3	1.7	2.1	1.5
	22	1.2	1.6	2.3	1.8	1.7
	29	1.7	1.5	1.5	1.4	1.5
BOTTOM	POSITION AVERAGE  C	1.5	1.3	1.9	1.8	1.6

Airflow

The standard deviation of the six MG measurements at each board is shown in Table F.8.

:

Table F.8: Standard deviation of six MG values on each board of stack 2, as seen from the end of  
the stack (Face A)

STACK 2: STANDARD DEVIATION OF 6 MG VALUES ON EACH BOARD - AS SEEN FROM END (FACE A)						
LAYER NO	BOARD POSITION IN EACH LAYER				LAYER AVERAGE  B	
	1	2	3	4		
TOP	2	0.4	0.3	0.3	0.5	0.4
	9	0.4	0.2	0.3	0.3	0.3
	16	0.4	0.3	0.4	0.4	0.4
	22	0.4	0.2	0.3	0.4	0.3
BOTTOM	29	0.3	0.4	0.4	0.5	0.4
	POSITION AVERAGE  C	0.4	0.3	0.3	0.4	0.4

Airflow

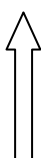
The average MC of the 20 boards of stack 7 and those of stack 2 did not differ much. An interesting phenomenon was the equally distributed standard deviation of the two stacks. The MG was low and the expectation was that the stresses would be small. The MG distribution was also random throughout the stacks.

## F.2 MC and MG variation over the length and width of the stacks, as seen from the top of the stack (B):

The average of five measurements along the height direction was taken on each position of the stack and at each location of a board. This would indicate the moisture variation in the direction of airflow and over the stack length.

Table F.9: Average of five MC values on all combinations of position and location of stack 7 at  $\frac{1}{3}$  depth, as seen from the top of the stack (Face B)


STACK 7: AVERAGE MOISTURE CONTENT AT $\frac{1}{3}$ DEPTH - AS SEEN FROM TOP							
BOARD POSITION NO.	LOCATION ALONG BOARD LENGTH (in metres) TOWARDS MIDDLE OF KILN						POSITION AVERAGE  C
	0.25	0.65	1.05	1.45	1.85	2.25	
1	11.8	12.4	12.3	11.9	11.8	11.9	12.0
2	11.3	11.5	11.5	11.7	11.6	11.4	11.5
3	11.1	11.3	11.5	11.7	11.6	11.2	11.4
4	12	12	11.9	11.7	11.9	12.1	11.9
LOCATION AVERAGE  A	11.6	11.8	11.8	11.8	11.7	11.7	11.7



Airflow

Table F.10: Standard deviation of five MC values on all combinations of position and location of stack 7 at  $\frac{1}{3}$  depth, as seen from the top of the stack (Face B)

STACK 7: STANDARD DEVIATION AT $\frac{1}{3}$ DEPTH - AS SEEN FROM TOP							
BOARD POSITION NO.	LOCATION ALONG BOARD LENGTH (in metres) TOWARDS MIDDLE OF KILN						POSITION AVERAGE  C
	0.25	0.65	1.05	1.45	1.85	2.25	
1	0.8	1.5	1.6	1.3	1.3	0.7	1.2
2	0.4	0.4	0.7	0.8	0.7	0.5	0.6
3	0.7	1.0	1.1	1.0	0.8	0.9	0.9
4	1.2	1.2	0.4	0.4	0.7	1.1	0.8
LOCATION AVERAGE  A	0.8	1.0	0.9	0.9	0.9	0.8	0.9




Airflow

Similarly for stack 2:

Table F.11: Average of five MC values on all combinations of position and location of stack 2 at  $\frac{1}{3}$  depth, as seen from the top of the stack (Face B)

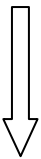
STACK 2: AVERAGE MOISTURE CONTENT AT $\frac{1}{3}$ DEPTH - AS SEEN FROM TOP							
BOARD POSITION NO.	POSITION ALONG BOARD LENGTH (in metres) TOWARDS MIDDLE OF KILN						POSITION AVERAGE  C
	0.25	0.65	1.05	1.45	1.85	2.25	
1	11.5	11.6	11.7	11.9	11.8	11.8	11.7
2	10.2	10.5	10.5	10.6	10.6	10.7	10.5
3	11.9	11.9	12.2	11.7	11.8	11.4	11.8
4	11	11.4	11.6	11.7	11.5	11.6	11.5
LOCATION AVERAGE  A	11.2	11.4	11.5	11.5	11.4	11.4	11.4



Airflow

Table F.12: Standard deviation of five MC values on all combinations of position and location of stack 2 at  $\frac{1}{3}$  depth, as seen from the top of the stack (Face B)

STACK 2: STANDARD DEVIATION AT $\frac{1}{3}$ DEPTH - AS SEEN FROM TOP							
BOARD POSITION NO.	POSITION ALONG BOARD LENGTH (in metres) TOWARDS MIDDLE OF KILN						POSITION AVERAGE  C
	0.25	0.65	1.05	1.45	1.85	2.25	
1	0.9	0.7	0.8	0.8	0.8	1.0	0.9
2	0.9	1.1	1.0	1.0	1.0	1.0	1.0
3	0.8	1.1	1.2	1.3	0.8	0.5	1.0
4	0.5	0.8	1.1	1.2	1.2	1.1	1.0
LOCATION AVERAGE  A	0.8	0.9	1.0	1.1	1.0	0.9	0.9

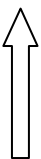


Airflow

The average of five MG measurements along the height direction of stack 7 was taken on each position of the stack and at each location of a board and is shown in Table F.13. This will indicate the MG in the direction of the airflow and over the stack length. The standard deviations for these average values are shown in Table F.14.

Table F.13: Average of five MG values on all combinations of position and location of stack 7, as seen from the top of the stack (Face B)

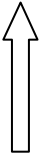
STACK 7: MOISTURE GRADIENT - AS SEEN FROM TOP							
BOARD POSITION NO.	LOCATION ALONG BOARD LENGTH (in metres) TOWARDS MIDDLE OF KILN						POSITION AVERAGE  C
	0.25	0.65	1.05	1.45	1.85	2.25	
1	1.3	1.6	1.6	0.9	1.5	1.3	1.4
2	1.2	1.2	1.3	1.2	1.2	1.6	1.3
3	1.5	1.6	1.5	1.4	1.5	1.2	1.5
4	1.3	1.7	1.4	1.5	1.2	1.6	1.5
LOCATION AVERAGE  A	1.3	1.5	1.5	1.3	1.4	1.4	1.4



Airflow

Table F.14: Standard deviation of five MG values on all combinations of position and location of stack 7, as seen from the top of the stack (Face B)

STACK 7: STANDARD DEVIATION OF MOISTURE GRADIENT - AS SEEN FROM TOP							
BOARD POSITION NO.	LOCATION ALONG BOARD LENGTH (in metres) TOWARDS MIDDLE OF KILN						POSITION AVERAGE  C
	0.25	0.65	1.05	1.45	1.85	2.25	
1	0.3	0.6	0.4	0.9	0.4	0.4	0.5
2	0.3	0.3	0.3	0.6	0.6	0.4	0.4
3	0.0	0.4	0.5	0.4	0.5	0.6	0.4
4	0.3	0.6	0.4	0.9	0.4	0.4	0.5
LOCATION AVERAGE  A	0.2	0.5	0.4	0.7	0.5	0.5	0.5

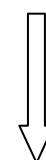


Airflow

Similarly for Stack 2:

Table F.15: Average of five MG values on all combinations of position and location of stack 2, as seen from the top of the stack (Face B)

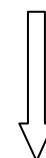
STACK 2: MOISTURE GRADIENT - AS SEEN FROM TOP							
BOARD POSITION NO.	LOCATION ALONG BOARD LENGTH (in metres) TOWARDS MIDDLE OF KILN						POSITION AVERAGE  C
	0.25	0.65	1.05	1.45	1.85	2.25	
1	1.2	1.5	1.7	1.7	1.6	1.3	1.5
2	1.1	1.3	1.2	1.3	1.5	1.3	1.3
3	1.9	1.9	2	1.8	1.9	1.6	1.9
4	1.4	2	1.7	1.8	2.1	1.6	1.8
LOCATION AVERAGE  A	1.4	1.7	1.7	1.7	1.8	1.5	1.6



Airflow

Table F.16: Standard deviation of five MG values on all combinations of position and location of stack 2, as seen from the top of the stack (Face B)

STACK 2: STANDARD DEVIATION OF MOISTURE GRADIENT - AS SEEN FROM TOP							
BOARD POSITION NO.	LOCATION ALONG BOARD LENGTH (in metres) TOWARDS MIDDLE OF KILN						POSITION AVERAGE  C
	0.25	0.65	1.05	1.45	1.85	2.25	
1	0.5	0.6	0.4	0.8	0.4	0.2	0.5
2	0.4	0.4	0.3	0.3	0.4	0.4	0.4
3	0.2	0.2	0.5	0.4	0.4	0.7	0.4
4	0.5	0.6	0.4	0.8	0.4	0.2	0.5
LOCATION AVERAGE  A	0.4	0.5	0.4	0.6	0.4	0.4	0.4



Airflow

The average MC of the 24 combinations of positions and locations in stack 7 and those in stack 2 did not differ much. The MG was also randomly distributed throughout the stacks. Again, wetter and drier measuring points were evenly spread through the stack and the only observation was that the MC and MG were a fraction lower at the board ends (0.2% lower). This could be because the measurements were taken 250mm from the end grain on both sides of the boards. However, the percentage being so small, it could be ignored.

The standard deviation of the values as seen from the top of the stack was generally higher than as seen from the end of the stack. This was to be expected because the measuring points were across different boards; the chances are greater that wood properties vary between boards, rather than within boards.

The standard deviation in stack 2 was a little lower and more equally distributed. However, this deviation was not as marked as it was when viewed from the stack end (Face A).

These results confirmed the tight final MC being achieved by the Saasveld solar kiln.

The standard deviation was generally higher. This was to be expected because the measuring points were across different boards; the chances are greater that wood properties vary between boards, rather than within boards.

The standard deviation was a little lower and more equally distributed, in stack 2. However, this deviation was not as marked as it was when viewed from the stack end (Face A).

These results confirmed the tight final MC being achieved by the Saasveld solar kiln.

### **F.3 MC and MG variation over the length and height of the stacks, as seen through the stickers of the stack (C), either from the back of the kiln or the plenum chamber**

The average of four measurements along the airflow direction was taken on each measuring location in a board and on each of the five layers. This would indicate the moisture variation in the height of the stack and over the stack length.

Table F.17: Average of four MC values on all locations of the five identified layers of stack 7 at  $\frac{1}{3}$  depth, as seen through the stickers from the back of the load (Face C)

<b>STACK 7: AVERAGE MOISTURE CONTENT AT <math>\frac{1}{3}</math> DEPTH - AS SEEN FROM BACK OF THE KILN AT AIRFLOW INLET</b>							
LAYER NO.	LOCATION ALONG BOARD LENGTH (in metres) TOWARDS MIDDLE OF KILN						LAYER AVERAGE  B
	0.25	0.65	1.05	1.45	1.85	2.25	
2	10.9	11.4	11.4	11.1	11.3	11.1	11.2
9	11.6	12.4	12.5	12.3	12.1	11.8	12.1
16	11.4	11.3	11.5	11.8	11.6	11.6	11.5
22	11.5	11.8	11.9	11.6	11.6	11.8	11.7
29	12.4	12.3	11.8	12.0	12.0	12.0	12.1
LOCATION AVERAGE  A	11.6	11.8	11.8	11.8	11.7	11.7	11.7

Table F.18: Standard deviation of four MC values on all locations of the five identified layers of stack 7 at  $\frac{1}{3}$  depth, as seen through the stickers from the back of the load (Face C)

<b>STACK 7: STANDARD DEVIATION AT <math>\frac{1}{3}</math> DEPTH</b> <b>- AS SEEN FROM BACK OF THE KILN AT AIRFLOW INLET</b>							
LAYER NO.	LOCATION ALONG BOARD LENGTH (in metres) TOWARDS MIDDLE OF KILN						LAYER AVERAGE  B
	0.25	0.65	1.05	1.45	1.85	2.25	
2	0.6	0.9	0.9	0.8	0.6	0.9	0.8
9	0.9	1.8	1.8	1.5	1.4	1.0	1.4
16	0.5	0.5	0.4	0.5	0.5	0.5	0.5
22	0.4	0.5	0.6	0.5	0.5	0.9	0.6
29	1.1	1.3	1.0	0.7	0.9	1.1	1.0
LOCATION AVERAGE  A	0.7	1.0	0.9	0.8	0.8	0.9	0.9

Similarly for stack 2:

Table F.19: Average of four MC values on all locations of the five identified layers of stack 2 at  $\frac{1}{3}$  depth, as seen through the stickers from the plenum (Face C)

<b>STACK 2: AVERAGE MOISTURE CONTENT AT <math>\frac{1}{3}</math> DEPTH</b> <b>- AS SEEN FROM PLENUM CHAMBER AT THE AIRFLOW OUTLET</b>							
LAYER NO.	LOCATION ALONG BOARD LENGTH (in metres) TOWARDS MIDDLE OF KILN						LAYER AVERAGE  B
	0.25	0.65	1.05	1.45	1.85	2.25	
2	11.1	11.0	11.4	11.0	10.8	10.9	11.0
9	10.8	10.9	10.9	11.0	11.4	11.5	11.1
16	10.9	11.4	11.5	11.8	11.6	11.6	11.5
22	11.4	11.6	11.6	11.8	11.5	11.4	11.5
29	11.6	11.9	12.1	11.9	11.9	11.5	11.8
LOCATION AVERAGE  A	11.2	11.4	11.5	11.5	11.4	11.4	11.4

Table F.20: Standard deviation of four MC values on all locations of the five identified layers of stack 2 at  $\frac{1}{3}$  depth, as seen through the stickers from the plenum (Face C)

<b>STACK 2: STANDARD DEVIATION AT <math>\frac{1}{3}</math> DEPTH</b> <b>- AS SEEN FROM PLENUM CHAMBER AT THE AIRFLOW OUTLET</b>							
LAYER NO.	LOCATION ALONG BOARD LENGTH (in metres) TOWARDS MIDDLE OF KILN						LAYER AVERAGE  B
	0.25	0.65	1.05	1.45	1.85	2.25	
2	1.4	1.6	1.5	1.6	1.0	1.1	1.4
9	1.0	0.5	1.0	1.1	1.2	1.4	1.0
16	0.9	0.9	1.3	1.3	1.5	1.4	1.2
22	0.9	1.1	0.8	1.0	0.7	0.3	0.8
29	1.0	1.0	1.3	0.9	0.6	0.6	0.9
LOCATION AVERAGE  A	1.0	1.0	1.2	1.1	1.0	1.0	1.1

The average of four MGs on each board is shown in Table F.21. This would indicate the MG in the direction of the airflow and over the stack length.

Table F.21: Average of four MG values on all locations of the five identified layers of stack 7, as seen through the stickers from the back of the load (Face C)

<b>STACK 7: MOISTURE GRADIENT</b> <b>- AS SEEN FROM BACK OF THE KILN AT AIRFLOW INLET</b>							
LAYER NO.	LOCATION ALONG BOARD LENGTH (in metres) TOWARDS MIDDLE OF KILN						LAYER AVERAGE  B
	0.25	0.65	1.05	1.45	1.85	2.25	
2	1.0	1.5	1.5	1.3	1.3	1.4	1.3
9	1.5	1.5	1.5	0.9	1.4	1.3	1.3
16	1.5	1.9	1.5	1.3	1.9	1.6	1.6
22	1.4	1.4	1.5	1.5	1.4	1.5	1.4
29	1.3	1.4	1.3	1.4	0.9	1.4	1.3
LOCATION AVERAGE  A	1.3	1.5	1.5	1.3	1.4	1.4	1.4

Table F.22: Standard deviation of four MG values on all locations of the five identified layers of stack 7, as seen through the stickers from the back of the load (Face C)

<b>STACK 7: STANDARD DEVIATION OF MOISTURE GRADIENT</b> <b>- AS SEEN FROM BACK OF THE KILN AT AIRFLOW INLET</b>							
LAYER NO.	LOCATION ALONG BOARD LENGTH (in metres) TOWARDS MIDDLE OF KILN						LAYER AVERAGE  B
	0.25	0.65	1.05	1.45	1.85	2.25	
2	0.7	0.4	0.4	0.9	0.3	0.5	0.5
9	0.7	0.6	0.6	0.6	0.5	0.3	0.5
16	0.4	0.5	0.6	0.6	0.3	0.5	0.5
22	0.3	0.5	0.4	0.4	0.5	0.4	0.4
29	0.3	0.5	0.3	0.8	0.3	0.8	0.5
LOCATION AVERAGE  A	0.5	0.5	0.5	0.7	0.3	0.5	0.5

Similarly for Stack 2:



Table F.23: Average of four MG values on all locations of the five identified layers of stack 2, as seen through the stickers from the plenum (Face C)

<b>STACK 2: MOISTURE GRADIENT</b> <b>- AS SEEN FROM PLENUM CHAMBER AT THE AIRFLOW OUTLET</b>							
LAYER NO.	LOCATION ALONG BOARD LENGTH (in metres) TOWARDS MIDDLE OF KILN						LAYER AVERAGE  B
	0.25	0.65	1.05	1.45	1.85	2.25	
2	1.5	2.0	2.1	1.9	2.0	1.5	1.8
9	1.1	1.4	1.5	1.5	1.6	1.5	1.4
16	1.5	1.4	1.5	1.9	1.6	1.3	1.5
22	1.4	1.8	1.9	1.8	1.9	1.5	1.7
29	1.5	1.9	1.3	1.3	1.8	1.5	1.5
LOCATION AVERAGE  A	1.4	1.7	1.7	1.7	1.8	1.5	1.6

Table F.24: Standard deviation of four MG values on all locations of the five identified layers of stack 7, as seen through the stickers from the plenum (Face C)

<b>STACK 2: STANDARD DEVIATION OF MOISTURE GRADIENT</b> <b>- AS SEEN FROM PLENUM CHAMBER AT THE AIRFLOW OUTLET</b>							
LAYER NO.	LOCATION ALONG BOARD LENGTH (in metres) TOWARDS MIDDLE OF KILN						LAYER AVERAGE  B
	0.25	0.65	1.05	1.45	1.85	2.25	
2	0.7	0.8	0.5	0.6	0.7	0.4	0.6
9	0.3	0.5	0.4	0.6	0.3	0.4	0.4
16	0.7	0.3	0.6	0.5	0.6	0.5	0.5
22	0.5	0.5	0.5	0.3	0.5	0.8	0.5
29	0.6	0.3	0.3	0.3	0.3	0.4	0.4
LOCATION AVERAGE  A	0.5	0.5	0.4	0.5	0.5	0.5	0.5

Once again, the average MC of the 30 measuring points on all locations of the five identified layers did not differ much. The slightly lower MC of 0.4% and 0.5 % below the average of the two stacks with layer number 2 was again observed.

The MG was randomly distributed throughout the stacks once again and the MC at measuring points was evenly spread. The MC and MG was fractionally lower (0.2%) at the board ends; however, the percentage was so small, it could safely be ignored.

These results confirm the tight final MC being achieved by the Saasveld solar kiln. The moisture distribution, as seen from all directions, confirmed an equal distribution of temperature, humidity and airflow. This proved that the air circulation through the stacks was properly baffled, the stacking was good and the geometry of the kiln assured efficient air circulation.